Calcified tissue structure in the distal condyle of the third metacarpal bone in young Thoroughbred horses

Michael Doube

Thesis submitted for the degree of Doctor of Philosophy

Barts and The London School of Medicine and Dentistry
Queen Mary, University of London

December 2007

Abstract

Aims: To determine improvements in third metacarpal (Mc3) condylar microanatomy attributable to preconditioning exercise. To investigate developmental causes of Mc3 condylar fracture. Methods: Twelve Thoroughbred horses were raised at pasture; six received preconditioning exercise from 10 days. Calcein labels were administered 19 and 11 days prior to euthanasia at 18 months. Six horses also received 2 seasons of race-training and were euthanised at 3 years. Slices were taken from the distal Mc3 condyle in the frontal and dorsal- and palmar-oblique frontal planes, scanned with DXA and macerated (frontal slices) or embedded in PMMA (oblique slices). Articular calcified cartilage (ACC) and subchondral bone (SCB) in oblique slices were imaged using confocal scanning light microscopy and quantitative backscattered electron scanning electron microscopy. ACC and SCB in the palmar slice lateral parasagittal grooves were imaged using μCT and nanoindentation tested. Results: Characteristic spatial variations in ACC and SCB histomorphometric parameters were present, none of which was significantly related to preconditioning exercise. Thickened, aberrantly mineralised ACC was found in 13/24 parasagittal grooves in the palmar slices and on the sagittal ridge of 4/12 dorsal slices of 18-month-old horses. Deep to thickened ACC, SCB had an open marrow structure, having not adopted the buttress morphology of the normal SCB plate. SCB in 3-year-old horses had incorporated early ACC defects as notches in parasagittal grooves and a hyaline cartilage island in a sagittal ridge. ACC was less stiff and SCB more stiff in affected than unaffected parasagittal grooves. Chondroclastic resorption in the parasagittal groove may be retarded as early as 3-6 months, possibly due to localised inhibition of ACC mineralisation. Linear defects in the Mc3 parasagittal groove may develop prior to entry to race training and are not significantly affected by preconditioning exercise. Early identification of affected individuals should aid in reducing condylar fracture risk.

Declaration

This thesis represents my own unaided work except where otherwise acknowledged.

Michael Doube

December 2007

Acknowledgements

I have written this thesis with the support of many people: first, my supervisors at Queen Mary, Professor Alan Boyde and Dr Andy Bushby. An auspicious meeting with Prof. Boyde in New Zealand in early 2004 culminated in an offer to join his lab in London. I am truly fortunate to have been supervised by such a critical, prolific and well-connected scientist. Dr Bushby has provided a fresh, engineering perspective to my study in his clear and patient style, all of which I hope to take beyond this PhD. Professor Elwyn Firth at Massey University, New Zealand, has been instrumental in my academic career, from guiding me through my first research projects as a veterinary undergraduate, to introducing me to Prof. Boyde and participating in every stage of the production of this document. Professor Jim Elliott as the head of Dental Biophysics has worked behind the scenes, navigating the laboratory through several bureaucratic obstacles; without Prof. Elliott this study would have been very difficult if not impossible.

Mrs Mo Arora has been invaluable in helping with specimen preparation, drawing on her years of experience in the lab. Dr Peter Howell's statistical and computing support has been invaluable, as I have processed tens of gigabytes of data with his applications. Mr Roy Radcliffe gave valuable advice and assistance while preparing specimens with the diamond ultramiller and at the University College London confocal microscope facility. Wayne Rasband and the members of the ImageJ email list have provided helpful suggestions on the use of ImageJ and its macro language.

I am grateful to the Horserace Betting Levy Board for the Veterinary Research Training Scholarship that has paid almost all of my expenses while living and studying in London, and for the several equipment and travel grants they have provided. In particular, Miss Jessica Dean has been a friendly and efficient first point of call in her role as Equine Grants Officer. The Overseas Research Students Awards Scheme has generously funded the difference between home and international tuition fees for the 2nd and 3rd years of my PhD.

Robert Barbour and Magdalena Barawas have given me their generous hospitality on more than one occasion, and as ever, Robert has given me timely introductions to useful techniques such as Perl and MySQL. Miss Sharlene Royal gave me more than she can know: an end and an ending. Tomos Williams introduced me to life in the UK. My many veterinary colleagues and friends have been a welcome source of motivation and simultaneously, distraction. It is a continuous pleasure to be associated with such a caring, down-to-earth and intelligent group of people. The veterinary nurses I have worked with over the past few years have been a constant source of practical tips and have always lent an ear to the latest 'cocktail synopsis' of this thesis. Dr Joanna Laurson has provided the final bit of inspiration to get things finished.

Dr Naomi Boxall has guided me through the PhD experience; as one of the several PhD students

I knew while an undergraduate at Massey University she gave me insight into coping with the varied challenges that postgraduate study entails. Naomi also helped correct my sometimes dubious spelling, grammar and punctuation while preparing documents for submission. Jen Swindlehurst provided a number of images of equine metacarpals from her own studies that I was kindly allowed to use in my presentations. Jen's work also (conveniently) supported my own, and it was nice to have a colleague who was so intimately familiar with the problem of condylar fracture.

Several of Professor Boyde's colleagues, some of whom received his supervision during their PhD's, have given their practical guidance and encouragement throughout this study: Dr Ginny Kingsmill, Dr Peter Howell, Dr Simon Rawlinson and Dr Helen Liversidge at Barts and The London's Dental Institute, and Professor Chris Riggs at the Hong Kong Jockey Club have been particularly supportive. Dr Elaine Murphy, Dr Duncan Bassett, Professor Graham Williams, Dr Allan Williams and Miss Rowan Swinhoe provided an insight into molecular techniques when I used their lab in the Royal Postgraduate Medical School, Imperial College London.

The postgraduates and postdoctoral staff in the Queen Mary Department of Materials were always welcoming and helpful when I visited the nanolab to perform my nanoindentation experiments: Aman Bembey, Tanya Ekers, Dr Chris Walker, Tingting Zhu, Dong Hou, Wei Roberts and Dr Ken Mok Yew p'Ng were vital sources of assistance, and tea.

My parents, Dr Alan Doube and Mrs Christie Doube, have been supportive from the beginning, and especially so during this PhD. My brothers and sisters are with me always, thank you all.

Attribution

This work has built upon and utilised the output from several sources. Collaborative assistance has been provided by colleagues in the Global Equine Research Alliance: Prof Elwyn Firth and Dr Chris Rogers at Massey University coordinated much of the original data collection in the GEXA experiment; race training was coordinated by Martin Johnston at Flock House; Dr Chris Kawcak and Professor Wayne McIlwraith at Colorado State University cut the 18-month-old metacarpal sections.

Dr Peter Howell's computer programs 'convert' and 'montage' were used extensively. Dr Virginia Ferguson wrote the Microsoft Excel spreadsheet with which all the UMIS tests were processed. Dr Graham Davis built the MuCat 2 μCT facility and performed the μCT scans.

Michael Doube, December 2007

For the horses

Contents

Appendices

Table List

Supplementary Materials

An electronic copy of this thesis in portable document format (PDF) is included on a CDROM in the inside back cover.

Equation List

Figure List

1: Literature Review

1.1 Introduction

Condylar fracture of the distal third metacarpal bone (Mc3) is the most common cause of racetrack fatality in Thoroughbred racehorses in the UK (Parkin, Clegg, French, Proudman, Riggs, Singer, Webbon and Morgan 2004a), and is a significant cause of lameness during training (Bathe 1994; Verheyen and Wood 2004). Musculoskeletal injuries accounted for the majority (358 / 432) of Thoroughbred fatalities between 1990 and 1992 at racetracks in California, USA, 62 of which were due to Mc3 condylar fracture (Johnson, Stover, Daft, Kinde, Read, Barr, Anderson, Moore, Woods and Stoltz 1994). Lameness was the most common health reason for loss of days in training in the UK (Rossdale, Hopes, Digby and Offord 1985) and New Zealand (Perkins, Reid and Morris 2005b), and the third most common of all reasons for days lost from training in Florida, USA, after the weather (rain) and respiratory disease (Hernandez and Hawkins 2001).

Condylar fracture results in withdrawal of affected horses from racing and training during the rehabilitation period. The economic consequences of fracture include veterinary expense, loss of income during convalescence and reduced likelihood of maintaining earnings once returned to racing (Rick, O'Brien, Pool and Meagher 1983; Zekas, Bramlage, Embertson and Hance 1999b), or euthanasia. Fillies and colts with ongoing lameness or failure to perform may be used for breeding, while geldings have no other use within the racing industry and may be euthanised or leave the industry to another equestrian discipline.

The cost to animal welfare is more difficult to quantify, but it includes pain associated with the acute fracture and that experienced during treatment. Moderate animal welfare groups such as the Royal Society for the Prevention of Cruelty to Animals seek to improve the welfare of racehorses (RSPCA 2006). More aggressive groups such as Animal Aid seek an outright ban on racing (Animal Aid 2006). Making racing safer for equine athletes must be a priority for the racing industry if it is to survive in the current social environment; indeed the UK Jockey Club's marketing catchphrase states that they are "working to promote public confidence in racing" (Jockey Club 2006). The primary responsibility of veterinary surgeons, however, should be not to the public perception of racing, but to the welfare of animals under their care (RCVS 2006; Veterinary Surgeons Act 1966).

1.2 Anatomy of Mc3

1.2.1 Gross Anatomy

The equine Mc3 is a component of the distal thoracic limb. Its proximal articulation is with the distal row of carpals and its distal articulation is with the proximal phalangeal bone (PP) and paired proximal sesamoid bones (PSB). The vestigial 2nd and 4th metacarpals ('splint bones') are attached to Mc3 by the interosseous ligaments on the palmaromedial and palmarolateral Mc3 respectively. The proximal Mc3 surface is approximately flat with facets that accommodate the distal surfaces of the 2nd, 3rd and 4th carpal bones. The distal articular surface of Mc3 is curved

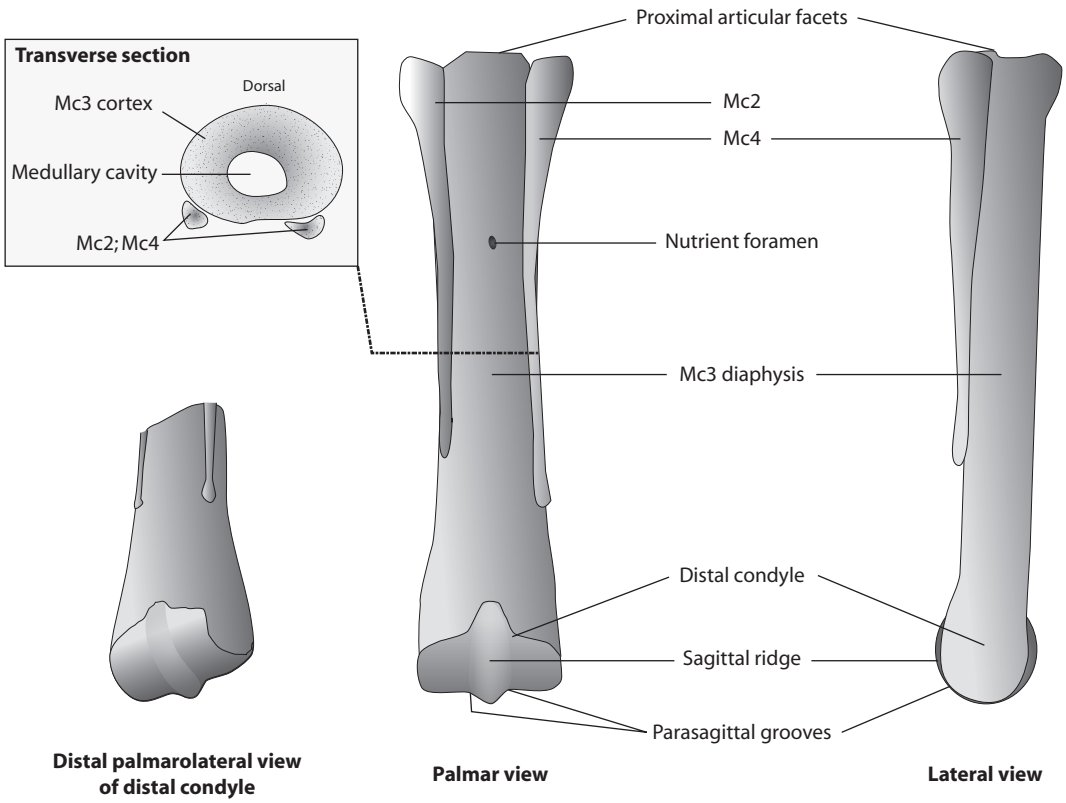

Figure 1-1: Gross Anatomy of Mc3

in the sagittal plane, through approximately 220°. In the frontal plane, the distal condyle is roughly symmetric about its mid-point, from which protrudes the sagittal ridge. The sagittal ridge glides within the central sulcus of PP, preventing axial rotation and lateromedial translation of the joint. A pair of parasagittal grooves flanks the sagittal ridge abaxially. The sagittal ridge and associated parasagittal grooves separate the distal condyle into lateral and medial parts, referred to as the lateral and medial condyles. The paired PSB articulate with the palmar aspect of the distal condyle of Mc3 in the standing horse, separated from each other by the sagittal ridge and the intersesamoidean ligament (Dyce, Sack and Wensing 1996). The diaphysis of Mc3 tapers gently as it rises from the distal metaphysis, then flares to form the proximal articular surface. It takes a generally ovoid cross-section with the long axis oriented mediolaterally. The dorsal surface is strongly convex, while the palmar surface is flatter or slightly concave, to allow free gliding movement of the interosseus tendon (IOT).

The third metatarsal bone (Mt3) is structurally and functionally similar to Mc3, except that its proximal articulation is with the distal row of tarsal bones. There are slight differences in the cross-sectional profiles and condylar shapes between Mc3 and Mt3, with the Mt3 diaphysis more circular in cross section (Richardson 1998) and the condyle somewhat smaller and more angular.

The common digital extensor (CDET) and lateral digital extensor (LDET) tendons run proximo-distally on the dorsal and dorsolateral surfaces of Mc3 (respectively), while the IOT, superficial

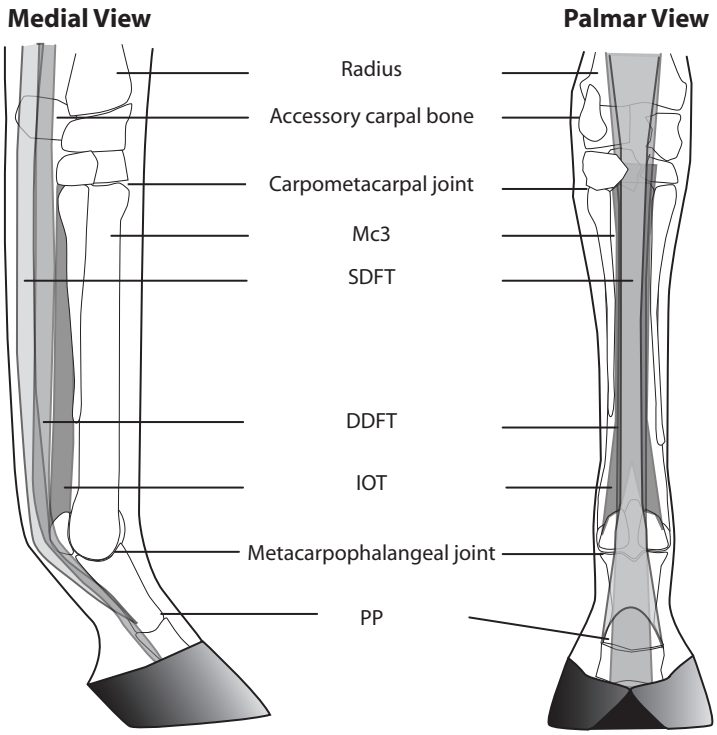

Figure 1-2: Equine Distal Thoracic Limb

digital flexor (SDFT) and deep digital flexor (DDFT) tendons run proximodistally on the palmar surface of Mc3. Palmar and palmar metacarpal arteries and veins accompany the flexor tendon group on their medial and lateral surfaces. A nutrient artery supplies the diaphysis of Mc3 through a nutrient foramen on its palmar surface approximately one third of the bone's length from its proximal extent. A thin covering of fascia and skin is tightly stretched around the distal limb. Skin directly overlies periosteum on the lateral and medial surfaces of Mc3, and those parts of the dorsal surface not covered by CDET or LDET (Dyce, Sack and Wensing 1996).

The fetlock joint is a synovial joint comprising the distal condyle of Mc3, proximal PP, paired PSB and supporting soft tissue structures. The primary articulation is between Mc3 and PP, the metacarpophalangeal joint (MCPJ). Mc3 also forms articulations with the lateral and medial PSB's, which are referred to in this thesis as the lateral and medial metacarposesamoidean joints (MCSJ). Articular surfaces are covered in articular cartilage. Collateral ligaments between Mc3 and PP, and Mc3 and PSB stabilise the fetlock joint against axial rotation and lateromedial flexion.

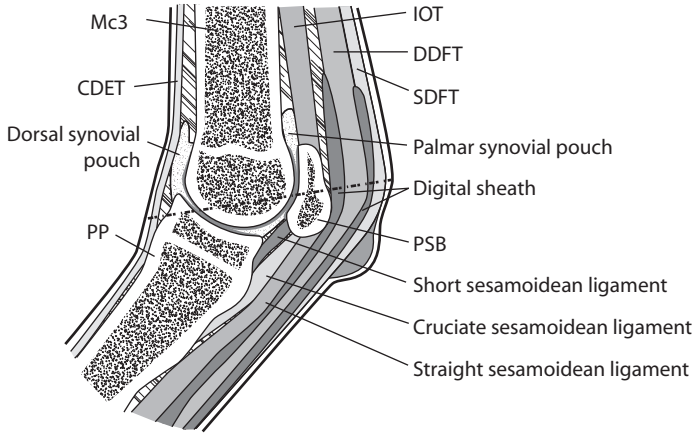

Figure 1-3: Fetlock joint in parasagittal section

Dashed line indicates approximate section plane illustrated in Figure 1-4. After Strand, Martin, Crawford, Kamerling and Burba (1998).

The suspensory apparatus comprises the SDFT, DDFT and IOT. PSB are embedded within medial and lateral branches of IOT, and are anchored to PP by the short, cruciate, oblique and straight sesamoidean ligaments. PSB are joined to each other by the fibrocartilagenous intersesamoidean ligament which passes between their axial borders, and are held in latero-medial position by annular ligaments. The extensor branches of IOT pass abaxially and dorsally from PSB to insert on the CDET as it passes over the dorsal surface of PP (Dyce, Sack and Wensing 1996).

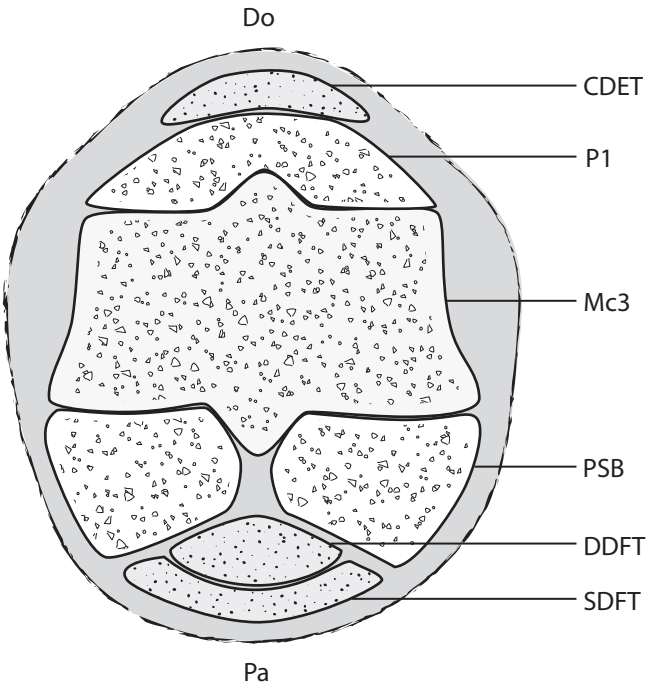

Figure 1-4: Fetlock joint transverse section

Transverse section through the extended fetlock, showing the relative positions of the major bony and tendinous elements. Note the close contact between PP and Mc3, and PSB and Mc3, while the apex of the palmar sagittal ridge of Mc3 has no bony articulation. CDET, common digital extensor tendon; PP, proximal phalangeal bone; Mc3, third metacarpal bone; PSB, proximal sesamoid bone; DDFT, deep digital flexor tendon; SDFT, superficial digital flexor tendon. After Riggs, Whitehouse and Boyde (1999b).

1.2.2 Development and Growth of Mc3

The Mc3 develops in utero by endochondral ossification, as is typical of long bones of the appendicular skeleton (Section 1.6 Endochondral Ossification). Endochondral ossification begins at the nutrient foramen and proceeds proximally and distally. A secondary centre of ossification forms at the distal condyle, but not at the proximal condyle (Krook and Maylin 1988). The majority of growth is complete before parturition; there is a 30% length increase in Mc3 in the final 7 weeks pre-partum but only an 8% length increase between parturition and adulthood (Krook and Maylin 1988) Fig. 9). Post-natal growth of Mc3 largely occurs prior to 2.5 months old in Thoroughbred/Quarter-Horse cross animals, with slight increases in length occurring up to 5 months old. Radiographic closure of the distal growth plate occurs at 7-9.5 months old (mean, 8.6 months old) (Fretz, Cymbaluk and Pharr 1984). Cortical cross-sectional area (Nunamaker, Butterweck and Provost 1989) and mineral density of the Mc3 diaphysis increase rapidly until around 18 months old, reaching a maximum at 4-7 years old (El Shorafa, Feaster and Ott 1979), reflective of maturation of the bone through cortical modelling and remodelling. Longer Mc3 tend to have thicker dorsal cortices as measured by plain radiography, which is thought to be a response to the greater bending moment experienced by longer bones (Davies and Watson 2005). Remodelling of Mc3 during the first 2 years results in a distinctive distribution of collagen fibre orientations that persists in adulthood (Riggs 1990).

Blood vessels run from the distal epiphysis, across the physis to the metaphysis in the growing Mc3 until at least 44 days old but are absent by 70 days old (Firth and Poulos 1982), correlating with the period of maximum post-natal growth (Fretz, Cymbaluk and Pharr 1984). These vessels enter from the entire circumference of the epiphysis and are present in the peripheral physis for a greater duration than in the central physis (Firth and Poulos 1982). As transphyseal vessels recede, vascular perfusion originating from extraosseous vessels maintains blood supply to the metaphyseal region (Firth and Poulos 1983).

1.2.3 Bone Structural Organisation

Bone tissue is comprised of cells and matrix. The organic component of bone matrix is primarily fibrous type-I collagen. The inorganic component is composed of carbonated apatite embedded within and throughout the collagen fibrils. Osteocytes reside within lacunae surrounded by mineralised bone matrix, sending cell processes through canaliculi to neighbouring osteocytes and osteoblasts. Osteoblasts secrete unmineralised bone matrix (osteoid) at the forming bone surface. The orientation and organisation of collagen within osteoid leads to bone being a felt-work of woven bone or more organised lamellar bone, with a common orientation of collagen in each layer.

The trabecular structure of Mc3 is notably anisotropic, with clear regional variation throughout the bone. Subchondral bone at the distal condyle has a high bone volume fraction, particularly in those portions that directly underlie the medial and lateral condyles (Yoshihara, Kaneko, Oikawa, Wada and Tomioka 1989; Firth, Rogers, Doube and Jopson 2005). The epiphyseal trabeculae are arranged as plates in the sagittal plane, which are joined by short transverse struts. Epiphyseal trabecular plates are angled slightly, so that they course proximo-axially. Metaphyseal trabeculae take the counter-course and angle slightly proximo-abaxially (Boyde, Haroon, Jones and Riggs 1999).

Osteoclasts resorb bone tissue by acidic and enzymatic digestion. Removal and replacement of bone with an overall change in bone shape is termed modelling, while the localised resorption and apposition of bone is termed remodelling. Modelling and remodelling result in two main bone structures: cortical bone that forms the shell of tubular long bones and trabecular bone that forms struts and plates within the cortical shell. Remodelling takes place on the cortical or trabecular surface by coordinated patches of osteoclasts and osteoblasts termed basic multicellular units (BMU) (Chenu and Delmas 1998). Remodelling within comapct bone in cortices and in more massive trabeculae is performed by specialised tunnelling osteons that produce channels through which dense bone may receive vascular perfusion (Ross, Romrell and Kaye 1995a).

1.2.4 Osteoblasts

Osteoblasts are the cells that produce bone matrix (osteoid) on bone forming surfaces. They differentiate from osteoprogenitor cells. Woven bone osteoblasts do not use a scaffold in the first instance. Lamellar osteoblasts may use a scaffold other than bone. Osteoid is the

unmineralised, largely proteinaceous substance produced by osteoblasts, comprising type-I collagen, glycosaminoglycans, proteoglycans and water. Woven bone osteoblasts may bud to form matrix vesicles and secrete alkaline phosphatase (ALP) that hydrolyses phosphate esters, leading to increased concentrations of inorganic phosphate that precipitate with calcium to form hydroxyapatite (Chenu and Delmas 1998). Osteoid is progressively mineralised under the control of ALP, matrix Gla protein (MGP) and biglycan. Biglycan is one of the major proteoglycans of bone. Its presence increases the rate of bone matrix mineralisation, by increasing osteoblastic differentiation and response to BMP-4 (Parisuthiman, Mochida, Duarte and Yamauchi 2005) in a sex-dependent manner and may also alter the manner in which mineral interacts with osteoid (Wallace, Rajachar, Chen, Shi, Allen, Bloomfield, Les, Robey, Young and Kohn 2006). Between 10-30 % of osteoblasts on a forming bone surface become encased in mineralised matrix (Franz-Odendaal, Hall and Witten 2006) and are then termed osteocytes.

1.2.5 Osteocytes

Osteocytes are mature bone cells whose primary function is widely considered to be to detect the mechanical environment within bone matrix and direct appropriate modelling or remodelling responses (Lanyon 1987; Klein-Nulend, Bacabac and Mullender 2005; Franz-Odendaal, Hall and Witten 2006). There is a relatively uniform distribution of osteocyte lacunae throughout Mc3, lending evidence to the argument that the number of osteocyte lacunae may not have any functional role in altering bone mechanotransduction pathways (Skedros, Grunander and Hamrick 2005). The primary function of osteocytes may be to down-regulate bone mineralisation (Steendijk and Boyde 1973). This inhibition may conceivably be associated with the more recently discovered osteocytic production of sclerostin which inhibits new bone formation (Poole, van Bezooijen, Loveridge, Hamersma, Papapoulos, Lowik and Reeve 2005). The production of sclerostin is down-regulated by intermittent parathyroid hormone (PTH) (Poole and Reeve 2005), partly accounting for the bone anabolic effects of PTH therapy.

1.2.6 Osteoclasts

Osteoclasts are multinucleate cells that differentiate from haematopoietic precursors under the influence of receptor activator of NF- κB ligand (RANKL) as well as other ligands including vascular endothelial growth factor (VEGF) (Niida, Kondo, Hiratsuka, Hayashi, Amizuka, Noda, Ikeda and Shibuya 2005) and Fas ligand (FasL) (Park, Jung, Park, Lee, Choi and Choi 2005). The primary function of osteoclasts is to resorb mineralised bone matrix, which they do under the influence of osteoblastic RANKL. RANKL may be inactivated by binding to osteoprotegrin (OPG), a diffusible 'dummy receptor' for RANKL also produced by osteoblasts (Kostenuik 2005). Because of the close association between osteoblastic RANKL and OPG production and osteoclast differentiation and activity, bone formation and resorption are often (but not always) seen to be coupled in BMU (Chenu and Delmas 1998). The BMU concept of coupled bone resorption-formation fails to explain rapid bone production without prior resorption that may be seen in horses recently brought into race training (Boyde 2003; Boyde and Firth 2005b) or bone resorption without formation seen in osteoporosis. Bone marrow-derived macrophages

cultured on demineralised bone or uncalcified cartilage do not become multicellular, produce tartrate-resistant acid phosphatase (TRAP) or form resorption pits, unlike those cultured on bone (Suzumoto, Takami and Sasaki 2005), suggesting that osteoclasts may only differentiate and resorb when in contact with mineralised matrices, though they certainly resorb non-mineralised matrices.

1.3 Biomechanics of Mc3 and the Fetlock Joint

1.3.1 Kinematics

Mc3 and Mt3 are loaded primarily in axial compression during the stance phase and experience slight sagittal bending with the dorsal cortex in tension and the volar cortex in compression (Turner, Mills and Gabel 1975; Biewener, Thomason, Goodship and Lanyon 1983; Biewener, Thomason and Lanyon 1988; Gross, McLeod and Rubin 1992). Brief periods of tensile strain have been measured in the Mc3/Mt3 dorsal cortex during the stride cycle, but tensile strains are much less than compressive strains (Davies 2005; Davies 2006). The medial cortex experiences approximately twice the compressive strain of the lateral cortex in young foals, a distribution that is adapted to and maintained after the hoof is made uneven by application of a lateral wedge (Firth, Schamhardt and Hartman 1988).

During galloping, the hoof contacts the ground with the MCPJ at 120º-130º in extension. The joint angle extends to 115º to 100º during mid-stance, then flexes to 180º as the foot leaves the ground and kinetic energy is released from the suspensory apparatus (Butcher and Ashley-Ross 2002). Shear is the dominant loading type during extension, with the majority of compressive load being placed when the MCPJ has reached maximum extension at approximately 110º (Colahan, Piotrowski and Poulos 1988). The disparity in angles at maximum extension reported by Butcher and Ashley Ross, and Colahan et al. may reflect that the former measured MCPJ angles from video images of galloping horses, while the latter used radiographs of dissected limbs held in a testing rig. Under the intense load and rapid forward motion of galloping, the contact between the proximal dorsal rim of PP and dorsal Mc3 condyle (Colahan, Piotrowski and Poulos 1988) might form a fulcrum causing distraction of the MCPJ and further fetlock hyperextension.

The contact area between Mc3 and PSB increases with increasing load, spreading from the parasagittal grooves across the condyles of Mc3 (Colahan, Piotrowski and Poulos 1988), but does not displace appreciably around the Mc3 condyle despite distal rotation of PSB around Mc3 during hyperextension of the digit. Instead, the MCSJ contact surface shifts from the basilar portion to the apical portion of PSB while PP and PSB rotate around the distal condyle of Mc3 (Vilar, Pinedo, Demier, Castejon and Riber 1995). The PSB's rotate only approximately 5º around the Mc3, while PP rotates through 15º (Lawson, Chateau, Pourcelot, Denoix and Crevier-Denoix 2007), implying that substantial strains occur in the distal sesamoidean ligaments. Example photographs of pressure-sensitive films in Colahan et al. (1988) show that when the MCPJ is at 150º (and relatively unloaded), only the axial edges of PSB are in contact with Mc3. During extension at full loading the axial and abaxial portions of PSB are compressed against Mc3 (Colahan, Piotrowski and Poulos

1988). The PSB may therefore rock on their axial borders within the Mc3 parasagittal groove as loading is applied, adding a lateromedial shear component to the axial portions of the MCSJ.

While Brama (1999) made detailed measurements of contact pressure distribution in the MCPJ, he did not report measurements of contact pressures in the MCSJ, nor did he map contact pressures onto the Mc3 articular surface (Brama 1999). Thus, the contact pressure distribution between Mc3 and PSB is unknown, as are any parameters that may influence it. This is of significance to our understanding of condylar fracture because the linear defect thought to precede fracture (Riggs, Whitehouse and Boyde 1999a) is found deep to the contact area between Mc3/Mt3 and the axial border of PSB.

A greater rate of MCPJ hyperextension has been observed in 2-year-olds compared to older Thoroughbred racehorses. The rate of MCPJ hyperextension was found to be independent of gallop velocity. A possible explanation for this observation is that younger horses may have less stiff suspensory apparatuses than older horses (Butcher and Ashley-Ross 2002).

Recent 3D kinematic studies of the MCPJ at the walk and trot indicate substantial individual variation in the degree of abduction-adduction and axial rotation, while flexion-extension is reasonably consistent between animals (Clayton, Sha, Stick and Elvin 2007). Excessive motion out of the sagittal plane may place abnormal stresses within the fetlock joint, possibly leading to more rapid fracture growth in some horses. Further studies are required to investigate the relationship between gait, fetlock joint kinematics and condylar fracture.

1.3.2 Bone Strain

The strain distribution within Mc3 is complex, with compressive, tensile, shear and torsional strains calculated within the same transverse level of the diaphysis (Gross, McLeod and Rubin 1992). Substantial individual variation in Mc3 strain distribution and magnitude results from preferential limb orientation during the stride (Biewener, Thomason, Goodship and Lanyon 1983). Tensile strains are found in the dorsal to dorsomedial cortex of Mc3 and the dorsolateral cortex in Mt3 (Turner, Mills and Gabel 1975) with tension being more pronounced during the swing phase (Gross, McLeod and Rubin 1992). Dorsal cortical tensile strains are an order of magnitude lower than compressive strains and are present over a minority of the stride cycle (Davies 2005). Piotrowski et al. (1983) calculated that the mid-diaphysis of Mc3 is stiffer in mediolateral bending than dorsopalmar bending. Bending stiffness of the distal Mc3 condyle has never been adequately determined. Piotrowski et al. (1983) describe their result as "questionable" (Piotrowski, Sullivan and Colahan 1983) and no further studies have made a serious attempt in this region.

While galloping on a treadmill, strain in the dorsal cortex of Mc3 was found to decrease substantially with age, from -4102 ± 722 μstrain in yearlings to -2530 ± 971 μstrain in 4-8 year-old horses, the negative sign denoting a compressive strain (Davies 1996). Assuming that similar loads were placed on Mc3 throughout life, this result indicates increased stiffness of Mc3 with

age. At low speeds (1-5 $m \cdot s^{-1}$), compressive strain in the Mc3 and Mt3 is proportional to speed (Biewener, Thomason and Lanyon 1983; Biewener, Thomason and Lanyon 1988). Compressive strain in the dorsal cortex of yearling horses' Mc3 was shown to be proportional to speed on a treadmill, ranging from approximately -1000 µstrain at a slow walk (2 $m \cdot s^{-1}$) to -7862 µstrain at a fast gallop (16.5 $m \cdot s^{-1}$; Davies 1994). Bone strain in the equine Mc3 was negatively correlated with diaphyseal cross-sectional area, particularly when the dorsal diaphyseal cortex contained a greater proportion of the total cross-sectional area (Davies 2001). Strain was also negatively correlated with single-photon absorptiometric bone mineral content (Davies 2001), although this method is dubious when used without proper correction for bone shape.

When galloping on the track, bone strains in the dorsal cortex of Mc3 are higher in the outside limb than the inside limb during turns and are higher in the non-lead limb than the lead limb on the straight. As horses tire and become fatigued, Mc3 cortical strains increase by around 20%, particularly when turning (Davies 1996).

1.3.3 Breaking Strength

Variation exists within Mc3 in its stiffness and fatigue resistance, being stiffer in the lateral than the dorsal cortex, but having greater fatigue resistance in the dorsal than the lateral cortex (Gibson, Stover, Martin, Gibeling, Willits, Gustafson and Griffin 1995). Collagen orientation varies within the Mc3 diaphysis (Riggs 1990), which has functional significance since collagen orientation forms a grain resulting in two orders of magnitude difference in fracture energy when crack growth is parallel or perpendicular to the grain (Peterlik, Roschger, Klaushofer and Fratzl 2006). Three-point bending tests on Mc3 demonstrated a rapid increase in breaking strength with age until around 3 years, when the rate of increase slowed. Maximum breaking strength was attained at 6.3 ± 1.2 years old. Breaking strength correlated positively with chemically determined bone mineral content, which peaked at 6.0 ± 1.8 years old (Lawrence, Ott, Miller, Poulos, Piotrowski and Asquith 1994).

Four-point breaking strength was greater in bone from Thoroughbred yearlings fed a high phosphate diet than those fed low and normal levels of phosphate, and was higher in horses fed grain than those fed alfalfa (Leach, Cymbaluk, Hendrix and Williams 1994). Increasing dietary protein and energy to 130% of the 1978 NRC recommendation did not result in significantly altered Mc3 diaphyseal breaking strength (Glade, Luba and Schryver 1986). The Ca:p ratio may affect equine cortical bone stiffness and breaking strength, as Shetland ponies fed with Ca:p ratios of 1.17:1 and 2.45:1 had a statistically non-significant tendency to stiffer and stronger bone than those fed a Ca:p ratio of 1:2 (Schryver 1978). However, like Sherman et al. (1995), these diaphyseal bending models failed to test Mc3 under natural loading conditions, including consideration for axial compression or the bending and compression caused by the action of the suspensory apparatus, PSB and PP on Mc3 (Biewener, Thomason, Goodship and Lanyon 1983). This was demonstrated by Leach et al. (1994), who described 17 of 41 of their test specimens breaking in a simple transverse fracture configuration at the level of the nutrient foramen – a configuration seen clinically

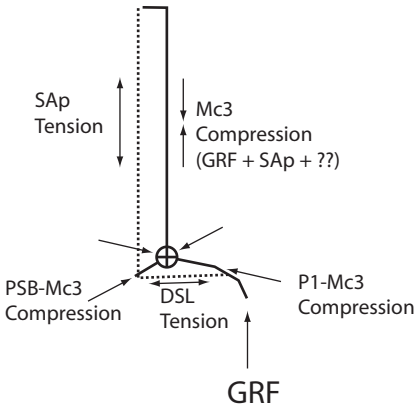

Figure 1-5: Summary of sagittal plane forces acting on Mc3 during the stance phase

This simplified scheme demonstrates the main forces acting on the Mc3 in the sagittal plane. Compression in the Mc3 diaphysis is the sum of the ground reaction force and tension in the suspensory apparatus (SAp). Tension in the distal sesamoidean ligaments (DSL) creates a horizontal component tending to reduce the angle between PP and PSB, and which causes opposing forces as they act on either side on the Mc3 condyle. If the horizontal components acting on Mc3 from the PSB and PP are unbalanced, a net horizontal (dorsopalmar) force will act on the distal condyle. Vertical components of the compression vectors from PSB and PP sum to increase Mc3 compression. GRF, ground reaction force.

in fewer than 5 per 1000 spontaneous Mc3/Mt3 fractures (McClure, Watkins, Glickman, Hawkins and Glickman 1998).

Generating fatigue in Mc3 by 3-point bending reduced monotonic failure load by 3%, but the authors considered this to be biologically insubstantial (Martin, Gibson, Stover, Gibeling and Griffin 1997), suggesting that an alternative cause of weakening in Mc3 is the normal fatigue repair process. Again, Mc3 was not loaded normally, making the result of this study doubtful at best.

Breaking strength of diaphyseal segments of Mc3 has been correlated to quantitative ultrasound (QUS) speed of sound (SOS). SOS increased rapidly from 50 days old to about 1 year old, and then showed a slight increase in SOS until 18 months old indicating that Mc3 diaphyseal breaking strength increases rapidly over the first year of life (Glade, Luba and Schryver 1986). This was corroborated by El Shorafa et al. (1979), who demonstrated a rapid increase in Mc3 breaking strength between 8 months old and 12 months old, reaching a maximum at 4-7 years old (El Shorafa, Feaster and Ott 1979). It must be noted that the breaking strength of the distal condyle of Mc3 has never been determined, despite its obvious relevance to sagittal condylar fracture.

1.4 Bone Mechanobiology

1.4.1 Paradigms

Bone is thought to model and remodel in order to produce a mechanically optimal structure that is strong enough to withstand normal loads and as light as possible to minimise the energy required for locomotion (Klein-Nulend, Bacabac and Mullender 2005). Work published by the anatomist von Meyer in 1867 (von Meyer 1867) inspired Culmann (an engineer) to propose that bone trabeculae in the human femoral head followed stress trajectories. Roux published the hypothesis that trabecular bone architecture is guided by mechanical load and regulated by cells in 1881 (Roux 1881). Wolff popularised the notion in 1892 in the oft-cited *Das Gesetz der Transformation der Knochen* (Wolff 1892), which he wrote as sole author because Roux rejected his offer of a co-authorship. Wolff's Law is the questionably-named legacy (Mow and Huiskes 2005). Experimental support for trabeculae being oriented parallel to tensile and compressive stresses was found in an in vivo experiment in which rosette strain gauges were glued to ovine calcanei. Trabeculae in the calcanei were found to be parallel to measured strain (Lanyon 1974).

Through the latter quarter of the 20th century, Frost and collaborators made extensive investigations into the regulation of bone turnover and remodelling, which culminated in the mechanostat theory of bone (Frost 1987; Frost 1996; Frost 2003). Briefly, mechanostat theory states that bone under load must resist a given strain, but to do so it must experience that strain. If the strain is insufficient, tissue is removed so that the same load produces more strain until the desired strain is achieved. If too much strain is experienced, for example due to increased body mass or exercise intensity, bone tissue is produced to resist the load, which reduces strain to the optimal value (Frost 1996; Frost 2003). Rubin and Lanyon provided the impetus for the mechanostat concept with their 1985 experiment that demonstrated increased bone deposition with increased peak strain, and net bone resorption when peak strain was less than 1 με (Rubin and Lanyon 1985).

The dual negative feedback system of the mechanostat theory results in the mechanical homeostasis of bone. Dual negative feedback loops are common physiological motifs, exemplified by the calcitonin-parathyroid hormone loop that maintains plasma calcium homeostasis and the insulin-glucagon loop that maintains plasma glucose homeostasis. The mechanostat theory does not propose the actual mechanisms by which load is sensed, information transmitted or changes in bone architecture made, rather it is a framework within which these functions may be understood. As such, it is likely to require revision as new discoveries of bone cell, tissue and organ function arise; for example it was recently shown that the mechanostat set-point is not absolute, but itself adapts to applied load (Schriefer, Warden, Saxon, Robling and Turner 2005), a suspicion that was raised in the 1980's (Lanyon 1987).

1.4.2 Bone Responses in Adult Horses

Trotting exercise (3.6 $m \cdot s^{-1}$, increasing distance with age, 5 days per week) was reported to be associated with increased rate of gain in Mc3 circumference but not absolute Mc3 circumference in

weanling horses (Raub, Jackson and Baker 1989), although this study contained a methodological flaw by the inclusion of all of the soft tissues of the digit in the Mc3 circumference measurement. Raub et al. (1989) also reported no change in bone density of Mc3 as determined by radiographic photometry using plain radiographs with an aluminium step-wedge imaged simultaneously as a reference standard (Raub, Jackson and Baker 1989). Radiographic photometry is a crude technique that would have been unable to resolve subtle changes in Mc3 volumetric bone mineral density (vBMD) (McCarthy and Jeffcott 1992), so the results of this study are questionable. No lameness or bone abnormalities were caused by the trotting exercise regime so it was considered to be safe (Raub, Jackson and Baker 1989).

Nine weeks of trotting and cantering exercise (< 12 $m \bullet s^{-1}$) followed by 5 weeks of galloping (12-14.5 $m \bullet s^{-1}$) exercise on a treadmill was associated with marked changes in Mc3 in 6 Thoroughbred horses (13-14 months old). Mid-diaphyseal transverse sections showed reduced porosity, reduced percentage of active intracortical bone surface, reduced osteoclast number, increased subperiosteal osteogenesis, increased vBMD and increased cortical bone area in exercised horses (McCarthy and Jeffcott 1992). McCarthy and Jeffcott (1992) suggested that gallop exercise was the specific stimulus that caused the changes in Mc3 diaphyseal cross-section. Similar changes were found in 18- to 24-month-old horses in response to gallop exercise (14.6 $m \bullet s^{-1}$) on turf (Firth, Rogers, Doube and Jopson 2005).

Maximum workout speed was positively correlated to an increased proportion of bone in the dorsal cortex of mid-diaphyseal Mc3 compared to medullary diameter, for speeds between 6 $m \bullet s^{-1}$ to 18 $m \bullet s^{-1}$ (Davies, Gale and Baker 1999). Sherman et al. (1995) demonstrated an increased cortical cross-sectional area, area moment of inertia and diaphyseal diameter with increased months in training in 24- to 48-month-old Thoroughbred racehorses' right Mc3. No change in breaking strength was found under 3-point bending (Sherman, Miller, Wronski, Colahan, Brown and Wilson 1995), but this may be due to the highly artificial load applied during testing compared to that experienced in vivo (Biewener, Thomason, Goodship and Lanyon 1983).

Yoshihara et al. (1989) noted substantial changes in digitised radiographs of trabeculae in the Mc3 condyle associated with age and physical exercise. They suggested that physical exercise results in "hypertrophy and hyperplasia" of the trabeculae, while ageing results in reorganisation and sclerosis of the condylar subchondral bone (Yoshihara, Kaneko, Oikawa, Wada and Tomioka 1989). An earlier study had indicated a positive correlation between Mc3 condylar subchondral bone vBMD and number of races run, age at last race and career length (Tomioka, Kaneko, Oikawa, Kanemaru, Yoshihara and Wada 1985).

Controlled training exercise designed to emulate typical New Zealand race preparation was associated with a number of changes in 2-year-old Thoroughbred Mc3 and Mt3 (Firth, Rogers, Doube and Jopson 2005). Peripheral quantitative computed tomography (pQCT) was used to measure vBMD, which was increased in subchondral bone (+37%) and epiphyseal bone (+14%)

of the distal Mc3. There was a tendency for subchondral bone in the medial Mc3 condyle to have higher vBMD than subchondral bone in the lateral Mc3 condyle; a tendency that was more significant in the right Mc3 than the left Mc3 and that was accentuated by exercise. Subchondral bone in the lateral Mt3 condyle had greater vBMD than in the medial Mt3 condyle, an effect that was accentuated by exercise (Firth, Rogers, Doube and Jopson 2005). Mc3 and Mt3 cortical vBMD were raised in 2-year-old Thoroughbred horses due to bone apposition within osteons during canter and gallop exercise. Cortical cross-sectional area was increased in horses that had been galloped. Osteonal, subperiosteal and subendosteal LAR increased with increased distance galloped (Firth, Rogers, Doube and Jopson 2005). Mc3 appears to respond to moderate exercise by infilling osteonal canals, while intense exercise results in increased cortical cross-sectional area.

Mc3 from Quarter-horses in race-training showed a decline in radiographic bone aluminium equivalence (RBAE) by radiographic photogrammetry that reached a nadir on day 60 of training. RBAE then increased for the remainder of the study period (250 days) but did not reach the RBAE measured at entry to the study (Nielsen, Potter, Morris, Odom, Senor, Reynolds, Smith and Martin 1997). Since RBAE is determined from plain radiographs, it cannot capture changes in the cross-sectional profile of the bone under study, and changes in cortical thickness will interfere with measures of bone density.

Increased cortical bone stiffness but no increase in bone mineral content, BMD or compact bone density was found in a study on 6 Standardbred horses (McCarthy and Jeffcott 1988). Shetland ponies given 16 km trotting (2.22 $m \bullet s^{-1}$) exercise per day from 14 months old to 18 months old had increased Mc3 cortical bone stiffness and ultimate breaking strength, an effect that was dependent on the diaphyseal quadrant from which each test specimen was cut. The medial quadrant was stiffest, followed by the cranial, lateral and caudal quadrants in declining order (Schryver 1978). The increased apparent bone density observed by plain radiography and pQCT in trained 2-year-old horses can be explained as the result of increased bone volume fraction (Boyde and Firth 2005b). Training exercise in young Dutch Warmblood horses caused a site-specific increase in type-I collagen cross linking, and increased calcium deposition in the subchondral bone of PP. The intermittently loaded region at the PP dorsal margin contained more calcium and type-I collagen cross links (Brama, Bank, Tekoppele and Van Weeren 2001).

1.4.3 Bone Responses in the Growing Animal

Physical activity is required for foals to attain maximum bone strength during growth. Stalling Arabian weanlings without access to exercise prevented maximal mineral deposition in Mc3, while those given 12 hours or less ad-hoc exercise at pasture had greater bone mineral density (Bell, Nielsen, Waite, Rosenstein and Orth 2001). Cornelissen et al. (1999) found that Warmblood foals given daily access to pasture had greater Mc3 diaphyseal cross-sectional area than those kept in boxes, or boxed and galloped at 5 months old but not at 11 months old (Cornelissen, van Weeren, Ederveen and Barneveld 1999). They also found that gallop exercise superimposed on

box confinement led to increased vBMD of trabecular bone in the apical PSB at 5 months old but not at 11 months old (Cornelissen, van Weeren, Ederveen and Barneveld 1999). Interestingly, they found that boxed foals had higher vBMD in the dorsal Mc3 cortex than boxed and sprinted, and pasture exercised horses at 5 months old, but not at 11 months old (Cornelissen, van Weeren, Ederveen and Barneveld 1999). These apparent reductions in vBMD occurred during the period in which Mc3 has ceased increasing in length (Fretz, Cymbaluk and Pharr 1984), so may be representative of secondary osteonal remodelling in the young adult bone.

Treadmill exercise in young horses (trot, canter and gallop at 3° incline) led to increased cortical bone stiffness, subperiosteal bone deposition and reduced bone remodelling compared to controls, although which gait caused the changes was not determined (McCarthy and Jeffcott 1992). No change in vBMD was seen in distal Mc3 subchondral bone taken from 18-month-old Thoroughbred horses given preconditioning exercise from 10 days old, although a distinct site-dependent effect on vBMD within the Mc3 was noted (Dykgraaf 2003).

1.5 Articular Cartilage

1.5.1 Tissue Structure

Articular cartilage is composed of chondrocytes embedded in specialised extracellular matrix. It may be thought of as the hyaline cartilage that escaped endochondral ossification at the articular growth plate. Chondrocytes produce and maintain cartilage matrix, which is mostly water, followed by type-II collagen and proteoglycans. Articular cartilage may be categorised into 4 zones; tangential, middle, deep and calcified based on tissue composition and arrangement (Figure 1-6: Osteochondral organisation). The mineralising front (tidemark) is the boundary between the hypertrophic and calcified zone, at which matrix water is replaced with an impure, carbonate-containing hydroxyapatite composite mineral. Articular calcified cartilage (ACC) provides the mechanical link between pliant hyaline cartilage and stiff subchondral bone. Its thickness is increased by progression of the mineralising front and decreased by endochondral ossification at the osteochondral junction (Ross, Romrell and Kaye 1995b; Mow, Gu and Chen 2005).

1.5.2 Cartilage Biomechanics

Articular cartilage serves dual functions – to evenly disperse and transmit loads on joints from one bone to the other, and to reduce friction between the two bones. In the first function, cartilage is aided by the large amount of water it contains tightly bound to proteoglycans, which are enmeshed and constrained by a regular collagen fibre network. This results in a structure that resists compression and deformation. Friction is reduced by cartilage interacting with synovial fluid during loading. A layer of synovial fluid lubricates the two cartilage surfaces (Mow, Gu and Chen 2005).

Cartilage is biomechanically heterogeneous. The collagen network is oriented perpendicular to the articular surface in the deep layers and tangential to the articular surface in the superficial layer (Hunziker, Herrmann, Schenk, Mueller and Moor 1984). This gives greater resistance to

shear at the articular surface. The stiffness of articular cartilage varies across the distal condyle of Mc3, with that in the parasagittal groove having lower stiffness than elsewhere on the condyle (Nugent, Law, Wong, Temple, Bae, Chen, Kawcak and Sah 2004). On a finer scale, hyaline cartilage interterrtorial matrix is stiffer than pericellular matrix when measured by nanoindentation (Allen and Mao 2004).

Abrupt transitions in mechanical properties occur at the mineralising front and at the osteochondral junction (Mow, Gu and Chen 2005). Shear forces cause articular cartilage to fracture along the mineralising front in mature bovine patellae (5 to 7 years old), but failure occurs through ACC directly above the osteochondral junction in immature tissue (2 to 3 years old) (Broom, Oloyede, Flachsmann and Hows 1996). This may be due to increased resilience of ACC, or a more organised mineralising front causing stress concentration and collagen fibre tearing in older animals. The elastic modulus of ACC was found to be an order of magnitude less than that of subchondral bone when pure subchondral bone and composite ACC-subchondral bone beams were tested under 3-point bending (Mente and Lewis 1994). However, ACC and subchondral bone had similar nanoindentation moduli (Ferguson, Bushby and Boyde 2003), indicating either a methodological flaw in Mente and Lewis (1994) or that the tissue-level organisation of ACC substantially affected Mente and Lewis' result. Stiffness could be less in ACC than subchondral bone because of its lower collagen volume fraction and/or the different collagen orientations of the two tissues; collagen in ACC is radially arranged and minimally interwoven whereas subchondral bone collagen in laid down in all directions in both lamellar and woven forms, giving subchondral bone much a much greater ability to prevent crack propagation.

1.5.3 Cartilage Mechanobiology

Oikawa et al. (1989) found that articular cartilage at the distal Mc3 reduces in thickness by half to two thirds between birth and 24 months old (Oikawa, Yoshihara and Kaneko 1989). Cartilage thickness was similar at all sites before 1 month old, but by 24 months old, a distinct heterogeneity had emerged. Regions within the MCPJ and MCSJ that experience high mechanical load had thinner articular cartilage than sites at the transverse ridge (Oikawa, Yoshihara and Kaneko 1989). The authors suggested that this was due to endochondral ossification. Cartilage thickness was measured on polyester-embedded undecalcified sections, a process that involves the removal of all tissue water by alcoholic substitution. Because articular cartilage is mostly water (65-73% for Mc3), and the water content of Mc3 articular cartilage shows regional variation (Brama, Tekoppele, Bank, Karssenberg, Barneveld and van Weeren 2000) that develops with age (Brama, Tekoppele, Bank, Barneveld and van Weeren 2000), the results of Oikawa et al. (1989) must be interpreted with caution. Some of the variation in thickness measured by Oikawa et al. (1989) could have been variable shrinkage artefact due to a change in water content rather than a true change in live cartilage thickness.

Strenuous treadmill exercise (19 weeks, 7-14 $m \bullet s^{-1}$) was related to increased ACC thickness in 18- to 21-month-old equine carpi, but no increase in hyaline cartilage thickness was seen (Murray,

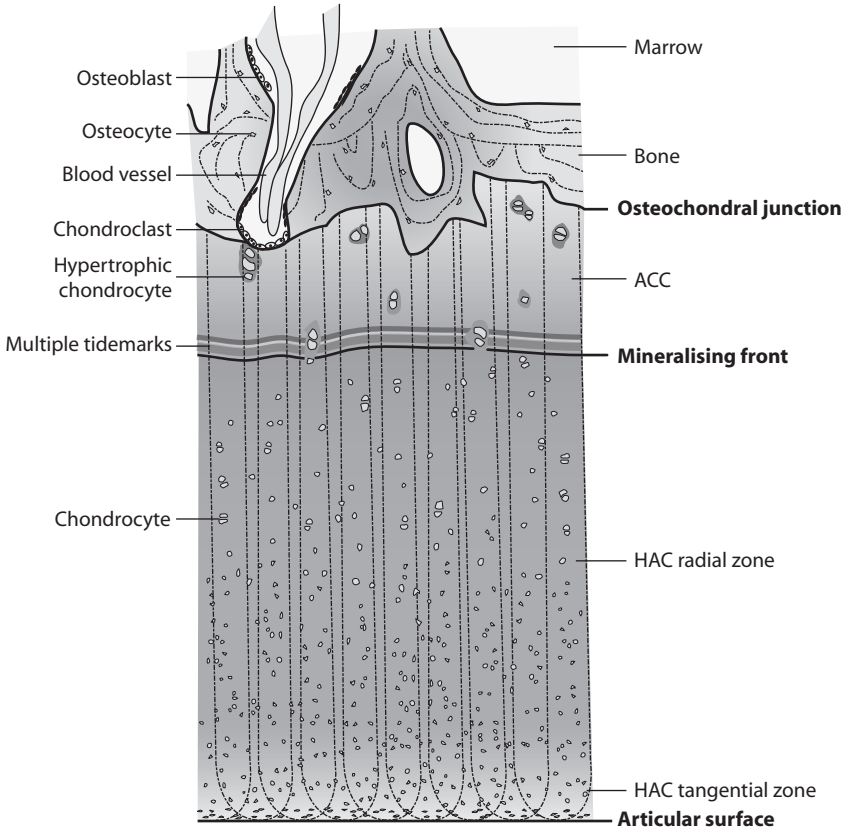

Figure 1-6: Osteochondral Organisation

Organisation of articular cartilage and subchondral bone. Bone and articular cartilage are intimately related at the osteochondral junction, where chondroclasts invade ACC. The vascular marrow space so formed is gradually filled with bone by osteoblasts, which are then buried in bone matrix and named osteocytes. ACC thickness increases as the mineralising front progresses into HAC and decreases as chondroclasts invade ACC at the osteochondral junction. Variation in mineralisation density as the mineralising front progresses results in multiple tidemarks. Dashed lines indicate collagen fibre orientation; note that cartilage collagen fibres pass through the ACC mineralising front and terminate at the osteochondral junction.

Whitton, Vedi, Goodship and Lekeux 1999). Dorsal sites were more affected by exercise and showed a greater increase in thickness than palmar sites, possibly because the dorsal articular surfaces experience higher strain than palmar articular surfaces. Murray et al. (1999) reach the conclusion that greater ACC thickness was due to increased ACC mineralising front advancement (linear accretion rate, LAR), however they did not directly measure LAR. The minimal change in hyaline cartilage thickness and increase in total cartilage thickness that was fully accounted for by increased ACC thickness suggests not increased ACC LAR, but decreased chondroclastic resorption. Further, Murray et al. (1999) measured hyaline cartilage thickness on paraffin embedded specimens, exposing the tissue to severe dehydration artefact and rendering the measurements of limited relevance to the hydrated state of live cartilage.

Martinelli et al. (2002) found age- and site-related variation in ACC thickness in sections taken in the sagittal plane from the medial parasagittal groove of Mc3. Horses younger than 5 years

had thinner ACC than those older than 5 years, while the main weight-bearing surfaces of the mid-palmar, mid-dorsal and dorsoproximal condyle had thicker ACC than the transverse ridge and palmaroproximal sites (Martinelli, Eurell, Les, Fyhrie and Bennett 2002). Interestingly, the authors note that the osteochondral border became less irregular with age (Martinelli, Eurell, Les, Fyhrie and Bennett 2002), indicating regular procession of the mineralising front and declining endochondral ossification with age.

ACC endochondral ossification and the ACC mineralising front may differ in response to shear and compression loading modes. Rats that had the majority of compressive loading removed from their femoro-tibial joints showed twice the ACC LAR of control rats, while those with neither compressive nor shear loading had similar ACC LAR to controls but increased endochondral ossification (O'Connor 1997). The cranial femoral condyle (which is not normally weight-bearing) experienced greater changes in ACC LAR than the weight-bearing caudal femoral condyle during hind limb unweighting. This observation may be due to the alteration in femoro-tibial joint angle that resulted from unweighting leading to contact between the cranial femoral condyle with the tibial plateau while the caudal femoral condyle was left in a non-contact position (O'Connor 1997). While O'Connor (1997) demonstrated independent responses of ACC endochondral ossification and ACC mineralising front to different loading modes, the altered joint position from normal in the experimental groups makes their results difficult to interpret, as the effect of altered joint position cannot be separated from the experimental loading conditions.

No difference in ACC thickness was found between the dorsal and palmar regions of the medial Mc3 condyle in 2- to 5-year-old horses (Norrdin, Kawcak, Capwell and McIlwraith 1999). Very few measurements were taken from each condyle, using an integration technique that cannot reflect the variation in ACC thickness present in each site. Norrdin et al. (1999) found that the number of invading osteochondral vessels was decreased in the distopalmar condyle and that ACC was thin in this region (Norrdin, Kawcak, Capwell and McIlwraith 1999) suggesting reduced ACC LAR.

Preconditioning exercise increased numbers of viable chondrocytes compared to rested horses, as determined by confocal scanning light microscopy (CSLM) on calcein AM / propidium iodide stained fresh cartilage explants from fetlock joints. Explants were taken from the mid-condyle in dorsal and palmar positions (Dykgraaf 2003). Impact loading may cause chondrocyte necrosis or apoptosis (Borrelli and Ricci 2004). High impact loads increase numbers of apoptotic cells in cartilage explants (Borrelli, Tinsley, Ricci, Burns, Karl and Hotchkiss 2003). Single applied loads as high as 45% of the joint fracture threshold do not cause significant cartilage disruption or degradation, although a loss of proteoglycan staining was noted in impacted cartilage (Borrelli, Zhu, Burns, Sandell and Silva 2004). Chondrocytes undergo apoptosis in a unique fashion, termed chondroptosis, with fewer apoptotic bodies than in classical apoptosis, and with autophagy and self-digestion rather than phagocytosis terminating the process (Roach, Aigner and Kouri 2004). The Golgi body is seen to expand during chondroptosis in osteoarthritic cartilage (Perez, Luna, Rojas and Kouri 2005). In addition, many chondrocytes may not die, but dedifferentiate, mitose and redifferentiate as osteoblasts (Bianco, Cancedda, Riminucci and Cancedda 1998).

Spatial variations are seen in the ultrastructural properties of distal Mc3 condylar articular cartilage. Collagen orientation was shown to vary with dorso-palmar position by small-angle X-ray scattering and may relate to stress distribution (Moger, Barrett, Bleuet, Bradley, Ellis, Green, Knapp, Muthuvelu and Winlove 2007). The parasagittal groove of 18-month-old Thoroughbred Mc3 contains thicker and less stiff articular cartilage with a lower reflectance score (indicative of less surface wear), higher water content and lower DNA content than the abaxial condylar surfaces. Cartilage from sites dorsal to the frontal plane was different to cartilage from sites palmar to the frontal plane, with increased thickness, lower reflection score, reduced stiffness, increased water content, lower glycosaminoglycan content, and increased DNA content seen in the palmar cartilage (Nugent, Law, Wong, Temple, Bae, Chen, Kawcak and Sah 2004). Reflectance scores use India ink adsorption to fibrillated cartilage surfaces as a marker of surface wear; however, Nugent et al. (2004) did not attempt to correct for differences in reflectance due to macroscopic condylar topography. Their example image shows specular reflective highlights on the sagittal ridge. Unlike other studies, Nugent et al. (2004) measured cartilage thickness on images of the cut surface of fresh cartilage rather than on processed histological sections, making their measurement of cartilage thickness more realistic than others (Nugent, Law, Wong, Temple, Bae, Chen, Kawcak and Sah 2004).

The proximal articular surface of PP is the primary mating surface for the dorsal aspect of the Mc3 distal condyle. Spatial variations in cartilage biomechanical characteristics develop in the cartilage of growing horses. Late-fetal horses have no variation in biomechanical characteristics within the proximal articular cartilage of PP. By 18 months, significant regional heterogeneity in Young's modulus and dynamic modulus develops within PP articular cartilage (Brommer, Brama, Laasanen, Helminen, van Weeren and Jurvelin 2005), evidence of functional adaptation of equine cartilage during growth. Further evidence for functional adaptation of articular cartilage is that regional variation in articular cartilage biochemical characteristics (DNA, glycosaminoglycan, collagen and hydroxyproline concentrations) develops during the first year of life from a biochemically homogenous cartilage (Brama, Tekoppele, Bank, van Weeren and Barneveld 1999b; Brama, Tekoppele, Bank, Karssenberg, Barneveld and van Weeren 2000).

Preconditioning exercise had a significant effect on hyaline articular cartilage (HAC) thickness in the dorsal but not the palmar distal condyle of Mc3/Mt3 in 12 18-month-old Thoroughbred horses. The same study demonstrated no effect of exercise on chondrocyte density measured by 3D CSLM on fresh cartilage explants, but an increased chondrocyte density in the palmar site compared to the dorsal site. Preconditioning exercise was associated with a 14% increase in the proportion of viable chondrocytes over all sites, the dorsal site seemingly more affected, with a 34% greater proportion of viable cells with preconditioning. The palmar site, which is under constant high load, had a 16% higher proportion of viable chondrocytes than the dorsal site, irrespective of treatment group. There was a tendency for non-viable chondrocytes to be found in the superficial and intermediate zones, rather than the deep zone (Dykgraaf 2003).

DNA content (ng•mg^{-1} wet weight) of cartilage from the tarsus and femoropatellar joints was less in trained and pasture exercised 5-month-old Warmblood foals than box-stalled foals, a difference that was maintained after 6 months break from training (van den Hoogen, van de Lest, van Weeren, van Golde and Barneveld 1999). This result indicates that exercise is associated with a greater quantity of ECM produced per chondrocyte. DNA content alone cannot indicate overall cellularity, as both viable and non-viable cells will contribute to DNA content.

Preconditioning exercise superimposed on ad-libitum exercise of Thoroughbred foals raised at pasture was found to have no effect on cartilage thickness, stiffness, reflectance score (again used as a measure of cartilage surface wear), water content, DNA content, glycosaminoglycan content or collagen hydroxyproline cross-linking (Nugent, Law, Wong, Temple, Bae, Chen, Kawcak and Sah 2004). The significance of this finding is that preconditioning exercise from 10 days old to 18 months old had no deleterious effects on cartilage beyond what was caused by the foals' normal behaviour.

Proteoglycan synthesis in adult fetlock cartilage increased as a result of a 19-week treadmill training regime, although the measured increases did not consistently meet the $p < 0.05$ criterion for satisfying statistical significance (Bird, Platt, Wells, May and Bayliss 2000). Five-month-old Warmblood foals raised in box stalls synthesised less articular cartilage proteoglycan than those given sprint training, but the difference was not seen in 11-month-old horses after the trained group had 6 months of rest (van den Hoogen, van de Lest, van Weeren, van Golde and Barneveld 1999).

1.6 Endochondral Ossification

1.6.1 Cartilage Anlagen

Endochondral ossification is the developmental process whereby cartilage models (anlagen) are replaced by bone during embryonic development and post-natal growth (Ross, Romrell and Kaye 1995a; Ballock and O'Keefe 2003; Kronenberg 2003). Embryonic cartilage anlagen are formed through condensations of mesenchymal cells, which proliferate and differentiate into chondrocytes (Figure 1-7, i-iii). Chondrocytes then undergo an orderly sequence of proliferation, maturation and hypertrophy (Figure 1-7, iv) under the influence of bone morphogenetic protein (BMP) (Anderson, Hodges, Aguilera, Missana and Moylan 2000), fibroblast growth factor (FGF) Indian hedgehog (Ihh) and parathyroid hormone related peptide (PTHrP) signalling (Kronenberg 2003). PTH/PTHrP stimulates the development of the hypertrophic chondrocyte phenotype (Bahrami, Plate, Dreier, DuChesne, Willital and Bruckner 2001).

The transcription factor core binding factor α1 (Cbfa1/Runx2, runt-related gene 2) is expressed by prehypertrophic and hypertrophic chondrocytes prior to cartilage mineralisation (Choi, Lee, Park, Bae, Shin, Nam, Kim, Kim and Ryoo 2002; Kuboki, Kanyama, Nakanishi, Akiyama, Nawachi, Yatani, Yamashita, Takano-Yamamoto and Takigawa 2003) and is essential for endochondral ossification. Cbfa1 expression has been seen in the articular surface of epiphyseal cartilage in the stifle

joints of normal 3-week-old mice but not in 10-week-old mice, while it is strongly expressed in hypertrophic chondrocytes deep to the articulating layer of cartilage (Kuboki, Kanyama, Nakanishi, Akiyama, Nawachi, Yatani, Yamashita, Takano-Yamamoto and Takigawa 2003). Cbfa1 may be a central control for the promotion of endochondral ossification of HAC and growth cartilages, and absence of Cbfa1 expression may be essential for the prevention of endochondral ossification of adult articular cartilage.

High mobility group box 1 protein (HMGB1) is a nuclear factor that also has a role as a secreted chemoattractant cytokine. It is expressed in the cytosol of hypertrophic chondrocytes but not resting or proliferating chondrocytes. HMGB1 knockout mice showed delayed chondroclastic and vascular invasion of growth plates, in part due to reduced recruitment of TRAP-staining (Taniguchi, Yoshida, Ito, Tsuda, Mishima, Furumatsu, Ronfani, Abeyama, Kawahara, Komiya, Maruyama, Lotz, Bianchi and Asahara 2007).

1.6.2 Cartilage Mineralisation

Hypertrophic chondrocytes in growth plate cartilage bud to produce matrix vesicles (Anderson 1969; Hwang, Cameron, Robinson, Cameron and Robinson 1978; Bullough and Jagannath 1983) that initialise cartilage mineralisation (Kirsch, Wang and Pfander 2003; Kirsch 2006). Vesicle-bound alkaline phosphatase (ALP) (Roach 1999; Kirsch 2006) hydrolyses inorganic pyrophosphate (PPi) to phosphate (Pi) outside the vesicle. Annexins and Na+/phosphate channel proteins modulate Ca++ and Pi transport into the vesicle lumen, where initial mineralisation occurs (Kirsch 2006). ALP hydrolysis of PPi outside the vesicle causes further matrix mineralisation. Trueta and Morgan demonstrated that hypertrophic chondrocytes produce ALP and that the physeal cartilage matrix mineralises when in close proximity (though still several hypertrophic chondrocyte diameters away) to invading capillary loops (Trueta and Morgan 1960). ALP expression is associated with progression of endochondral ossification (Bahrami, Plate, Dreier, DuChesne, Willital and Bruckner 2001). Physeal matrix vesicles are associated with MMP-2, -9, and -13 and contain TGF-β. MMP-2 and -9 are integral to matrix vesicles, while MMP-13 is peripheral. MMP-13 activates latent TGF-β (D'Angelo, Billings, Pacifici, Leboy and Kirsch 2001).

Calcification at the mineralising front of articular cartilage takes the form of multiple, tiny spherules, however these particles occur in much greater density and are smaller than calcospherites associated with matrix vesicles in the growth plate. Thus articular cartilage mineralisation occurs without matrix vesicle formation (Boyde and Jones 1983). Articular cartilage mineralisation proceeds as a front that can be labelled with fluorescent markers such as tetracycline (Lemperg 1971; Revell, Pirie, Amir, Rashad and Walker 1990).

Bone-marrow derived macrophages fail to differentiate into osteoclasts and do not form resorption lacunae when cultured on hyaline cartilage or demineralised bone (Suzumoto, Takami and Sasaki 2005), but differentiated osteoclasts do not stop resorbing when they contact a non-mineralised tissue matrix (Jones, Boyde and Ali 1986). Chondrocytes are alive and usually not apoptotic as they

are enclosed by the mineralising front. Hunziker et al. (1984) found by TEM that chondrocytes in mineralising epiphyseal cartilage had a morphology typical of live cells and suggested that they may directly control cartilage mineralisation (Hunziker, Herrmann, Schenk, Mueller and Moor 1984). Further TEM micrographs demonstrated that hypertrophic chondrocytes at the mineralising front in adult lapine articular cartilage are non-degenerate even as they are being enveloped by the advancing mineralisation front (Eggli, Hunziker and Schenk 1988). Cultured avian chondrocytes mineralise extracellular matrix in a normal fashion when apoptosis is retarded; when chondrocyte apoptosis is stimulated, matrix mineralisation is reduced and aberrant (Pourmand, Binderman, Doty, Kudryashov and Boskey 2007).

Cartilage ECM concentrations of aggrecan, hyaluronic acid and the C-terminal propeptide of type-II collagen are maximal just before mineralisation, while a rapid decrease in total ECM collagen occurs (Alini, Matsui, Dodge and Poole 1992). The type-II collagen triple helix unwinds as a result of enzymatic digestion (Alini, Matsui, Dodge and Poole 1992), and hypertrophic chondrocytes produce type-X collagen immediately prior to cartilage mineralisation (Gannon, Walker, Fischer, Carpenter, Thompson and Oegema 1991; Claassen and Kirsch 1994; Bai, Lu and Bai 1995; Walker, Fischer, Gannon, Thompson and Oegema 1995).

Vascular invasion of the hypertrophic zone is stimulated by the production of VEGF by hypertrophic chondrocytes. Vascular invasion may be followed by chondrocyte apoptosis (Kronenberg 2003), although chondrocytes are often alive and functional when contacted by invading vasculature (Hunziker, Herrmann, Schenk, Mueller and Moor 1984). Apoptosis is not the only fate for hypertrophic chondrocytes (Boyde and Shapiro 1983; Alvarez, Costales, Lopez-Muniz and Lopez 2005), which may transform to an osteoblastic phenotype and have a function in initial bone formation (Bianco, Cancedda, Riminucci and Cancedda 1998).

1.6.3 Primary Ossification Centre

Perichondrial cells superficial to hypertrophic chondrocytes of the cartilage anlagen differentiate into osteoblasts and form a bone collar under the stimulation of Ihh (Kronenberg 2003; Figure 1-7, v). Formation of a primary ossification centre occurs when vascular channels enter the nascent diaphysis in the region of the bone collar and expand into the hypertrophic zone, under the influence of VEGF signalling (Figure 1-7 vi). Bone morphogenetic proteins (BMPs) stimulate angiogenesis through stimulating osteoblasts to produce VEGF, thus coupling angiogenesis to bone formation (Deckers, van Bezooijen, van der Horst, Hoogendam, van der Bent, Papapoulos and Lowik 2002). PTHrP, FGFR3 and VEGF interact to regulate the depth of the hypertrophic chondrocyte layer and vascular invasion (Amizuka, Davidson, Liu, Valverde-Franco, Chai, Maeda, Ozawa, Hammond, Ornitz, Goltzman and Henderson 2004). A disc of ossification progresses towards each end of the anlage, termed the metaphyseal growth plate (Byers and Brown 2006; Figure 1-7 vii). Osteoblasts and osteoclasts accompany blood vessels as they penetrate the mineralised cartilage matrix surrounding hypertrophic chondrocytes (Figure 1-7, viii). Osteo(chondro)clastic resorption of mineralised cartilage matrix may not be necessary during this phase as it is loosely

packed, and vascular invasion has been observed to occur in the presence of clodronate-inhibited osteoclasts (Deckers, Van Beek, Van Der Pluijm, Wetterwald, Van Der Wee-Pals, Cecchini, Papapoulos and Lowik 2002). It is thought that osteoclasts mainly function to remove remnants of mineralised longitudinal septa, while endothelial cells remove unmineralised transverse septa (Deckers, Van Beek, Van Der Pluijm, Wetterwald, Van Der Wee-Pals, Cecchini, Papapoulos and Lowik 2002).

1.6.4 Secondary Ossification Centre

At either extremity of the developing anlage, resting chondrocytes may undergo further proliferation, forming epiphyses. Chondrocytes then hypertrophy and produce matrix vesicles that cause calcification of the matrix. Pericellular calcification is followed by vascular invasion and bone formation (Cameron and Robinson 1956; Trueta and Buhr 1963). TGF-ß1 prevents terminal differentiation of epiphyseal chondrocytes into hypertrophic cells (Ballock, Heydemann, Wakefield, Flanders, Roberts and Sporn 1993). Cartilage canals are formed within the epiphyses by invading perichondrial cells that express matrix metalloproteinases (MMP) -9, -13 and membrane type-1 MMP (MT1-MMP). Viable chondrocytes are released from the cartilage anlage and may differentiate into other cell types as the canals progress (Alvarez, Costales, Lopez-Muniz and Lopez 2005).

MT1-MMP (MMP-14, MT-MMP14) appears to be essential for penetration of vascular canals into uncalcified epiphyseal cartilage. Its absence in knock-out mice severely retarded secondary ossification (Zhou, Apte, Soininen, Cao, Baaklini, Rauser, Wang, Cao and Tryggvason 2000), which only occurred once epiphyseal cartilage was mineralised to its periphery (Holmbeck, Bianco, Caterina, Yamada, Kromer, Kuznetsov, Mankani, Gehron Robey, Poole, Pidoux, Ward and Birkedal-Hansen 1999). Mice deficient in MT1-MMP also displayed decreased chondrocyte proliferation in proliferative physeal cartilage (Zhou, Apte, Soininen, Cao, Baaklini, Rauser, Wang, Cao and Tryggvason 2000). MMP-13 is expressed during chondrocyte hypertrophy associated with collagen-X expression, and is possibly activated by MMP-2 or MT1-MMP (D'Angelo, Yan, Nooreyazdan, Pacifici, Sarment, Billings and Leboy 2000). Mmp9-/- mice have normal chondrocytes but have delayed removal of mineralised cartilage, thought to be due to impaired release of matrix-bound VEGF at the metaphysis (Colnot, Thompson, Miclau, Werb and Helms 2003).

Secondary ossification begins with the arrival of blood vessels, osteoclasts and osteoblasts in the centre of the cartilaginous epiphysis, attracted by VEGF and Ihh secreted by hypoxic chondrocytes (Maes, Stockmans, Moermans, Van Looveren, Smets, Carmeliet, Bouillon and Carmeliet 2004). The ossification front progresses radially, forming the articular growth plate towards the extreme of the anlage and the epiphyseal growth plate towards the diaphysis. When the epiphyseal growth plate meets the metaphyseal growth plate, the conjoined growth plates are recognised as the physis (Byers and Brown 2006).

Indian hedgehog null mice (Ihh-/-) display a lack of ossification in the extremities. Cartilage differentiation and VEGF expression are normal, but invading vessels do not expand to form a marrow cavity (Colnot, de la Fuente, Huang, Hu, Lu, St-Jacques and Helms 2005), indicating that Ihh signalling is essential for post-vascular invasion bone deposition.

Cathepsin B has been found in chondrocytes at the articular surface and in the hypertrophic zone of most growing horses, but in a minority of fetuses or neonatal horses. Cathepsin L was expressed in a different distribution to cathepsin B, being found in the proliferating chondrocytes of fetal and neonatal cartilage. Cathepsin B appears to be important for cartilage resorption during post-natal endochondral ossification at the articular physis in growing horses (Gläser, Davies and Jeffcott 2003). Cathepsin D degrades proteoglycans, which may be a necessary precursor to matrix mineralisation. It has been shown to be highly expressed by equine chondrocytes in the deep zone of articular cartilage taken from the lateral trochlear ridge of the femur and absent from the hypertrophic zone of radial growth cartilage (HernandezVidal, Jeffcott and Davies 1997).

While it is not generally recognised in contemporary literature, epiphyseal and articular growth plates show different cartilage morphologies and bony invasion proceeds in a different pattern than that seen in the metaphyseal growth plate. Columns of hypertrophying chondrocytes are present in the metaphyseal growth plate, while hypertrophic chondrocytes in the articular and epiphyseal growth plates show a less organised, scattered orientation during ossification (Byers and Brown 2006). In the equine distal Mc3, chondrocytes maintain a scattered orientation until after 6 months old, at which point chondrocytes of the superficial zone are found arranged parallel to the articular surface (Oikawa, Yoshihara and Kaneko 1989), indicating that maturation of the articular growth plate continues for several months after foaling.

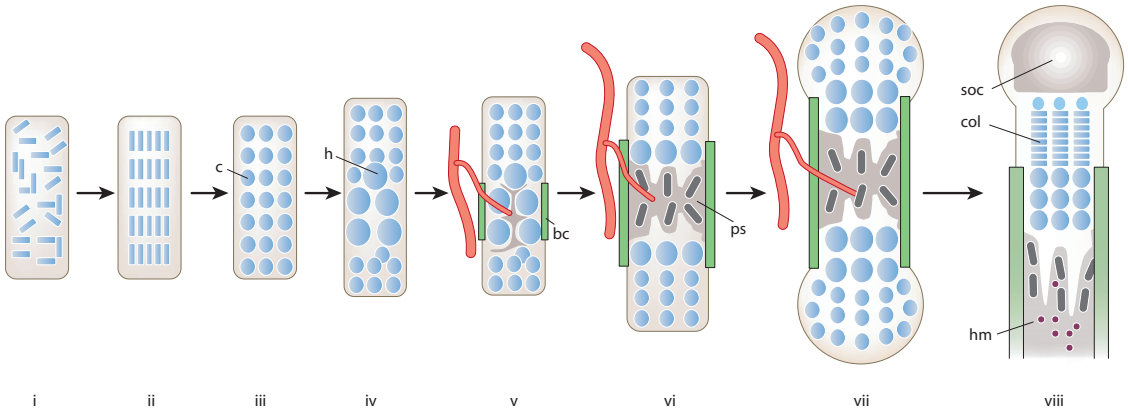

Figure 1-7: Early events in long bone development

See text for full description. C, chondrocyte; h, hypertrophic chondrocyte; bc, bone collar; ps, primary spongiosa; Soc, secondary ossification centre; col, chondrocyte columns; hm, haematopoietic marrow. Adapted by permission from Macmillan Publishers Ltd: NATURE (Kronenberg 2003), copyright (2003)

1.6.5 Matrix Gla Protein

Matrix gamma-carboxyglutamic acid (Gla) protein (MGP) is an 84 residue produced by chondrocytes and vascular endothelium that has a major function in preventing matrix calcification in cartilage and blood vessels (OMIM *154870). $Mgp^{-/-}$ (knockout) mice exhibited inappropriate calcification of physes and articular cartilage, which led to short stature, osteopenia, and fractures (Luo, Ducy, McKee, Pinero, Loyer, Behringer and Karsenty 1997). MGP is also present in the circulation, but this MGP pool has no effect on calcification of any ECM (Murshed, Schinke, McKee and Karsenty 2004). $Mgp^{-/-}$ mice develop calcification within blood vessels with an associated transformation of vascular endothelial cells to a chondrocytic phenotype (El-Maadawy, Kaartinen, Schinke, Murshed, Karsenty and McKee 2003). Bone Gla protein (BGLAP, BGP, osteocalcin) is a matrix Gla protein specific to bone and teeth, similar to MGP in structure but lacking any inhibitory effect on matrix mineralisation (Murshed, Schinke, McKee and Karsenty 2004).

1.6.6 Osteopontin

Osteopontin (OPN) is secreted by chondrocytes and is associated with chondrocyte and osteoblast differentiation and osteo(chondro)clast activation. Bone sialoprotein and osteopontin may participate in the regulation of mineralisation as they are found in high levels at the epiphyseal osteochondral junction. Osteopontin is also expressed in the centre of the epiphysis (deBri, Reinholt, Heinegard, MengarelliWidholm, Norgard and Svensson 1996).

1.6.7 Vascular Endothelial Growth Factor

VEGF's regulate bone remodelling by attracting endothelial cells and osteoclasts and by stimulating osteoblast differentiation (Deckers, Karperien, van der Bent, Yamashita, Papapoulos and Lowik 2000) and as such are critical for normal endochondral ossification. VEGF is expressed by mammalian hypertrophic chondrocytes (Kusafuka, Hiraki, Shukunami, Kayano and Takemura 2002) during medullary cavity formation but not during cartilage canal formation (Alvarez, Costales, Serra, Balbin and Lopez 2005). An in vitro avian model showed that only chondrocytes with a hypertrophic phenotype expressed VEGF. VEGF was chemotactic for endothelial cells, and had an autocrine feedback loop within hypertrophic chondrocytes (Carlevaro, Cermelli, Cancedda and Cancedda 2000). Hypoxia induces expression of VEGF isoforms by hypertrophic and proliferating zone chondrocytes through activation of the transcription factor, hypoxia-inducible factor-1 (HIF-1) (Cramer, Schipani, Johnson, Swoboda and Pfander 2004). Osteoclasts express VEGF receptor 1 (VEGFR-1) and resorb bone in response to exogenous VEGF (Niida, Kondo, Hiratsuka, Hayashi, Amizuka, Noda, Ikeda and Shibuya 2005).

There are 3 spliced isoforms of VEGF, differing in the number of exons transcribed; in the mouse, they are $VEGF_{120}$, $VEGF_{164}$ and $VEGF_{188}$. $VEGF_{120}$ is the diffusible form and appears to have less potent effect than the heparan sulfate-binding $VEGF_{164}$ and $VEGF_{188}$. Abolition of $VEGF_{164}$ and $VEGF_{188}$ expression reduced mineralisation around hypertrophic chondrocytes and inhibited vascular invasion of the growth plate during endochondral ossification (Maes, Carmeliet,

Moermans, Stockmans, Smets, Collen, Bouillon and Carmeliet 2002). Reduced endothelial and osteoclastic invasion was associated with a reduction in MMP-9 expression, indicating that MMP-9 expression is upregulated by the release of matrix-bound $VEGF_{164}$ and $VEGF_{188}$ during vascular invasion of the metaphysis. Reduced cartilage mineralisation was associated with continued expression of collagen-X indicating delayed terminal differentiation of hypertrophic chondrocytes in mice expressing only $VEGF_{120}$ (Maes, Carmeliet, Moermans, Stockmans, Smets, Collen, Bouillon and Carmeliet 2002). Mice expressing only $VEGF_{188}$ had reduced size and mineral content of all skeletal elements compared to wild-type littermates, largely explained by reduced epiphyseal vascular invasion as metaphyseal vascular invasion was inhibited. Mice expressing only the $VEGF_{164}$ isoform were skeletally normal (Maes, Stockmans, Moermans, Van Looveren, Smets, Carmeliet, Bouillon and Carmeliet 2004). These data indicate a central role for VEGF signalling in coordinating the vascular invasion stage of endochondral ossification, and that the most important isoform is $VEGF_{164}$.

Leukocyte cell-derived chemotaxin 1 (LECT1; chondromodulin, CHM1) is a potent inhibitor of VEGF-, FGF-2- and TGF-β-stimulated vascular invasion of cartilage, and is found in the inter-territorial cartilage matrix (Kusafuka, Hiraki, Shukunami, Kayano and Takemura 2002). The balance between LECT1 and VEGF determines the rate of vascular invasion of ACC (Amil, Fernandez-Fuente, Molinos, Rodriguez, Carbajo-Perez, Garcia, Yamamoto and Santos 2004). Expression of LECT1 decreases with age in articular cartilage, and is almost absent in mature articular cartilage, indicating that its role may be to inhibit vascular invasion of immature articular cartilage (Kitahara, Hayami, Tokunaga, Endo, Funaki, Yoshida, Yaoita and Yamamoto 2003). LECT1 expression in articular cartilage is lower than that in the epiphyseal cartilage (Kitahara, Hayami, Tokunaga, Endo, Funaki, Yoshida, Yaoita and Yamamoto 2003) perhaps reflective of a reduced requirement to modulate vascular invasion once the majority of endochondral ossification has occurred.

1.7 Tendons and Ligaments

Tendons and ligaments are critical supporting organs in the equine distal limb (Section 1.2.1: Gross Anatomy p.14). Their arrangement and stiffness must impact greatly on fetlock joint biomechanics but the contribution of soft tissues to fetlock stiffness and stability is not well defined. Partial transection of the medial branch of the IOT led to increased stress in the lateral Mc3 condyle, presumably through compensatory stress transmission through the lateral branch of the IOT and lateral PSB. The authors postulated that this might increase the likelihood of a lateral condylar fracture (Le Jeune, Macdonald, Stover, Taylor and Gerdes 2003).

Tendon is biochemically heterogenous at birth, with rapid, substantial changes occurring in the first 5-12 months of life in water content and concentrations of DNA, degraded collagen, hyaluronic acid, hydroxylysylpyridinoline crosslinks, pentosidine, glycosaminoglycan and hydroxyproline crosslinks (Lin, Brama, Kiers, Vanweeren and Degroot 2005). Sprint exercise given to foals in the 5-11 month age range, superimposed on stall confinement, may have detrimental effects on tendon compared to foals kept in stalls or given daily pasture turnout. Foals turned out to pasture

showed the greatest increase in tendon cross sectional area, rupture stress and compliance, while collagen fibril diameters were smaller (Cherdchutham, Becker, Spek, Voorhout and van Weeren 2001; Cherdchutham, Meershoek, van Weeren and Barneveld 2001).

Two-year old Thoroughbred fillies showed an increased cross-sectional area of the superficial digital flexor tendon in response to a 13-week race training program but no increase in echogenicity (Perkins, Rogers, Firth and Anderson 2004), indicating that tendon in young adult horses has some ability to adapt to exercise. Increases in superficial digital flexor tendon cross-sectional area were demonstrated after additional exercise was given during the first 15 months of life (Kasashima, Smith, Birch, Takahashi, Kusano and Goodship 2002). Accumulated data indicate that tendon may respond to exercise in the young, growing horse but that it becomes poorly or non-responsive in the adult horse, and that the number of load cycles is more important than intensity of load (Dowling and Dart 2005).

1.8 Parasagittal Condylar Fracture of Mc3/Mt3

1.8.1 Classification

Condylar fractures of the distal condyle of Mc3 may be partial, complete and non-displaced or complete and displaced, and always involve the articular surface (Meagher 1976). Simple incomplete and simple complete fractures are more common than complete comminuted (catastrophic) fractures, the latter making up 5-10% of all condylar fractures (Alexander and Rooney 1974; Bathe 1994). Mc3 and third metatarsal bones (Mt3) fracture in a similar pattern, although the most common limb, condyle and fracture-type combination appears to vary by breed, exercise type and study (Meagher 1976; Richardson 1984; Bathe 1994; Ellis 1994; Bassage and Richardson 1998). Of the medial and lateral condyles of Mc3 and Mt3, the lateral condyle of Mc3 is the most common site of condylar fracture (Bassage and Richardson 1998). Earlier reports suggested that only the lateral condyle could be affected (Meagher 1976), while it is clear from later data that fractures may occur in either lateral or medial condyles (Riggs 1999). Fractures may be simple, with one oblique fissure separating a wedge of bone comprising the lateral or medial distal condyle and a portion of the metaphysis and diaphysis from Mc3/Mt3, or they may spiral proximally, causing catastrophic, comminuted failure of the diaphysis. Occasionally, the fracture progresses proximally, spiralling through the diaphysis without causing catastrophic failure. This configuration has been termed long incomplete longitudinal fracture (Barr, Sridhar and Denny 1989).

1.8.2 Diagnosis

The standard clinical approach to condylar fracture is to assess lameness, obvious swelling, crepitus, malformation and pain on palpation localised to the fetlock joint. Horses may or may not be lame, and may be fully or partially weight-bearing on the affected limb (Schneider and Jackman 1996; Stashak 2001). High metacarpal nerve blocks or intra-articular anaesthesia may be required to localise pain to the fetlock joint in cases of subtle, incomplete fractures, but is contraindicated in cases of suspected displaced fracture.

Condylar fracture occurring during a race is most likely to be diagnosed after completion of the race than during the race (Peloso, Mundy and Cohen 1994). This is likely due to the relative prevalence of fracture severity, since most condylar fractures are simple (Ellis 1994) they are more likely to be investigated at the conclusion of a race. Horses with less common, catastrophic fractures may be diagnosed and euthanised while the race is still being run.

Plain radiography follows, with standard projections taken and oblique views as required to project the fracture line (Wyn-Jones 1988). In addition to the standard fetlock views, the flexed dorso-palmar and flexed dorso-35º-distal-palmaroproximal oblique projections are useful in diagnosing condylar fracture as PSB are elevated away from the condylar silhouette (O'Brien, Hornof and Meagher 1981; Pilsworth, Hopes and Greet 1988; Kawcak, Bramlage and Embertson 1995). In addition, a view that projects the distal palmar condyle is essential to diagnose intra-articular comminution (Wyn-Jones 1988; Schneider and Jackman 1996; Richardson 1998).

Incomplete fractures may be difficult to diagnose using standard radiography, in which case gamma scintigraphy (Ross 1998), xeroradiography or digital radiography may aid in diagnosis (Kawcak, Bramlage and Embertson 1995). Gamma scintigraphy may aid the clinician in localising lameness to the fetlock joint, but cannot provide a definitive diagnosis of condylar fracture due to its lack of specificity and resolution (Ross 1998). Computed tomography (CT) may be more sensitive than plain radiography at detecting small cracks in the parasagittal groove and intra-articular comminution in severe condylar fracture (Morgan, Santschi, Zekas, Scollay-Ward, Markel, Radtke, Sample, Keuler and Muir 2006), but the routine use of CT is limited at present due to the lack of a scanner that can be used in the standing horse.

Magnetic resonance imaging (MRI) has been used to generate 2D and 3D reconstructions of the fetlock joint on post-mortem specimens (Martinelli, Baker, Clarkson, Eurell, Pijanowski, Kuriashkin and Carragher 1996; Martinelli, Kuriashkin, Carragher, Clarkson and Baker 1997; Denoix 1999), to correlate with serial images of dissected limb anatomy (Martinelli, Baker, Clarkson, Eurell, Pijanowski, Kuriashkin and Carragher 1996; Denoix 1999), and to image condylar fractures post-mortem (Tapprest, Audigie, Radier, Anglade, Voisin, Foucher, Collobert-Laugier, Mathieu and Denoix 2003). Tapprest et al. (2003) also demonstrated a nascent fracture line in the contralateral Mc3 to a fractured Mc3 (Tapprest, Audigie, Radier, Anglade, Voisin, Foucher, Collobert-Laugier, Mathieu and Denoix 2003), indicating that MRI could be useful in preventing displaced condylar fracture by identifying premonitory lesions. There is no published study that describes the use of MRI for the clinical diagnosis of condylar fracture, probably due to the poor resolution, expense, rarity and impracticality of MRI scanners in current equine practice. Many clinical condylar fractures can be visualised by plain radiography, so MRI is not often required. Equine patients can be difficult to image as they do not readily stand still and often require sedation or general anaesthesia in order to reduce movement artefact. However, as MRI technology improves in resolution, speed, affordability and clinical practicality it will become an important tool for diagnosing condylar fracture, particularly occult stress fractures.

Computed tomography (CT) has not been used extensively for lameness diagnosis in equine practice. Like MRI, CT has enormous potential for use in equine orthopaedics, particularly in imaging the distal limb. Firth et al. (2005) demonstrated the use of a compact pQCT unit as a research tool in anaesthetised horses, finding substantial changes in the Mc3 in response to training exercise (Firth, Rogers, Doube and Jopson 2005). A 2D detector array high-resolution pQCT (HR-pQCT) unit has been used for clinical imaging of the cortical and trabecular structure of human extremities in 3D at a nominal voxel size of 82 μm (Boutroy, Bouxsein, Munoz and Delmas 2005), but the unit is currently too slow and bulky to be practical for use in the standing horse. HR-pQCT could be used in combination with 3D finite element analysis (FEA) to assess condylar fracture risk (Morgan and Bouxsein 2005), as has been demonstrated in isolated human vertebrae imaged with QCT (Crawford, Cann and Keaveny 2003; Morgan and Bouxsein 2005). FEA relates the spatial arrangement of voxels of varying densities to bone strength, as opposed to measuring mineral density in isolation from its organization (Crawford, Cann and Keaveny 2003). QCT combined with 3D finite element analysis outperforms densitometric and cross-sectional QCT measures in predicting vertebral compressive strength; however, it is time and computationally expensive at present.

QUS returns a composite measure of bone elasticity, density and trabecular architecture. SOS measured by QUS has been correlated to BMD determined by dual energy X-ray absorptiometry (DXA) in equine Mc3 but measures different bone characteristics (Carstanjen, Duboeuf, Detilleux and Lepage 2003). QUS is reasonably precise with a 1-2% between-operator error (Carstanjen, Duboeuf, Detilleux and Lepage 2003). SOS determined by QUS was found to be highly correlated with diaphyseal breaking strength in the Mc3 from 18-month-old ponies and horses (Glade, Luba and Schryver 1986), but this is likely to be of limited relevance to condylar fracture which initiates in the condyle, not in the diaphysis. SOS measures of horses with clinical dorsal metacarpal disease were no different to normal horses, although differences in SOS were found with sex, age, training intensity and site (Carstanjen, Lepage, Hars, Langlois, Duboeuf and Amory 2003). Because of its lack of specificity and inherently low resolution, QUS is unlikely to be clinically useful for diagnosing condylar fracture or bone changes predisposing to condylar fracture.

DXA of equine Mc3 has shown poor repeatability in pilot studies on disarticulated limbs (Swindlehurst, J. pers. comm, RVC, Herts November 2005). DXA is fundamentally limited to two dimensional imaging, suffering from projection artefact and relatively poor spatial resolution and does not report bone mineral density accurately (Bolotin 2007). For these reasons, DXA is unlikely to be useful in clinical equine practice.

1.8.3 Treatment and Outcome

Treatment of parasagittal condylar fracture of Mc3 may be either conservative or surgical. Incomplete, non-displaced fractures tend to be treated conservatively, while complete, displaced fractures or those that spiral are generally treated surgically (Stashak 2001). Return to racing may

be achieved by 65% of horses after either approach, providing that fracture healing is evident on 2-4 month post-fracture radiographs. However, horses take around 10 months to return to racing (9.7 months, Zekas, Bramlage, Embertson and Hance (1999b); 306 ± 67 days, Galuppo, Simpson, Greenman, Dowd, Ferraro and Meagher (2006)). Early diagnosis of incomplete condylar fractures carries a good prognosis with conservative management, which comprises stall rest and hand walking until radiographic union is evident (Kawcak, Bramlage and Embertson 1995).

Surgical management by lag-screw fixation is the usual treatment for complete condylar fractures (Alexander and Rooney 1974; Meagher 1976; Wyn-Jones 1988; Richardson 1998; Galuppo, Simpson, Greenman, Dowd, Ferraro and Meagher 2006). Screw number, size, type and position have a substantial influence on fracture healing. In equine Mc3, 5.5 mm diameter cortical bone screws had a greater pullout and breaking strength than 4.5 mm screws (Yovich, Turner and Smith 1985b). A more recent study recommended the use of shafted 4.5 or 5.5 mm screws due to greater shear strength than fully-threaded screws, with no difference found between 4.5 and 5.5 mm cortical screws' shear strength (Rahm, Ito and Auer 2000). It is probably more useful to consider screws' shear strength than their pullout strength, because in the case of condylar fracture repair the primary load experienced by screws is shear across the fracture gap, rather than direct tension on the screw head. Recent investigations support the use of variable-pitch, tapered, headless screws for fixation of non-displaced condylar fracture, as they do not impinge upon surrounding ligaments and other soft tissues (Carpenter, Galuppo and Stover 2006; Galuppo, Simpson, Greenman, Dowd, Ferraro and Meagher 2006). Arthroscopy may be required when intra-articular comminution is present (Ellis 1994). Surgical repair of long, spiralling condylar fractures may be performed in the standing horse under sedation and local anaesthesia, with outcomes similar to those achieved using general anaesthesia (Russell and Maclean 2006). Avoiding general anaesthesia is advantageous as horses often irreparably damage their fracture repair or cause other self-injury during anaesthetic recovery, leading to euthanasia.

Euthanasia is the treatment of choice for severely comminuted fractures due to the difficulty in achieving a satisfactory outcome with surgery. Incomplete medial condylar fractures of Mt3 are reported to have a high incidence of post-operative complications, such as progression of apparently simple, incomplete fractures into comminuted catastrophic fractures (Richardson 1984).

Complete lateral condylar fracture reduces the likelihood of returning to racing compared to incomplete fracture (Bassage and Richardson 1998) possibly because of a higher complication rate (Ellis 1994). Horses with non-displaced fractures were 17 times more likely to resume racing than horses with displaced fractures after treatment with lag-screw fixation (Martin 2000). Similar fracture configurations may carry a better prognosis if found in the Mt3 rather than Mc3 (Bassage and Richardson 1998). Intra-articular comminution bears an unfavourable prognosis because accurate surgical reduction of the joint surface becomes difficult or impossible, increasing the likelihood of arthritis (Richardson 1998).

1.8.4 Distribution

The typical origin of condylar fractures is in or near the medial or lateral parasagittal grooves of Mc3 and Mt3 (Alexander and Rooney 1974), as demonstrated in example radiographs in Vaughan and Mason (1975); Rick, O'Brien, Pool and Meagher (1983); Greet (1987); Krook and Maylin (1988); Barr, Sridhar and Denny (1989); Ellis (1994); Riggs (1999); Zekas, Bramlage, Embertson and Hance (1999a); Tapprest, Audigie, Radier, Anglade, Voisin, Foucher, Collobert-Laugier, Mathieu and Denoix (2003) and Galuppo, Simpson, Greenman, Dowd, Ferraro and Meagher (2006); MRI images in Tapprest, Audigie, Radier, Anglade, Voisin, Foucher, Collobert-Laugier, Mathieu and Denoix (2003); and pathological specimens in Alexander and Rooney (1974); Vaughan and Mason (1975); Rick, O'Brien, Pool and Meagher (1983); Greet (1987); Boyde, Haroon, Jones and Riggs (1999); Riggs (1999); Riggs, Whitehouse and Boyde (1999a) and Parkin, Clegg, French, Proudman, Riggs, Singer, Webbon and Morgan (2006).

Medial condylar fractures make up a greater proportion of Mt3 fractures than Mc3 fractures (Ellis 1994). Rick et al. (1983) described a case series of 77 condylar fractures, all of which originated within 20 mm (mean, 12 mm) abaxial of the middle of the sagittal ridge (Rick, O'Brien, Pool and Meagher 1983). Barr (1989) demonstrated that 8 long incomplete longitudinal condylar fractures originated 8-13mm abaxial to the centre of the sagittal ridge (Barr, Sridhar and Denny 1989). Ellis (1994) showed that 87% of 124 condylar fractures originated within 4 mm of the edge of the sagittal ridge (Ellis 1994). Mean distance from the centre of the sagittal ridge was 10 mm, with a range of 4-25 mm in a series of 75 fatal lateral condylar fractures sustained while racing in the UK (Parkin, Clegg, French, Proudman, Riggs, Singer, Webbon and Morgan 2006). Fractures may originate in the condyle itself (Kaneko, Kiryu, Oikawa, Kanemaru, Yamamoto and Satoh 1980; Krook and Maylin 1988; Norrdin, Kawcak, Capwell and McIlwraith 1998), but these points of origin are much less common. The weight of evidence in multiple studies shows that the majority of condylar fractures initiate in the parasagittal groove, but the reasons for this are not yet clear.

The length of simple complete lateral condylar fractures is reasonably consistent at 74-88 mm from fracture origin at the condyle to fracture exit on the abaxial diaphysis (Alexander and Rooney 1974; Vaughan and Mason 1975; Rick, O'Brien, Pool and Meagher 1983; Ellis 1994; Zekas, Bramlage, Embertson and Hance 1999a; Parkin, Clegg, French, Proudman, Riggs, Singer, Webbon and Morgan 2006), indicating a common cleavage pattern through Mc3. This may be a result of the combination of the gross shape of the bone, the forces acting on it and the sagittal plate trabecular structure of Mc3 (Boyde, Haroon, Jones and Riggs 1999). Evidence to date implicates a pre-existing lesion in the palmar parasagittal groove acting as a stress-riser exacerbating trabecular microfracture and failure of the bone organ (Riggs, Whitehouse and Boyde 1999a).

1.8.5 Pathogenesis

Rooney (1974) and Alexander and Rooney (1974) suggested that Mc3 condylar fractures might be produced by a single, high intensity, asynchronous movement between Mc3 and the proximal phalanx, producing shear forces across the condyles of Mc3 (Alexander and Rooney 1974; Rooney

1974). Vaughan and Mason (1975) reiterated the suspicion that "some incoordinate movement" caused condylar fracture, but of the 9 condylar fractures in their study, 8 came from horses that were reported to be galloping, cantering or finishing a race in the normal fashion when fracture occurred (Vaughan and Mason 1975). No subsequent study has confirmed Rooney's hypothesis, and condylar fractures are now considered stress fractures resulting from chronic bone damage because they occur after cyclic loading within the normal range (Riggs 1999; Riggs 2002; Stepnik, Radtke, Scollay, Oshel, Albrecht, Santschi, Markel and Muir 2004). Despite the changing opinion amongst researchers and lack of supporting evidence, Rooney continued to publish his hypothesis as late as the mid-1990's (Rooney and Robertson 1996). Notably, Rooney and Robertson (1996) eschewed the notion that lesions affecting the distal condyle of Mc3 might predispose to condylar fracture, stating that "the reports [of lesions] are trivial and not cited" (Rooney and Robertson 1996).

More recent evidence indicates that raising the lateral or medial sides of the hoof during loading, such as might occur when exercising on an uneven surface, causes rotation and 'collateromotion' (similar to adduction/abduction) at the MCPJ, which widens the joint space (Chateau, Degueurce, Jerbi, Crevier-Denoix, Pourcelot, Audigie, Pasqui-Boutard and Denoix 2001). The findings of Chateau et al. (2001) implicate uneven hoof placement and out-of-axis joint motion as a source of increased stress in the fetlock, but they do not support Rooney's hypothesis that a single, asynchronous rotation is enough to cause condylar fracture in a normal Mc3.

The intense loading of the fetlock joint during galloping is undoubtedly responsible for causing condylar fracture. Fracture occurs when the applied load is greater than the structure's ability to resist loading. Condylar fracture is not usually associated with specific traumatic accidents such as being kicked by another horse or colliding with a fence. Instead, condylar fracture usually occurs during normal loading, particularly high speed exercise (Riggs 1999).

Incomplete, non-displaced condylar fractures are well known (Section 1.8.1) but may be clinically silent in an unknown proportion of cases, through lack of clinical motivation for investigation. Tapprest et al. (2003) found evidence by magnetic resonance imaging of a clinically silent, incomplete condylar fracture in a horse's right Mc3. The horse had been destroyed due to a catastrophic, comminuted condylar fracture of its left Mc3. Both lesions originated in the lateral parasagittal groove (Tapprest, Audigie, Radier, Anglade, Voisin, Foucher, Collobert-Laugier, Mathieu and Denoix 2003) and together suggest that a presumptive fracture line may exist prior to complete bone failure, meaning that condylar fractures occur through material fatigue.

Several authors have noted an association between condylar fracture and pre-existing pathology. Kaneko et al. (1980) and Krook and Maylin (1988) observed damage to the palmar articular surface (palmar osteochondral disease, POD) of the distal Mc3 condyle and proposed that this might predispose to condylar fracture (Kaneko, Kiryu, Oikawa, Kanemaru, Yamamoto and Satoh 1980; Krook and Maylin 1988). Kaneko et al. (1993) noted an association between condylar fracture and "focally thickened and discolourated [sic] articular cartilage, focal brittle and

reddish-brown subchondral bone, and osteosclerosis", but they found no statistical relationship between these lesions and fracture incidence (Kaneko, Oikawa and Yoshihara 1993). A semi-circular area of lysis (termed osteoporosis by the authors) was found in the palmar condyle of non-fractured Mc3, while contralateral fractured Mc3 from the same horses contained regions of 'osteoporosis' bordering fracture fragments (Stover, Read, Johnson, Harrington, Ardans, Anderson, Barr, Daft, Kinde, Moore, Stoltz and Woods 1994). Other examinations of this hypothesis failed to reveal any predisposition to condylar fracture by POD (Pool and Meagher 1990; Ellis 1994; Riggs 1999). Swindlehurst et al. (2005) found a negative correlation between the presence of POD and fatal condylar fracture (Swindlehurst, Parkin and Morgan 2005), indicating that POD is an incidental finding in most cases of condylar fracture.

Linear fissures in HAC and ACC in the palmar/plantar aspect of the parasagittal groove were found to be present in at least one Mc3/Mt3 in 75% of horses (Riggs, Whitehouse and Boyde 1999a). There was a close similarity between the site and dimensions of the fissures and the usual plane of condylar fracture (Riggs, Whitehouse and Boyde 1999a). This fissure may extend into the subchondral bone where a concentration of resorption spaces may be found. There was a breach in the ACC layer, continuous with underlying bone resorption cavities. The fissure can be visualised as a lucent region in CT images and correlates well with the usual condylar fracture site (Riggs, Whitehouse and Boyde 1999a). Strenuous exercise was associated with the presence of wear lines in PP articular cartilage, in which water content was increased and hydroxyproline collagen cross-links were decreased (Brama, Tekoppele, Bank, Barneveld, Firth and van Weeren 2000), indicating disruption of the cartilage collagen network.

Horses with fatal lateral condylar fracture had a greater likelihood of having fissures in the parasagittal groove detected by gross pathologic examination (Swindlehurst, Parkin and Morgan 2005) and CT (Swindlehurst, Parkin and Morgan 2006) than case-control horses that died of other causes. Linear fissures were found in 55% of medial and 63% of lateral parasagittal grooves of non-fractured contralateral limbs taken from horses euthanised on-track with lateral condylar fracture. The degree of parasagittal groove cartilage pathology was not associated with age, number of years in racing or number of career starts (Parkin, Clegg, French, Proudman, Riggs, Singer, Webbon and Morgan 2006), suggesting that linear fissures of the parasagittal groove arise independent of racing and training activity.

Bone is toughened in 4 major ways against fracture: viscoplastic flow, microcracking, crack bridging and crack deflection (Peterlik, Roschger, Klaushofer and Fratzl 2006). Osteons usually act to prevent the propagation of microcracks in bone by deflecting them around cement lines (Gibson, Stover, Gibeling, Hazelwood and Martin 2006) but where penetration occurs, osteons may facilitate extension of the crack (O'Brien, Taylor and Lee 2005; Mohsin, O'Brien and Lee 2006). Cortical bone failure tends to occur as a result of the extension of a single microcrack rather than as a coalescence of multiple small microcracks (O'Brien, Taylor and Lee 2005). Linear microcracks occur under compression and diffuse damage occurs under tension (Cotton, Zioupos,

Winwood and Taylor 2003). Fracture toughness parallel to the axis of long bones is less than that perpendicular to the long axis (Peterlik, Roschger, Klaushofer and Fratzl 2006). It follows that cracks originating from a stress riser in condylar ACC and subchondral bone could easily propagate through the Mc3 if they enter and continue proximally within osteonal spaces.

Absence of a "'V' shaped region of mineralised cartilage" (Riggs, Whitehouse and Boyde 1999a) in Mc3 linear fissures suggests that they may be manifestations of osteochondrosis or an osteochondrosis-like process. Osteochondrosis has been simplistically defined as, "a failure of cartilage to convert into bone" (Krook and Maylin 1988) and "a focal disturbance in endochondral ossification" (Ytrehus, Carlson and Ekman 2007), which may result in a number of manifestations in the metaphyses and epiphyses. Despite intensive investigation, the causes of osteochondrosis are not understood, possibly because of a general failure to define clearly sub-types of osteochondrosis (Ytrehus, Carlson and Ekman 2007). Given that condylar fractures propagate from points of cartilage damage and poor osteochondral integration, it is pertinent to consider some features of osteochondrosis (OC) in the horse.

OC is a common finding in the fetlock joint. OC may be related to reduced plasma IGF-I, cortisol, copper and calcium, and increased plasma 1,25-dihydroxy-vitamin D, PTH and zinc (Sloet van Oldruitenborgh-Oosterbaan, Mol and Barneveld 1999), although the specific biochemical and developmental lesions that lead to OC have not been identified. Liver copper levels were not significantly associated with the prevalence of OC in Warmblood foals, but low liver copper levels were associated with a reduction in the normal resolution of OC lesions during growth (van Weeren, Knaap and Firth 2003). Copper supplementation of pregnant mares had no observed effect on the incidence of OC in their foals (Gee, Davies, Firth, Jeffcott, Fennessy and Mogg 2007). Hanoverian Warmblood horses had a reduced incidence of fetlock osteochondral fragments in response to a selective breeding programme (Stock and Distl 2005), indicating a genetic element to OC. Exercise during the first year of life has a limited effect on the prevalence or natural resolution of OC lesions in Warmblood foals, although foals kept in box stalls and not exercised had a tendency to more severe lesions (van Weeren and Barneveld 1999). OC may present as a subchondral cyst-like lesion, typified by a region of subchondral lysis that communicates with the joint space via a narrow cloaca (Nixon 1990). The most common site of cyst-like lesions in Mc3 is the medial condyle (Hogan, McIlwraith, Honnas, Watkins and Bramlage 1997), although they may occur at any site within Mc3 (Nixon 1990).

Osteochondrosis dissecans (OCD) may occur on the dorsal sagittal ridge and condylar surface of Mc3 and Mt3, in multiple limbs within the same animal. It is characterised by variable lameness, flattening of the dorsal sagittal ridge, subchondral bone irregularity and bone sclerosis. Intra-articular osteochondral fragments may be present (Yovich, McIlwraith and Stashak 1985; Nixon 1990).

Ihh expression was significantly increased in osteochondrotic cartilage compared to normal cartilage taken from equine joints, and was found mostly in the deep zone of articular cartilage adjacent to ACC (Semevolos, Strassheim, Haupt and Nixon 2005). Ihh stimulates ossification, but acts after VEGF signalling has attracted blood vessels to the site of cartilage resorption (Maes, Stockmans, Moermans, Van Looveren, Smets, Carmeliet, Bouillon and Carmeliet 2004; Colnot, de la Fuente, Huang, Hu, Lu, St-Jacques and Helms 2005). Increased Ihh expression in this regions of osteochondrosis indicates that ossification per se is likely to be increased, but is not necessarily occurring in an appropriately directed manner.

Full-thickness osteochondral injury leads to chondrocyte apoptosis as observed by TUNEL staining, particularly in the superficial tangential zone and middle zone of articular cartilage (Costouros, Dang and Kim 2004). Loss of chondrocyte signalling due to apoptosis or necrosis may explain failure of endochondral ossification in linear fissures.

Some authors have noted that the condylar fracture plane passes through a region of trabecular bone with a high density gradient, with sclerotic subchondral bone deep to the condyle abaxial and less dense bone deep to the sagittal ridge axial to the fracture (Riggs 1999; Riggs, Whitehouse and Boyde 1999b). No association between fracture risk and density gradient (Swindlehurst, Parkin and Morgan 2006) or preconditioning exercise and density gradient (Kawcak, pers. comm. 2005) has been demonstrated. It is possible, however, that regions of sclerotic bone serve to guide the fracture line, as Riggs et al. (1999) observed, "the fracture line … passed along the axial margin of the most dense portion of the lateral condyle. Once proximal to the area of intense sclerosis, it deviated laterally [abaxially]" (Riggs, Whitehouse and Boyde 1999a).

Stepnik, Radtke and Scollay (2004) claim to have observed branching arrays of microcracks at the failure surface of catastrophic Mc3 fractures by scanning electron microscopy (SEM) (Radtke, Danova, Scollay, Santschi, Markel, Da Costa Gomez and Muir 2003; Stepnik, Radtke, Scollay, Oshel, Albrecht, Santschi, Markel and Muir 2004). A thin layer of ACC was reported to overlay remodelled, dense subchondral bone in which branching arrays of microcracks were seen. Critical evaluation of the published images reveals severe processing damage to the tissue so that in most frames the bone ultrastructure is not visible. In addition, gold microspheres that were supposed to adhere within microcracks to prove the cracks' existence prior to tissue processing are not convincingly displayed inside any microcracks.

Boyde et al. (1999) noted a tendency for ACC to split in the sagittal plane more readily than in the frontal plane when Mc3 condyles were prepared for electron microscopy, and suggested that this tendency may be involved in condylar fracture initiation (Boyde, Haroon, Jones and Riggs 1999). Further, they found that trabeculae deep to the subchondral bone of the Mc3 epiphysis were arranged as sheets in the sagittal plane, joined by sparse transverse struts. This normal, developmental anisotropy gives Mc3 a 'grain' that condylar fracture tends to follow (Boyde, Haroon, Jones and Riggs 1999). Collagen fibres in the lateral cortex of Mc3 are arranged more longitudinally than those in the dorsal cortex which was

associated with increased stiffness in bending and reduced remodelling activity (Riggs 1990; Gibson, Stover, Martin, Gibeling, Willits, Gustafson and Griffin 1995; Martin, Lau, Mathews, Gibson and Stover 1996). An increased proportion of longitudinal collagen in the lateral cortex may contribute to the grain through which condylar fracture propagates.

1.8.6 Epidemiology

In the UK, as many as 78% (Verheyen and Wood 2004) to 84% (Bathe 1994) of fractures occur during training, rather than on the racetrack. The metacarpus is always strongly represented in Thoroughbred fracture statistics (Mohammed, Hill and Lowe 1991; Mohammed, Hill and Lowe 1992; Bathe 1994; Johnson, Ardans, Stover, Daft, Kinde, Read, Barr, Moore, Woods, Anderson, Stoltz and Blanchard 1994; McKee 1995; Riggs 1999; Verheyen and Wood 2004). Mc3 condylar fractures accounted for 5.3% of racing injuries at 4 US racetracks in a 17-month period (Peloso, Mundy and Cohen 1994).

Two-year-old horses were more likely to experience lateral condylar fracture later in the racing season than 3-year-old horses, while 2-year-old horses tended to have medial condylar fractures more frequently and earlier in the season than 3-year-olds (Ellis 1994). Colts may be slightly predisposed to condylar fracture compared to fillies (Ellis 1994).

Horses doing no gallop work during training and those in their first year of training are at greater risk of sustaining a fracture during racing (Parkin, Clegg, French, Proudman, Riggs, Singer, Webbon and Morgan 2004b). Fracture risk varies by trainer (Ely, Verheyen and Wood 2004; Verheyen and Wood 2004), indicating that individual training regimes may increase fracture risk. Geldings, horses whose most recent race was more than 33 days previous to injury and horses running long races (8-12 furlongs, 1 furlong = 201.17 m) on turf were at greater risk of catastrophic musculoskeletal injury (Hernandez, Hawkins and Scollay 2001).

The likelihood of any catastrophic musculoskeletal injury during racing has been associated with sex (increased in geldings), duration since the horse's previous race and a lower cumulative number of furlongs run at high speed in the 30-60 days preceding the fracture (Hernandez, Scollay, Hawkins, Corda and Krueger 2005). Horses given excessive exercise distances during a 2-month training period had an estimated relative risk of fatal musculoskeletal injury 15.5 times that of horses which completed average exercise distances (Estberg, Stover, Gardner, Johnson, Case, Ardans, Read, Anderson, Barr, Daft, Kinde, Moore, Stoltz and Woods 1994). The risk of fatal condylar fracture was between 7 and 17 times higher when horses wore shoes with toe grabs than without (Kane, Stover, Gardner, Case, Johnson, Read and Ardans 1996), indicating a deleterious alteration in stance phase kinematics.

Fatal musculoskeletal injury was more likely to occur while the horse was on the final turn and the straight section of track before the final turn of a race than elsewhere during the race, and were more likely to result from shorter races with fewer turns than non-fatal injuries (Peloso, Mundy and Cohen 1994). Mohammed et al. (1992) found the converse; fatal injuries were more likely to occur in the first 6 furlongs (1206 m) than the final 6 furlongs. One study found no association

between fatal injuries and track type (dirt vs. turf) or track condition (Hill, Carmichael, Maylin and Krook 1986), while Mohammed et al. (1991; 1992) found that non-fatal (Mohammed, Hill and Lowe 1991) and fatal injuries (Mohammed, Hill and Lowe 1992) were more likely to occur on dirt than turf. Further, some tracks may present an increased risk of injury when compared to others with similar surfaces (Mohammed, Hill and Lowe 1991).

In Thoroughbred horses in New Zealand, the risk of sustaining musculoskeletal injury of the distal limb was greater for 5-year-old (and older) horses than for 2-year-old horses. However, horses in their first year of race preparation were at higher risk of musculoskeletal injury than horses in their third or subsequent preparations (Perkins, Reid and Morris 2005a). This is echoed by the finding that there was a diminished risk of injury depending on the number of seasons raced, being 2, 3, 4 and 100 times lower for horses in their second, third, fourth, fifth (and above) seasons respectively, than horses in their first season (Mohammed, Hill and Lowe 1991). The mean age of Thoroughbreds sustaining condylar fracture was 3.4 ± 1.2 years, with a tendency to suffer medial condylar fracture of Mt3 at a younger age than lateral condylar fracture of Mt3 (2.9 ± 1.0 vs. 3.6 ± 1.2 years) (Bassage and Richardson 1998).

1.8.7 Genetic Factors

Ellis (1994) noted that heredity was a possible factor in condylar fracture, but the number of horses in his study (n = 122) was too small to draw any definite conclusion. The prominent stallion Mill Reef (USA, 1968) suffered Mc3/Mt3 fracture, and sired 7 horses that also suffered Mc3/Mt3 fracture. His offspring accounted for 5.9% of Mc3/Mt3 fractures (in a population that Ellis did not define) between 1973 and 1990 (Ellis 1994). No further epidemiological evidence was given to substantiate the suspicion of a genetic predisposition to condylar fracture. Little mention is made in prior or subsequent literature regarding the heritability of condylar fracture, and no published study exists that defines a genetic component to the disease. Swindlehurst et al. (2005) found in a case control study of that horses sustaining fatal condylar fracture of Mc3 on UK racecourses (n = 23) had narrower medial condyles than control horses (n = 42) (Swindlehurst, Parkin and Morgan 2005). Fracture risk reduced by an odds ratio of 0.45 for each millimetre increase in medial condylar width (Swindlehurst 2007). While conformational traits can be highly heritable (Love, Wyse, Stirk, Stear, Calver, Voute and Mellor 2006), and could conceivably increase condylar fracture risk, Swindlehurst et al. (2005) are the only group who have successfully related condylar fracture to any conformational variable – yet they only included fatal, on-track condylar fractures. Conformational influences on less severe, non-fatal condylar fractures have not yet been defined, but are the subject of current enquiry (Archer and Wade 2006). Anderson et al. (2004) found less specific relationships: that 'offset knees' were related to increased incidence of all fetlock joint diseases combined and that PP length was related to left forelimb fracture (Anderson, McIlwraith and Douay 2004). Computer modelling of the fetlock joint showed substantial variation in digital flexor tendon strains with minor variation in the tendons' insertion points (Lawson, Chateau, Pourcelot, Denoix and Crevier-Denoix 2007), suggesting that individual variation in the soft tissues of the digit could have a major impact on stress distribution in the fetlock joint.

Osteochondral diseases in horses and other species are often found to have a genetic component. Fetlock osteochondral fragment prevalence was examined in Hanoverian Warmblood horses, and was found to be of reasonable heritability (h^2 = 0.21-0.23) (Stock, Hamann and Distl 2005). Furthermore, the prevalence of fetlock osteochondral fragmentation in Hanoverian Warmblood horses may be reduced through selective breeding (Stock and Distl 2005). Quantitative trait loci relating to osteochondrosis in South German Coldblood horses have been identified and implicate genes for collagen type-III, type-V and type-XXVII, as well as interleukin 6 (among others) as heritable components (Wittwer, Lohring, Drogemuller, Hamann, Rosenberger and Distl 2007).

1.8.8 Related Pathologies

Concurrent fracture of PSB may be present in cases of Mc3 condylar fracture, particularly when there is displacement of the condylar fragment (Alexander and Rooney 1974; Meagher 1976; Barclay, Foerner and Phillips 1985; Greet 1987). A characteristic appearance is an axial fracture of the PSB on the same side (medial or lateral) as the fracture, and an apical fracture of the other PSB of the pair (Vaughan and Mason 1975). Four of 18 horses with Mc3 or Mt3 condylar fracture had concurrent axial sesamoid fractures (Barclay, Foerner and Phillips 1985). Recovery from axial sesamoid fracture has been associated with severe degenerative joint disease and prolonged lameness, and a poorer prognosis for return to racing form than recovery from condylar fracture alone (Barclay, Foerner and Phillips 1985; Greet 1987; Bassage and Richardson 1998). Of fatal condylar fractures sustained during racing, 69% had an associated PSB fracture and 17% had associated fractures of both PSB and PP (Parkin, Clegg, French, Proudman, Riggs, Singer, Webbon and Morgan 2006).

Dorsal metacarpal disease (DMD; bucked shins, sore shins) is a common, painful, exercise-related condition of the dorsal Mc3 diaphysis in young Thoroughbred racehorses. DMD is characterised by painful swelling on the dorsal mid-diaphysis of Mc3. Rapid sub-periosteal bone deposition is visible in an extreme saltatory form (Stover, Pool, Martin and Morgan 1992; Firth, Rogers, Doube and Jopson 2005). DMD may extend as a macroscopic, incomplete stress fracture of the dorsal cortex. It is possible that the latent microfractures of DMD fulminate by extension of parasagittal condylar fractures, resulting in catastrophic fractures of Mc3. DMD is most common in Thoroughbred horses in their first year of training. Decreased training distance at 'breezing' speed (15-16 $m \bullet s^{-1}$) and increased distance 'galloped' (US definition, 11 $m \bullet s^{-1}$) were associated with an increased risk of DMD (Boston and Nunamaker 2000). These results were supported by findings in UK Thoroughbreds that demonstrated a clear increase in risk with increasing distance cantered and galloped in short periods, but decreased risk with relatively increased training distances over longer periods (Verheyen, Henley, Price and Wood 2005). Small amounts of high speed exercise may have a protective effect against DMD if introduced prior to race training.

Cohen, Carter & Watkins (2006) showed that radiographic abnormalities of the proximal dorsal sagittal ridge at Texan yearling sales resulted in a reduced sale price but no diminution of racing performance as 2-year-olds. No other radiographic abnormality observed at yearling sales affected either 2-year-old race performance or sale price (Cohen, Carter, Watkins and O'Conor 2006).

Palmar/plantar osteochondral disease (POD; traumatic OCD) of the distal condyles of Mc3/Mt3 is found on the condylar surface that bears against PSB. It is characterised by collapsed or ulcerated articular cartilage, with or without exposure of discoloured mineralised cartilage or subchondral bone, osteonecrosis, osteosclerosis, focal bone resorption, bone microcracking and collapse (Kaneko, Oikawa and Yoshihara 1993; Riggs, Whitehouse and Boyde 1999a; Norrdin and Stover 2006). Flattening of the condyle may be seen at or palmar to the transverse ridge, associated with thin articular cartilage (Norrdin, Kawcak, Capwell and McIlwraith 1998). Additionally, cartilage fibrillation, erosion, wear lines or collapse may be found, along with subchondral micro-fracture, haemorrhage and fibroplasia (Norrdin, Kawcak, Capwell and McIlwraith 1998). These authors also noted the presence of a calcified cartilage layer subsiding into subchondral bone and concluded that this was evidence of an acquired, rather than developmental aetiology (Norrdin, Kawcak, Capwell and McIlwraith 1998). Kaneko et al. (1993) noted increased prevalence of POD with increasing age, races run and training duration (Kaneko, Oikawa and Yoshihara 1993), indicating that POD may result from the accumulation of and response to cyclic trauma. POD may be present in severe form with little apparent loss of joint function (Norrdin and Stover 2006). Radiographic diagnosis may be made using routine (dorsopalmar, lateral and lateral oblique) as well as special views (flexed dorsopalmar and lateral) of the fetlock (O'Brien, Hornof and Meagher 1981; Pilsworth, Hopes and Greet 1988). Despite commonly being found in fractured condyles, POD does not seem to be directly related to condylar fracture incidence in the majority of cases (Kaneko, Oikawa and Yoshihara 1993; Swindlehurst, Parkin and Morgan 2005).

1.9 Summary

Parasagittal condylar fracture of Mc3/Mt3 is a common injury that usually occurs during normal racing and training activity. Several predisposing factors have been identified, including the presence of linear fissures, years in training, distance galloped and cantered, track surface and shoe type. Most condylar fractures initiate in the parasagittal groove, where linear fissures are commonly found in articular cartilage. Excess bone resorption has been identified deep to these fissures, which may be detected with clinical imaging methods. Linear defects of the parasagittal groove are likely to act as stress-risers, increasing fatigue accumulation and reducing the amount of force required to initiate ultimate bone failure. The trabecular bone structure of the distal Mc3 has high regional anisotropy as an adaptation to the extreme loads experienced during full-speed exercise. However, this normal anisotropic structure in many cases does not adequately prevent fracture propagation and may promote fracture propagation as the condyle splits between sagittally-oriented trabecular plates.

There is a complex interplay between HAC, ACC and subchondral bone in the parasagittal groove of Mc3, which under intense loading results in linear defects and subchondral bone lysis. This process is not well understood yet is a potential key to the prevention of condylar fracture in racing and training Thoroughbred horses. Events in the parasagittal groove during growth may contribute to the development of linear defects and later condylar fracture.

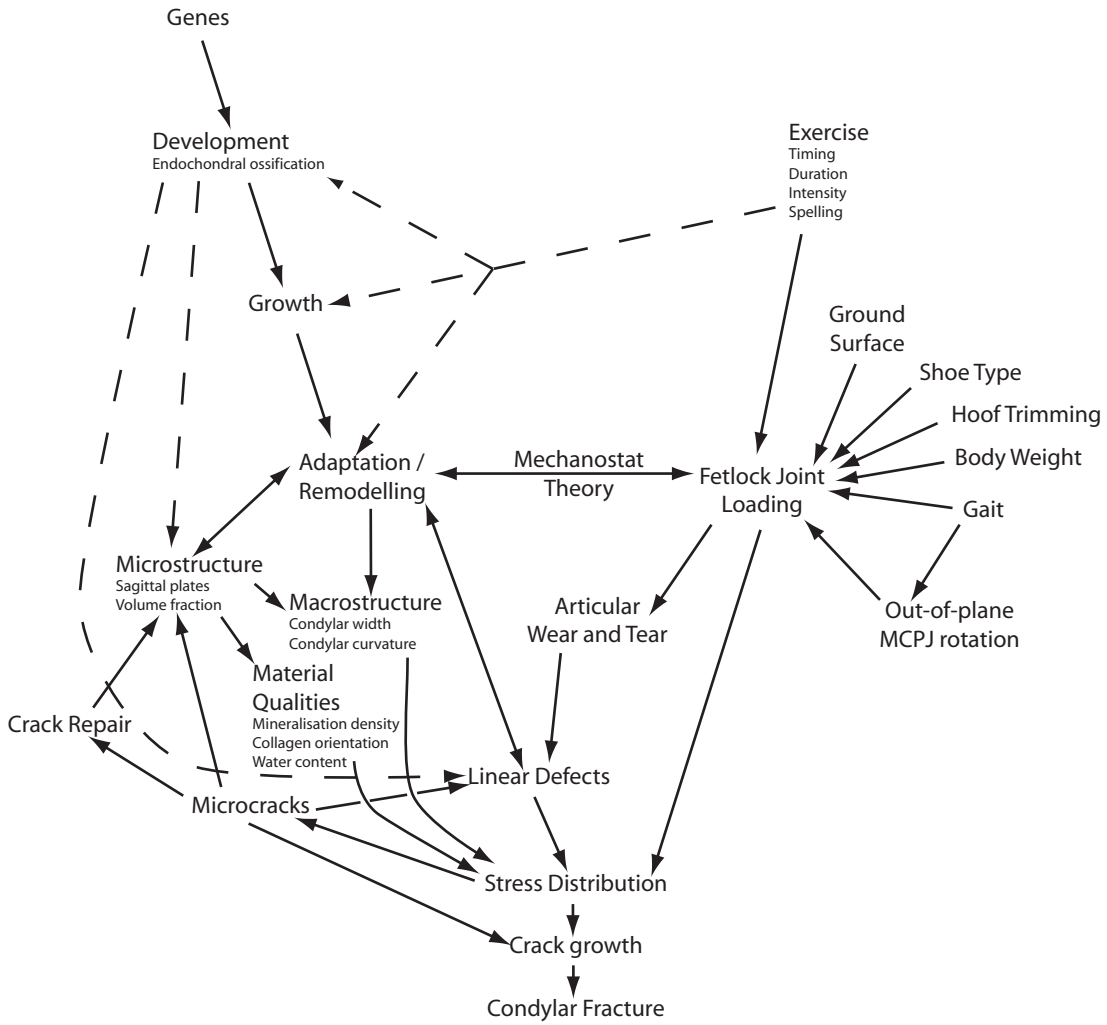

Figure 1-8: Condylar Fracture Concept Web

Concept web summarising the paradigm for condylar fracture. Themes explored in this thesis are shown by dashed lines, while pre-existing or externally-developed concepts are shown in solid lines.

Preconditioning exercise is controlled training given to foals prior to their entry to race-training. Its goal is to expose developing tissues to loads that will stimulate an adaptive response, and thus protect organs from mechanical failure while training and racing. Tendon and cartilage in the adult horse are considered largely unable to adapt to mechanical stress, while bone actively remodels throughout life. The configuration of subchondral bone and ACC in the distal Mc3 condyle is relevant to the development of condylar fracture. Manipulating tissue configuration through preconditioning exercise may prove to be beneficial in preventing pathological changes later in life.

1.10 Aims

This thesis aims to determine if variations in the 3-dimensional microstructure of the distal condyle of the Mc3 of 18-month-old Thoroughbred horses can be related to preconditioning exercise. It also seeks to demonstrate site-specific differences in bone and ACC and to argue that linear defects of the parasagittal groove have a strong developmental component with features in common with osteochondrosis.

1.11 General Experimental Plan

Mc3 specimens from an international collaboration on preconditioning exercise (GEXA) were processed and investigated using a variety of high resolution 2D and 3D imaging techniques. Particular attention was paid to HC, ACC and subchondral bone of the parasagittal grooves. Imaging modalities included microradiography, DXA, CSLM, SEM and μCT. Bone and ACC stiffness was determined by nanoindentation. Where possible, quantitative image analysis was used. Where practicable, results from each technique weree correlated to other techniques to discover interrelationships between data types. Tissues were explored for previously unobserved phenomena, which were documentedI in detail. Statistical tests were used to determine effects of site and preconditioning exercise where quantitative data were collected. Comparisons were drawn between results of the current study and those from collaborators who had worked on other tissues from the GEXA horses, and who had used complementary experimental techniques on the same tissues.

2: Experimental Design

2.1 Exercise Regime

Thirty-three Thoroughbred foals born in the 2000 breeding season at Flock House Thoroughbred Research Stud, Bulls, New Zealand, were matched for sire and sex and allotted into treatment (preconditioned) and control (non-preconditioned) groups for a research project investigating the effects of early exercise on the musculoskeletal system. Details of animal management, preconditioning exercise regime, race training and in-vivo experimental observations are reported in detail by Rogers et al. (papers in press, *Equine Veterinary Journal*: Rogers, Firth, McIlwraith, Barneveld, Goodship, Kawcak, Smith and Van Weeren (in press); Rogers, Firth, McIlwraith, Barneveld, Goodship, Kawcak and Smith (in press). All live animal procedures were performed with ethical approval from the Massey University Animal Ethics Committee, Palmerston North, New Zealand.

From birth, the horses were managed at pasture in paddocks of approximately 2 ha. Four or five mares with foals at foot shared each paddock prior to weaning, after which 8 weanlings shared each paddock. Weaning occurred at approximately 130 days old. Colt foals were castrated as yearlings. Diet was predominantly ryegrass/clover pasture, with supplementary meadow hay during winter.

From 10 days (21 ± 19 days) to 18 months old, the preconditioned group underwent a programme of incremental controlled preconditioning exercise superimposed on their normal paddock activity. Control horses exercised spontaneously at pasture only. Preconditioned horses were encouraged from 10 days post partum to trot, canter and gallop on a purpose-built track. Prior to weaning, 3 or 4 foals at a time were exercised alongside their mares. The velocity of the horses was regulated by the use of two four-wheeled 'quad' bikes equipped with mobile barriers. The track surface was turf covered with a thin layer of sand to improve the consistency of the surface and prevent slipping during wet conditions.

Foals exercised 1020 m each day, 5 days a week in clockwise and counter-clockwise directions on alternate days. Speed and distance were altered during growth to increase the intensity of the exercise. The exercise load was increased twice during the study. Initially the foals exercised at an average base speed of 5.36 ± 0.89 $m \bullet s^{-1}$, which was increased to 7.52 ± 1.75 $m \bullet s^{-1}$ in February 2001 when the foals were weaned at 4 months old (138 ± 10 days). At 6 months old (236 ± 31 days) the base speed was increased to 9.62 ± 0.71 $m \bullet s^{-1}$ and a 129 m sprint at 12.52 ± 3.39 $m \bullet s^{-1}$ was introduced after the first 500 m at base speed.

A cumulative work index (CWI) was calculated for each horse using the method described in Rogers and Firth (2004). CWI is the product of distance travelled and the average velocity worked at each subjectively-identified gait, which can be calculated for any period of activity for an individual horse and expressed in $m^2 \bullet s^{-1}$ (Rogers and Firth 2004). The behaviour patterns of

the preconditioned and control group were monitored. Observations included the duration of rest, grazing and play periods during the day. Preconditioned and control horses had similar overall levels of voluntary activity at pasture, although the intra-day timing of activity was different between groups. Preconditioned horses were estimated to have experienced CWI approximately one third greater than control horses at the termination of the preconditioning exercise programme (Rogers, Firth, McIlwraith, Barneveld, Goodship, Kawcak, Smith and Van Weeren In press).

All horses were observed by the stud manager daily for clinical abnormalities. Condition scores and weighing were carried out twice weekly. Full clinical examinations were conducted monthly by experienced equine clinicians. Any veterinary treatment was recorded in individual foal records. All horses contracted low-grade respiratory illness and were withdrawn from exercise for periods of up to 3 weeks in weeks 45-47. The average age in the middle of this 3 week period (13 August 2001) was 285 ± 28 days. Horses worked an average of 96 ± 22 days before and 102 ± 25 days after the outbreak of respiratory signs.

One control horse sustained a comminuted intra-articular fracture of the pelvis and was euthanised 5 weeks prior to the termination of the preconditioning exercise programme. Post-mortem tissue from this horse was not made available for study.

Twelve horses were selected for euthanasia at the end of preconditioning exercise. The intent was to retain a homogenous cohort of 20 horses that would enter race training and be available for study during and at the end of 2 racing seasons, so those horses that reduced cohort homogeneity were favoured for euthanasia. Six control and 6 preconditioned horses were selected from the original group based on being born early or late in the season, and were weighted for sex and sire. Injury, disease and difficult temperament were also considered as factors favouring euthanasia at 18 months old. Intravenous calcein injections (25 $mg \bullet kg^{-1}$) were administered as 2 single boluses separated by an 11 day interval, beginning 15 to 20 days prior to euthanasia (Table 2-1). The treatment groups each contained 3 geldings and 3 fillies. The 12-horse cohort was euthanised between 20th and 25th April 2002 by free bullet at 533.5 ± 29.2 days old (17.5 months). Specimens from these horses only were used for all experiments in this thesis except the final experimental chapter (Chapter 8, p. 114) in which they were compared against specimens from the horses that received 2 seasons of race training.

Twenty horses entered race training and raced for 2 seasons, under the management of an experienced, licensed trainer who was blinded to previous preconditioning exercise. The trainer was selected on the basis of known skill in previous training, standard of care of horses, and enthusiasm for the project. Although blinded to treatment group, the trainer was informed about the project to motivate his inquisitiveness and care in observing and managing the horses. Results of experimental clinical and radiographic examinations were not revealed to the trainer, but if he requested veterinary opinion then the results of the examination were made available so that appropriate training decisions could be made.

Horses were housed and trained at a commercial racetrack located in the lower North Island of New Zealand. Breaking to saddle, basic preparatory fitness work and introduction to grain feeding began when the horses were 18-21 months old and lasted about 8 weeks; from August 2002 they were trained to typical Australasian standard. Three sand-based tracks and 5 grass tracks were available for training, all oval.

In general, 2-year-old training consisted of 6 days per week slow cantering (7-9 $m \bullet s^{-1}$) for about 4 weeks, fast cantering (9-11 $m \bullet s^{-1}$) for another month, and then continuation of fast cantering with galloping (14-15 $m \bullet s^{-1}$) 3 times a week. After being taught to enter and leave the starting barrier, horses were started with others at a similar stage in jump-outs or time trials. Jump-outs are pre-race training sessions to habituate the horse to the starting gate and the start of a race, and usually involve a 400 - 600 m sprint at near-racing speed. Time trials, managed by the New Zealand racing authorities, are unofficial races used to assess race potential and readiness; 2-year-old trials were at 450, 600 and 800 m and 3-year-old trials were at 800 and 1000 m. After suitable performance, the horse was entered in an official race.

The 2-year-olds were to be trained until the end of the season in March 2003. Each horse was trained according to its individual merits and racing ability. Decisions concerning training were by the trainer, who worked within rough guidelines concerning the need to achieve each horse's athletic potential. The trainer agreed that horses were to be progressed toward participation in competitive events (jump-outs, trials or races) as promptly as possible within the racing season, and not spared for hopefully better prospects later. Conversely, the trainer was charged with maximising the chance that all horses had the best chance to achieve competitive starts, rather than subject horses to high workloads and see which survived to compete. At the completion of 2-year-old training the horses were subjected to a full clinical and imaging examination, then lived in 2 ha paddocks during the spelling (lay-up) period of at least 4 months before returning to training for racing as 3-year-olds in July 2003.

Withdrawal of any horse from training was at the discretion of the trainer, based on various criteria including reaching the end of the season, physical or 'mental' immaturity, or clinician-diagnosed illness or orthopaedic injury requiring withdrawal from training. The horses received no medications that may have affected the musculoskeletal system, except when specifically indicated for the treatment of clinically established disease.

The initial intent of the GEXA study was for tissue from all 20 race-trained horses to be made available at 3 years old. One horse sustained a displaced physeal fracture of the right proximal humerus and was euthanised 4 weeks after the transition from preconditioning to race conditioning. Tissue from this horse was collected and prepared as for the other horses, but was not included in statistical analyses. Of the 19 horses that completed 2 race seasons, only 6 were euthanised (3 preconditioned, 3 control) at 3 years old due to ethical objections from persons opposed to the experiment. These 6 horses had been shown to have no athletic potential for racing, or did not have the temperament required to be safe and reliable equine athletes. Tetracycline labels had been given to some of the 6 3-year-old horses prior to euthanasia (Table 2-2).

2.2 Specimen Preparation

Limbs were dissected free immediately after euthanasia and transported to the laboratory within 15 minutes of death. The fetlock joints were opened and synovial fluid and cartilage samples were taken for other studies. Initial tissue handling was completed within 4 hours of death. The digits were either frozen at -20 ºC and shipped on dry ice to Colorado State University, Fort Collins, Colorado, USA (18-month specimens), or fixed in 70% ethanol and retained in New Zealand (3-year specimens). All distal Mc3 condyles were cut according to a standard protocol (Boyde and Firth 2005b) with a low speed, water cooled diamond saw (LabCut; DR Bennett Ltd, London, UK), giving a dorsal-25º-oblique frontal slice (A slice), a frontal slice (B slice), and a palmar-35º-oblique frontal slice (C slice) (Figure 2-1). Bone slices (2.5-3 mm thick, 3 per condyle) were fixed in 70% ethanol and transported to London, UK. Tissue from both left and right distal Mc3 condyles was used in this study.

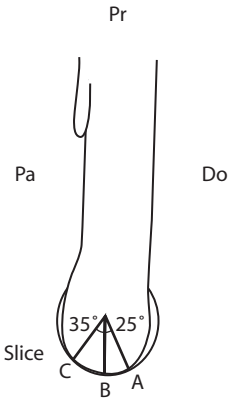

Figure 2-1: Slice orientation, lateral view

Table 2-1: Treatment group, calcein label and euthanasia data for 18-month-olds

Horse ID / sex		Control / Precondition	1st calcein label time (05/04/2002)	2nd calcein label time (13/04/2002)	Interlabel time (dd:hh:mm)	Date of euthanasia	Age at euthanasia (days)
1	M	Precon.	10:36:00	14:36:00	11:04:00	23/04/2002	584
3	M	Control	11:27:00	17:15:00	11:05:48	20/04/2002	569
13	F	Control	10:41:00	17:09:00	11:06:28	20/04/2002	552
16	F	Precon.	11:29:00	14:39:00	11:03:10	23/04/2002	546
17	M	Control	10:45:00	17:25:00	11:06:40	23/04/2002	543
19	M	Precon.	10:51:00	14:29:00	11:03:38	24/04/2002	533
20	F	Precon.	10:54:00	14:40:00	11:03:46	24/04/2002	531
24	M	Control	11:00:00	17:16:00	11:06:16	22/04/2002	517
29	M	Precon.	11:06:00	14:32:00	11:03:26	24/04/2002	511
30	F	Control	11:10:00	14:27:00	11:03:17	23/04/2002	495
31	F	Precon.	11:12:00	14:27:00	11:03:15	24/04/2002	482
33	F	Control	11:19:00	17:24:00	11:06:05	25/04/2002	539

Table 2-2: Tetracycline label schedule for 3-year-olds

Horse ID	1st Tetracycline	2nd Tetracycline	3rd Tetracycline
14	27/11/2003	not given	not given
26	28/11/2003	30/11/2003	5/12/2003
27	8/12/2003	14/12/2003	not given
10	8/12/2003	17/12/2003	not given

All bone slices were imaged in DXA (Lunar PIXImus, GE Medical Systems, WI, USA) and with an optical flatbed scanner (UMAX Astra 5400) upon arrival in London. B-slices were macerated in an alkaline bacterial pronase detergent solution (Terg-A-Zyme, Alconox, New York, NY, USA) and dried. A- and C-slices were fixed in 70% ethanol and dehydrated in absolute ethanol. Ethanol was substituted with xylene, which was subsequently drained off and replaced with 2 changes of methyl-methacrylate monomer (BDH Ltd, Poole, UK). Polymerisation of methyl-methacrylate to polymethylmethacrylate (PMMA) was initiated by the catalyst α-azo-iso-butyronitrile (BDH Ltd, Poole, UK). Embedded sections were ground flat on increasing fineness of abrasive, from P120 to P4000 silicon carbide paper and finishing with diamond paste polishing, imaged in quantitative backscattered electron scanning electron microscopy (qBSE; Section 4.3.2: p. 72), then diamond ultramilled (Reichert-Jung Ultramiller; Leica UK Ltd, Milton Keynes, UK) and imaged in both qBSE and CSLM (Section 3.3.4: p. 59). PMMA casts were made of the embedded A- and C-slices by alternate peroxide and bleach digestion, which removes mineralised tissue while soft tissue spaces are retained. Thirteen standard sites per specimen were identified based on previous experience and used consistently throughout the study (Figure 2-2).

2.3 Image Analysis

Digital image analysis involves the use of a powerful and growing set of tools based on computer algorithms applied to digitised images. Continued development of fast central processing units (CPU) and graphical processing units (GPU) with large amounts of random access memory (RAM) has made digital image analysis progressively cheaper and more accessible. Open source image analysis software such as ImageJ (Rasband 2005) and Drishti (Limaye 2007) is available on the Internet, is free to download and may be modified to the user's requirements.

The earliest application of digital image analysis to the equine Mc3 was by Yoshihara et al., who in 1989 measured trabecular surface areas, thickness, perimeter length, skeleton length, number of intersections and orientation on digitised radiographs of Mc3 condyles (Yoshihara, Kaneko, Oikawa, Wada and Tomioka 1989). Complementary work by Riggs (Riggs 1990), Boyde and others (Boyde, Reid and Howell 1983; Reid and Boyde 1987; Boyde, Howell, Bromage, Elliott, Riggs, Bell, Kneissel, Reid, Jayasinghe and Jones 1992; Boyde, Elliott and Jones 1993; Boyde, Haroon, Jones and Riggs 1999; Goldman, Blayvas, Boyde, Howell, Clement and Bromage 2000; Boyde, Lovicar and Zamecnik 2004)led to improvements in the resolution and accuracy of mineral density determination in bone specimens, and allowed for correlated studies of intra-vital labels and mineralisation density.

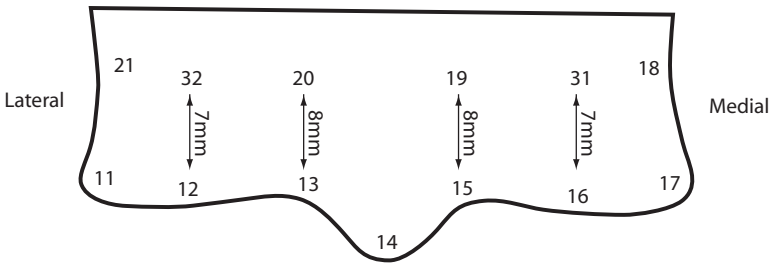

Figure 2-2: Site locations

2.4 Statistical Analysis

Table 2-3 illustrates the rapid data multiplication that occurs when making several measurements on individuals. While comparing exercise or age effects, the number of observations (*n*) was limited to the number of horses in each group and repetitive or nested measurements averaged to summarise results by horse. When comparing tissue types, *n* was taken as the number of individual observations rather than the number of horses. SPSS (SPSS v11.0.0, SPSS Inc, Chicago, IL, USA) was used for the majority of statistical analyses while additional data manipulation was handled with ImageJ, Excel (Microsoft Corp., Redmond, CA, USA), Perl and MySQL (MySQL AB, Uppsala, Sweden).

Table 2-3: Data Multiplication

Level	Factor	*n*	Notes
Treatment group	2	2	Control vs. exercised
Horses	6	12	6 horses per treatment group (NB: while testing age effects, *n* = 12 18-month-olds and *n* = 6 3-year-olds)
Legs	2	24	2 forelimbs per horse
Slices	3	72	3 slices per leg
Sites	13	936	13 sites per slice (NB: Not all sites were used in every study)
Measures	1 to ~500	936 to 0.5×10^6	Variable numbers of measurements per site, depending on the experimental technique. Measures were averaged by site before site and treatment comparisons.

3: Variation in Condylar Microanatomy

3.1 Summary

Multiple imaging modalities were applied to Mc3 specimens. Examination of the resulting data-sets revealed patterns that guided detailed quantitative experiments, which are described in the following chapters of this thesis.

Gross examination of PMMA-embedded specimens showed that thickened, discoloured and poorly embedded cartilage was distributed on the sagittal ridge of the A-slice and in the parasagittal grooves of the C-slice. Examination of these regions on the flat surfaces of polished and ultramilled embedded blocks with backscattered electron scanning electron microscopy (BSE-SEM) showed thickened, poorly mineralised ACC. CSLM of the same regions showed plentiful and bright double calcein labels in bone surrounding disorganised marrow spaces deep to thickened regions of ACC. The association between thickened ACC and unusually active subchondral bone modelling was suggestive of localised aberrations in endochondral ossification. Anomalous morphology of bone and ACC in the parasagittal grooves is of particular concern because they are predilection sites for condylar fracture of Mc3.

BSE-SEM of embedded specimens, macerated specimens and PMMA casts showed variation in trabecular size, orientation and anisotropy within specimens (in common with previous studies), but variation was also identified between individuals. X-ray microtomography and microradiography confirmed this finding. ACC thickness, mineralisation density and tidemark calcein label gap appeared to vary across the condyle.

The specimens could not easily be sorted into treatment groups based on morphological observations, indicating that any relationship between preconditioning exercise and Mc3 condylar microanatomy was subtle at most. This contrasts with the results of the samples from the (second) Bristol treadmill training experiment and the Massey University Grass Exercise Study (MUGES) in which the diffrence between control (untrained) and exercise (trained) groups was obvious (Boyde and Firth 2005b). Statistical analysis of semi-quantitative scoring of morphological parameters confirmed this.

3.2 Introduction

Bony architecture within the Mc3 condyle varies widely, from dense, i.e., high volume fraction bone immediately deep to the main weight-bearing condyles, to a more open sagittal plate structure proximally (Boyde, Haroon, Jones and Riggs 1999; Riggs, Whitehouse and Boyde 1999b). Low volume fraction bone in the parasagittal grooves has been associated with condylar fracture (Riggs 1999). Previous studies have utilised random-source tissue from animals whose histories were not fully available. The current study uses tissue from an experimental cohort of horses that were born in the same season to a limited number of sires. Management of the horses was as described earlier (Section 2.1: Exercise Regime p. 50).

Training exercise was related to increased volume fraction of bone within Mc3 of 2-year-old Thoroughbred horses (Boyde and Firth 2005b). The response of Mc3 to preconditioning exercise is unknown, but is potentially important in generating adaptations to condylar structure that are better able to resist condylar fracture.

ACC varies across the distal condyle of Mc3 (Boyde and Firth 2004) and may be involved in condylar fracture. Microcracks within ACC of Mc3 may propagate into the subchondral bone plate and thence into macroscopic fracture lines (Riggs, Whitehouse and Boyde 1999a; Radtke, Danova, Scollay, Santschi, Markel, Da Costa Gomez and Muir 2003; Muir, McCarthy, Radtke, Markel, Santschi, Scollay and Kalscheur 2006).

This chapter describes qualitative and semi-quantitative observations of the structure of 12 Mc3 condyles from 18-month-old Thoroughbred horses using gross observation, BSE SEM, microradiography, μCT and CSLM.

3.3 Materials and Methods

3.3.1 Visual assessment

Left and right A- and C-slices were evaluated macroscopically in the embedded state. Defects within the parasagittal grooves and sagittal ridges were identified and scored from 0 (no change) to 3 (severe change), giving 12 sites per horse. Discolouration and extent of affected tissue contributed to the severity score. Data were coded for exercise group, slice and site and analysed with the Mann-Whitney test for exercise effects and the Kruskal-Wallis test for site effects in SPSS (SPSS v11.0.0, SPSS Inc, Chicago, IL).

3.3.2 Microradiography

Microradiography is the application of general radiographic technique at the sub-millimetre scale. The limits to resolution of radiography include the size of the X-ray source (focal spot size), film grain size or detector pixel size, specimen thickness and X-ray scatter. Magnification may be achieved by increasing the distance between the specimen and the detector (Cosslett and Nixon 1952; Dunn, Bowes, Rothert and Greer 1975). All specimens were imaged in a digital X-ray cabinet with a 20 μm nominal spot size (Faxitron MX-20, Qados Ltd., Sandhurst, Berks, UK) and either a 118 x 117 mm Hamamatsu camera with 50 μm pixels (model DC12), or a 49 x 95 mm Dalsa camera with 46 μm pixels (model DC4). Exposure settings were as appropriate for the thickness of each specimen (24-32 kV, 19 s). Magnification was controlled by placing the specimen on a tray that could be moved between slots set at factory-defined heights within the cabinet. Initial survey radiographs were made at the highest magnification that allowed the entire specimen to be imaged in a singe frame (1.5 – 2x), and regions of interest imaged at up to 5x magnification. Images were saved as 8-bit TIFF and 16-bit DICOM files for later viewing. This method could be applied retrospectively to unembedded or PMMA embedded blocks.

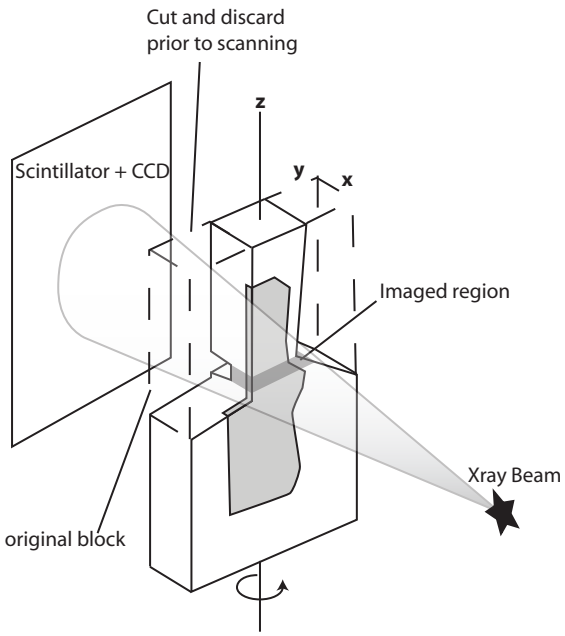

Figure 3-1: Schematic diagram of µCT set-up

3.3.3 Micro Computed Tomography

Computed tomography is the process whereby a set of projections of an object made at a large number of angles are reconstructed to give an image of the object. Mathematical principles of tomographic reconstruction are described by Kak and Slaney (2001). Briefly, each x-y slice can be reconstructed by performing an inverse Fourier transform on the 2D image produced by combining, at the angles of projection, the Fourier transforms of a set of 1D projections (Kak and Slaney 2001). Micro-computed tomography (microCT, µCT) applies the principles of computed tomography on a reduced scale in order to gain resolution at the micron level (Elliott and Dover 1985). Early instruments scanned a 1D source-detector couple in tandem across a 2-dimensional x-z raster, while the specimen rotated in the z-axis. Modern instruments, such as the MuCat 2 developed in this department and used in this thesis, utilise a 2D detector array and cone-shaped X-ray beam, greatly reducing scanning time because the source-detector raster-scanning motion is no longer necessary. Reconstruction is performed with a modified Feldkamp cone-beam algorithm to account for cone-beam projection geometry (Davis and Elliott 2003). Between 450 and 580 z-slices can be scanned in a single specimen rotation by the MuCat 2; if more slices are required to image a specimen, the specimen is translated in the z-axis and re-scanned until full coverage has been achieved. The MuCat 2 has a unique design feature, time delay integration (TDI), whereby the 2D CCD is scanned horizontally during each projection, thus averaging pixel values and avoiding ring artefacts that can be introduced by variation in sensitivity and output between pixels (www.smd.qmul.ac.uk/dental/oralgrowdev/biophysics/xmt).

Voxels with sides as small as 1-2 µm (or less) are possible using synchrotron radiation, in part because synchrotron radiation is monochromatic so reconstructions do not suffer from beam-hardening artefacts (Jiang, Zhao, White and Genant 2000), and because synchrotron sources are coherent, polarised and have very high flux. The Belgian commercial firm SkyScan claims that 400 nm isotropic voxels are possible in their SkyScan-2011 X-Ray NanoTomograph machine (2006). The MuCat 2 is capable of 8.7 µm voxels, although decreasing voxel size results in a substantial increase in scanning and reconstruction time – scanning the same specimen with 15 and 10 µm voxels resulted in scan times of just over 5 hours, and just over 2 days and 5 hours respectively.

μCT overestimates bone biopsy BVF and trabecular thickness when compared to histomorphometry. 3D modelling algorithms and volumetric resolution (voxel size e.g. 14.63 μm^3) are the greatest influence (Chappard, Retailleau-Gaborit, Legrand, Basle and Audran 2005). However, μCT has the advantage of being able to analyse 3D connectivity while 2D techniques rely on either serial sections or stereology to estimate 3D structure.

PMMA was cut away around the region of interest to reduce the loss of contrast that excess, non-informative material would otherwise cause (Figure 3-1). The specimen was held in a custom-built rotating clamp. Top and bottom limits in the z-axis were set, defining the imaged region. Voxel size was set to 15 μm isotropic. The standard reconstruction algorithm resulted in small artefacts of apparently increased attenuation, particularly at the junctions between trabeculae. A specialised wobble-correction algorithm was written to reduce this artefact, which functioned by finding and removing periodic noise. Reconstructed TOM files were imported into ImageJ and Drishti (Limaye 2007) as stacks of 2D slices, in which they were visualised as resliced 2D stacks and volume renderings. Animated volume renderings of typical and atypical parasagittal grooves were created in Drishti using transfer functions that displayed calcified tissue, marrow space or the calcified tissue boundary.

3.3.4 Confocal Scanning Light Microscopy

CSLM is a technique whereby pinhole apertures are included in the illumination and collection light paths to prevent light radiating from outside the subject focal plane from reaching the image plane. Optical sectioning is achieved by the confocal microscope, so that large and difficult to cut specimens such as bone and ACC may be viewed through the top surface. Images are sharp due to the reduction of scattered or fluorescent light emanating from other than the desired focal plane. Serial optical sections may be made through the z-axis and reconstructed into 3-dimensional models (Inoué 1995).

Point illumination and detection increases resolving power by reducing scatter. By scanning a point source of light across the specimen, a whole image is built up. A scanning point source is provided by either a laser whose path is bent by mirrors to produce a raster, or a conventional incoherent light source shone through small holes in a spinning Nipkow disc. Reflected or fluorescent light radiates from the point of reflection / excitation and a small fraction of this enters the objective lens.

For digital imaging, light is separated into colour channels either by coloured filters or by prisms. Each channel is fitted with a photomultiplier whose voltage can be altered to amplify the light signal. Incident light on a photodetector causes an electric charge which is converted into a digital signal for further processing. The photodetector may be an array of small photodetector elements, each of which is represented by a pixel in the final digital image, or it may be a single element whose signal is coordinated with the specimen scan to construct an image. The photodetector for each channel is assigned a colour look-up table (LUT), and if multi-channel imaging is used, the channels are combined to form a red-green-blue (RGB) colour image. At low light levels,

photomultiplier noise is increased, necessitating increased exposure time, which may be achieved by either increasing the number of passes of the laser over each point on the object within the raster, or by increasing the dwell time of the laser on each point of the raster.

Confocal microscopy has a major advantage over conventional microscopy in that physical sections do not need to be cut; meaning that large and difficult to cut specimens such as undecalcified horse bone may be examined. Epifluorescence and reflection modes may be used on specimen surfaces; however, image quality diminishes as specimen penetration increases, as scattered light and out of focus light is included in the image.

3.3.5 Scanning Electron Microscopy

Scanning electron microscopy (SEM) employs a focussed beam of electrons passed in a scan pattern (usually a rectangular raster) across a specimen to generate an image of the specimen surface. Electrons extracted from a white hot tungsten filament serve as electron source. Electrons are accelerated towards an annular anode, which is maintained at 1-50 kV, then focussed through a series of electromagnetic coils where the imaging spot is formed and the scan pattern generated (Goldstein 1975b). Electrons are emitted as either high energy backscattered electrons (BSE: hundreds of eV to nearly the accelerating voltage) or lower energy secondary electrons (SE: <50eV) after the primary beam interacts with the atoms in the specimen surface (Goldstein 1975a). Backscattering results from collision between incident electrons and specimen atomic nuclei, while secondary electrons result from electron-electron interactions (Goldstein 1975a). Once emitted, electrons are collected by either solid state or scintillating detectors.

The specimen scan raster is coordinated with the image formation raster such that the detector signal represents the brightness of a pixel in the image, relating to the position of the electron beam (Newbury 1975). Direct visualisation may be achieved by synchronising the raster scan of a cathode ray tube (CRT) monitor with the scan in the SEM. Alternatively, the detector signal is digitised and stored on electronic media for later visualisation and analysis.

3.4 Results

3.4.1 Visual Assessment

A highly significant relationship between defect severity, slice and site was found, with the A-slice sagittal ridge and C-slice parasagittal grooves most severely affected (Table 3-1). Half (6/12) of the horses had at least one site graded as severely affected (Figure 3-2). No score was logged for the sagittal ridge tip of 19rc, which had been lost during specimen polishing. No relationship was found between preconditioning exercise and macroscopic defect severity (Figure 3-2; Table 3-2).

3.4.2 Microradiography and µCT Images

Results of microradiographic and microtomographic imaging are presented as figures on the following pages.

Table 3-1: Macroscopic Defect Scores by Site (method in section 3.3.1)

	Site	*n*	Mean Rank
A-Slice	Lateral Parasagittal Groove	24	60.52
	Sagittal Ridge	24	77.85
	Medial Parasagittal Groove	24	71.94
C-Slice	Lateral Parasagittal Groove	24	92.58
	Sagittal Ridge	23	40.09
	Medial Parasagittal Groove	24	87.69
All Sites	**Total**	143	
Kruskal-Wallis Test	**Asymptotic Significance**		< 0.001

Table 3-2: No effect of preconditioning exercise on macroscopic defect score

	Treatment Group	*n*	Mean Rank	Sum of Ranks	Asymptotic Significance
Medial groove pathology	Control	24	24.50	588.00	
	Exercised	24	24.50	588.00	
	Total	48			1.000
Lateral groove pathology	Control	24	25.83	620.00	
	Exercised	24	23.17	556.00	
	Total	48			0.477
Sagittal ridge pathology	Control	24	24.33	584.00	
	Exercised	23	23.65	544.00	
	Total	47			0.844

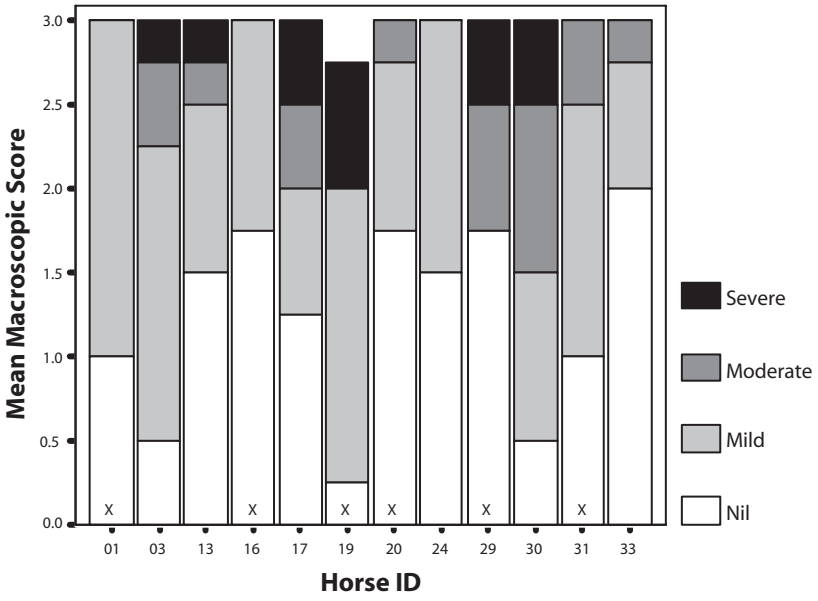

Figure 3-2: Proportionate Macroscopic Defect Scores Pooled by Site and Horse

Preconditioned horses marked with 'X'

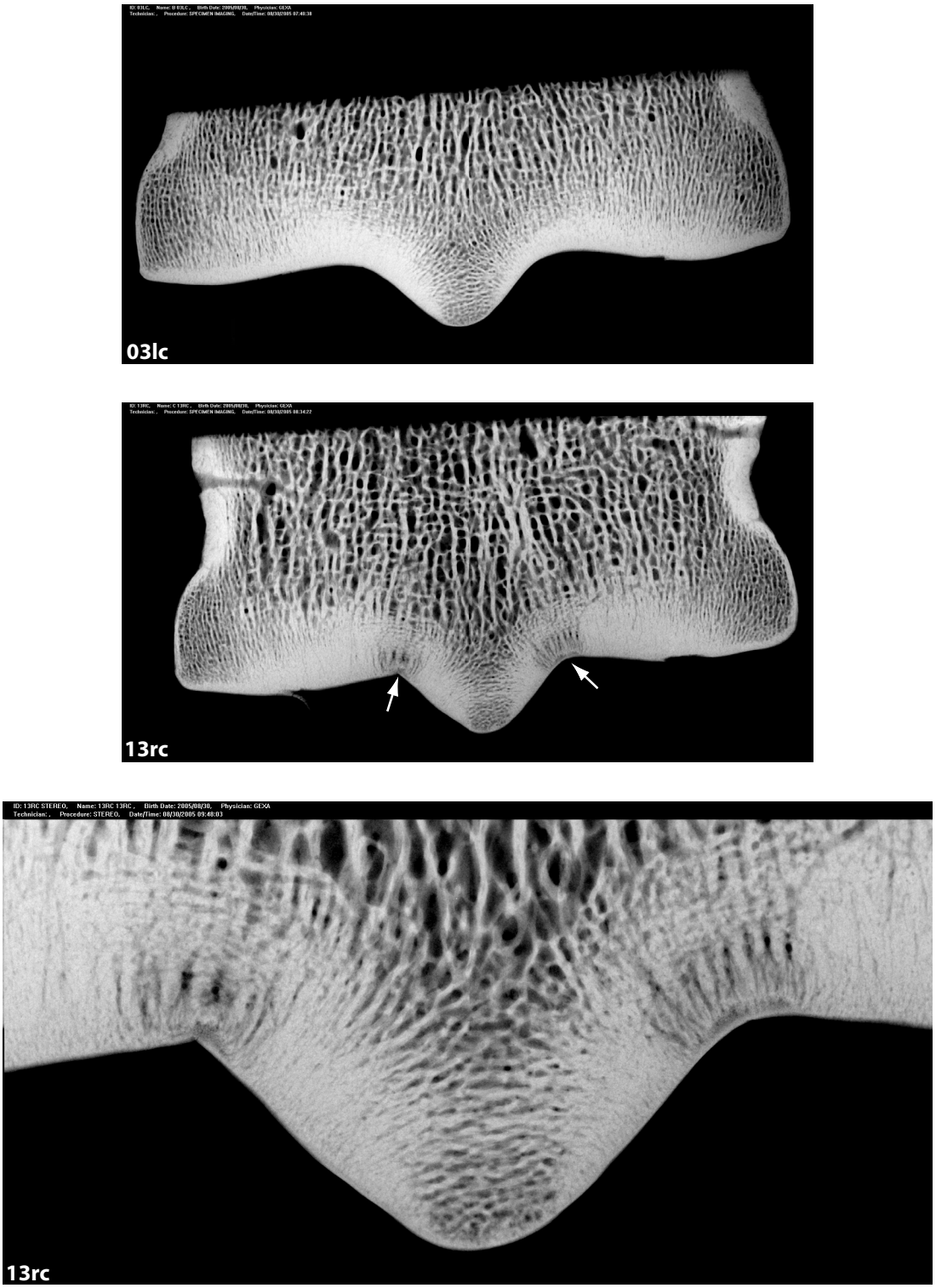

Figure 3-3: Variation in palmar slice morphology - digital microradiographs

Left and right C-slices (lc & rc) from two horses' Mc3. Note the variation in the parasagittal grooves' radii of curvature and subchondral bone morphology. The lateral parasagittal groove in 13rc has a very small radius of curvature and both grooves show evidence of subchondral bone lysis (arrows). Field width 59.3 mm (top, middle); 29.7 mm (bottom). Lateral to left.

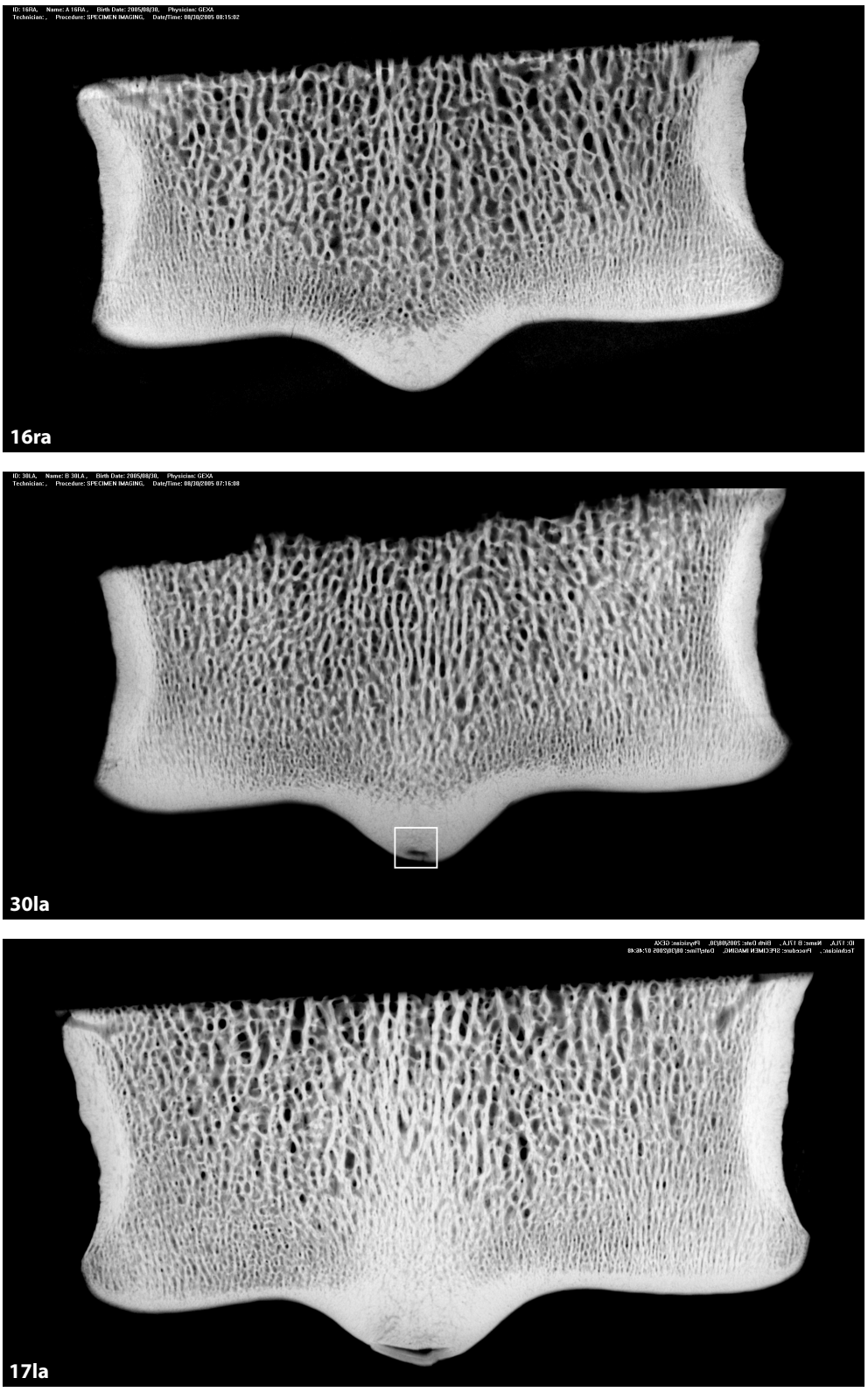

Figure 3-4: Variation in dorsal slice morphology - digital microradiographs

A-slices displaying subchondral bone densification and osteochondral defects of the sagittal ridge. Box in 30la is enlarged in Figure 3-5. Note the axial region of bone sclerosis, in contrast to sclerosis deep to the condyles seen in the C-slices (Figure 3-3). Field width 59.3 mm.

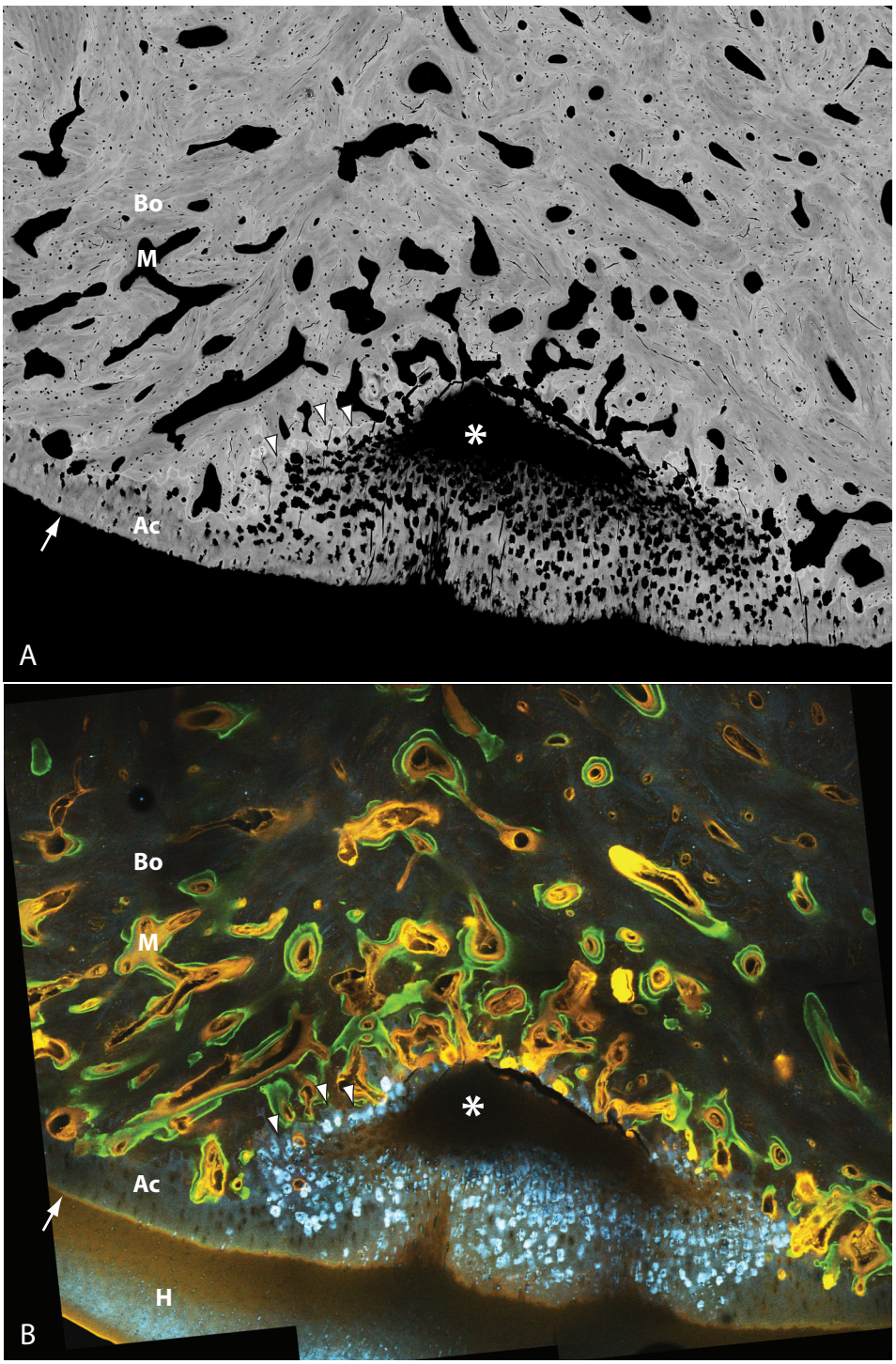

Figure 3-5: Thickened ACC on sagittal ridge in qBSE and CSLM

Montaged and registered BSE SEM (A) and CSLM (B) images demonstrating a region of thickened ACC on the sagittal ridge of the dorsal slice from the left Mc3 of horse 30. Grey level in A is proportional to mineralisation density; in B, green bands are calcein labels, blue is reflected light and yellow / orange is mainly tissue autofluorescence. Note partial to complete lack of mineralisation in deep portions of thickened ACC (*) surrounded by intense bone remodelling activity. H, hyaline articular cartilage; Ac, ACC; Bo, bone; M, marrow space; single arrow, ACC mineralising front; arrowheads, cement line at osteochondral junction. Image width 3.44 mm, 6 fields per image.

3.5 Discussion

A wide variety of morphologies was seen in the distal condyles of Mc3 from the 12 18-month-old horses examined in this chapter. Variation was particularly notable in the parasagittal grooves of the C-slices and on the sagittal ridges of the A-slices. Parasagittal grooves displayed variation in their radii of curvature and the apparent density and orientation of subchondral bone. Of particular interest was the appearance of linear defects involving ACC and subchondral bone within the parasagittal grooves of several C-slices: 4 of 12 lateral parasagittal grooves (horses 13, 20, 24 & 29) showed cracks extending through the ACC layer into subchondral bone in μCT reconstructions. Minor cracks are expected to be caused as artefacts of ethanolic dehydration, conceivably the PMMA oligomer-to-polymer polymerisation shrinkage and super-drying in the SEM vacuum. However, the cracks seen in these specimens were larger than the usual artefacts and were associated with evidence of bony remodelling, and must therefore have existed prior to tissue processing.

Variation in the radius of curvature of the parasagittal grooves was evident. Stress concentration increases as the radius of curvature decreases, so it is likely that stress distribution is greater in those Mc3 with a sharp angle or linear defect in the parasagittal groove than those with a smoothly curved parasagittal groove. In an elliptical crack of length 2a and width 2b, under an applied external stress σ, the stress at the ends of the major axes is given by:

Equation 3.1

$$\sigma_{max} = \sigma\left(1 + 2\frac{a}{b}\right) = 2\sigma\sqrt{\frac{a}{\rho}}$$

where ρ is the radius of curvature of the crack tip. A stress concentration factor is the ratio of the highest stress (σ_{max}) to a reference stress (σ) of the gross cross-section. As the radius of curvature approaches zero, the maximum stress approaches infinity. The stress concentration factor is a function of the geometry of a crack, and not of its size (Anderson 2005). Thus, a deep, narrow trench in ACC and subchondral bone is likely to reduce the energy required to initiate fracture in this region.

Linear defects of the distal condyle of Mc3 have not previously been demonstrated in horses prior to race training, though they have been associated with clinical fracture in trained, racing Thoroughbreds. Preconditioning exercise was not statistically related to the occurrence of linear defects in the 12 horses under study, perhaps due to its relatively low intensity and because it was superimposed upon ad-libitum pasture exercise. It was previously thought that linear defects were the result of fatigue failure due to the physical demands of training and racing, however the existence of linear defects prior to race training whose incidence or severity is not appreciably affected by 30% increased CWI rather suggests an aetiology independent of training activity.

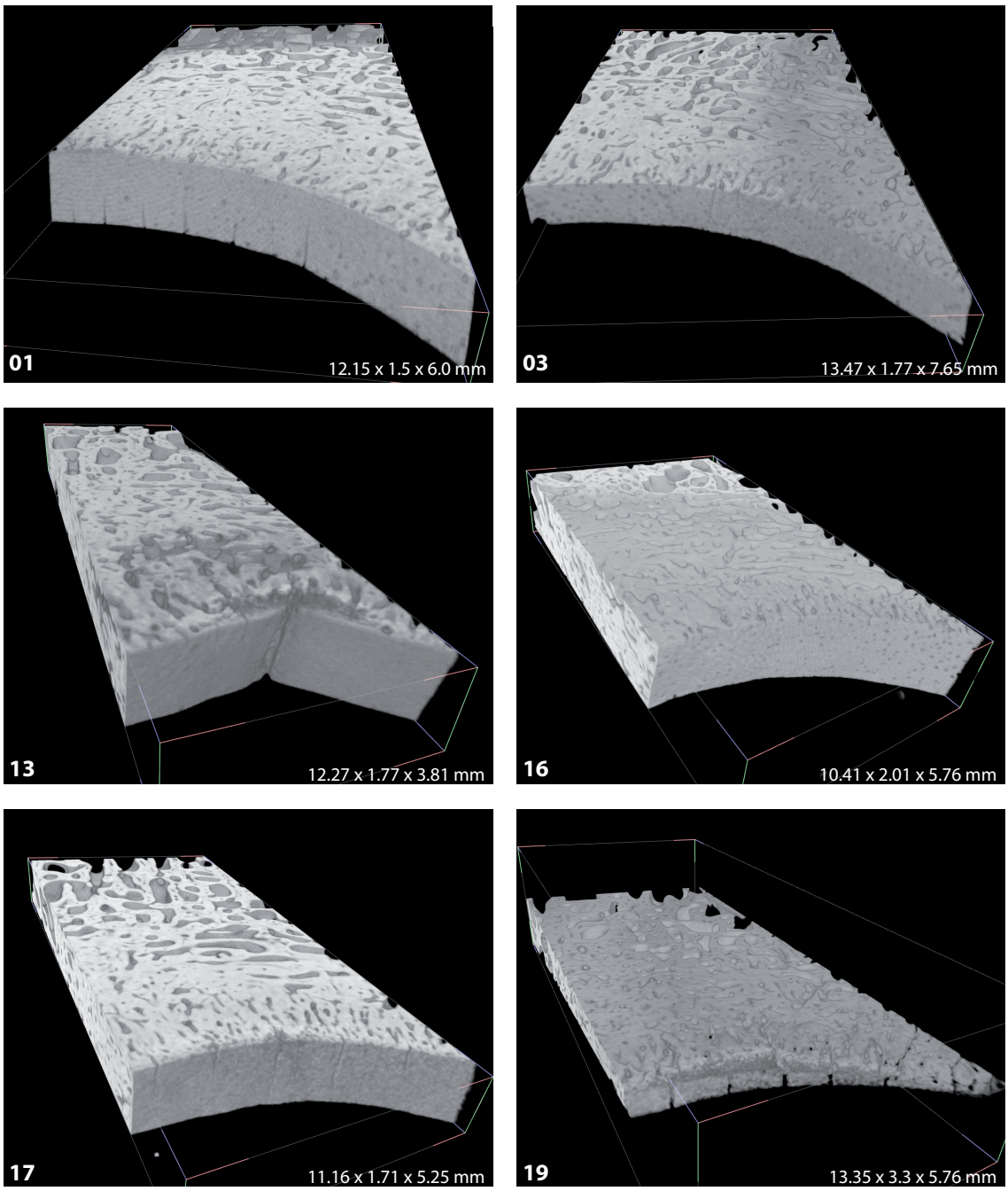

Figure 3-6: 3D rendered reconstructions of µCT data showing mineralised tissue

Lateral parasagittal grooves from the right C-slices of the 12 18-month-old horses were imaged in µCT and rendered in Drishti. Specimen dimensions are indicated on each projection. All projections show the ACC layer in the foreground and the proximal cut surface in the background. Note the variation in parasagittal groove curvature, ranging from a high radius of curvature (03, 16) to low radius of curvature (13). Also note the defects in the superficial ACC layer (13, 29, 33), which are closely related to thickened, poorly mineralised ACC and enlarged subchondral bone marrow spaces.

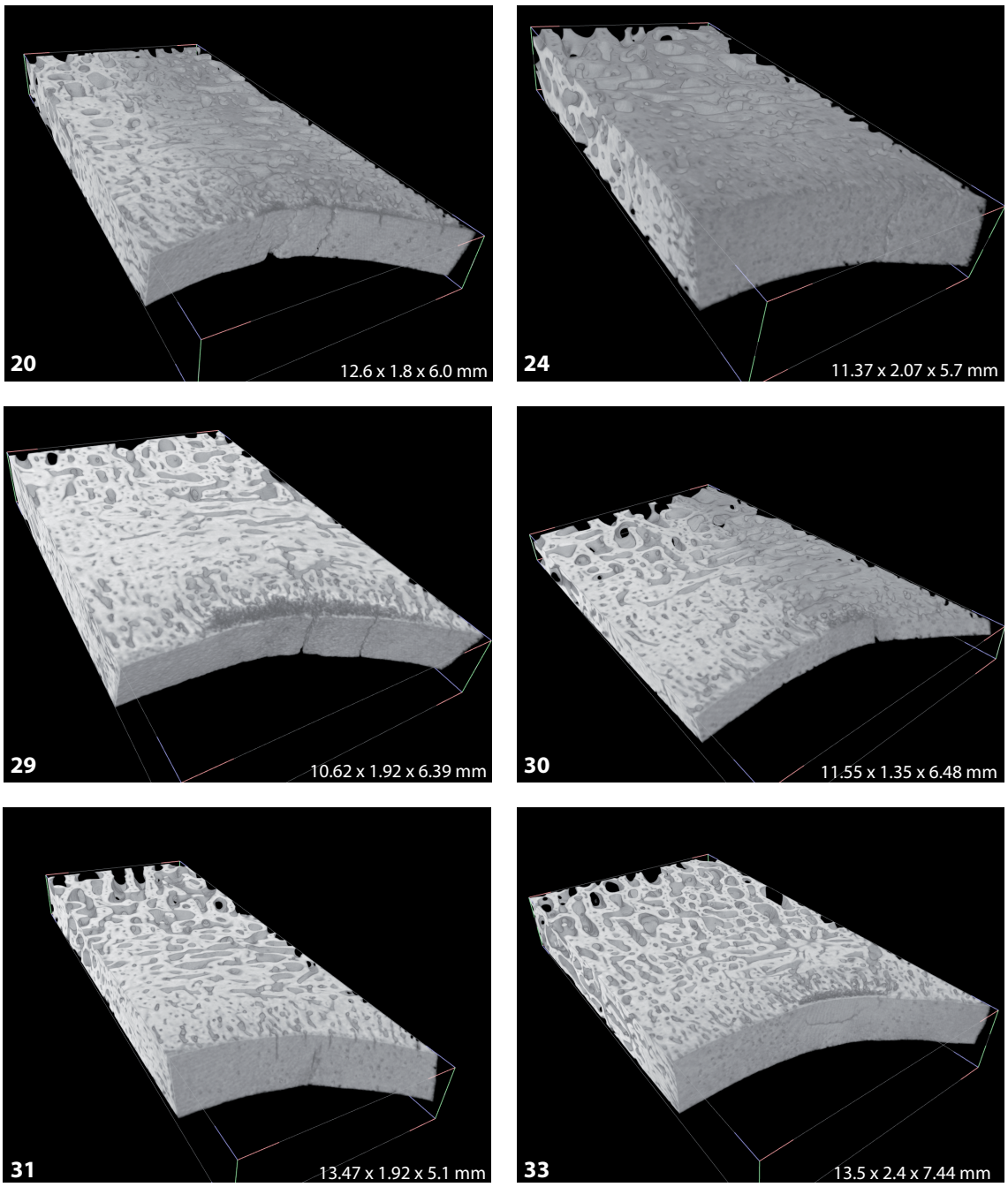

Given the limited number of horses in the study, it can only be cautiously estimated that as many as one third of Thoroughbred horses entering race training as rising 2-year-olds might already have moderate to severe linear defects in their lateral parasagittal grooves. Thorough investigations using high-resolution non-invasive imaging techniques and/or opportunistic post-mortem examinations on a larger number of Thoroughbreds are required to define fully the linear defect prevalence prior to race training. Whether such defects contribute to condylar fracture is not yet known. However, it is known that notches within bone substantially reduce fracture energy by as much as an order of magnitude (Currey, Brear and Zioupos 2004). Interestingly, the subchondral

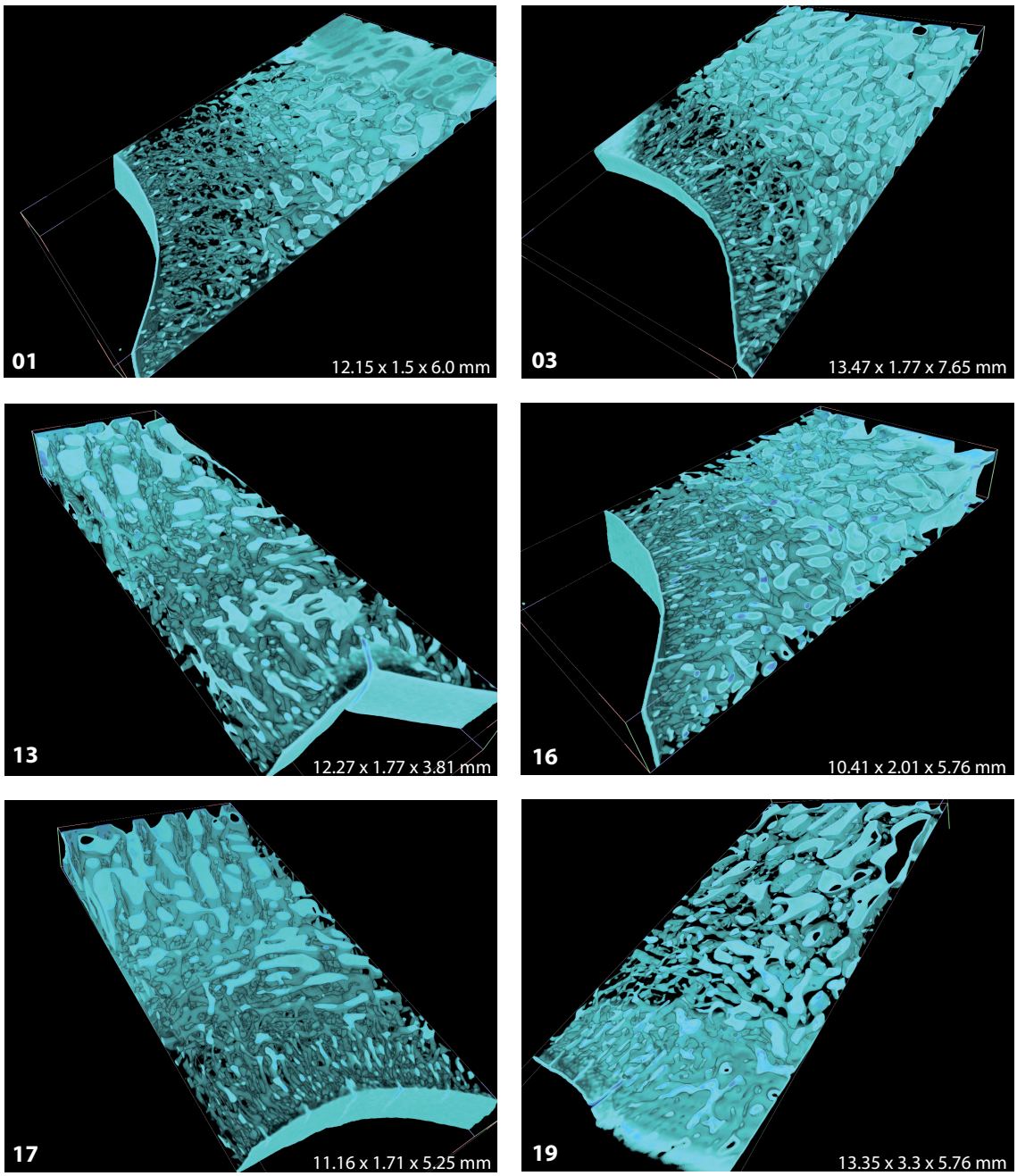

Figure 3-7: 3D rendered reconstructions of µCT data showing marrow spaces

The µCT data were rendered with Drishti using a transfer function that rendered the mineralised tissue / unmineralised tissue boundary as blue and all other components (bone, ACC, HAC, PMMA, air) as transparent. Variation in marrow space size and orientation is obvious: note the enlarged marrow spaces just deep to ACC in the parasagittal grooves communicating with cracks penetrating ACC (13, 20). Other parasagittal grooves (01, 03, 17) show small, organised marrow spaces deep to ACC, with a layer in a radial orientation immediately deep to ACC, a tangentially oriented layer deep to that, and finally, proximo-distally oriented marrow spaces in the trabecular plate portion of the epiphysis.

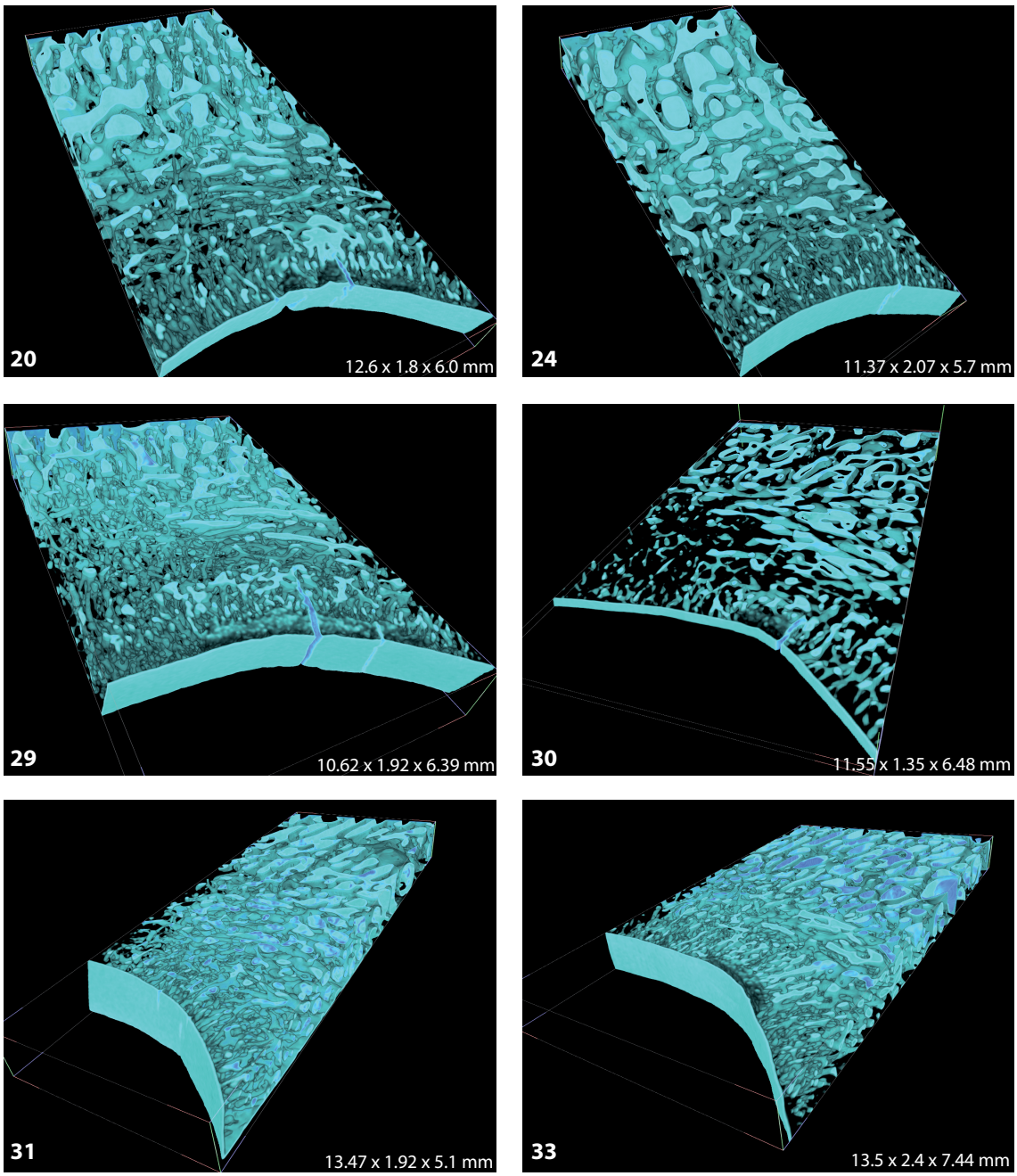

bone defects in the parasagittal grooves of specimen 13rc are on a very similar scale to the stress risers artificially induced by Currey, Brear et al. (2004), being on the order of 2 mm long with a 400 µm diameter crack tip (Figure 3-3). It follows that linear defects existing prior to race training are likely to act as stress risers, hastening the development of fatigue fracture and ultimately leading to condylar fracture of Mc3.

4: CSLM and qBSE Co-registration studies

4.1 Summary

Combined backscattered electron scanning electron microscopy (BSE SEM) and CSLM was used to put tissue mineralisation data into the context of soft tissue histology and fluorescent label information. Mineralisation density (Dm) and linear accretion rate (LAR) are quantifiable parameters associated with mineralising fronts within calcified tissues. Quantitative BSE (qBSE) may be used to determine Dm, while CSLM may be used to detect label fluorescence, from which LAR is calculated. Eighteen-month-old Thoroughbred horses received single calcein injections 19 and 8 days prior to euthanasia, labelling sites of active mineralisation with fluorescent bands. CSLM images of ACC from distal third metacarpal condyles were registered to qBSE images of the same sites using an in-house program. ImageJ and Sync Windows enabled the simultaneous collection of LAR and Dm data. The repeatability of the registration and measurement protocols was determined. Dm profiles between calcein labels were explored for an association with time. Dm was 119.7 ± 24.5 (mean ± SD) grey levels (where 0 = backscattering from monobrominated and 255 from monoiodinated dimethacrylate standards respectively), while modal and maximum LAR were 0.45 and 3.45 $\mu m \bullet d^{-1}$ respectively. Coefficients of variation (CV) for Dm were 0.70 % and 0.77 % with and without repeat registration respectively. CVs for LAR were 1.90 % and 2.26 % with and without repeat registration respectively. No relationship was identified between Dm and time in the 11 day inter-label interval. Registration of CSLM to qBSE images is sufficiently repeatable for quantitative studies of equine ACC.

4.2 Introduction

Mineralisation density (Dm) of hard tissues is a key component of their structural and functional biology; for example, increased Dm of ACC is associated with increased elastic modulus (Ferguson, Bushby and Boyde 2003; Gupta, Schratter, Tesch, Roschger, Berzlanovich, Schoeberl, Klaushofer and Fratzl 2005). Quantitative backscattered electron scanning electron microscopy (qBSE) is a well-established technique for the determination of mineral content within the ultrastructure of biological specimens (Boyde, Reid and Howell 1983; Howell and Reid 1986; Reid and Boyde 1987; Mechanic, Arnaud, Boyde, Bromage, Buckendahl, Elliott, Katz and Durnova 1990; Boyde, Howell, Bromage, Elliott, Riggs, Bell, Kneissel, Reid, Jayasinghe and Jones 1992; Boyde, Elliott and Jones 1993; Gomez and Boyde 1994; Vajda, Skedros and Bloebaum 1995; Roschger, Fratzl, Eschberger and Klaushofer 1998; Misof, Roschger, Tesch, Baldock, Valenta, Messmer, Eisman, Boskey, Gardiner, Fratzl and Klaushofer 2003; Zizak, Roschger, Paris, Misof, Berzlanovich, Bernstorff, Amenitsch, Klaushofer and Fratzl 2003; Loveridge, Power, Reeve and Boyde 2004). The cubic micron resolution afforded by qBSE offers a significant advantage over other methods of densitometry, such as DXA (110 μm x 110 μm x sample thickness in GE Lunar PIXImus), peripheral quantitative computed tomography (pQCT; 8x106 to 512x106 μm^3), μCT (typically 1000-8000 μm^3) and bulk chemical analysis. Quantitative BSE is the only method currently available that can study Dm at less than 1 μm resolution on specimens as large as 70 mm x 70 mm.

CSLM is especially well suited to the examination of hard tissues due to its ability to section thick specimens optically, thus obviating thin section preparation and the resultant damage to the tissue. The CSLM pinhole greatly reduces blurring in the image due to reflected and fluorescent light produced outside the optical section (Inoué 1995). Images of labels obtained with CSLM are thus of much greater spatial resolution than those obtained with conventional reflection or fluorescence microscopy.

Intra-vital labelling of mineralised tissues is an established method for the identification of active mineralising fronts (Frost 1962). Fluorescent dyes that localise at mineralising fronts are injected into the subject prior to euthanasia and the time of injection recorded. Periodic injection of labels documents the changing position of the mineralising front. Regions containing multiple labels can be used for the measurement of the rate of advancement of the mineralising front. The distance between labels, linear accretion (LA), is divided by the time between labels to calculate linear accretion rate (LAR).

Little attention has been paid to the LAR of ACC, despite the importance of ACC in osteoarthritis, osteochondrosis and intra-articular fracture. Thoroughbred racehorses commonly fracture the distal condyle of the Mc3 (Verheyen and Wood 2004). Typically, pathological changes are found in the ACC and subchondral bone adjacent to the fracture (Riggs 1999; Riggs, Whitehouse and Boyde 1999a). Similar changes may be identified in intact Mc3 condyles, indicating that pathology precedes the fracture. Qualitative work in Chapter 3 identified osteochondral anomalies in the parasagittal grooves of horses that had not yet entered race training. Work described in this chapter sought to develop microscopic techniques with which the dynamics of cartilage mineralisation and resorption in endochondral ossification of ACC can be studied.

Registration of CSLM and qBSE images of bone and cartilage results in a unique qualitative and aesthetic effect by combining soft tissue, intra-vital label and mineralised matrix Dm information (Boyde 2003; Boyde and Firth 2004; Boyde, Lovicar and Zamecnik 2004; Boyde and Firth 2005a). An analogous approach has been used to correlate bone collagen orientation information determined by circularly polarised light (CPL) microscopy with bone mineralisation information determined by qBSE (Goldman, Blayvas, Boyde, Howell, Clement and Bromage 2000). However, in this case the CPL contrasts derive from the entire section thickness of, e.g., 100 µm, whilst the CSLM data can be derived from the superficial 1µm, closely matching the BSE escape depth. Unmineralised tissues and intra-vital labels can be clearly visualised in the context of the mineralised components of bone and cartilage. While CSLM and qBSE have been used independently for the measurement of mineralised tissue parameters, their combined use for quantitative study had not been previously validated. This study tested the hypothesis that registration of CSLM to qBSE images is sufficiently repeatable to be used for quantitative analyses of mineralising tissues.

4.3 Techniques

4.3.1 Labelling of Mineralising Fronts

The identification of mineralising fronts in animal tissue by injection of intravital dyes has its origins in the observation of red discolouration of pig bone and dentine after their feeding on madder-contaminated bran (Belchier 1738a). Feeding of madder-root to a rooster resulted in red-discoloured bones (Belchier 1738b), leading to the hypothesis that the animals' circulation delivered the dye from ingested madder to bone. Refinement of the technique resulted in the modern practice of injecting pure dyes such as tetracyclines, calcein green, calcein blue and alizarin red S - the latter originally being derived from red madder (Frost 1962). These dyes have the property of selective and long-term incorporation into active mineralising fronts. Multiple injections over time result in a series of coloured bands deposited in the mineralised tissue, from which the rate of mineralising front advancement may be calculated. The double (or multiple) labelling technique has been successfully applied to observe progression of the ACC mineralising front (Lemperg 1971; Revell, Pirie, Amir, Rashad and Walker 1990; O'Connor 1997).

Calcein is a fluorescent dye originally derived from fluorescein isothiocyanate (FITC). It is incorporated into mineralising fronts in bone, cartilage and dentine through its ability to bind to divalent cations, including Ca++. Calcein fluorescence is readily detected by the use of fluorescein filter sets or spectral detection in the green range. Calcein fluorescence is excited maximally by the 488 nm band of light produced by Kr/Ar laser sources commonly employed in CSLM (Invitrogen 2006).

4.3.2 Quantitative Backscattered Electron Scanning Electron Microscopy (qBSE)

qBSE is an established histological method for the determination of compositional contrast within mineralised tissues including bone (Reid and Boyde 1987; Boyde, Howell, Bromage, Elliott, Riggs, Bell, Kneissel, Reid, Jayasinghe and Jones 1992; Boyde, Travers, Glorieux and Jones 1999), ACC (Ferguson, Bushby and Boyde 2002; Ferguson, Bushby and Boyde 2003), cement line (Skedros, Holmes, Vajda and Bloebaum 2005) and dentine (Angker, Nockolds, Swain and Kilpatrick 2004b). The backscatter current is proportional to the mean atomic number of the region of the specimen under examination. The analogue current signal is digitised into 256 bins, which are subsequently given grey values for visualisation and analysis. More densely mineralised tissues have higher average atomic numbers (Z) and therefore have higher digital bin values. Comparison of specimen backscatter current to known standard backscatter objects allows the normalisation of BSE current readings to a quantitative scale.

Halogenated methacrylates have been validated as effective standards for bone and calcified cartilage as they have backscatter coefficients just greater and lesser than mineralised bone and cartilage. This is in contrast to elemental backscatter standards such as Al and C, whose backscatter coefficients are well beyond those typically found in mineralised tissues and in which channelling contrast due to cystallographic grain orientation occur and may override the *Z* contrast. Histogram peaks within BSE images of backscatter standards yield two standard grey levels. Pixel grey values within the specimen image (p) are normalised (p_n) by subtracting the grey value of the lower standard (b), multiplying by the bin range (r, 255 for 8-bit images) and dividing by the difference between the higher (i) and lower standard grey values (Equation 4.1). Standards used for this thesis were polymers of monobrominated-dimethacrylate and monoiodinated-dimethacrylate.

Equation 4.1

$$p_n = \frac{(p-b)\cdot r}{i-b}$$

Mean atomic number changes during exposure to the electron beam, resulting in an increase in backscatter coefficient and bleaching of the image. Prolonged exposure of bone specimens to the electron beam leads to loss of the embedding PMMA (as is extremely well known in electron beam fabrication) leading to elevated BSE signal after over-exposure. Energy dispersive x-ray (EDX) analysis has been used to confirm the loss of carbon, mainly from PMMA (Bloebaum, Holmes and Skedros 2005). To avoid this artefact it is important to minimise specimen exposure and to ensure that all sites receive similar and minimal exposure to the electron beam.

Surface topography is detected in BSE mode and may interfere with measurements of mean atomic number. Ridges give greater surface area for the escape of backscattered electrons so are artefactually bright, while grooves reduce the amount of backscattering and appear artefactually dark. It is imperative for strictly compositional backscattered imaging that the surface under examination be as flat as possible. Diamond ultramilling produces a flatter surface than polishing and consequently less than half the topographic contrast caused by polishing (Howell and Boyde 1999).

4.4 Materials and Methods

4.4.1 Microscopy

For CSLM, specimens were coverslipped with glycerol and examined using a Leica DMRBE with an SP2 confocal scanhead and 40x/1.0 NA objective (Leica Microsystems Ltd, Knowlhill, Milton Keynes, UK). A 40x/1.0 NA objective was used because the lower magnification lens (25x/0.75 NA) did not give adequate spatial resolution to quantify LAR, and the higher magnification lens (63x/1.4 NA) reduced the field of view to approximately 238 μm, limiting the length of ACC imaged at each site. Excitation was at 488 nm: orange-red (mainly tissue autofluorescence), green-yellow (dominated by calcein fluorescence where present) and reflection signals were collected into red, green and blue channels respectively. Images were saved as 1024 x 1024 pixel RGB TIFF files. Seven defined sites within ACC were examined per specimen. Images were made only if double calcein labelling was present at a site. Care was taken to sample only the

most superficial image plane of the specimen. Blocks were levelled in a custom device using Plasticine™ on a glass slide.

Following CSLM, specimens were carbon coated and the same ACC sites imaged with a Zeiss DSM 962 SEM (Zeiss UK Ltd, Welwyn Garden City, Herts, UK) in BSE mode at nominal 200x magnification (field width 446 µm). This magnification gave a qBSE image field larger than that of the CSLM image, allowing for some adjustment in the position of the CSLM image without loss of information. Standard settings (20 kV accelerating voltage, 17 mm working distance, filament current saturated, beam current 0.8 – 1.0 x 10^{-9} A) were used on all images. The BSE detector contrast and brightness settings were altered to set the monobrominated dimethacrylate standard to a grey level of around 50/255, and the monoiodinated dimethacrylate standard to a grey level of around 200-235/255 to allow maximum dynamic range in ACC image grey levels. Kontron IBAS external control was used to automate image acquisition of specimen sites and monobrominated and monoiodinated dimethacrylate standards. Images were collected in 8-bit greyscale at 2048 x 2048 pixels in the Zeiss IMG file format. Standard grey levels were automatically extracted from images of the halogenated dimethacrylate standards with an ImageJ macro (TwinPeaks: Appendix 3.1.1, p. 159). Specimen IMG files were converted to TIFF and their grey level normalised against the standards (Howell, Davy and Boyde 1998).

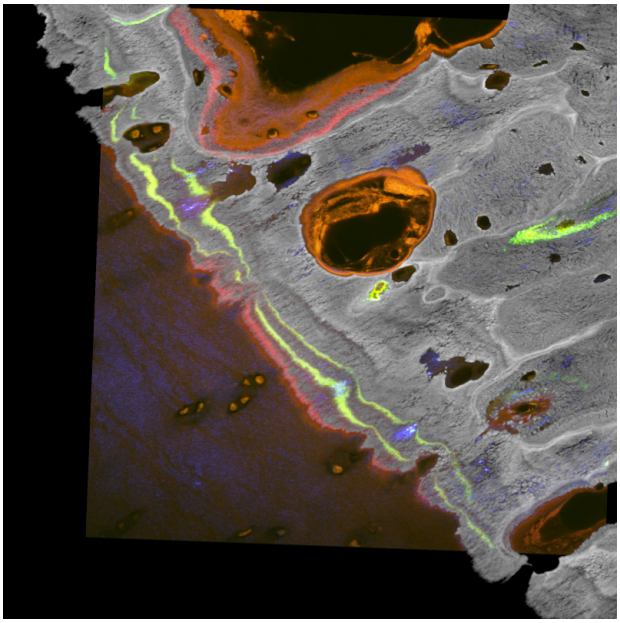

Figure 4-1: CSLM image registered to qBSE image.

Image pair registered using in-house Honza's program. The qBSE image is retained unaltered while the CSLM image is scaled, translated, rotated and sheared to align 3 pairs of user-defined points. Calcein labels are clearly visible as green bands within ACC, marking the positions of the mineralising front 8 and 19 days prior to euthanasia. A third red line of endogenous fluorescence can be seen at the mineralising front, most likely originating as a post-mortem artefact from an haematogenous porphyrin. Field width 446 µm.

An in-house program ('Honza's') was used to register CSLM images to qBSE images (Boyde, Lovicar and Zamecnik 2004). Three matching structural features were identified on each image. The program applied scale, translation, rotation and shear transformations to the CSLM image, while leaving the qBSE image in place. Successful registration was judged as a state where morphological features were aligned across the entire image (Figure 4-1).

Often, several combinations of points were tested before registration was deemed correct. Registered image pairs were then analyzed in ImageJ v1.34 (Rasband 2005) with the Sync Windows plugin (Walter 2004) activated (Figure 4-2). Sync Windows enables measurements of qBSE image grey level to be made using spatial references from a CSLM image of calcein labels.

Repeatability of the registration process was quantified by registering the 5 image pairs 5 times each, then measuring Dm and linear accretion (LA) multiple times per registration attempt. Five image pairs from one bone slice were selected due to their bright calcein labels. Dm and linear accretion were measured with ImageJ's straight line measurement tool, set to 5 pixels width. Dm was the mean grey value of pixels within the 5-pixel-wide line tool selection. LA was the distance between the start and endpoints of the selection. A series of measurements (n = 59 to 110 per image) were made along the entire length of paired calcein labels in the ACC, at approximately

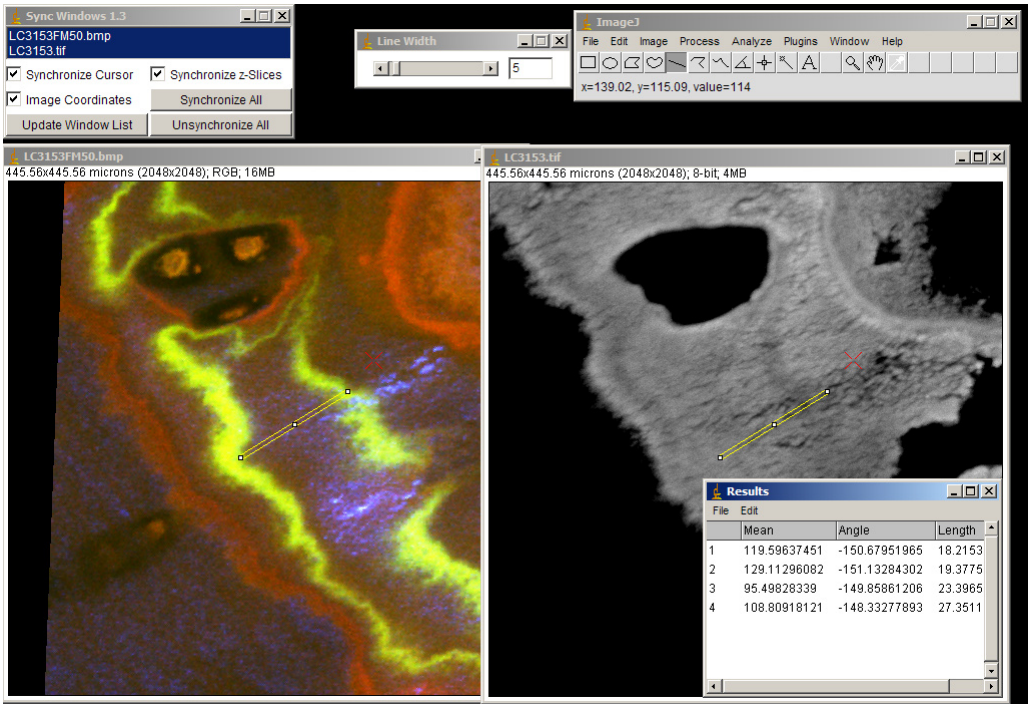

Figure 4-2: Measurement of Dm using calcein labels as reference points.

The original qBSE image and registered CSLM image are opened in ImageJ and synchronised using Sync Windows. The cursor and ROI positions are identical in each image, so that the ROI can be placed on the qBSE image using the calcein labels in the registered CSLM image as spatial references. ROI length marked on image = 27.35 µm.

5 µm intervals. Means of Dm and LA were calculated for each image pair and these were used to calculate coefficients of variation (CV) for the 5 registration attempts of each image pair (Excel 2002, Microsoft). Dm and LA were measured as above and repeated 5 times on one registration attempt from each of the 5 image pairs in order to isolate the effect of registration from the effect of the measurement protocol. LAR was calculated by dividing LA by 11 days. Regression and Pearson correlation (measures of linear association) were calculated to examine relationships between LAR and Dm (SPSS v11.0.0, SPSS Inc, Chicago, IL).

To investigate a potential trend in Dm versus time, Dm versus displacement was measured with the ImageJ Profile Plot function. Dm data were recorded from 5-pixels-wide line selections at 5 µm intervals along paired labels in ACC. One registration attempt on each of 20 sites total from 3 horses was examined. Because LAR varied markedly within and between each site, Dm versus displacement data was converted into Dm versus time data by stretching displacement data to the inter-label time (11 days).

4.5 Results

Measurement sets from 5 registration attempts on images from 5 sites had a mean CV of 0.70 % and 1.90 % for Dm and LA respectively (Tables 4-1 and 4-3). Five sets of repeat measurements on one registered image pair per site gave a mean CV of 0.77 % and 2.26 % for Dm and LA respectively (Tables 4-2 and 4-4). ACC Dm was normally distributed with a mean ± SD of 119.7 ± 24.5 grey units.

ACC LAR was positively skewed with a peak at 0.45 $\mu m \cdot d^{-1}$, mean ± SD of 0.89 ± 0.51 $\mu m \cdot d^{-1}$ and maximum of 3.45 $\mu m \cdot d^{-1}$ (Figure 4-3). A small but statistically significant Pearson correlation was identified between LAR and Dm ($r = 0.114$, $p < 0.01$), while regression analysis showed $R^2 = 0.013$ ($p < 0.001$). No significant correlation between Dm and time was found in the 11 day inter-label period.

4.6 Discussion

Registration of CSLM and qBSE images can be performed with sufficient repeatability for large scale surveys of ACC. No loss of repeatability was caused by the registration step. The greatest source of variability appears to be the measurement protocol itself, which requires substantial user interaction. Subtraction of images from sequential CSLM registration attempts reveals imperfectly repeated processes as the resulting images are not all black, highlighting discrepancies. In our hands, these variations are not great enough to affect the outcome of LAR and Dm measurements substantially.

It is interesting to note that repeatability of LA measurement was worse in 3 out of 5 sites when only repeated measurement - and no repeated registration - was performed. Inter-session random operator error is a factor that will require attention. This highlights the need for clear criteria for the placement of regions of interest.

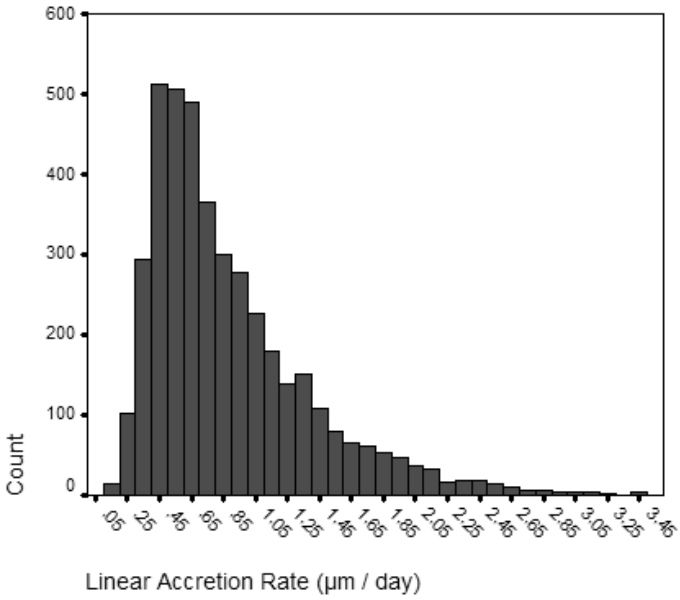

Figure 4-3: Histogram of ACC LAR.

The peak corresponds to an LAR of 0.45 µm•d^{-1}, while the mean ± SD LAR was 0.89 ± 0.51 µm•d^{-1}. The maximum of 3.45 µm•d^{-1} demonstrates significant range within which LAR may be regulated.

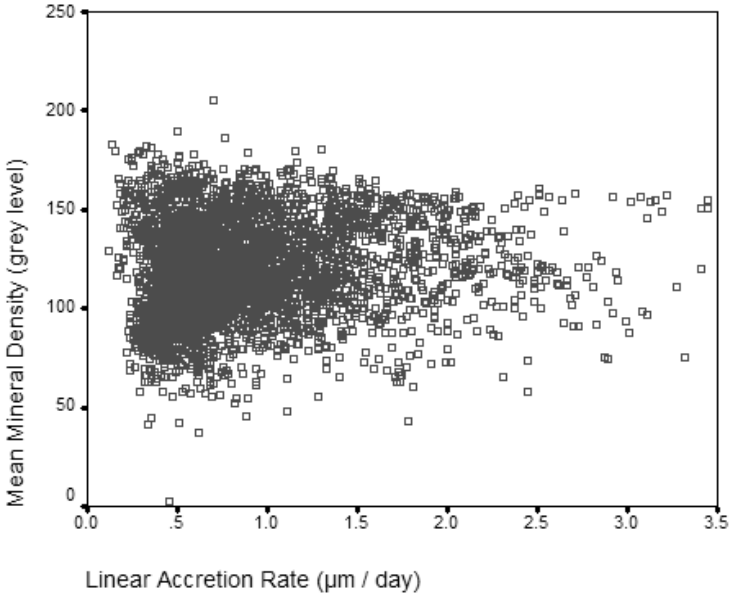

Figure 4-4: Dm versus LAR scatter plot

The slight trend indicated by Pearson correlation ($r = 0.114$, $p < 0.01$) is difficult to identify, and may be caused by the string of outliers to the top right of the plot.

Table 4-1: Mean value of each Dm measurement set per site for each repeated registration attempt

Site	Dm Repeat Registration 1	Dm Repeat Registration 2	Dm Repeat Registration 3	Dm Repeat Registration 4	Dm Repeat Registration 5	Mean ± SD	CV
1	118.81	119.95	121.15	120.99	119.83	120.14±0.96	0.80%
2	118.76	119.20	119.51	119.23	116.99	118.74±1.01	0.85%
3	128.28	129.44	128.34	129.15	130.89	129.22±1.06	0.82%
4	154.31	154.84	156.03	155.12	155.16	155.09±0.63	0.40%
5	125.55	125.30	123.40	123.44	123.45	124.23±1.10	0.88%
Mean CV							0.70%

Table 4-2: Mean value of each Dm measurement set per site for 5 repeated measurement sets

Site	Dm Repeat 1	Dm Repeat 2	Dm Repeat 3	Dm Repeat 4	Dm Repeat 5	Mean ± SD	CV
1	118.87	117.23	120.38	119.70	120.12	119.26±1.27	1.06%
2	118.71	119.91	119.08	119.06	120.67	119.48±0.80	0.67%
3	127.70	128.65	129.33	125.90	125.85	127.49±1.58	1.24%
4	154.85	154.45	153.19	154.23	154.25	154.20±0.61	0.40%
5	125.37	124.30	123.87	123.98	124.81	124.46±0.62	0.50%
Mean CV							0.77%

Table 4-3: Mean value of each LA measurement set per site for each repeated registration attempt

Site	LA Repeat Registration 1	LA Repeat Registration 2	LA Repeat Registration 3	LA Repeat Registration 4	LA Repeat Registration 5	Mean ± SD	CV
1	13.52	12.81	12.81	13.08	13.35	13.11±0.32	2.42%
2	12.65	11.98	12.56	12.34	12.56	12.42±0.27	2.17%
3	8.57	8.86	8.59	8.58	8.54	8.63±0.13	1.51%
4	15.43	15.79	15.78	16.19	15.88	15.82±0.27	1.72%
5	10.53	10.03	10.28	10.17	10.36	10.28±0.19	1.83%
Mean CV							1.9%

Table 4-4: Mean value of each LA measurement set per site for 5 repeated measurement sets

Site	LA Repeat 1	LA Repeat 2	LA Repeat 3	LA Repeat 4	LA Repeat 5	Mean ± SD	CV
1	13.82	12.71	13.26	13.28	13.02	13.22±0.41	3.09%
2	12.20	12.13	12.01	12.04	11.92	12.06±0.11	0.87%
3	8.49	8.24	8.20	8.34	8.36	8.33±0.11	1.33%
4	15.54	15.76	16.62	16.50	15.11	15.91±0.64	4.04%
5	10.27	10.28	10.49	9.93	10.25	10.24±1.96	1.96%
Mean CV							2.26%

Calcein labelling in ACC is much more irregular than that seen in lamellar bone. The borders of chondrocyte lacunae at the mineralising front are frequently labelled. Labels from newly deposited bone within resorption cavities within the ACC merge into the ACC labels in places, obfuscating the interpretation of label morphology. Three-dimensional reconstructions of CSLM image stacks from equine ACC show the mineralising front to have a pocked and wrinkled morphology, further complicating the interpretation of ACC mineralising zone labelling. ACC labels must be interpreted in the context of tissue morphology. The labels themselves vary from approximately 0.5 to 6 µm wide (2-30 pixels), and they tend to have bright centres and indistinct edges. The determination of ACC label position is not straightforward, so the logical conclusion is that this is the major source of variability in LAR and Dm measurement.

Alternative methods of label gap determination such as tracing labels, then either calculating the area and dividing by label length or semi-automatic line measurement were rejected. This was due to the complexity of the ACC mineralising zone compared to osteonal and peri- or endosteal mineralising fronts and because these methods still require the operator to identify the label with a cursor. Thresholding, erosion and skeletonisation to find the centres of labels may offer some advantage especially in those images with bright, wide labelling. Faint, narrow or irregular labels are not well identified by the skeletonisation procedure, so it can only be considered as an aid to measuring from the RGB CSLM image. Skeletonisation may offer a better solution for finding the centres of bright regular labels as are typically found in osteonal and trabecular bone systems.

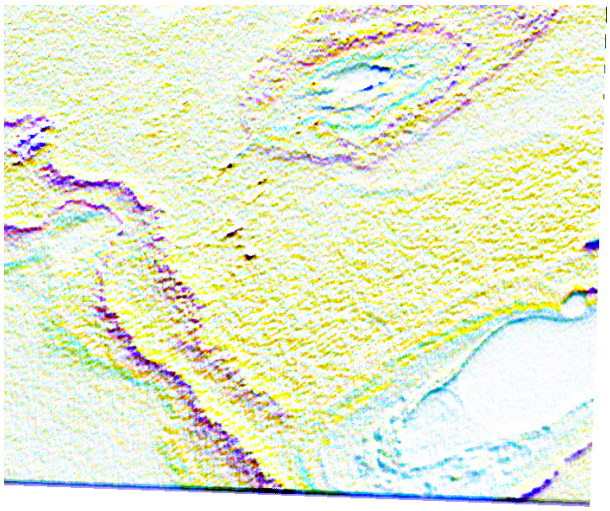

Figure 4-5: Negative of subtracted repeated registration attempts.

Two images from sequential registration attempts using Honza's program were subtracted from each other and colours inverted. The white background of the resulting image indicates only slight variability. The dark line at the bottom of the image represents the region of overhang between the two registration attempts. It is approximately 4 pixels wide, which is a 0.2 % error in a 2048 x 2048 pixel image. Field width = 155 µm.

A slight positive Pearson correlation was found between Dm and LAR, indicating that more rapid advancement of the mineralising front is related to increased deposition of mineral at each point in mineralising cartilage. The regression relationship is weak but statistically significant, indicating that most variation in Dm arises from a source indirectly related to LAR. Similarly, the lack of any significant relationship between Dm and time may be due to the large amount of high frequency noise in Dm vs. time data. It will be interesting to examine these relationships in more regularly mineralised tissue, such as lamellar bone. Labelling animals at greater intervals may demonstrate longer-term trends in mineralised tissue, such as gradual mineral accretion behind the mineralising front, while shorter labelling intervals may highlight short period regulation of Dm and LAR.

Within each site, there were often trends in Dm versus time. No particular trend generalised across all sites. Observed trends were related to the grey level gradients within tidemarks as mineralisation density increased or decreased. Attempts to show changing Dm with respect to time gave no consistent result, perhaps because of small fluctuations in LAR within the inter-label period leading to an inability to assume constant LAR. More frequent labelling may help to overcome this problem.

The spacing of tidemarks relative to the labels indicates that ACC may regulate Dm and LAR over periods of hours to days. This has clear implications for our understanding of endochondral ossification at the epiphysis, as it indicates the responsiveness of chondrocytes to their environment. The lack of consistent correlation between Dm and time may indicate that very little mineral, if any, is deposited or removed from ACC after initial calcification at the mineralising front. Alteration in matrix mineralisation density behind the mineralising might have helped to explain the presence of multiple tidemarks, however, the lack of any correlation between Dm and time suggests that multiple tidemarks are cuased by varying mineralisation density at the mineralising front itself. The interval under study (11 days) may be insufficient to examine this question thoroughly, however.

The term LAR, not mineral accretion rate (MAR), was used in this study to avoid ambiguity. MAR usually refers to the distance between labels divided by inter-label time, but the term does not clearly distinguish whether it is measuring a chemical accretion, millimoles of mineral deposited per unit time, or a spatial accretion. The term MAR was avoided because this experiment measured Dm directly. Monitoring of Dm versus LAR plots by site indicated that there might be a correlation between Dm and LAR within each site, but that the correlation is not consistent between sites and that it generalises weakly. Future measurements may indicate a stronger relationship between Dm and LAR, from which the quantity of mineral deposited per unit space and time may be deduced. Dm measurements at the mineralising front may be the best place to study this phenomenon.

An advantage of measuring Dm from only those tissue regions bounded by labels is that tissue mineralisation occurring during a known period can be studied. Thus, the instantaneous effects on

mineralisation density of in vivo manipulations during the inter-label period can be determined. Dm measurements are not biased or diluted by measurements of bone, or of measurements of tissue mineralised during other periods. Thus, direct comparisons may be made between animals that received or did not receive experimental treatment at a known time.

If we assume constant LAR, an estimate of the lag time between ACC mineralisation and resorption by bone can be made by comparing ACC thickness to LA and the interval between labels. This delay between cartilage mineralisation and vascular invasion must be an important feature of the osteochondral junction. It is clear from the present observations that there is substantial regional variation in Dm, LAR and ACC thickness within individual joints. Thickened regions of ACC are associated with pathologies such as sagittal condylar fracture of Mc3 and osteochondrosis. Understanding the time frame over which pathology occurs may be central to the prevention of disease. ACC LAR and Dm might be considered together as an historical record of the condition of the osteochondral junction. Registration of qBSE and CSLM images is an excellent technique for the examination of this question.

Accurate registration requires that the imaged volumes are as similar as possible, which can only be achieved when the specimen is flat and level. Small landmarks, such as osteocyte lacunae, must be visible in both images for successful registration. Diamond ultramilling is superior to hand polishing specimens in achieving a flat surface. Increased BSE image contrast and consequent inaccuracies in Dm measurements may be caused by topographic relief after polishing, which is substantially reduced after ultramilling (Howell and Boyde 1999).

Prior to the development of CSLM, cathodoluminescence (CL) was used for the simultaneous collection of light and BSE for the detection of fluorescent labels in the SEM (Boyde, Reid and Howell 1983). The obvious advantage of CL is that the specimen need only be prepared for and imaged in one device rather than two. A further advantage is that since the light and BSE radiate from the same point of excitation, image registration is automatic: however, the excitation volume for CL is substantially greater than that for BSE, albeit that the electron beam impact point is identical. Thus CSLM currently far outperforms CL in label detection efficiency, and can be used to distinguish wavelengths in several detection channels and information can be acquired in depth to view the 3D scene. Multicolour label experiments can be performed in the CSLM that are impossible in the SEM unless major advances are made in CL excitation and detection efficiency. This study has shown that registration of qBSE and CSLM images is a repeatable and informative method with clear advantages over CL for the combined study of Dm and LAR in mineralising tissues.

5: Variations in ACC

5.1 Summary

The objective of this study was to relate LAR, mineralisation density, tidemark number and ACC thickness in ACC from multiple regions of the equine third metacarpal distal condyle. Additionally, the effects of exercise during early life on ACC were determined. Six of 12 pasture-raised Thoroughbred horses were exercised from 10 days old. Calcein labels were given 19 and 8 days prior to euthanasia at 18 months old. Osteochondral specimens were cut from the distal Mc3 and embedded in PMMA. Blocks were imaged using CSLM and quantitative backscattered electron scanning electron microscopy (qBSE). ACC thickness and total thickness mineralisation density (TTDm) were measured on montaged qBSE image sets, and LAR (LAR), inter-label mineralisation density (ILDm) and tidemark number on registered CSLM-qBSE image pairs. ACC thickness, mineralisation density, LAR and tidemark count varied significantly between sites. ACC thickness was negatively correlated with LAR. Mineralisation density was positively correlated with LAR. Tidemark count was negatively correlated with LAR. Lag time between the tidemark and cement line was estimated (180 days; range 0-648 days). Exercise had little effect on most parameters, in most sites. Strong site effects indicate sensitivity of the tidemark to biomechanical factors. Coupling of the tidemark and chondroclastic resorption may occur, but the mechanism remains obscure. The major determinant of ACC thickness in 18-month-old Thoroughbred horses' Mc3 is the rate of chondroclastic resorption, not tidemark LAR. Exercising pasture-reared foals causes little additional adaptation in distal Mc3 cartilage. ACC growth flaws may contribute to Mc3 condylar fracture in adulthood.

5.2 Introduction

The mineralising front (tidemark) of ACC is thought to be regulated in response to loading (O'Connor 1997; King, Opel and Rempel 2005), but this process is not well understood. To date, the literature describing the mineralising front is dominated by casual observations of human surgical and post mortem material supplemented by observations in small mammals, particularly rabbits, guinea pigs and rats. Very little quantitative data on the mineralising front exists, and none describes a joint larger than the rat femoro-tibial joint (O'Connor 1997). Advancement of the tidemark may result in thinning of HAC (Lemperg 1971) and play a part in osteoarthritis (Burr and Schaffler 1997; Burr 2004). Chondroclastic resorption of deep ACC at the osteochondral junction may decline with increasing skeletal maturity, but may be more active in areas of high load in people over 60 (Lane, Villacin and Bullough 1977) or during limb casting (Kiviranta, Jurvelin, Tammi, Saamanen and Helminen 1987). ACC thickness represents the balance between tidemark progression and chondroclastic resorption. Tidemark advancement and chondroclastic resorption may be coupled in adult cartilage (Oegema, Carpenter, Hofmeister and Thompson 1997). Multiple tidemarks are commonly observed in the normal ACC of many species (Oegema, Carpenter, Hofmeister and Thompson 1997) including horses (Muir, McCarthy, Radtke, Markel, Santschi, Scollay and Kalscheur 2006) so their presence is not unique to osteoarthritis as is sometimes suggested (Casey, Fhied and Oegema 2004). Tetracycline labelling of multiple tidemarks

has been reported (Revell, Pirie, Amir, Rashad and Walker 1990), indicating that cartilage mineralisation may occur deep to the tidemark. Variation in ACC mineralisation density (Dm) and tidemark LAR may occur within the ACC of a single joint (Chapter 3) but the relationship between Dm and LAR is unclear.

The Thoroughbred racehorse is a large athletic animal in which the responses of cartilage to controlled exercise may be investigated. The equine fetlock joint is a high-motion, high-load joint comprising of articulations between the distal condyle of Mc3 and PP, and Mc3 and paired PSB (Section 1.2.1, p. 10). The MCPJ is a frequent site of pathology compared to other joints in the horse, but changes such as cartilage wear lines and collapse are often clinically silent (Pool and Meagher 1990; Firth, Rogers, Perkins, Anderson and Grace 2004; Firth and Rogers 2005b). The most common cause of racetrack fatality in the United Kingdom is lateral condylar fracture of the distal Mc3 condyle (Parkin, Clegg, French, Proudman, Riggs, Singer, Webbon and Morgan 2004a), a fracture that originates within the MCPJ. Linear defects involving the ACC and subchondral bone (subchondral bone) of the parasagittal groove of the distal Mc3 condyle have been implicated in the initiation of condylar fracture (Riggs, Whitehouse and Boyde 1999a; Swindlehurst, Parkin and Morgan 2005). ACC microcracking may also be found in this region (Muir, McCarthy, Radtke, Markel, Santschi, Scollay and Kalscheur 2006).

Foals are born with biochemically homogeneous HAC in the MCPJ, in which regional heterogeneity develops within 5 months of age (Brama, Tekoppele, Bank, Barneveld and van Weeren 2000; Brama, Tekoppele, Bank, Karssenberg, Barneveld and van Weeren 2000). Significant site- and exercise-related variation in HAC stiffness, thickness and water content was found in the Mc3 condyle of 18-month old horses (Nugent, Law, Wong, Temple, Bae, Chen, Kawcak and Sah 2004). Notably, HAC in the parasagittal groove had a higher water content, was thicker and less stiff than elsewhere on the condyle (Nugent, Law, Wong, Temple, Bae, Chen, Kawcak and Sah 2004).

The present study examines ACC in specimens adjacent to those used by Nugent et al. (Nugent, Law, Wong, Temple, Bae, Chen, Kawcak and Sah 2004) for variation in thickness, Dm, tidemark count and LAR. The relationships between these parameters are explored to gain insight into load-related regulation of the tidemark and chondroclastic resorption, and the potential role of ACC in condylar fracture of the equine distal Mc3.

5.3 Method

Animal husbandry and exercise were as described earlier (Section 2.1: Exercise Regime p. 50). Specimen production was as per Section 2.2, p.53. CSLM and quantitative backscattered electron scanning electron microscopy (qBSE) image registration technique was developed to correlate ACC LAR and Dm at the micron scale (Chapter 3: Variation in Condylar Microanatomy p. 56). Combined reflection (blue), autofluorescence (red) and calcein fluorescence (green) images were made with a Leica SP2 CSLM using 488nm excitation and a 40x/1.0NA objective. Seven

anatomically distinct ACC sites were imaged per specimen (Figure 5-1 A), taking care to include only the specimen surface in the confocal image plane.

Specimens were then carbon-coated and qBSE images made in a Zeiss DSM 962 SEM. Montages of the entire lateromedial extent of the ACC layer were made at a nominal 50x magnification, 17 mm working distance, 20.0 kV accelerating voltage (Figure 5-1 B, C). Sites matching the CSLM images were identified and imaged in qBSE at 200x magnification. Spatial calibration was performed by making images of a 10 µm 'checkerboard-in-checkerboard' pattern etched in a silicon wafer, using the same instrument parameters as used for specimen imaging. Monoiodinated- and monobrominated-PMMA standard density objects were used to calibrate atomic number contrast. Zeiss IMG format images were converted to TIFF images and the image grey levels stretched so that the BSE coefficient of the mono-Br-PMMA standard image grey was set to 0, and that of the mono-I-PMMA to 255.

ACC thickness, mineralised fraction and total thickness mineralisation density (TTDm) were measured in the nominal 50x (1782 µm field width) qBSE lateromedial montage images. Each montage was opened as a stack in ImageJ (Rasband 2005). ACC in each slice of the stack was measured with several regions of interest (ROIs) extending from the tidemark to the cement line, placed perpendicular to the tidemark and spaced 250 µm apart. Care was taken to avoid measuring specimen regions twice when they appeared within overlapping montage tiles. Relative position was calculated to standardise the anatomic location of each measurement. The number of images distant from the most lateral image was divided by the total number of images in each montage to give a value between 0 (most lateral) and 1 (most medial). Relative position was divided into 20

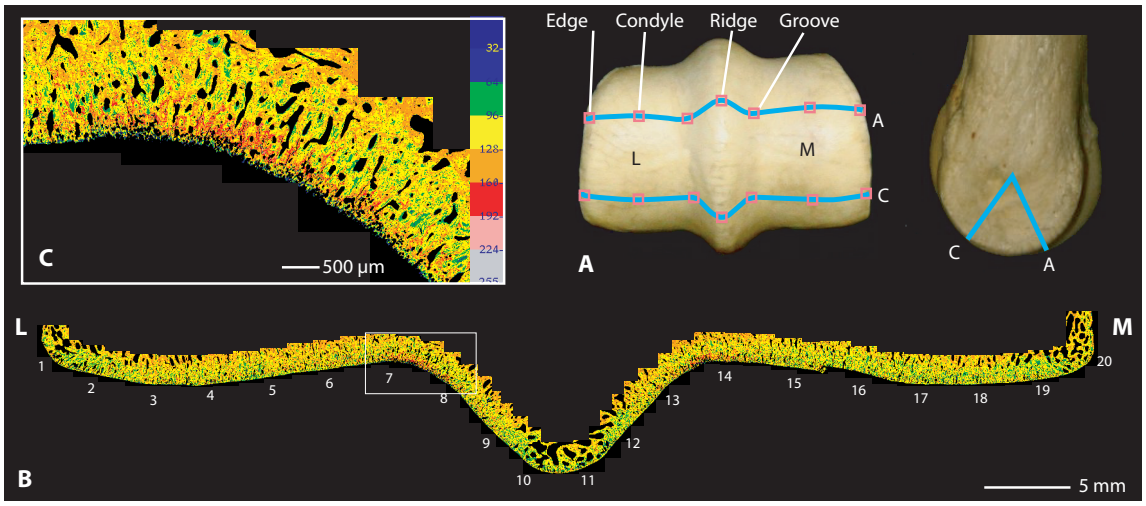

Figure 5-1: Site Locations

Sample locations and qBSE montage of lateromedial extent of Mc3 ACC. (A) A- and C- slices were taken at the line marked in cyan, pink squares mark the 7 sampling sites. (B) qBSE montage demonstrating entire lateromedial extent of distal Mc3 ACC. ACC thickness and TTDm measures were made on every tile of each montage, numbers 1-20 indicate relative positions, white rectangle is enlarged in (C).

n-tiles for analysis, with n-tile 20 occupying the most medial position on the Mc3 condyle. Mean thickness and TTDm were calculated for each n-tile and specimen.

CSLM images were registered to 200x qBSE images of matching sites using in-house software (Honza's; Boyde, Lovicar and Zamecnik (2004)) and loaded into ImageJ with the Sync Windows plugin (Walter 2004) activated. LAR and inter-label mineralisation density (ILDm; Dm of ACC bounded by calcein labels) were measured on the qBSE image (Figure 5-2 B), using calcein label bands in the CSLM image (Figure 5-2 A) as a temporospatial reference as described in Chapter 4. ROIs were placed at 10 µm intervals, using the proximal label edges as start and endpoints (Figure 5-2). Multiple tidemarks were counted in the 200x qBSE images at 4 evenly-spaced sites per image. Mean LAR, ILDm and tidemark counts were calculated for each site and specimen and used in subsequent analyses.

Lag time between the tidemark and cement line was estimated by dividing ACC thickness by LAR for each site and specimen. Lag time reflects the time elapsed between cartilage mineralisation and chondroclastic resorption (Section 4.6 p. 76).

Data were collected and analysed in SPSS v 11.0.0 (SPSS Inc., Chicago, IL). Univariate ANOVA was used to test for variation in each parameter with respect to site or relative position. Student's t-tests were performed for each parameter by site or relative position to test for differences between exercise groups. Parameters were compared to each other by Pearson's correlation.

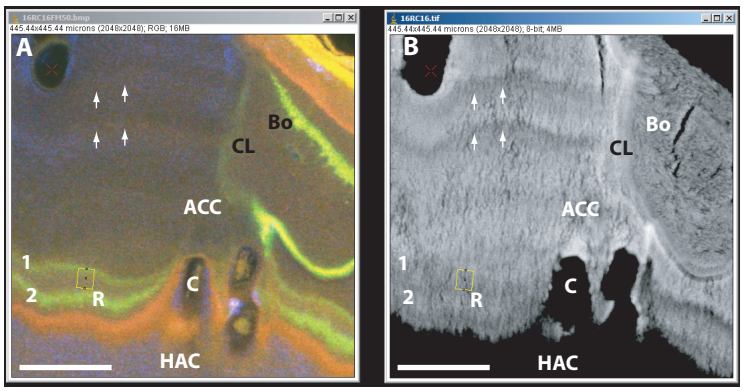

Figure 5-2: Registered CSLM and qBSE Images

Correlated measurement of LAR and ILDm using ImageJ. Registered CSLM (A) and qBSE (B) images were loaded into ImageJ and cursor motion synchronised using Sync Windows. Measurements of ILDm were made on (B) using calcein labels in (A) as reference points. Bo, bone; CL, cement line; ACC, articular calcified cartilage; C, chondrocyte; HAC, hyaline articular cartilage; R, region of interest; arrowheads demonstrate a multiple tidemark; bar = 30 µm.

5.4 Results

5.4.1 Site Effects

ACC thickness, mineralised fraction and TTDm varied significantly with relative position and bone slice ($p < 0.001$). A subtle mediolateral trend in ACC thickness was seen in the A-slice, with the medial condyle showing thicker ACC than the lateral condyle (Figure 5-3 C). Regions of greatly increased ACC thickness (>500 μm) were seen in the sagittal ridge of 4 A-slices and the parasagittal grooves of 4 C-slices (Figure 5-3 C, D). ACC ILDm ($p < 0.001$), LAR ($p < 0.001$) and tidemark count ($p = 0.014$) varied significantly with site (Figure 5-4). Greatest LAR was seen on the sagittal ridge of the C-slice and the joint edges of both slices.

5.4.2 Exercise Effects

LAR was less in exercised horses than control horses in one site only, the lateral condyle of the A-slice (0.65 ± 0.14 vs. 0.94 ± 0.15 μm•d^{-1}, $p = 0.01$). ILDm was greater in exercised horses than control horses in one site only, the medial edge of the C-slice (141.2 ± 7.2 vs. 124.8 ± 7.8 greys, $p = 0.032$). Multiple tidemarks were less frequent in exercised horses than in control horses in one site only, the sagittal ridge of the C-slice (0.98 ± 0.47 vs. 2.45 ± 0.79, $p = 0.024$). TTDm was significantly greater ($p < 0.05$) in exercised horses than control horses in 7 positions distributed

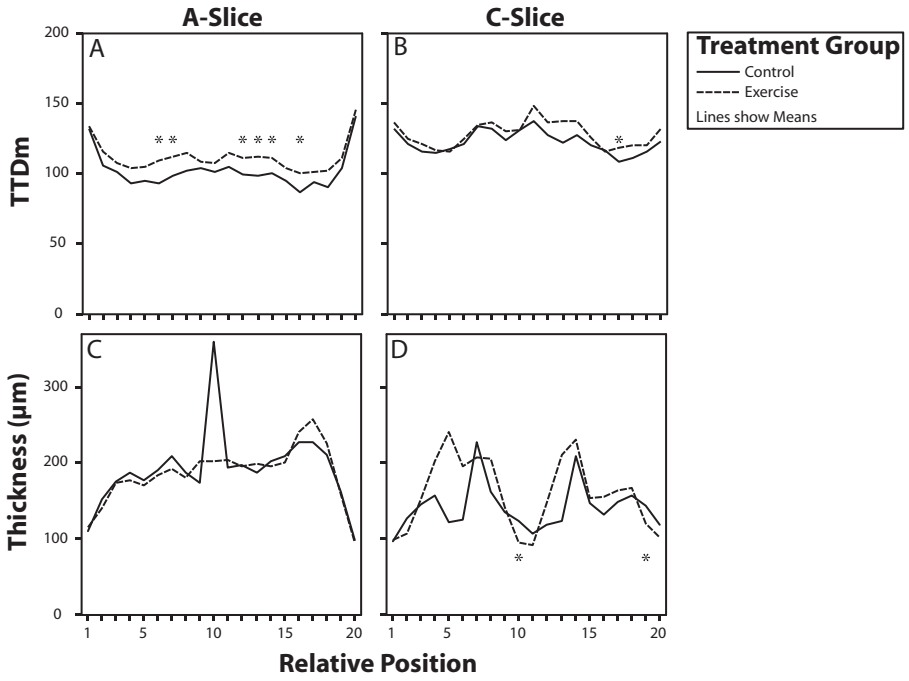

Figure 5-3: ACC TTDm and Thickness by Relative Position

Clear spatial trends may be seen, notably on joint edges, where ACC is thin and mineralisation density is high; this trend is seen around the midpoint (relative positions 9-11) of the C-slice. Peak ACC thickness was seen at relative position 10 in the A-slice (C) and relative positions 7 and 14 in the C-slice (D). A third peak is present at relative position 5 of exercised horses' ACC thickness in the C-slice; this was due to a single individual with very thick ACC on the lateral condyle of Mc3. * denotes significant effect of exercise ($p < 0.05$). Dashed line exercised, solid line control.

across the A- and C-slices. Thickness was greater in control horses than exercised horses in 2 positions on the C-slice (Significant differences denoted by * on Figure 5-3 and Figure 5-4).

5.4.3 Interrelationships

Three continuous clusters of points were visible in the ACC thickness versus TTDm scatter plot. Most points were confined within TTDm of 50-200 grey levels and below 400 μm thickness. The second cluster had very high thickness, occasionally greater than 1000 μm and TTDm of around 100 grey levels, while the third cluster had moderately high thickness (400-800 μm) and TTDm (100-200 grey levels) (Figure 5-5). Site-by-site plots of ACC thickness versus TTDm revealed that the two less populous clusters were contained within the A-slice sagittal ridge and C-slice parasagittal groove regions (data not shown).

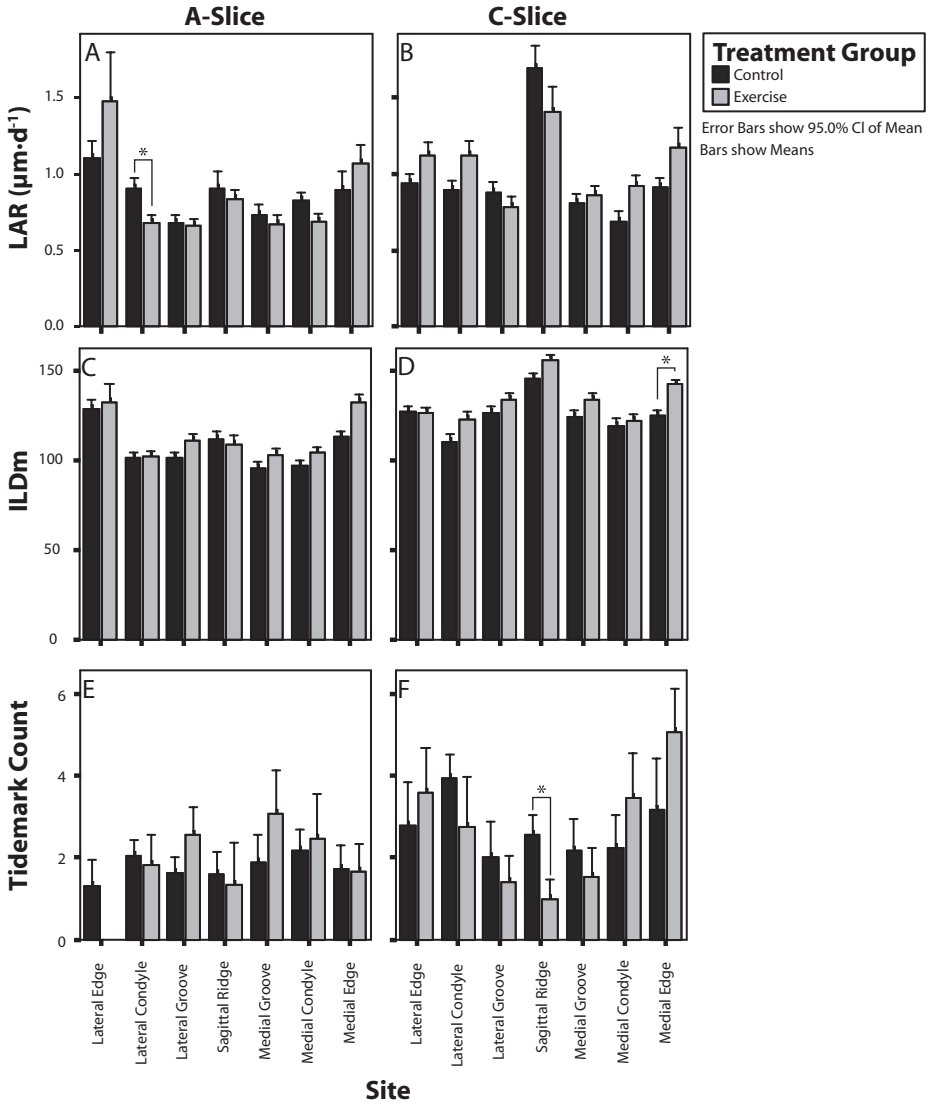

Figure 5-4: LAR, ILDm and Tidemark Count by Site

Spatial trends in LAR and ILDm are clear, but not those of tidemark count. High LAR is seen on the joint edges and C-slice sagittal ridge, where there is a tendency to high ILDm.

ILDm was significantly positively correlated with LAR ($r = 0.178$, $p < 0.001$) (Figure 5-6). A significant negative Pearson correlation existed between ACC thickness and mineralised fraction ($r = -0.440$, $p < 0.001$).

Comparing data sets by horse and site revealed that regions with very thick ACC did not have a proportional increase in LAR; instead, a negative correlation was found between LAR and ACC thickness ($r = -0.220$, $p = 0.015$). Median estimated lag time was 180 days. In some sites, vascular invasion reached the mineralising front, in which case the lag time was 0 days. Maximum lag time was 648 days, longer than the horses' post-natal life. Subtracting these values from the age at euthanasia (18 months) gives an indication that vascular invasion was occurring in ACC that was mineralised around 6 months earlier, i.e., at 12 months of age in most sites. Chondroclastic resorption may have been substantially delayed in other sites, where lag times were greater.

A negative correlation was found between tidemark count and LAR ($r = -0.280$, $p = 0.002$; Figure 5-7). In thick ACC, multiple tidemarks were visible in the most superficial layers, occupying only a quarter to one third of the total ACC thickness. No significant relationship existed between tidemark count and ACC thickness. No more than 2 calcein bands were observed in any site, including those with obvious multiple tidemarks.

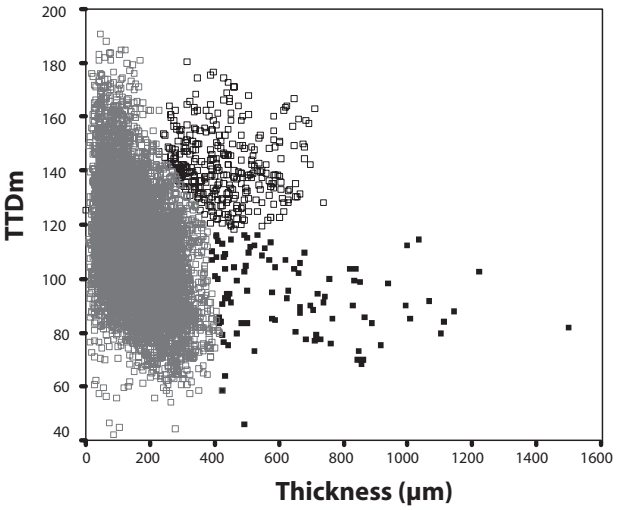

Figure 5-5: ACC TTDm versus Thickness

Three clusters of points are visible. The bulk of measurements are confined to a group on the left of the graph (open grey squares), while 2 extra clusters can be seen extending to the right (filled black squares; thick ACC) and upper right (open black squares; thick ACC, high ILDm). The extra 2 clusters of points were from the C-slice parasagittal grooves and A-slice sagittal ridge.

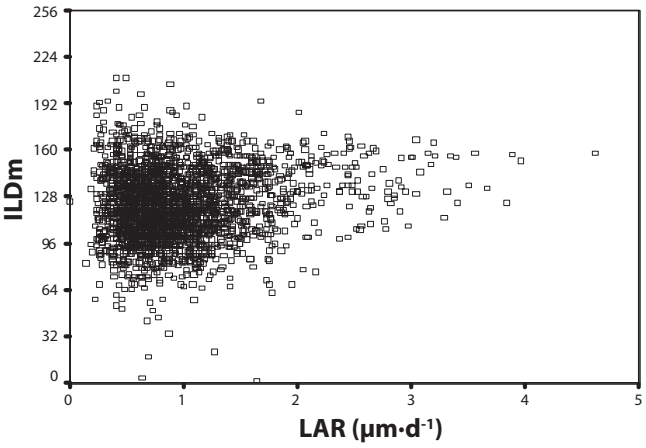

Figure 5-6: ACC ILDm vs LAR

ILDm vs. LAR. A slight, significant positive correlation was found ($r = 0.178$, $p < 0.001$).

5.5 Discussion

These are the first data, other than the preliminary data acquired in method development, for ACC mineralisation density in 18-month-old horses, and the most comprehensive data for ACC LAR in any mammalian joint. The only other published study that quantifed ACC LAR used 4 sites from rat femoro-tibial joints (O'Connor 1997) where a similar range of LAR was found.

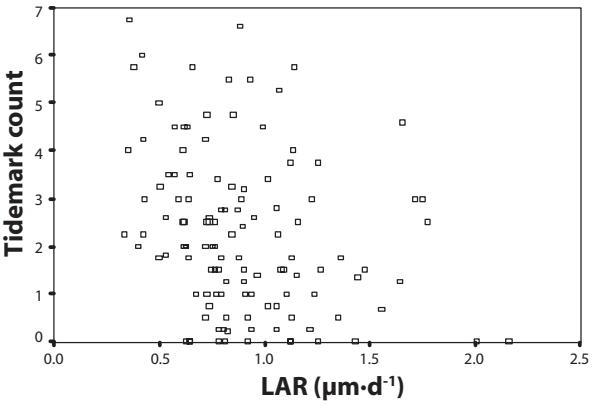

Figure 5-7: Tidemark Count versus LAR

A slight negative correlation was seen between tidemark count and LAR ($r = -0.280$, $p = 0.002$).

Several spatial trends emerged in ACC parameters in the equine distal third metacarpal condyle. Edge regions and the C-slice sagittal ridge tended to have high mineralisation density, high LAR, thin ACC and short lag times. These sites experience low loads, at least in the standing animal, as they are not on the bearing surface of the condyle (Brama 1999; Easton and Kawcak 2007). Chondroclastic cutting cones have previously been shown to penetrate the tidemark more especially in low-load regions of the distal metacarpal condyle (Boyde and Firth 2004). It must be noted that in vivo data on equine fetlock joint load distributions are scant at present (though see Brama (1999), Vilar, Pinedo, Demier, Castejon and Riber (1995), Colahan, Piotrowski and Poulos (1988) and Easton and Kawcak (2007) for ex vivo experimental data), so it is difficult to draw definite conclusions regarding load effects on ACC.

Spatial trends in ACC parameters appeared to correlate with subchondral bone trends: thick and poorly mineralised ACC tended to be situated on high volume fraction bone, while thin and highly mineralised ACC was found on low volume fraction bone, agreeing with previous findings on ACC thickness in the equine third carpal bone (Firth and Rogers 2005a). Subchondral bone responds to high load by increasing volume fraction, so it may be inferred that ACC overlying high volume fraction bone experiences a similarly high load. It appears that ACC under high loads mineralises to a lesser degree, and is removed by chondroclastic resorption more slowly, than ACC under low load. High LAR and rapid chondroclastic resorption in regions of low load would lead to progression of the subchondral bone plate towards the opposing joint surface. As low-loaded joint surfaces grow towards each other an increase in joint congruence may occur, as has been described in the human elbow (Goodfellow and Bullough 1967).

Decreased mineralised fraction with increased ACC thickness was seen in the A-slice sagittal ridge and C-slice parasagittal grooves, regions that are under constant load in the standing horse (Colahan, Piotrowski and Poulos 1988). These regions had a 'moth-eaten' pattern to their mineralisation, suggesting localised failure to mineralise as the tidemark mineralisation front passed through HAC. Cross-sectional studies are required to differentiate between failure of hyaline

cartilage mineralisation and ACC demineralisation. Regional variations in mineralisation density found in this study are likely to be related to variation in ACC stiffness, since a positive correlation exists between ACC mineralisation density and nanoindentation modulus (Ferguson, Bushby and Boyde 2003; Gupta, Schratter, Tesch, Roschger, Berzlanovich, Schoeberl, Klaushofer and Fratzl 2005).

High compressive loads on the growth plate have been reported to suppress cartilage mineralisation and vascular invasion in rats (Ohashi, Robling, Burr and Turner 2002) and rabbits (Trueta and Trias 1961). When loading was removed, cartilage mineralisation resumed rapidly, but a delay was seen in vascular invasion (Trueta and Trias 1961; Ohashi, Robling, Burr and Turner 2002). Bone marrow-derived macrophages failed to differentiate into osteoclasts and did not form resorption lacunae when cultured on hyaline cartilage or demineralised bone (Suzumoto, Takami and Sasaki 2005), confirming the widely held view that osteoclastic activity may be inhibited, or less encouraged by a non-mineralised substrate. It is possible that constant loading in regions within the fetlock joint leads to failure of articular cartilage mineralisation and a subsequent retardation of chondroclastic resorption.

LAR and ACC thickness are negatively correlated, meaning that the major determinant of ACC thickness must be chondroclastic resorption in the 18-month-old equine distal third metacarpal condyle. In general, sites with rapid LAR have thinner ACC than sites with slow LAR (Figure 5-3 and Figure 5-4), which can only have occurred if chondroclastic resorption advanced more rapidly when tidemark LAR increased. The apparent regional relationship between LAR, mineralisation density and thickness suggests coordination of the progression of the ACC mineralisation front and chondroclastic resorption. This might be direct, for example through chondrocyte-chondroclast signalling, or indirect, as each cell type responds independently to local loading conditions.

Lag time estimation may be useful to describe the relationship between cartilage mineralisation and its subsequent removal during chondroclastic resorption. Lag time estimation assists the determination of chondroclastic activity, since decreased lag times imply rapid advancement of chondroclasts towards the tidemark. Estimating lag time may aid researchers when they wish to ascribe causes of change in hyaline and ACC thickness either to the tidemark or to chondroclastic resorption. In any case, it is clear from the current study that it should not be assumed that thick ACC has resulted from rapid LAR.

This study further demonstrates substantial variation in lag time within the ACC of the distal third metacarpal, from 0 days to 21 months. In those regions with short lag times, chondroclastic resorption appears to be advancing aggressively into ACC, calcein bands are typically distinct and bright, mineralisation density is higher and LAR is more rapid, suggesting an overall activation of endochondral ossification. O'Connor (1997) showed that limb unweighting increased tidemark LAR, and that joint immobilisation increased chondroclastic invasion of ACC in rats (O'Connor 1997), suggesting that mechanical sensitivity of chondrocytes at the tidemark and chondroclasts

at the osteochondral junction may be related to variations in ACC thickness.

The parasagittal grooves of four horses showed increased ACC thickness and increased lag times, indicating that chondroclastic resorption had been reduced in this region. The lag time of '648 days' in a parasagittal groove of an 18-month-old horse indicates that chondroclastic resorption may have been delayed during early growth. In regions where the estimated lag time was greater than the horse's age, it is possible that LAR had been greater earlier in growth than at 18 months. More extended intra-vital labelling protocols are required to define changes in ACC LAR during joint development.

Defects in the parasagittal groove region are a consistent feature of condylar fracture in adult ($\geq$ 2-year old) racehorses (Riggs, Whitehouse and Boyde 1999a; Parkin, Clegg, French, Proudman, Riggs, Singer, Webbon and Morgan 2006). Thickened, poorly mineralised ACC without increased tidemark LAR was found in the parasagittal grooves of 18-month-old horses, indicating delayed chondroclastic resorption of ACC during early growth. This is the first evidence that developmental events prior to race training might contribute to linear defects in the parasagittal groove and, subsequently, the possibility of increased risk of fracture during racing and race training. Extensive future work is required to determine whether variations in parasagittal groove morphology at 18 months old are related to later condylar fracture.

The exercise regimen used in this study resulted in few statistically significant differences in measured parameters, in common with the study of Nugent et al. (2004). Here, a gentle exercise protocol was designed to minimise the likelihood of causing injury to young animals. Very few controlled exercise programmes have been evaluated in very young horses (Raub, Jackson and Baker 1989; Brama, Tekoppele, Bank, van Weeren and Barneveld 1999a), so no clear precedent for appropriate exercise intensity existed prior to this experiment. Furthermore, the foals in this study had free access to ad-libitum exercise on pasture, unlike previous studies in which foals received sprint exercise superimposed upon stall rest, or ad-libitum pasture exercise only (van de Lest, Brama and Van Weeren 2002). Inclusion of a stall-rested group may have highlighted exercise-related effects on ACC because joint unweighting and immobilisation are known to influence LAR and chondroclastic resorption (O'Connor 1997). For reasons of animal welfare, horses were not raised to 18 months old without access to exercise. Also, the parent (GEXA) study aimed to test increased over "normal" exercise, rather than imposing exercise on an atrophy model. In view of the fact that many of the world's athletic horses are confined for considerable periods, such a model does need to be tested, but this was not possible in the present study for several reasons besides the welfare concern.

High-intensity treadmill exercise was related to increased ACC thickness in adult horses' middle carpal bones (Murray, Whitton, Vedi, Goodship and Lekeux 1999), but 13 weeks of training on grass and sand did not affect ACC thickness of 2-year-old horses' third carpal bones (Firth and Rogers 2005a). The GEXA exercise program may have been insufficiently intense at the appropriate stage to alter regulation of the tidemark or chondroclastic resorption. Juvenile animals' ACC may be relatively unresponsive to exercise since growth cues might override responses to mechanical stimuli. It is possible that ad-libitum pasture exercise is sufficient to cause functional adaptation of hyaline and ACC, and that additional imposed exercise may have little beneficial effect. The regions of very thick ACC found in this study were distributed evenly between control and exercised horses, indicating that their presence was not an effect of the exercise regimen.

The negative correlation between LAR and tidemark count may represent intermittent arrest of the mineralisation front leading to reduced average LAR and increased tidemark count. The failure of calcein to bind strongly at levels other than that of the tidemark indicates that the majority of cartilage mineralisation occurs at the tidemark and not at multiple tidemarks. This contrasts with one previous study in which it was concluded that tetracycline labelled multiple tidemark levels simultaneously (Revell, Pirie, Amir, Rashad and Walker 1990). This may, however, reflect a difference in tetracycline and calcein binding mechanisms, experimental dose levels or prior therapeutic administration of tetracycline in that study's aged human subjects (Revell, Pirie, Amir, Rashad and Walker 1990). It is important to note that the horses in the current study received low dose, intravenous calcein administration to ensure short, sharp uptake and clear labels for reading with confocal microscopy. Deep ACC mineralisation may be diffuse and weak, so that calcein would not form identifiable bands as it does at the tidemark. Previous work (described in Chapter 4) failed to identify any temporal trend in mineralisation density between calcein labels, supporting the concept that the principal site of cartilage mineralisation is the tidemark.

Distinctive variations in ACC thickness and mineralisation density were found in the equine distal third metacarpal condyle, which are likely to have structural importance. Material failure in the parasagittal groove is a consistent feature of sagittal condylar fracture of the third metacarpal in adult Thoroughbred racehorses. Thick, poorly mineralised calcified cartilage in the parasagittal grooves of 18-month-old horses, prior to race training, might contribute to later condylar fracture. Detailed investigation into osteochondral biology in the palmar parasagittal grooves of the distal third metacarpal condyle during early growth is warranted.

6: Bone Morphometrics

6.1 Summary

Condylar fracture of the Mc3 is a common cause of racetrack fatality in Thoroughbred horses. Fractures propagate through subchondral bone of the distal Mc3 condyle, typically originating in parasagittal groove ACC. Bone microstructure in the Mc3 is likely to influence fracture propagation. Preconditioning exercise may affect bone development in young horses and could protect against later athletic injury, but its effects are poorly understood.

Twelve Thoroughbred horses were raised at pasture in New Zealand. Six were given preconditioning exercise from 10 days old. Intravenous injections of calcein were given 19 and 8 days prior to euthanasia at 18 months old. Osteochondral specimens were cut from the distal Mc3 in the dorsal and palmar oblique frontal planes, imaged with DXA, fixed in ethanol and embedded in PMMA. Surfaces were finished to a diamond polish and imaged using quantitative backscattered electron scanning electron microscopy (qBSE). Montages of 56-120 images (each 4.46 mm field width) were made of entire specimen surfaces. Specimens were then diamond ultramilled and imaged with confocal scanning light microscopy (CSLM) and qBSE. Montages were repeated on the ultramilled surface, and 13 defined sites imaged at higher magnification (445 μm field width). CSLM images were registered to matching qBSE images with Honza's (Boyde, Lovicar and Zamecnik 2004). Montaged image sets were used to measure bone volume fraction (BVF); bone mineralisation density (Dm); mean volumetric density (VDm); marrow space Feret diameter (MSFD) and marrow space orientation (MSO). Linear accretion rate (LAR) and inter-label mineralisation density (ILDm) were determined in registered image pairs. All measurements were made in 13 identical sites.

No significant effect of preconditioning was found in any parameter ($p < 0.05$). All parameters except MSFD, LAR and ILDm varied significantly by site ($p < 0.05$). LAR and ILDm were negatively correlated ($r = -0.328$, $p < 0.001$). DXA bone mineral density (BMD) was positively correlated with BVF and VDm ($r = 0.851$ & 0.881, $p < 0.001$) and negatively correlated with Dm ($r = -0.155$, $p < 0.001$). MSO was highly variable in the parasagittal groove and was related to MSFD. Bone structure and composition in the distal Mc3 condyle was not detectably altered in preconditioning exercise. Individual variation exists in Mc3 condylar microstructure, which may result in an increased fracture risk for some horses.

6.2 Introduction

Condylar fracture of the distal third metacarpal bone (Mc3) is a significant cause of lameness during Thoroughbred racehorse training (Bathe 1994; Verheyen and Wood 2004), as well as being the most common cause of racetrack fatality in the UK (Parkin, Clegg, French, Proudman, Riggs, Singer, Webbon and Morgan 2004a) and a substantial cause of fatality in the USA (Johnson, Stover, Daft, Kinde, Read, Barr, Anderson, Moore, Woods and Stoltz 1994).

Mc3 condylar fractures are considered to be stress fractures because they occur during normal loading in the course of training and racing (Riggs 2002), and because fracture lines may develop prior to total material failure (Tapprest, Audigie, Radier, Anglade, Voisin, Foucher, Collobert-Laugier, Mathieu and Denoix 2003), possibly as a culmination of microfractures (Stepnik, Radtke, Scollay, Oshel, Albrecht, Santschi, Markel and Muir 2004). Simple complete condylar fractures typically travel from the parasagittal grooves of the condyle (Alexander and Rooney 1974; Rick, O'Brien, Pool and Meagher 1983; Barr, Sridhar and Denny 1989; Ellis 1994; Parkin, Clegg, French, Proudman, Riggs, Singer, Webbon and Morgan 2006) to the abaxial diaphysis, resulting in a reasonably consistent fracture length of 74-88 mm (Alexander and Rooney 1974; Vaughan and Mason 1975; Rick, O'Brien, Pool and Meagher 1983; Ellis 1994; Zekas, Bramlage, Embertson and Hance 1999a; Parkin, Clegg, French, Proudman, Riggs, Singer, Webbon and Morgan 2006). In 5-10 % of condylar fractures, the fracture line propagates proximally through the diaphysis resulting in long, minimally-displaced fractures (Barr, Sridhar and Denny 1989) or comminuted fractures with multiple, irreducible fragments (Rooney 1974; Bathe 1994). Surgical reduction of condylar fracture is usually successful (Zekas, Bramlage, Embertson and Hance 1999b; Russell and Maclean 2006), except in heavily comminuted fractures for which euthanasia is the only humane recourse.

Linear defects involving articular cartilage and subchondral bone of the parasagittal groove of Mc3 are associated with condylar fracture (Riggs 1999; Riggs, Whitehouse and Boyde 1999a; Swindlehurst, Parkin and Morgan 2005). Microcracking of ACC and resorption of subchondral bone are typically present at the base of linear defects (Riggs 1999; Muir, McCarthy, Radtke, Markel, Santschi, Scollay and Kalscheur 2006). Parasagittal groove linear defects precede overt failure and are not associated with age, career length or number of race starts (Parkin, Clegg, French, Proudman, Riggs, Singer, Webbon and Morgan 2006), suggesting that they arise independent of exercise. A density gradient between high volume fraction bone deep to the condyle and low volume fraction bone in the sagittal ridge has been demonstrated in some condyles and together with linear defects might increase stress concentration in the parasagittal groove (Riggs, Whitehouse and Boyde 1999b).

The trabecular structure of the distal Mc3 is highly anisotropic, with plates in the sagittal plane joined by short lateromedial struts (Boyde, Haroon, Jones and Riggs 1999). This configuration provides little resistance to disto-proximal fracture propagation and promotes cleavage in the sagittal plane. The combination of parasagittal groove linear defects acting as stress-concentrators, sagittal plate bone architecture and intense, repetitive mechanical loading is thought to lead to condylar fracture (Riggs 1999).

Preconditioning exercise is training delivered during growth with the intent of strengthening musculoskeletal tissues against the future rigours of racing and race-training. The distal Mc3 is a target for preconditioning exercise since it often fails in condylar fracture. Very little data has been produced on the effects of preconditioning exercise on equine musculoskeletal tissues,

yet if successful programmes can be developed, preconditioning exercise has the potential to reduce injury to animals and financial losses for owners. A small amount of literature supports exposure of Mc3 to light exercise during growth; daily access to ad-libitum exercise at pasture was related to increased diaphyseal radiographic bone aluminium equivalence in Arabian weanling horses' Mc3 (Bell, Nielsen, Waite, Rosenstein and Orth 2001), while controlled trotting exercise on an automatic walker between weanling and yearling age was related to increased Mc3 radiographic bone aluminium equivalence and limb circumference at the mid-metacarpal level (Raub, Jackson and Baker 1989). These studies used low-resolution, plain radiography and so could not determine the effects of preconditioning exercise on bone microstructure in the distal Mc3, which is critical for resistance to condylar fracture.

Exercise-related variation in Mc3 condylar bone microarchitecture has been observed after race preparation of 2-year-old horses (Boyde and Firth 2005b), but inter-individual variation has not been documented for either adult or juvenile horses. Mc3 from 12 18-month-old horses were examined with electron microscopy, confocal scanning light microscopy and dual x-ray absorptiometry (DXA) to determine any changes in microstructure that may have occurred due to a preconditioning exercise program, to investigate individual variation in Mc3 microstructure, and to investigate interrelationships between structural parameters.

6.3 Materials and Methods

6.3.1 Specimen Preparation

Horses were raised and given preconditioning exercise as described in Section 2.1, p. 50. Specimen preparation was as described in Section 2.2, p. 53.

6.3.2 Dual X-Ray Absorptiometry (DXA)

DXA is an established technique for the determination of areal BMD and is commonly employed to monitor human patients at risk of osteoporosis (Lewiecki 2005). DXA measures relative attenuation as two wavelengths of X-rays pass through an object, from which 'bone mineral density' or content is calculated. It is an inherently 2D imaging modality (unlike CT), so increased subject thickness will result in an apparent increase in material density. DXA is well suited to regularly-shaped subjects, particularly plane-parallel sections, as thickness artefact is minimal. The resolution of DXA is usually limited to the 0.5-2.0 mm range, so fine structural detail cannot be visualised.

All specimens were imaged with a small animal DXA unit (PIXImus DXA, GE Lunar) prior to embedding. Speciman thickness (h; cm) was measured with digital callipers and the areal bone mineral density (aBMD; g•cm^{-2}) reported by the DXA unit converted into volumetric bone mineral density (vBMD; g•cm^{-3}) using Equation 6.1.

Equation 6.1

$$vBMD = \frac{aBMD}{h}$$

6.3.3 Correlated CSLM and qBSE

A confocal scanning light microscopy (CSLM) and quantitative backscattered electron scanning electron microscopy (qBSE) image registration technique was developed to correlate mineralising front LAR and matrix mineralisation density at the micron scale (Chapter 4). Thirteen anatomically distinct subchondral bone sites were imaged per specimen (Figure 6-1 A), taking care to include only the specimen surface in the confocal image plane.

Specimens were then carbon-coated and qBSE images made in a Zeiss DSM 962 scanning electron microscope. Montages of entire specimen surfaces (56-120 images) were made at a nominal 20x magnification (4456 µm field width), 17 mm working distance and 20.0 kV accelerating voltage

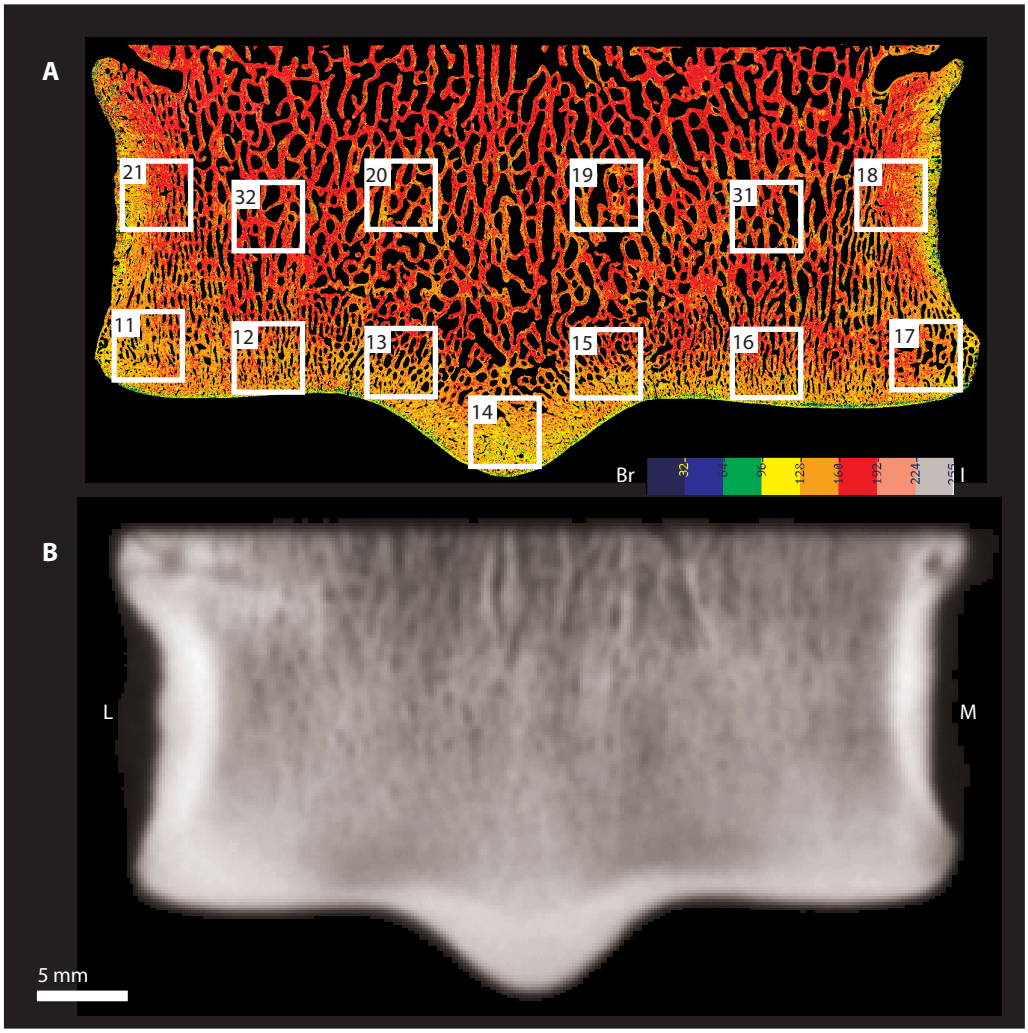

Figure 6-1: Site Locations for qBSE and DXA Measurements

(A) qBSE montage comprised of 91 image tiles showing the 13 sampling sites used for all measurements. A false-colour look-up table has been applied according to the scale at right, with 8-bit grey equivalent to monobrominated-dimethacrylate (Br) set to black and 8-bit grey equivalent to monoiodinated-dimethacrylate (I) set to white. Note variation by site in qBSE composition, marrow space size and orientation and volume fraction. Pixel size in original, 4.35 µm. (B) PIXImus DXA image of the same specimen for comparison; pixel size in original approximately 180 µm. L, Lateral; M, Medial; Specimen is an A-slice.

(Figure 6-1 A). Sites matching the CSLM images were identified and imaged in qBSE at 200x magnification (445 µm field width). Spatial calibration was performed by making images of a 10 µm 'checkerboard-in-checkerboard' pattern etched in a silicon wafer, using the same instrument parameters as used for specimen imaging. Monoiodinated- and monobrominated-dimethacrylate standard density objects were used to calibrate compositional contrast for mineralisation density measurement. Zeiss IMG format images were converted to 8-bit greyscale TIFF images and the image grey levels stretched so that the backscatter coefficient of the monobrominated-dimethacrylate standard image grey was set to 0, and that of the monoiodinated-dimethacrylate to 255.

Montages were constructed by aligning sets of 20x qBSE image tiles (Figure 6-1 A). Several parameters were measured in 13 identical regions of interest with ImageJ. Bone volume fraction, mean mineralisation density of the region of interest (ROI) and mean mineralisation density of bone matrix were calculated. Montages were converted to binary for morphological operations. The mean Euclidean distance transform was calculated with ImageJ's EDM function, which returned the distance from each foreground pixel (bone) to the nearest background pixel (marrow), so estimating trabecular thickness. Marrow spaces were measured with ImageJ's Analyze Particles function, which returned marrow space cross-sectional area, orientation and Feret diameter. The

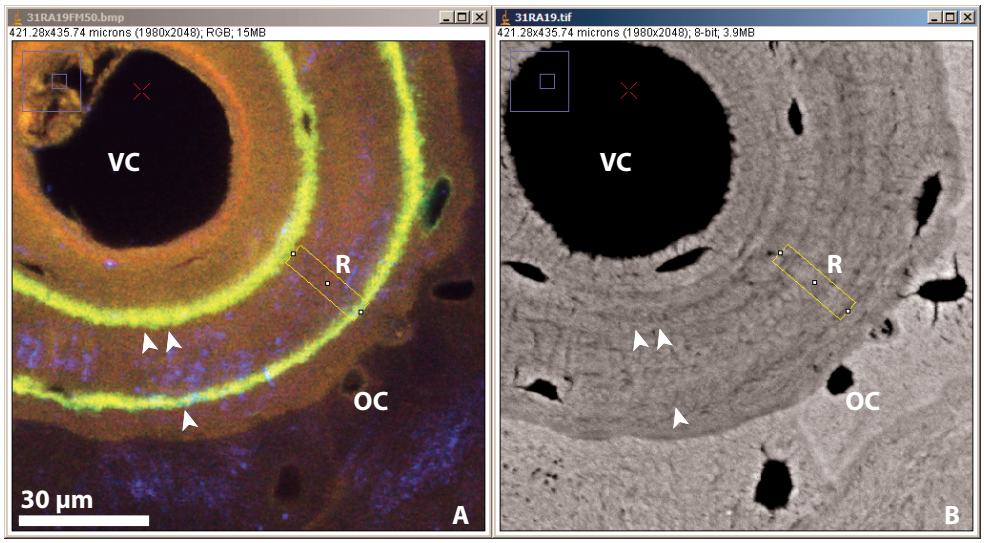

Figure 6-2: Correlated Measurement of LAR and Dm

Correlated measurement of mineralising front LAR and inter-label mineralisation density of bone using ImageJ. Registered CSLM (A) and qBSE (B) images were opened with ImageJ and cursor motion synchronised using Sync Windows. The cursor is visible as red cross-hairs to the top left of both image windows. Measurements of inter-label mineralisation density were made on (B) using calcein labels in (A) as reference points. Calcein labels identify the position of the mineralising front 19 days (single arrowhead) and 8 days (paired arrowheads) prior to euthanasia. LAR was calculated by dividing the region of interest's length by the inter-label period (11 days). VC, vascular canal; OC, osteocyte lacuna; R, region of interest. Markers are replicated in each window to show the positions of features that are invisible to qBSE.

Feret diameter is the greatest distance between any 2 pixels on the selection boundary. Osteocyte lacunae were excluded from analysis by restricting Analyze Particles to particles greater than 25 pixels (473 μm^2) in area. Examination of the montages revealed an abrupt transition from smaller marrow spaces to larger marrow spaces at 1500 pixels (28383 μm^2) at the boundary between the subchondral bone plate and trabecular bone, which was used to separate marrow spaces into 'small' and 'large' categories for later analysis. The 'large' class of marrow space sizes was examined further by examining a subset of 'very large' marrow spaces (> 5000 pixels), to examine the likelihood of finding very large marrow spaces in the lateral parasagittal grooves. Variation in specimen orientation in each montage was corrected for by drawing a single line tangent to both lateral and medial condyles and assuming that the proximo-distal axis was normal to it.

CSLM images were registered to 200x qBSE images of matching sites using Honza's program and loaded into ImageJ with the Sync Windows plug-in activated, as described in Section 4.4, p. 73. LAR and mineralisation density of bone matrix bounded by calcein labels (inter-label mineralisation density) were measured on the qBSE image (Figure 6-2 B), using calcein label bands in the CSLM image (Figure 6-2 A) as a temporospatial reference. ROIs were placed at 10 μm intervals, using the proximal label edges as start and endpoints. Mean LAR and inter-label mineralisation density were calculated for each site and specimen and used in subsequent analyses.

Data were analysed in SPSS v 11.0.0 (SPSS Inc., Chicago, IL). Univariate ANOVA was used to test for variation in each parameter with respect to site. Mann-Whitney U tests were performed for each parameter by site to test for differences between exercise groups. Parameters were compared to each other with Pearson's correlation. Circular statistics were calculated according to Batschelet (1981).

6.4 Results

6.4.1 Site Variation

No statistically significant variation by site was found in LAR, LAR angle, ILDm or large or small marrow space Feret diameter. Highly significant site variation ($p < 0.001$) was found in VFb, BMMD (qBSE), vBMD (DXA) and EDM (Figure 6-4). High mean EDM was seen in C-slice lateral parasagittal grooves (site 13; Figure 6-4 F), and deep condyle positions (sites 31, 32; Figure 6-4 F).

In general, large marrow spaces in the C-slice were more lateromedially aligned, whereas in the A-slice they were more proximodistally aligned. Mean marrow space orientations and angular variances by site are presented in Figure 6-3. Low angular variance is evident in marrow spaces in the proximal row of sites, while high variance in angle in the A-slice sagittal ridge and C-slice parasagittal groove. Note the axially-deviated mean orientation and high angular variance of marrow spaces in the C-slice lateral parasagittal groove (Figure 6-3).

6.4.2 Exercise Variation

No effect of preconditioning exercise was found for LAR, LAR angle or ILDm. Very few significant differences were found when comparing treatment groups by site. Using a cutoff for significance of p = 0.05, one test per 20 repeats would be expected to achieve significance randomly for each variable. Given the 26 sites per horse (13 sites per slice), just over one site per horse would erroneously achieve significance and give rise to rejection of the null hypothesis and a Type I error (Petrie and Watson 1999).

No effect of preconditioning exercise was seen for VFb or BMMD. Marrow space area did not vary significantly with preconditioning exercise when large and small marrow spaces were considered separately or pooled together.

Angular variance in marrow space angle was significantly different in preconditioned specimens in A-slice sites 16 (p = 0.004, greater in control) and 32 (p = 0.041, greater in preconditioned), and in C-slice site 11 (p = 0.041, c greater). No significant differences in marrow space Feret diameter were found associated with exercise.

Preconditioned specimens had generally higher DXA vBMD than control specimens. Of the 39 sites per condyle (13 in each A-, B- and C-slice), vBMD was greater in preconditioned specimens in 27 sites, though statistical significance was not reached in any site. Pooling sites and slices had no effect on statistical significance for vBMD by exercise.

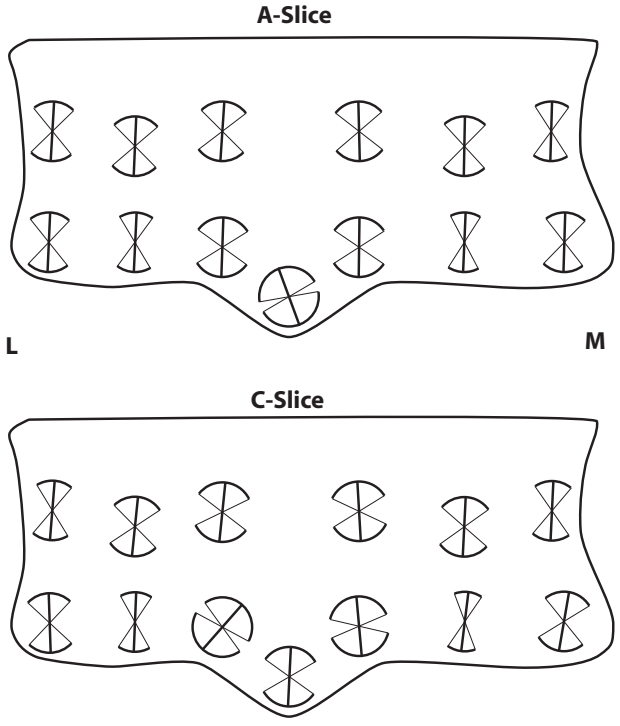

Figure 6-3: Marrow Space Orientation Angular Mean and Variance by Site

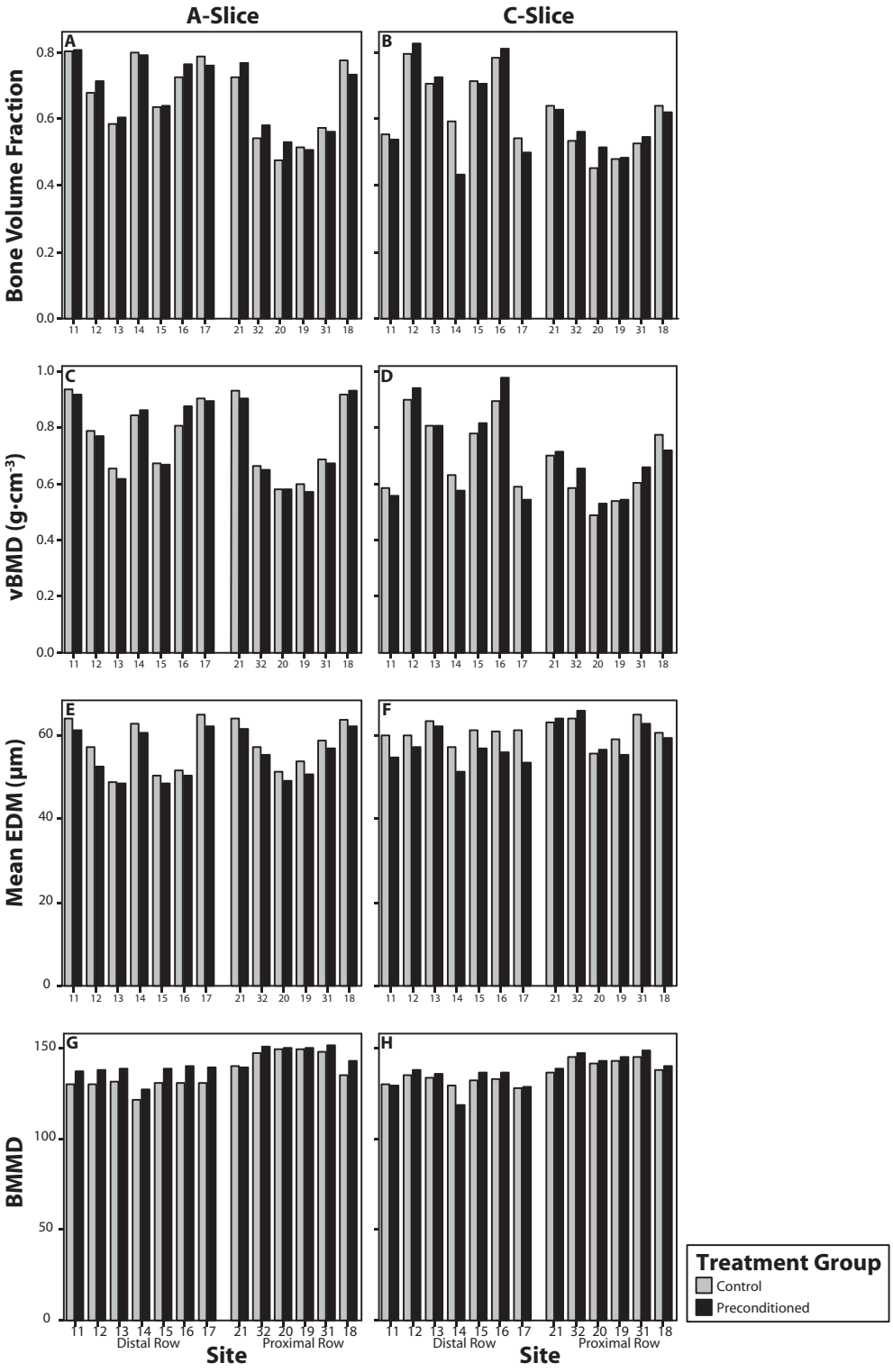

Figure 6-4: Bone Morphological Paramters by Site

Mean marrow space area and variance of marrow space area varied significantly by site ($p < 0.001$) for all sites and both size classes. There were more very large marrow spaces in the A-slice (69.7 +- 25.5) lateral parasagittal groove than in the C-slice (22.6 +- 10.3) lateral parasagittal groove ($p < 0.001$). However, this difference was not evident when all marrow spaces greater than 1500 pixels in area were included in the comparison.

6.4.3 Correlations

LAR was found to be anisotropic. LAR angle was not randomly distributed, with more LAR measurements in the lateromedial direction than in the proximodistal direction. This was probably due to proximodistal marrow space orientation leading to a greater proportion of the bone surface facing the lateromedial direction, hence a greater length of label available to measure. The highest mean interlabel distances were measured at a label angle of ±90º, that is, parallel to the long axis of Mc3 at the proximal and distal ends of marrow spaces. The proximodistal orientation of marrow spaces meant that they had a shorter radius of curvature at their proximal and distal extent than on their lateromedial sides. This would result in rapid narrowing of the space being filled with bone so that the same volume of matrix deposited on the bone surface would result in a greater apparent LAR in the narrow ends than on the sides. In other words, greater proximodistal LAR may be a simple geometric effect of filling concave spaces rather than being a response to the direction of mechanical load (Equation 6.2). Alternatively, it is possible that increased obliquity of label cross-sectioning in the more highly-curved proximodistal portions of marrow spaces artificially increased their apparent LAR.

Equation 6.2

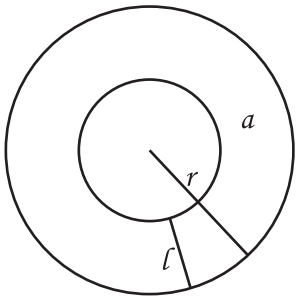

$$l = r - \sqrt{r^2 - \frac{a}{\pi}}$$

As the radius of curvature (*r*) decreases, a constant area of matrix deposited (*a*) is achieved by increased linear accretion (*l*).

A negative correlation was found between LAR and ILDm ($r = -0.328$, $p<0.001$), in contrast to ACC, in which a subtle positive correlation was found (Section 5.4.3, p. 87). ILDM and BMMD were positively correlated ($r = 0.316$, $p< 0.001$), indicating that initial matrix mineralisation accounts for almost a third of the variability in bone matrix mineralisation density. LAR did not correlate with VFb or EDM.

A strong positive correlation was found between vBMD and VFb ($r = 0.851$, $p < 0.001$) (Figure 6-5), whereas subtle negative correlations were found between vBMD and BMMD ($r = -0.155$, $p < 0.001$) and between BMMD and VFb ($r = -0.129$, $p < 0.001$). A moderate positive correlation existed between EDM and VFb ($r = 0.312$, $p < 0.001$), indicating that as bone volume fraction increases, the distance of each osteocyte from the nearest vascular space also increases.

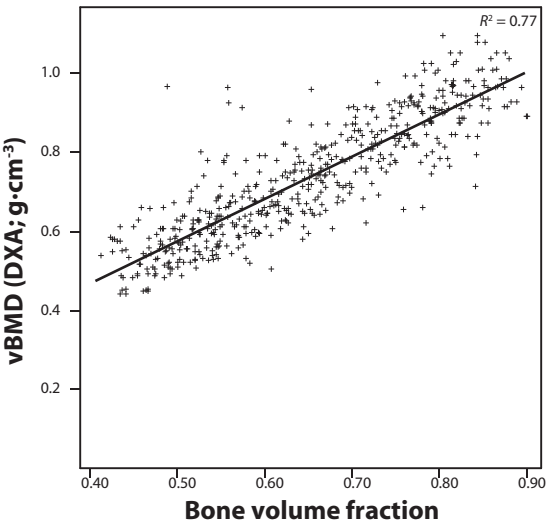

Figure 6-5: vBMD versus Bone Volume Fraction

6.5 Discussion and Conclusions

Substantial site variation was evident in the mineralisation density and structural organisation of Mc3 subchondral and trabecular bone, but little (if any) effect of preconditioning exercise was found. Individual variation in structural parameters such as marrow space size and orientation are likely to have profound implications for fracture growth, meaning that some horses may be less able to resist condylar fracture once the Mc3 experiences the intense loading of racing and race training. It is possible that the trabecular structure of the distal condyle guides the fracture line either abaxially towards the cortex, resulting in a simple condylar fracture, or more axially into the centre of the diaphysis resulting in a heavily comminuted, fatal fracture. Further investigation into variation in Mc3 condylar trabecular structure and its interaction with fetlock loading and linear defects will aid in discovering why some horses suffer fatal fracture while others only experience simple, surgically reparable injury.

The lack of consistent bony changes associated with preconditioning exercise echoes the findings in ACC (Section 5.5, p. 89), however, bone is known to adapt rapidly in the face of changes in loading while little evidence supports mechanobiological adaptation in ACC. The explanations given in Section 5.5 largely stand in the case of a lack of bone response: the exercise regime may not have been sufficiently intense; the horses were allowed ad-lib pasture exercise, and growth cues may have interfered with loading cues. Possibly the most significant factor is the small number of animals in the study, and the small effect size relative to individual variation leading to low statistical power.

In common with Chapter 5, this chapter has found no negative effect of preconditioning exercise, as given to this group of foals. If convincing positive benefits of preconditioning are found in other injury sites, in general fitness or behavioural readiness for racing then it may be delivered with minimal likelihood of damage to the Mc3 condyle.

The discovery of a correlation between EDM and VFb is in agreement with the observation that bone remodelling in the Mc3 primarily occurs by apposition on existing bone surfaces without prior resorption (Boyde 2003). As bone is laid down, VFb increases along with the mean distance to the bone surface. This has clear implications for osteocyte metabolism, as osteocytes deep within bone may become starved of nutrition by rapid apposition. In addition, increased VFb reduces the amount of marrow space that blood vessels can use to increase in diameter when

increased demands are placed on blood flow, further restricting osteocytes' nutrient supply. While osteocyte starvation is difficult to relate to condylar fracture, it may have important ramifications for POD, in which a zone of osteocyte necrosis might be closely related to extremely high VFb (0.9 – 0.95 and greater) deep to the portions of the condyles that bear the greatest loads (Norrdin, Kawcak, Capwell and McIlwraith 1998). It is possible that increased VFb cuts off osteocytes' nutrient supply, which then die and stop signalling, while the limited vascularity reduces the delivery of osteoclasts and osteoblasts which are required to repair damaged bone.

The EDM measurement in this study was strictly 2D, so bone surfaces out of the plane of section could not contribute to the estimation of distance to bone surface, which has likely been overestimated. 3D EDM is possible, but requires specialised algorithms and high resolution 3D datasets, such as sub-10 µm µCT stacks, that were not available to this study.

The technique used to determine the proximodistal axis for directional measures was inherently variable because of obvious variation in condylar shape, which may have been due to the exact plane that each slice was cut from and because of individual variation in the curvature of the medial and lateral condyles. The error between the calculated proximodistal axis and anatomic proximodistal axis is unknown because only the distal condyle was available for measurement.

vBMD reflects the amount of X-ray attenuation as the beam passes through a specimen, thus is strongly affected by the proportion of minimally-attenuating material such as water- and fat-filled, non-mineralising marrow space. The most common single mineralisation density in a distal Mc3 bone specimen is 0.0 g•cm^{-3}, which is the mineralisation density of marrow space. Figure 6-6 shows a typical ImageJ histogram of qBSE backscatter coefficients from bone in an Mc3. Note the main peak at 159 to the centre-right of the histogram, as well as a sharp peak at the far left at exactly 0, which forms the modal peak of the graph. While the modal backscatter coefficient of the mineralised portion is 159, the mean backscatter coefficient of the mineralised plus unmineralised portions is reported as 92.021. Of the 230,545 pixels in this example, 77,816 pixels represented unmineralised tissue, so the VFb was calculated as per Equation 6.3.

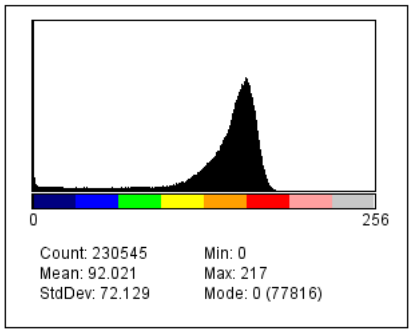

Figure 6-6: Histogram of Typical qBSE Values in Bone with topo9c LUT

Note the high peak at the very left of the graph that represents the modal backscatter coefficient of 0.

Equation 6.3

$$VFb = \frac{n_{total} - n_0}{n_{total}} = \frac{230{,}545 - 77{,}816}{230{,}545} = 0.6624$$

Thus, the inclusion of marrow space when calculating vBMD means that a large amount of unmineralised tissue is contributing 'zero' values to the measurement of tissue mineralisation density, dragging vBMD lower than BMMD as a function of volume fraction. A clear linear association between VFb and vBMD is evident (Figure 6-5), which can be expressed as:

Equation 6.4

$$vBMD \approx BMMD \cdot VFb$$

In other words, vBMD is a composite of BMMD and VFb: bone matrix contains the entire mineral complement of a bone volume, so the volumetric mineral density is the amount of mineral in the bone matrix reduced by the fraction of the organ which is unmineralised bone.

This study corrected the raw DXA result, which is an areal bone mineral density, by dividing by specimen thickness to give a volumetric bone mineral density. Most DXA scanners in clinical practice report areal BMD (often of the femoral neck or vertebrae) with no consideration for bone geometry, meaning that the results are a composite not only of BMMD and VFb but also of an unknown thickness of projected bone. 3D techniques such as pQCT help to eliminate bone thickness artefact but due to poor resolution (usually > 250 μm) can only report vBMD and not BMMD. The sole exception in clinical pQCT imaging is Scanco's XtremeCT (Scanco Medical AG, Bassersdorf, Switzerland), which can just resolve individual trabeculae with its 82 μm resolution. However, even μCT with 10 μm or better resolution contains partial volume artefacts, where voxels may be partially-filled with mineralised matrix as they intersect the bone surface. The partial-volume artefact leads to difficulties in estimating the true BMMD of surface voxels, since the attenuation coefficient of a single voxel will be a composite of its volume occupancy and the BMMD of the intersecting portion that is bone. As voxels increase in size relative to features of interest, the greater the partial volume effect and hence, uncertainty in determining VFb and BMMD.

7: Nanoindentation of ACC and Subchondral Bone

7.6 Introduction

Condylar fracture of Mc3 usually initiates in or near the parasagittal grooves but a full explanation for fracture predilection in these sites is lacking. Earlier experiments in this thesis identified regions of thickened, aberrantly mineralised ACC in the parasagittal grooves of 18-month-old Mc3 distal condyles associated with disorganised, high-turnover subchondral bone and enlarged marrow spaces. The elastic modulus of ACC and subchondral bone has previously been determined on healthy, normal equine specimens (Bushby, Ferguson and Boyde 2004) and osteoarthritic human specimens, and correlated to matrix mineralisation density using correlated nanoindentation testing and qBSE imaging (Ferguson, Bushby and Boyde 2003). Material properties of ACC and subchondral bone have not been determined in Mc3 parasagittal grooves, yet may be important for understanding condylar fracture initiation.

Correlated qBSE and nanoindentation testing allows a greater understanding of tissue mineralisation than qBSE alone. Material stiffness is related to both the amount and arrangement of mineral within tissue, as well as collagen orientation and tissue hydration. Both stiffness and mineralisation density are related to fracture energy and sensitivity to stress concentration (notch sensitivity) in bending tests on bone (Currey, Brear and Zioupos 2004). Aberrant regions of ACC and subchondral bone in the Mc3 parasagittal grooves may act as stress concentrators, particularly if ACC and bone are mechanically weaker in such regions. This study sought to discover material deficiencies within ACC and subchondral bone that may be related to previously identified histomorphological variations in the parasagittal grooves.

7.7 Materials and Methods

7.7.1 Nanoindentation

Nanoindentation is a materials testing technique whereby a diamond-tipped indenter is depressed into the surface of the specimen with a known force and rate of application. The specimen's indentation modulus may be calculated from the resulting force versus displacement curve and probe tip geometry. Nanoindentation differs from other indentation techniques because the probe tip is very fine (typically 5-20 μm), the tip's movement in the z axis may be controlled with nanometre accuracy and x-y movements may be controlled at the micron scale. This makes nanoindentation ideal for studying variations in tissue ultrastructure by correlating indentation modulus with histological features.

Nanoindentation modulus of Mc3 cortical bone increases as bone is dehydrated in ethanol then embedded in PMMA, and correlates well with traditional 3-point bending tests (Bushby, Ferguson and Boyde 2004). Nanoindentation modulus has been shown to correlate to qBSE mineralisation density in ACC, bone (Ferguson, Bushby and Boyde 2002; Ferguson, Bushby and Boyde 2003) and carious dentine (Angker, Nockolds, Swain and Kilpatrick 2004a).

7.7.2 UMIS Set-Up

Two sites were tested per specimen: one in the lateral parasagittal groove and one in a control region 5 mm lateral to the parasagittal groove. Arrays of between 708-1492 indentations were designed individually for each site, using 50x qBSE images (from Chapter 5) as tissue maps and an ImageJ macro (Appendix 3.1.3: UmisArrayDesigner.txt p. 161) that produced a scaled layout file for the UMIS 2000. The macro also drew the desired array on the tissue map and gave an estimated time to completion (Figure 7-1). Each array incorporated HAC, ACC and subchondral bone, contained at least 500 μm width of subchondral bone and incorporated sufficient ACC to result in at least 50 usable ACC indentations. Indentations were spaced at 20 μm intervals in *x* and *y*. Because there was substantial variation in ACC thickness, consistency in mineralisation and flatness of the prepared surface, geometry of indentation arrays varied in width and depth. The number of indentations per array was limited by the time available for each run: since each indentation test required 3.7 minutes to complete, approximately 390 tests could be completed per 24 hours. The shortest run took just under 2 full days to complete (1 day 19 h), while the longest required 3 days and 20 hours. Twenty-four sites in total were tested, comprising 2 sites from each of the 12 right C-slices.

Specimens were used as previously processed for qBSE imaging. Surfaces had been embedded in PMMA and diamond ultramilled, which leads to smoother and flatter surfaces than polishing. Each specimen was glued to a steel stub with cyanoacrylate adhesive and mounted on the UMIS stage. The indenter tip was aligned in x, y and z axes with a microscope mounted to the indentation apparatus. Visualisation of the specimen in the microscope allowed rotational orientation of the specimen and accurate placement of the array in the desired microanatomical location. The working distance was set and the indentation run initiated.

Parameters for indentation were similar to those used in earlier experiments on calcified tissues (Ferguson, Bushby and Boyde 2002; Ferguson, Bushby and Boyde 2003; Bushby, Ferguson and Boyde 2004; Bembey 2007). A 5 μm radius spherical diamond indenter tip was used to make indentations with 40 load increments, with 75% partial unloading between each increment. The same tip was used for all indentations. Measurements of force (mN) versus Z-displacement (nm) were logged to hard disk at each load increment. Mineralised tissues are known to have viscoplastic as well as elastic properties so the dwell time at each incremental loading was set to the minimum allowed by the apparatus (0.1 seconds) to avoid time-dependent strain (creep) effects on measurements of elastic modulus. A spherical indenter tip was used rather than a Berkovich tip, increasing the loading rate during unloading and reducing the severity of the stress field, resulting in lesser effects of creep.

A set of marker indents were included in the array layout to facilitate localisation of the array in later qBSE imaging; these were incremented to a maximum force of 50 mN. Indentations in the body of the array were incrementally loaded to a maximum of 20 mN with a square root progression. Contact force was set to 0.3 mN.

7.7.3 UMIS Data Processing

Each indentation resulted in a dataset comprising 40 force-displacement data points, each point corresponding to a loading increment. Previous work found a low-modulus surface layer and stabilisation of elastic modulus once this surface layer had been passed (Bushby, Ferguson and Boyde 2004). For this reason, force-displacement data from the deepest 10 loading increments only were used to determine elastic modulus.

Elastic modulus was calculated as a function of contact depth (Field and Swain 1993) for each load-partial unload data pair, and a mean value of indentation modulus (E) was derived for each indentation site from the 10 deepest increments. E' may be calculated for spherical indentations to allow for better comparison with Berkovich indenter data. The reduced modulus, E_r, is calculated using Hertzian contact mechanics from the elastic penetration depth (h_e) of the sphere under force P, given by

Equation 7.1

$$E_r = \frac{3}{4} \times \frac{P}{h_e^{3/2}} \left(\frac{1}{R} - \frac{1}{R'} \right)^{1/2}$$

where

Equation 7.2

$$\left(\frac{1}{R} - \frac{1}{R'} \right)$$

is the relative curvature between the sphere and residual impression in the surface (Bushby 2001). E' is derived from E_r again, using Equation 7.3:

Equation 7.3

$$\frac{1}{E_r} = \frac{1}{E'_s} + \frac{1}{E'_i}$$

Equation 7.4

$$E'_x = \frac{E_x}{1 - \nu_x^2}$$

v is Poisson's ratio for material x.

Data were processed with an Excel macro in batches of 25 indentations and mean ± standard deviation of elastic modulus collated for each indentation array.

7.7.4 Array Imaging in qBSE and Topographic BSE

Each completed nanoindentation array was imaged in the SEM at a nominal 150x magnification (field width 599.5 μm) in two modes: qBSE and topographic backscattered electron (BSE)

imaging. qBSE imaging has been described earlier in this thesis (Section 4.3.2 p. 72). Topographic BSE imaging requires that half of the BSE detector be reversed in polarity, highlighting surface topography by creating a directional lighting effect on the specimen surface. The specimen was not moved between qBSE and topographic BSE imaging, so image pairs were automatically in register. Most of the nanoindentation arrays were bigger than a single field so montages of up to 5 image fields were constructed manually, ensuring that matching tiles in qBSE and topographic BSE images remained exactly in register in the resulting montage images.

A program (Appendix 3.1.4: Umis_Array.txt, p. 164) was written in the ImageJ macro language to correlate topographic images with registered qBSE images. It ensured that the indentation modulus at a given point was accurately correlated with backscatter coefficient from the same point. Topographic images showed residual impressions left at many but not all indentation sites (Figure 7-2). A small amount of skew was present in the SEM images, due to a slight deviation in the x:y aspect ratio being sent from the SEM's scan rotation unit to the electron beam scan generator. The indentation array could also be in any rotational and translational position within the images. UmisArray corrected for translation, scale, rotation and shear transformations between the indentation array layout file and the images of the indentation array, and was designed for rapid, error-free user interaction. Three key points on the array, bottom left (0,0); bottom right (xmax, 0) and top left (0, ymax), were identified by the operator. The macro calculated the pixel position within the image of each indentation by relating the user-dentified key points to the layout file and drew a circular ROI at each position in the qBSE image. Registration errors between individual indentations' topographic and qBSE images could be corrected by moving the ROI to the appropriate position with the mouse; however, this function was rarely required.

The operator identified the tissue type at each position or rejected the data from the position by entering a number; 0 = reject, 2 = ACC, 3 = cement line, 4 = bone. A position was rejected if it fell on a crack, an uneven surface, a cell lacuna, marrow space or HAC. Positions that were

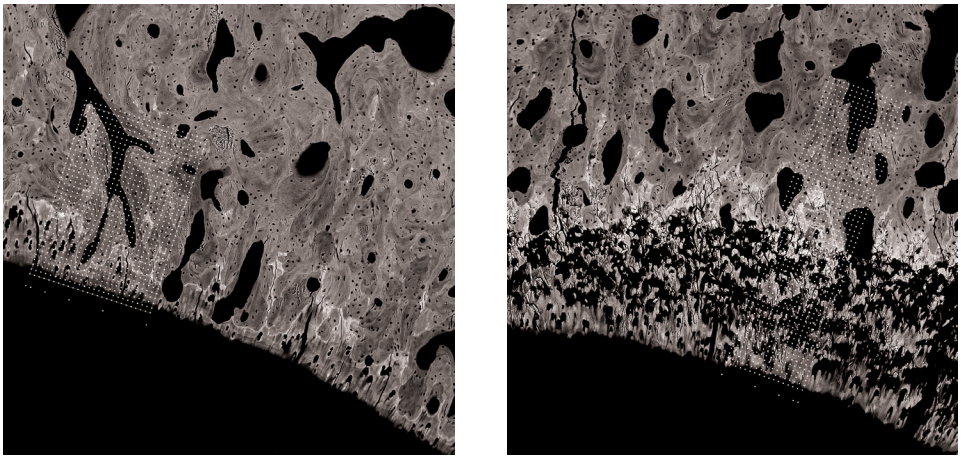

Figure 7-1: Nanoindentation Array Maps

Nanoindentation array layouts designed with UmisArrayDesigner.txt on unaffected (left) and affected (right) parasagittal grooves. Field width 1591 µm.

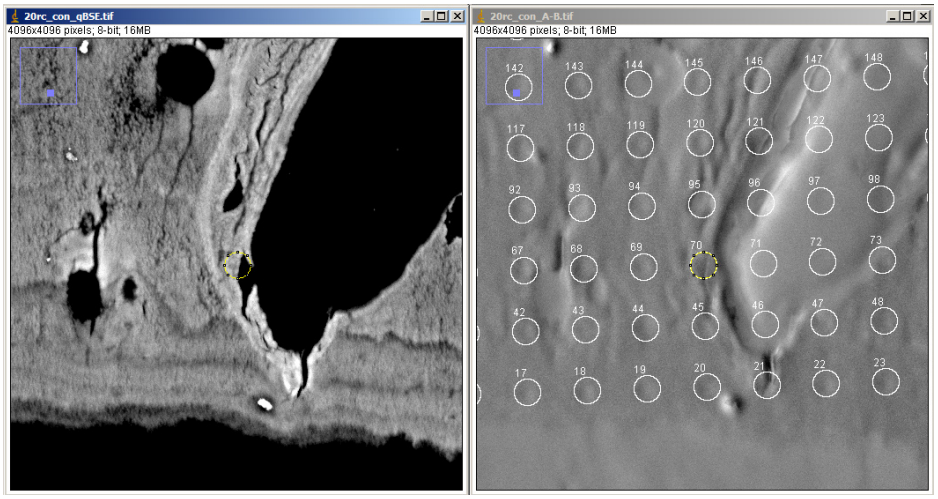

Figure 7-2: Use of UmisArray

affected by high electron backscatter from topographic ridges were rejected to avoid artefactually increased interpretation of mineralisation density. Repeat measurement resulted in approximately 10% of positions being classified differently in successive runs (Table 7-1). Therefore, all arrays were measured and classified twice and positions with non-matching classifications reclassified as 0 (reject). qBSE data were matched to elastic moduli and entered into SPSS for statistical analysis. Exercise effects were assessed with the non-parametric Mann-Whitney U and Kolmogorov-Smirnov Z tests on means calculated for each horse, site and tissue. Specimens were designated 'affected' or 'non-affected' based on criteria developed in previous chapters: those specimens with at least one site containing thickened, poorly mineralised ACC were 'affected' and those with thin ACC and well-integrated ACC and subchondral bone in both sites were 'non-affected'. Elastic moduli and mineralisation density in affected ACC and bone were compared to non-affected ACC and bone with univariate ANOVA and Tamhane's T2 post-hoc comparisons, using pooled indentations grouped by site and tissue.

7.8 Results

Several indentations per array yielded no elastic modulus data, usually because the indentation tip had proceeded beyond its maximum Z-range of 2,000 nm. Such measurements may have been the result of the indenter tip testing non-flat regions, or causing subsidence of inhomogeneous matrix components.

Table 7-1: Duplicate Classification of Indentations

Counts		First Run				
		Reject	**ACC**	**Cement Line**	**Bone**	**Subtotal**
Second Run	**Reject**	**11319**	126	78	458	11981
	ACC	558	**2256**	65	41	2920
	Cement Line	56	19	**324**	29	428
	Bone	1267	16	101	**6945**	8329
	Subtotal	13200	2417	568	7473	**23658**

Table 7-1 summarises the results of repeated tissue typing with UmisArray. 23,658 indentations were made, from which 2,256 were accepted into the ACC dataset and 6,945 accepted into the bone dataset. This represented approximately 1,500 hours of indentation testing.

No effect of preconditioning exercise was found for either *E* or mineralisation density in ACC or bone in either the condyle or parasagittal groove. Highly significant differences ($p < 0.001$) were found between affected and unaffected ACC and bone in both sagittal ridge and condyle sites (Figure 7-5).

A smear of data tending towards high mineralisation density and low nanoindentation was seen in affected parasagittal groove ACC (Figure 7-4F). Cut-off values of Dm > 100 and *E* < 10 GPa were introduced in order to explore the data that fell outside the expected trend, i.e. those indentations of tissue that was apparently well mineralised but which yielded lower than expected values for *E*. Two-hundred indentations fell into this range, 115 of which were from ACC and 85 from bone. Examination of indentation sites using UmisArray's GoTo feature revealed that most should have been excluded in the first 2 rounds of typing based on the defined criteria. However, several of the filtered indentations appear in sites in which there was no obvious cause for a low *E* and were in sites that satisfied the criteria for inclusion. 200 indentations out of over 20,000 represents less than 1% of the total, so was considered mainly classification error and occasionally an indentation on a thin remnant of ACC overlying a cellular lacuna or marrow space. The predominance of such indentations in ACC from affected parasagittal grooves may be explained by the irregular pattern of mineralisation increasing the likelihood that an indentation will fall on an edge or rough

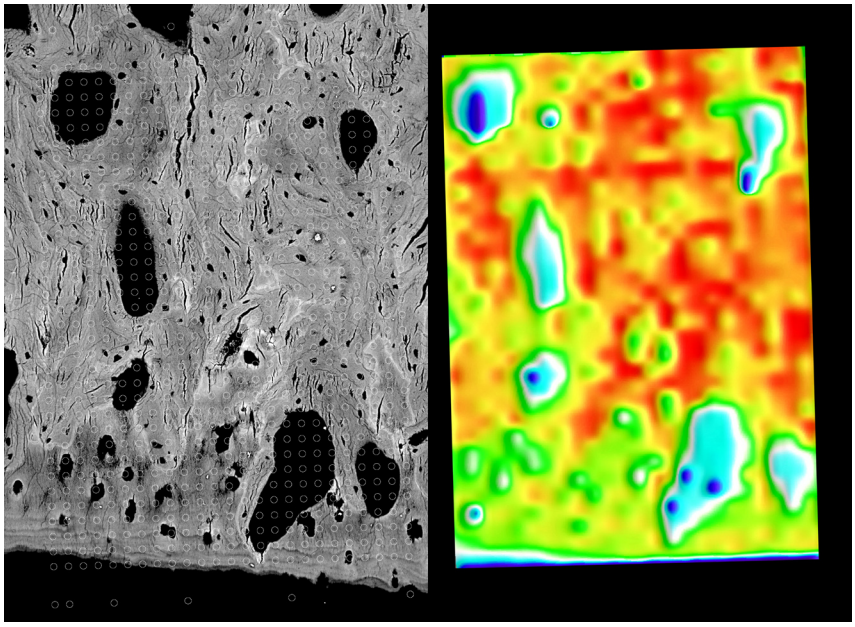

Figure 7-3: Correlated qBSE and Nanoindentation Modulus Maps

qBSE image (left) and map of *E* (right) of an unaffected site showing spatial variation in *E* relating closely to tissue morphology. Note the lower *E* in ACC (yellow-green, to bottom of image) than subchondral bone (yellow-red). Dark blue is the lowest modulus (0-5 GPa); red is the highest modulus (20-25 GPa).

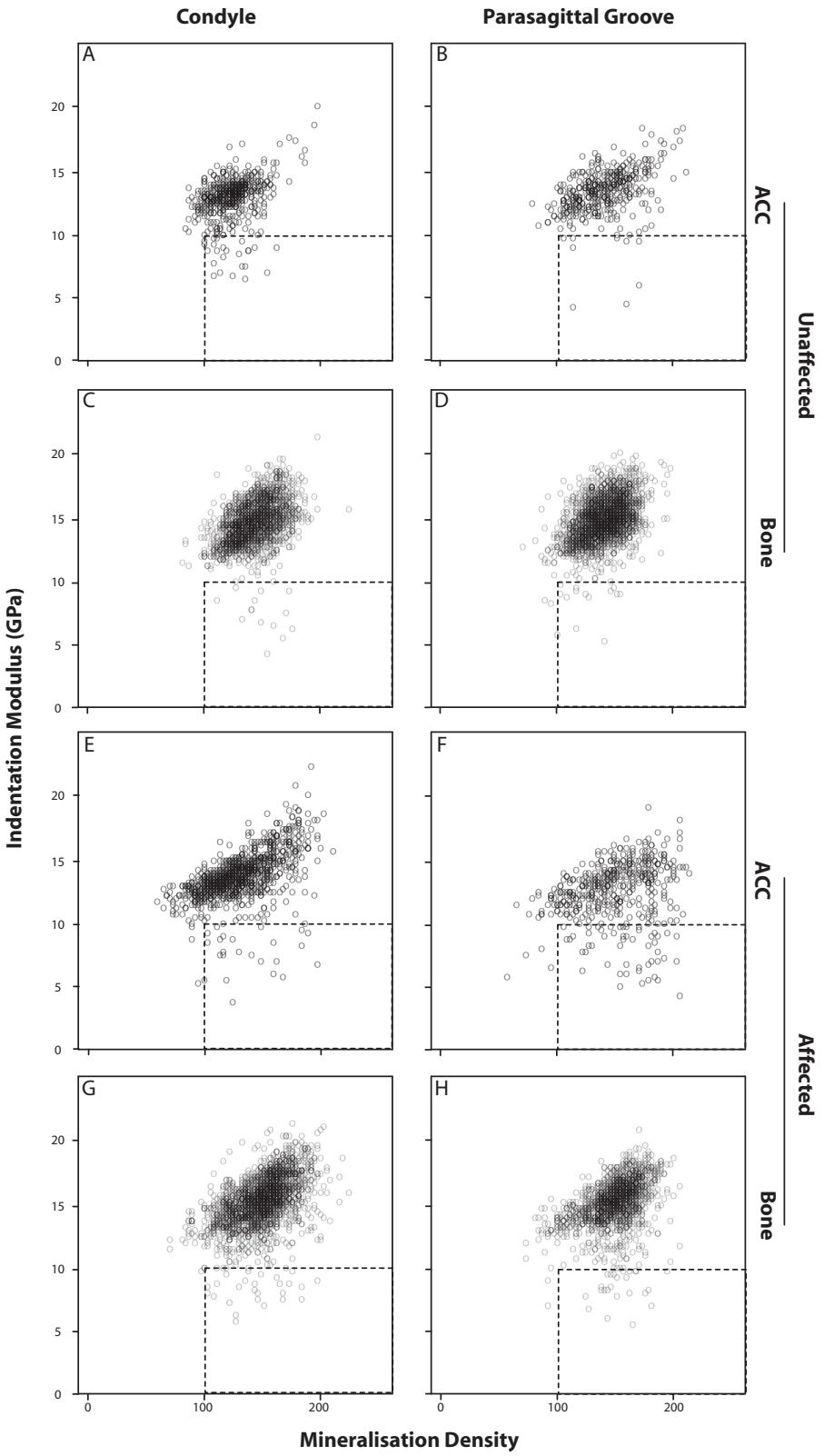

Figure 7-4: Indentation Modulus versus Mineralisation Density by Site and Tissue Type

Scatter plots of all data that remained after 2 rounds of tissue typing in UmisArray. Dashed lines bound data that were excluded from analysis after individual examination of outlying points showed that they usually failed the criteria for inclusion.

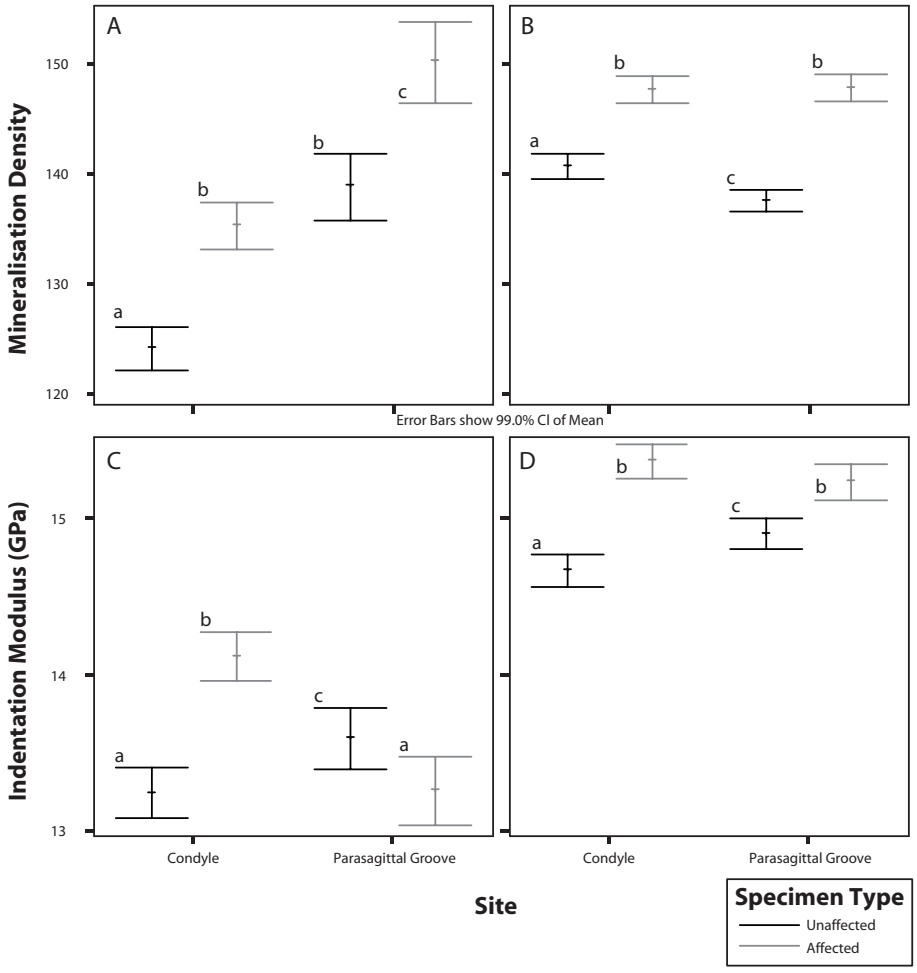

Figure 7-5: Mineralisation Density and Indentation Modulus by Site

Significant differences ($p < 0.01$) denoted by different letters within each graph. Note the inconsistent relationship between mineralisation density and indentation modulus in ACC, in particular, the lower than expected indentation modulus for ACC in the parasagittal groove.

surface (resulting in a low reading of *E*), compared to normal ACC, which was usually smooth and evenly mineralised. One specimen with normal-looking ACC gave several low *E* values for ACC, possibly because of surface contamination resulting in asperity contacts well above the true surface of the specimen. All 200 dubious indentations were excluded from analysis.

7.9 Discussion

Nanoindentation calculations assume that the specimen is a homogenous, isotropic material with a mathematically flat surface. Normal bone and ACC are neither homogenous nor isotropic, being variably hydrated and oriented mixtures of organic, inorganic and cellular components. Thus, testing of irregularly mineralised tissue in specimens with sometimes imperfectly flat surfaces presents a challenge to nanoindentation testing. The approach here, of using a very large number of indentations and excluding invalid tests based on morphological characteristics at each position, has resulted in a usable data set. Regional variations in bone matrix anisotropy may lead to averaging and elimination of bias if a large enough area is included in the indentation array.

Arrays were made as large as possible in this study, given the constraints of time and the field width of a 150x SEM image. Collagen within ACC is highly organised and in the sections used in this study was aligned parallel to the plane of section so site-related bias referable to collagen orientation in ACC should not be present in the data. Islands of mineralisation were present in affected ACC making indentation data difficult to obtain because a large number of indentations fell on unmineralised tissue or small cracks within mineralised tissue. Such sites were excluded from analysis to improve data fidelity.

There is a general positive correlation between mineralisation density and *E* for both bone and ACC, however, this relationship is not as strong as sometimes suggested (Seeman 2007) and appears to break down in affected parasagittal grooves. A cluster of indentations with high mineralisation density and low *E* can be seen on the *E* versus mineralisation density scatter graph (Figure 7-4F). These data were mainly concentrated in affected parasagittal groove ACC and related to indentations failing to be excluded after 2 rounds of typing despite not meeting the criteria for inclusion. The occasional indentation would be expected to fall upon a thin layer of mineralised matrix overlying a cell lacuna or marrow space, leading to unusually low values of *E* as the tip broke through this thin layer into PMMA. Further investigation showed that these aberrantly low *E* values mainly came from indentations that fell upon cracks, edges and irregular surfaces, which were plentiful in affected ACC.

The pattern of mineralisation within affected ACC is clearly abnormal, as has been discussed throughout this thesis. Patchy islands of mineralised ACC are separated by strands of unmineralised cartilage matrix and chondrocytes. This may represent a loss of control of the mineralisation process, or damage to hyaline cartilage resulting in mineralisation of disrupted extracellular matrix. Alternatively, the pattern of mineralisation may be different in the epiphyseal growth cartilage and adult ACC, and such thickened, 'affected' areas of ACC might represent normally mineralised (but slowly resorbing) epiphyseal growth cartilage.

Bone is known to be notch sensitive, that is, the inclusion of a stress concentrator dramatically reduces fracture energy. However, bone's notch sensitivity is dependent on its mineralisation density and Young's modulus, increasing as mineralisation density and Young's modulus increases (Currey, Brear and Zioupos 2004). Mineralisation density of both ACC and bone was raised in affected parasagittal grooves, while the *E* of ACC was reduced and the *E* of bone was raised. Together, these findings support the presence of materially inferior ACC forming a stress concentrator in the lateral parasagittal groove and the underlying bone being more notch-sensitive than elsewhere in the condyle. It is likely that stress concentration within the parasagittal groove due to materially inferior ACC increases the probability of fatigue failure in the distal Mc3.

8: Effects of Age and Unloading

8.1 Introduction

Bone is known to be highly responsive to its mechanical environment; however, the exact mechanisms of load-sensing and tissue remodelling are still being elucidated (Section 1.4: Bone Mechanobiology, p. 20). Training exercise is known to result in rapid, profound changes in Mc3 trabecular structure through the apposition of on existing bone surfaces without prior resorption (Boyde and Firth 2005b). Bone apposition results in increased VFb, which is evident on pQCT as increased vBMD (Firth, Rogers, Doube and Jopson 2005). The timing of bone apposition within a training season is unknown, but is thought to be associated with exercise at canter-intensity and greater.

Unloading results in rapid bone resorption (Section 1.4.1, p. 20). Riggs et al. demonstrated massively decreased VFb in a Warmblood horse that had been non-weight bearing on its left forelimb for 8 weeks prior to euthanasia. Resorption had occurred in both the affected (left) and unaffected (right) Mc3 (Riggs, Whitehouse and Boyde 1999b) despite the normal expectation of increased weight bearing in the non-lame limb. It is possible that the horse had adjusted its stance to shift weight bearing to the hindlimbs, which would unload both forelimbs and result in bone resorption in both Mc3.

Cracks in ACC may heal by infilling with high mineralisation density, amorphous material (Boyde 2003). No evidence of this phenomenon was observed in the 18-month-old specimens, indicating that any cracks that had formed either had been removed by chondroclastic resorption or had not been in-filled. In rapidly turning over ACC, it is possible that there is insufficient time for infilling to occur prior to normal endochondral ossification. The timing of crack infilling with or without resorption is unknown.

This chapter examines material from horses raised contemporaneously with the animals described in earlier chapters of this thesis, but which were euthanised after 18 months old. Six horses trained in real race-training conditions for 2 seasons and were euthanised as 3-year-olds. One horse suffered a broken humerus and was non-weight bearing until its euthanasia several weeks later. Mc3 from these horses were available for study so were prepared and analysed in a similar manner to the 18-month-old Mc3 and examined for changes related to age, exercise and unloading. Special attention was paid to the ACC of the parasagittal grooves of the C-slice, to identify changes that might be related to the development of condylar fracture.

8.2 Materials and Methods

Methods from previous sections were repeated on tissue from 6 3-year-old horses, 2 of which had received preconditioning exercise, and all of which race-trained and raced in 2 successive seasons (Section 2.1). Quantitative and qualitative comparisons were made between age groups to investigate changes related to maturation of the Mc3 condyle. Specimens from the horse that

was euthanised at 19 months old due to a displaced physeal fracture of the right proximal humerus were prepared and examined for effects that might be associated with its 4 weeks of non-weight bearing and box rest.

8.2.1 Microradiography

Microradiography was performed as in Section 3.3.2, p. 57.

8.2.2 qBSE

qBSE was performed as in Section 4.3.2, p. 72, except that montages were constructed from tiles of 256 x 256 pixels rather than 1024 x 1024 pixels. ACC was imaged at 50x in the 7 previously-defined sites and thickness and mineralisation density measured on all 3-year-old specimens.

8.2.3 DXA

DXA was performed on all 3-year-old specimens prior to embedding, as in Section 6.3.2, p. 95.

8.2.4 Confocal Microscopy

CSLM montages and individual images were made of sites selected from BSE images. The carbon coat was removed by briefly polishing with 2000-grit carborundum paper moistened with distilled water. The 3-year-old horses had not received calcein labels at 18 months, although 4 did receive tetracycline labels just prior to euthanasia (Table 2-1, p. 53).

8.3 Results

8.3.1 Parasagittal Groove Cracks

Cracks in ACC in-filled with high mineralisation density, amorphous material were present in at least 2 sites in all 6 3-year-old horses' Mc3 (Figure 8-1), totalling 19 sites out of 252 imaged (6 horses, 2 Mc3 per horse, 3 slices per Mc3, 7 sites per slice). Only parasagittal groove sites contained in-filled cracks, with medial (n = 10) and lateral (n = 9) parasagittal grooves evenly represented. Sites with in-filled cracks were found mainly in the C-slice (n = 16), sometimes in the B-slice (n = 3) and never in the A-slice (X^2, p = 0.003). Thus, 19 out of 72 (26.3 %) parasagittal groove sites, and 16 out of 24 (66.7 %) C-slice parasagittal groove sites contained in-filled ACC cracks. All the affected B-slice sites were in medial parasagittal grooves, 2 of which were in the left and right B-slices in a single horse, which also had bilaterally affected C-slice lateral parasagittal grooves but unaffected C-slice medial parasagittal grooves. The left Mc3 appeared to be affected more frequently (n = 12) than the right Mc3 (n = 7), however this was not statistically significant (X^2, p = 0.251).

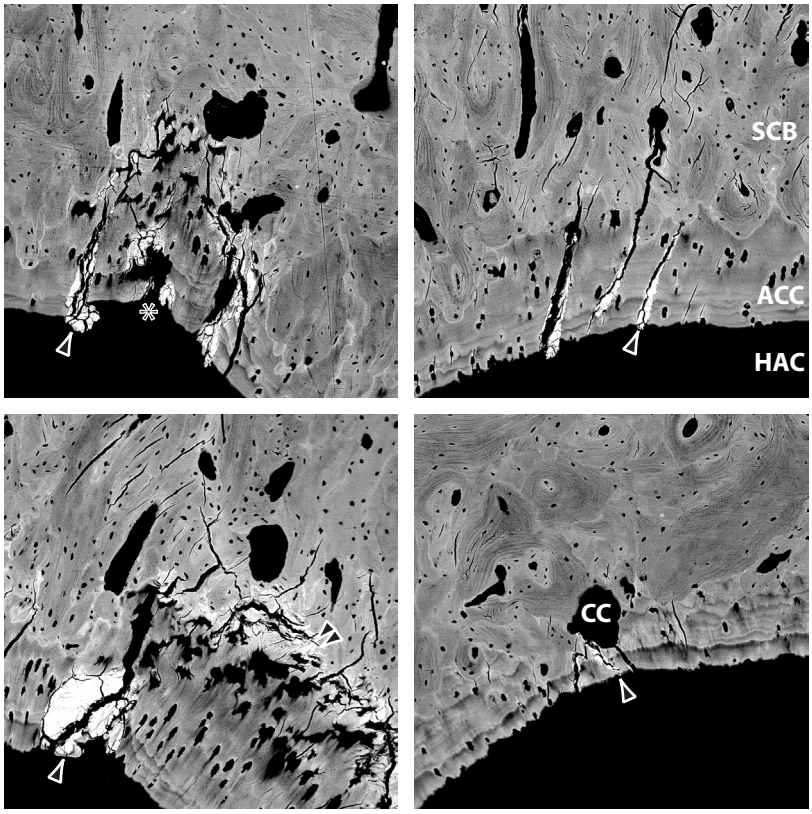

Figure 8-1: ACC Crack Infilling

Amorphous, mineralised material fills cracks in ACC and penetrates mineralising front (arrowheads). Double arrowheads indicate hypermineralisation of osteochondral junction. CC, chondroclastic resorption removes crack filler material. Mineralisation front may be damaged and delayed (*). SCB, subchondral bone; ACC, articular calcified cartilage; HAC, hyaline articular cartilage. Field width 891 µm.

One C-slice contained single fissures approximately 2 mm deep and 140 µm wide in both parasagittal grooves, comprising a cleft through HAC and into a trench lined by a thin layer of ACC and supported by subchondral bone (Figure 8-2). It appears that crack infilling and subsequent resorption and replacement by bone failed or did not initiate in these sites. Extrapolation from the morphology of the thickened, poorly mineralised ACC in 18-month-old parasagittal grooves (Figure 7-1B, p. 108) to the trench morphology in 3-year-old parasagittal grooves led to a hypothetical model for linear defect development (Figure 8-3).

Figure 8-2: ACC Trenches

(Facing page) Defects in the joint profile were found in both parasagittal grooves of one specimen, 28RA. (A) qBSE montage of the whole slice. Arrows indicate defects, box enlarged in B and C. Image width 55.4 mm. (B & C) qBSE and CSLM images of a defect showing a bony trench lined with ACC and HAC. Arrowheads show the cement line; SCB, subchondral bone. Blue = reflection, green & red = spectrally separated tissue autofluorescence. (D) Bony repair of the defect is underway but does not penetrate further than the mineralising front between ACC and HAC. (E) Deep zone HAC is obliterated between ACC and tangential zone HAC. Field width 600 µm.

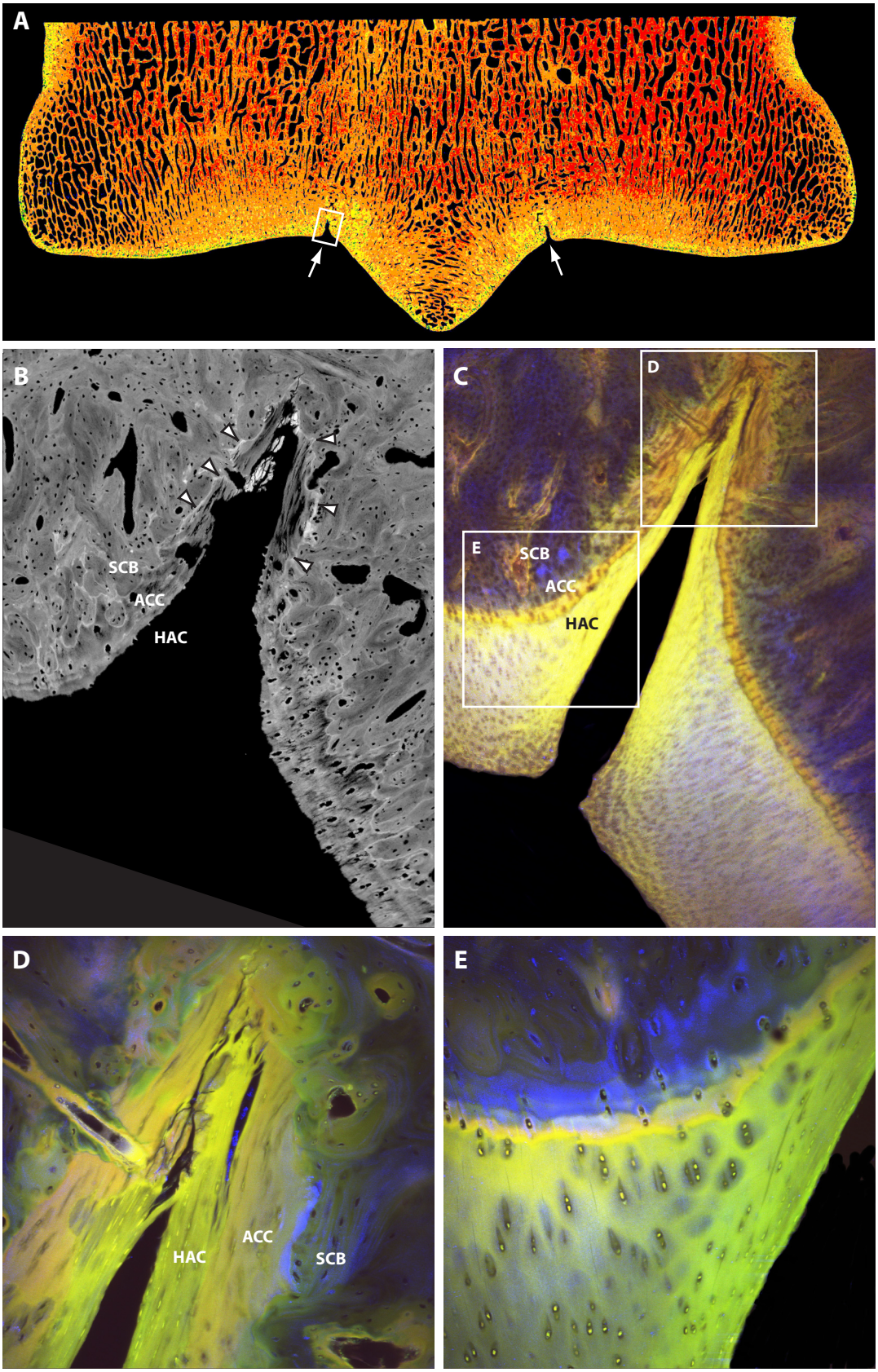

Figure 8-2: ACC Trenches

One specimen (10LA) contained an island of unmineralised cartilage surrounded by bone, just deep to ACC on the sagittal ridge (Figure 8-4). Bony replacement of ACC appeared to have occurred, isolating this piece of HAC from the main articular cartilage (Figure 8-5). Extrapolation from the morphology seen in Figure 3-5 (p. 64), where a thickened piece of poorly-mineralised ACC was being ineffectually removed by chondroclastic resorption at 18 months old, to the morphology seen at 3 years old (Figure 8-4), led to the development of a hypothetical model of endochondral ossification in foci of unmineralised ACC (Figure 8-5).

8.3.2 Microradiography

A-slice sagittal ridge lesions were present at about the same frequency at 3 years old as at 18 months old, but appeared to be deeper in some cases than seen at 18 months (28ra_5x, 32rd_5x). ACC/subchondral bone defects in the sagittal ridge were well-supplied by blood vessels that had to penetrate very high volume fraction bone. Cracks in the parasagittal groove were present, involving ACC and subchondral bone (28rc_5x). One specimen showed moderate subchondral bone collapse in the palmar condyles, in the region that POD is found (10rc_4x_lc).

8.3.3 DXA and qBSE of ACC and Bone

ACC was significantly thicker and more highly mineralised in 3-year-old than 18-month-old horses (Figure 8-6). Correlation of qBSE data to intra-vital labelling could not be repeated on the 3-year-old specimens because the would-be fluorochrome labels were not visible in bone or ACC in any 3-year-old Mc3 when examined under CSLM (488 nm Kr/Ar laser excitation) and standard epifluorescence (mercury vapour excitation). LAR and inter-label mineralisation density could not be measured because both require clear bands of labelling.

VFb was strongly related to vBMD, while BMMD was not related to vBMD at all (Figure 8-7). vBMD (and by association, VFb) was significantly higher in 3-year-old than 18-month-old Mc3 in most sites (Figure 8-9). The site-related trends in ACC and bone in 3-year-olds echo those seen in 18-month-olds (Sections 5.4.1, p. 86; 6.4.1, p. 98).

Figure 8-3: Hypothetical mechanism for early development of linear defects

(Facing Page) (A) Normal endochondral ossification during growth. HAC mineralises regularly and is converted into ACC, which is then replaced by subchondral bone (SCB). (B) An insult to HAC damages chondrocytes (*) and reduces their competency to initiate mineralisation at the mineralising front (MF) and stimulate chondroclastic resorption at the osteochondral junction (OCJ). (C) The mineralising front becomes delayed, while HAC accumulates wear damage at the articular surface (AS). (D) Chondroclastic resorption reduces the thickness of ACC while HAC tears and the mineralising front circumvents unmineralisable HAC. (E) The HAC tear reaches ACC and chondroclastic resorption removes most poorly mineralised ACC. (F) A trench is formed as SCB surrounds the rift in HAC and ACC.

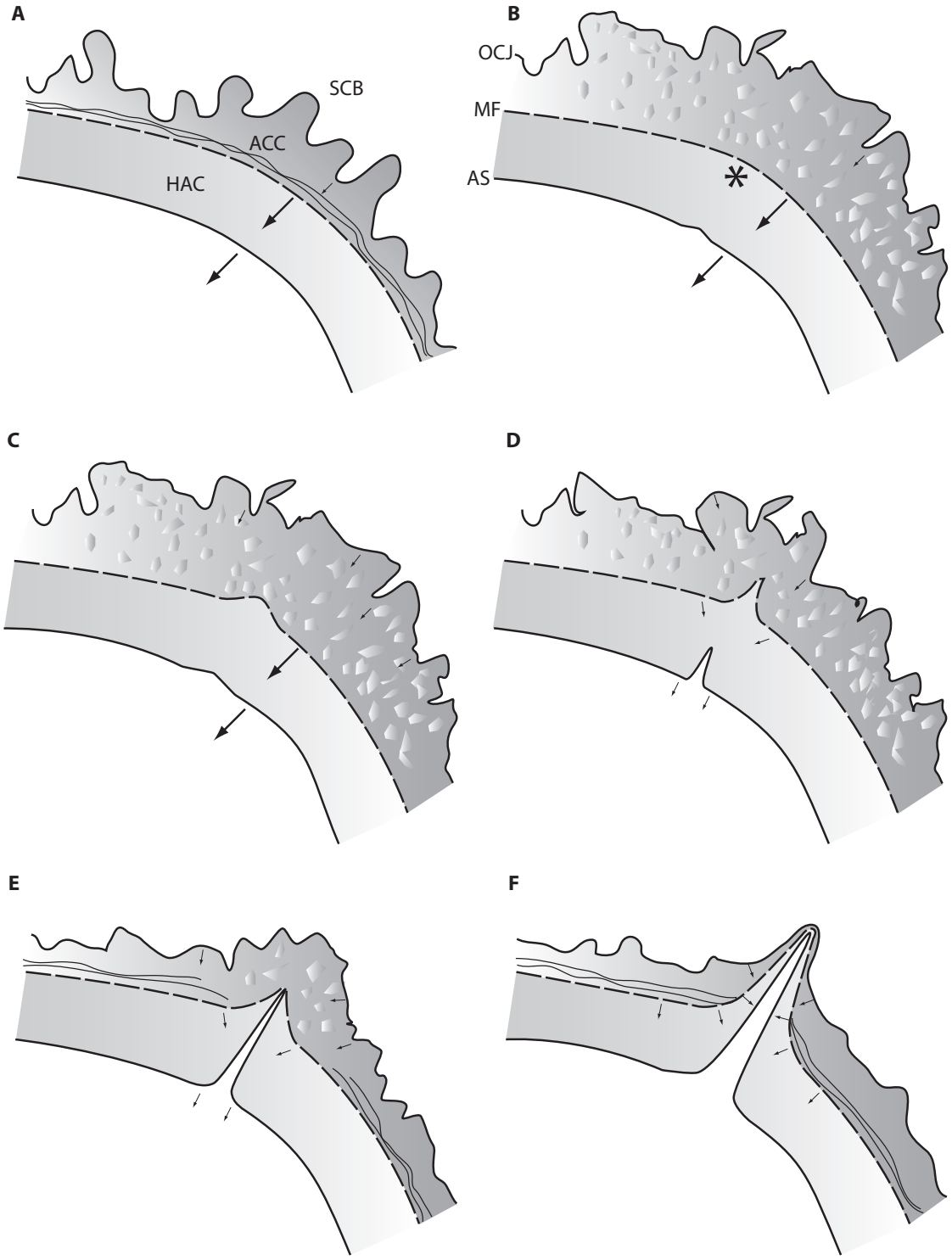

Figure 8-3: Hypothetical mechanism for early development of linear defects

8.3.4 Unloading

Gross resorption of trabecular bone and the subchondral bone plate was evident in Mc3 specimens from horse 09, which had been non-weight bearing on the right forelimb for 4 weeks prior to euthanasia (Figure 8-10). The specimens were extremely fragile: both the A- and C- slices from the right Mc3 snapped during handling, while specimens from the left Mc3 (and all other horses) survived intact. Low VFb was evident in both the fractured and weight bearing Mc3, being 0.40 and 0.50 respectively (Figure 8-10C, B), while VFb in the normal Mc3 A-slice of a similar-aged horse (16) was 0.59 (Figure 8-10A). Trabecular thinning and some resorption of the subchondral bone plate was apparent in the weight bearing limb (Figure 8-10B), while wholesale lysis occurred in the non-weight bearing limb (Figure 8-10C).

8.4 Discussion

In-filled cracks in bone and ACC were frequently present in parasagittal grooves, with a tendency to be found in the palmar C-slices more often than in the dorsal A-slices. Infilling and chondroclastic resorption prove that these cracks definitely preceded specimen preparation. In contrast, ACC cracks were present without evidence of repair in 18-month-old specimens, so cracks were more likely to be preparation artefacts or else specimens were prepared before the infilling repair process had occurred. Differentiating real cracks that existed prior to specimen collection from cracks that are artefacts of specimen preparation is critical if meaningful quantification of crack frequency is desired. Cracks may occur whenever tissue distortion is produced, such as during cutting, dehydration and under vacuum. PMMA casts demonstrate cracks that existed prior to methacrylate infiltration (Boyde, unpublished data), however, these may include cracks that occurred during dehydration. It is clear that cracks appear during SEM imaging as their growth can be observed in real time, however, quantification of the rate of SEM-related crack appearance in has never been performed.

That cracks in 18-month-old ACC showed no evidence of infilling suggests that the infilling process may only occur in older, more stable ACC, and that it requires some time to complete: young ACC may be removed before cracks have a chance to be repaired. C-slice parasagittal grooves of older horses are a fruitful region for the future study of ACC cracking and healing as two-thirds contained some degree of hypermineralised crack infilling. Hypermineralisation of ACC as observed at the osteochondral junction of 18-month-old horses may represent a similar phenomenon of matrix disruption followed by fluid leakage and subsequent mineralisation of the fluid-filled space. Infilling cracks with mineralised substrate may improve crack stability by bonding together crack surfaces or may function to improve chondroclastic resorption and subsequent replacement by bone, since mineralised substrates are usually necessary for osteochondroclasis.

ACC was significantly thicker in 3-year-old Mc3 than in 18-month-old Mc3, in 7 out of 14 sites. In no site was ACC significantly thinner in 3-year-old Mc3 than 18-month-old Mc3. This indicates a general ‘pulling-away’ of the mineralising front from the osteochondral junction, resulting in an overall increase in ACC thickness in the older animals. Neither LAR or lag time could be

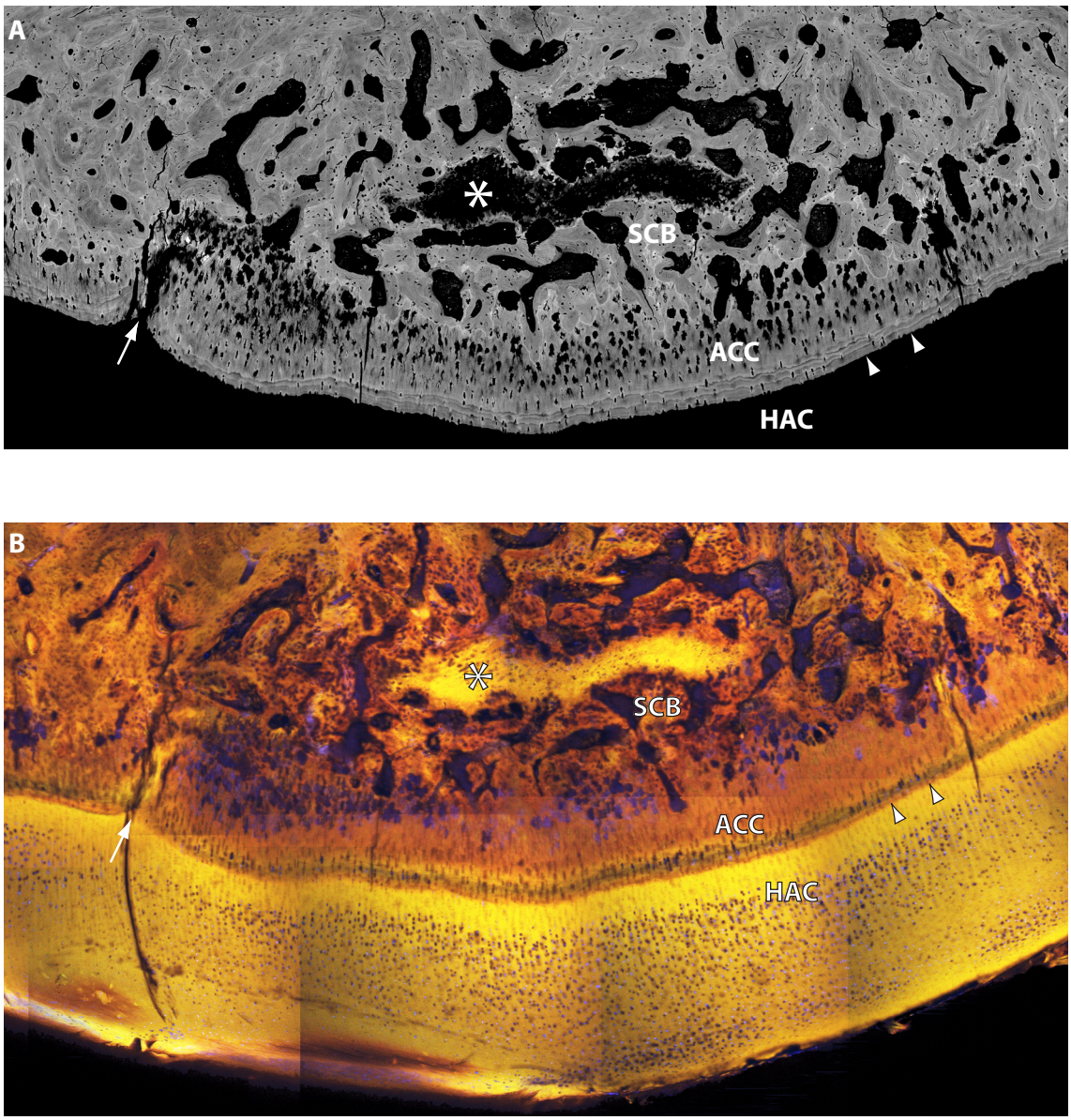

Figure 8-4: Hyaline articular cartilage inclusion in subchondral bone

qBSE (A) and CSLM (B) montages of the A-slice sagittal ridge of a 3-year-old horse's Mc3. The feature indicated by the asterisk (*) is unmineralised, hyaline cartilage surrounded by subchondral bone. The arrow indicates a region of retarded mineralisation and the development of an ACC trench filled with HAC. SCB, subchondral bone; ACC, articular calcified cartilage; HAC, hyaline articular cartilage; arrowheads, mineralising front. Image width 4.7 mm.

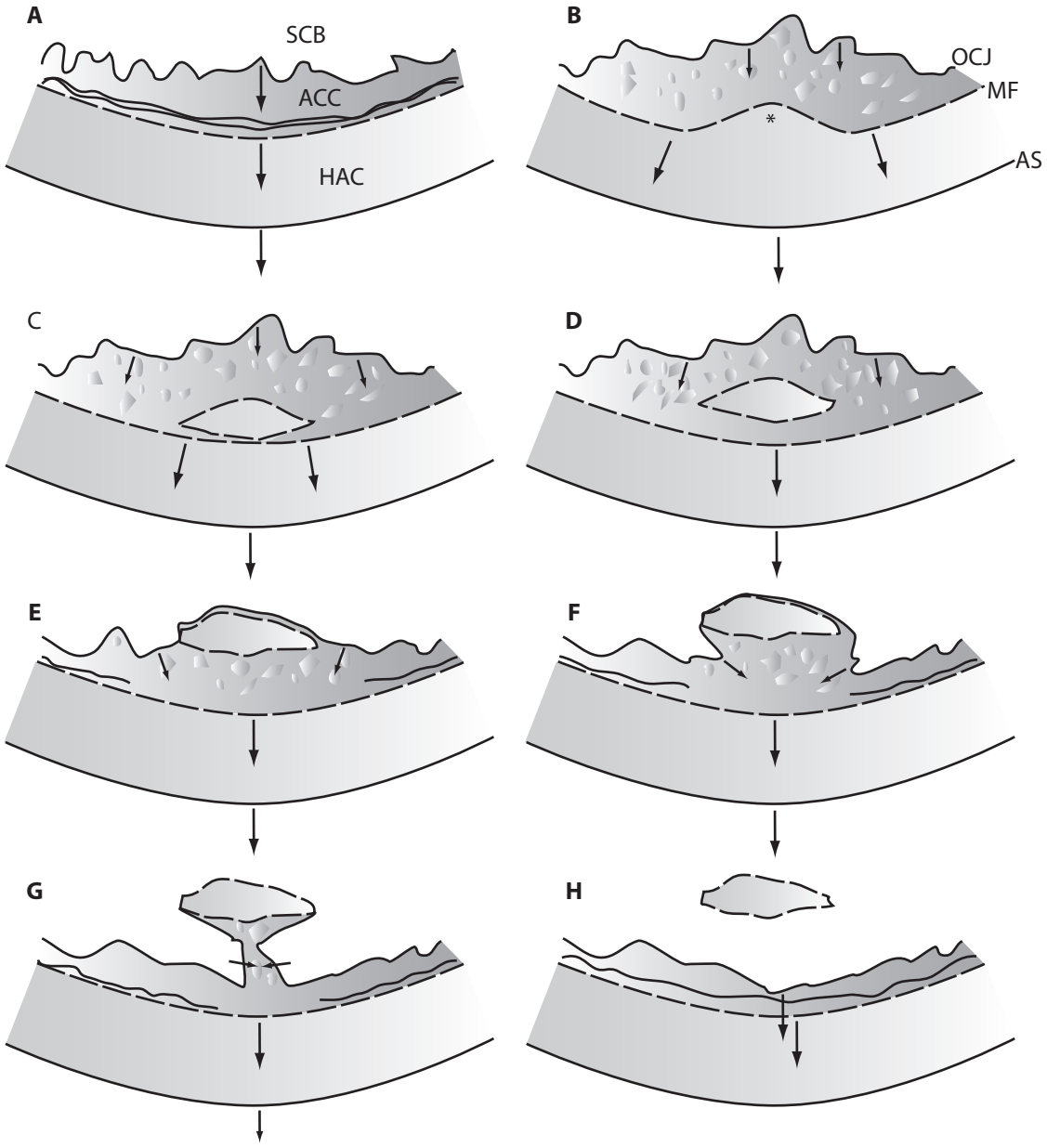

Figure 8-5: Hypothetical Development of HAC Inclusions

Endochondral ossification occurs as normal in the young (0-6 month-old) Mc3 epiphysis (A). Some defect occurs (*) in the progress of the mineralising front (MF) in (B), probably due to mechanical overload and chondrocyte injury or death. Impaired mineralisation occurs in surrounding ACC. (C, D) Healthy hypertrophic chondrocytes overlying the injured site resume cartilage mineralisation, leaving an unmineralised portion behind. (E,F,G) Chondroclastic invasion of mineralised cartilage and replacement with bone by osteoblasts circumvents the unmineralised portion of cartilage, resulting in (F), its isolation from the parent articular cartilage.

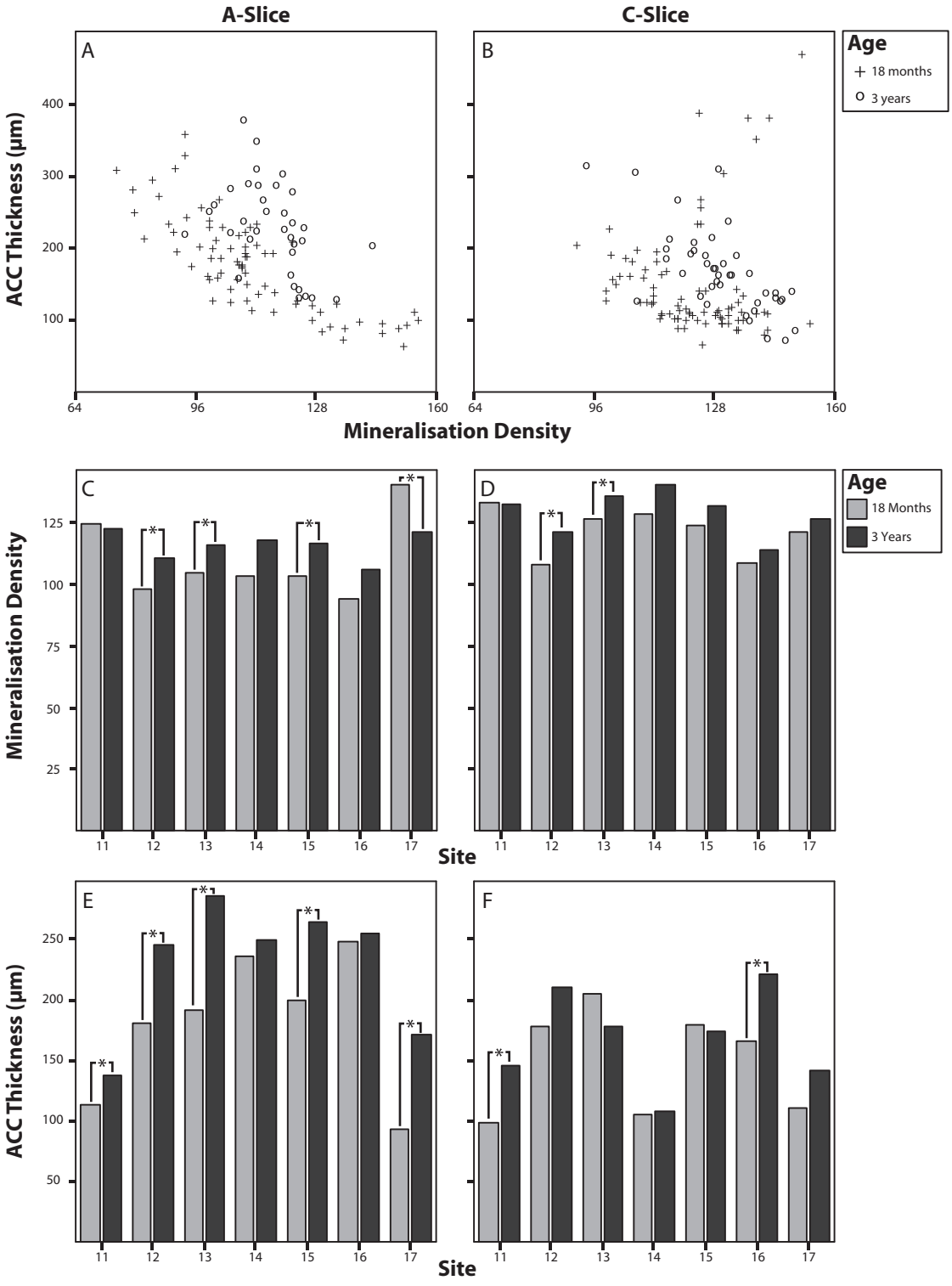

Figure 8-6: Age effects in ACC

ACC mineralisation density and thickness varied by site and age. Significant differences ($p < 0.05$) denoted by *. Note the generally greater mineralisation density and thickness in the older specimens (C-F).

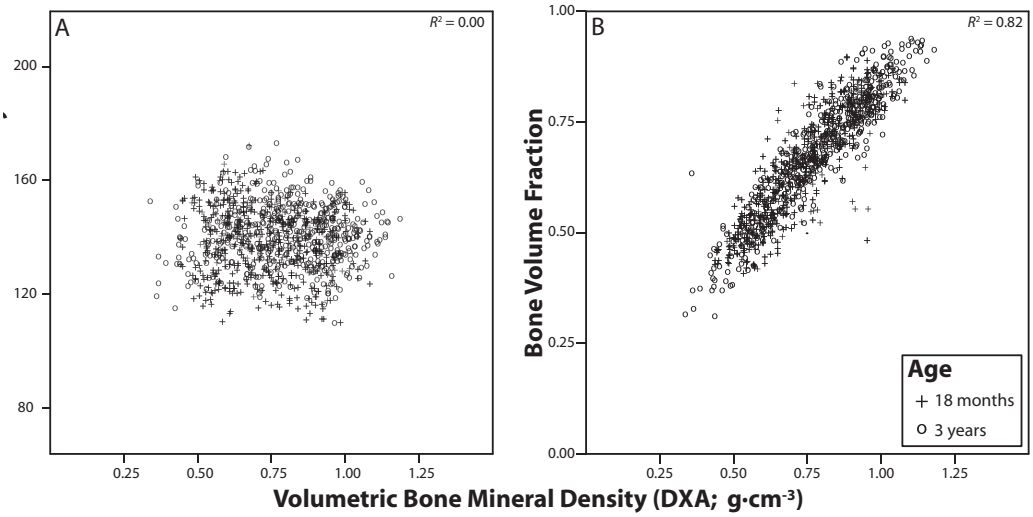

Figure 8-7: qBSE Matrix Mineralisation Density and Bone Volume Fraction versus DXA vBMD

Matrix mineralisation density (A) and bone volume fraction (B) determined on qBSE montages vs. volumetric bone mineral density determined by PIXImus DXA. There is a strong relationship between volume fraction and volumetric bone mineral density and no relationship between matrix mineralisation density and volumetric bone mineral density.

calculated due to failure of the injected fluorochrome labels, so it is impossible to ascribe increased ACC thickness to either increased mineralising front LAR or decreased chondroclastic activity at the osteochondral junction.

ACC was more highly mineralised in 11 of 14 sites in 3-year-old Mc3 than in the same sites in 18-month-old Mc3, however, a significant increase ($p < 0.05$) was found in only 5 sites. Increased mineralisation may have occurred at the mineralising front, or mineral may have gradually accrued behind the mineralising front between 18 months and 3 years. Only total-thickness and not inter-label mineralisation density could be measured in the 3-year-old specimens because of a lack of intra-vital labelling. Whether increased ACC mineralisation density with increased skeletal maturity is due to the mineralising front depositing more mineral or due to gradual mineral accretion behind the mineralising front is a question that could have been easily answered within the bounds of this study. All the horses could have received 2 doses of calcein at 18 months. Those that were to be euthanised as 3-year-olds could have received 2 doses of another label such as alizarin or a tetracycline just prior to euthanasia. Thus, the inter-label mineralisation density could be measured between calcein labels in 18-month-olds and 3-year-olds, testing the rate of mineral accretion or dissolution over time in mineralised ACC. Further, mineralisation density at the mineralising front could be compared between 18-month-old and 3-year-old horses. This experiment should be considered in future studies, with the possible inclusion of more time points.

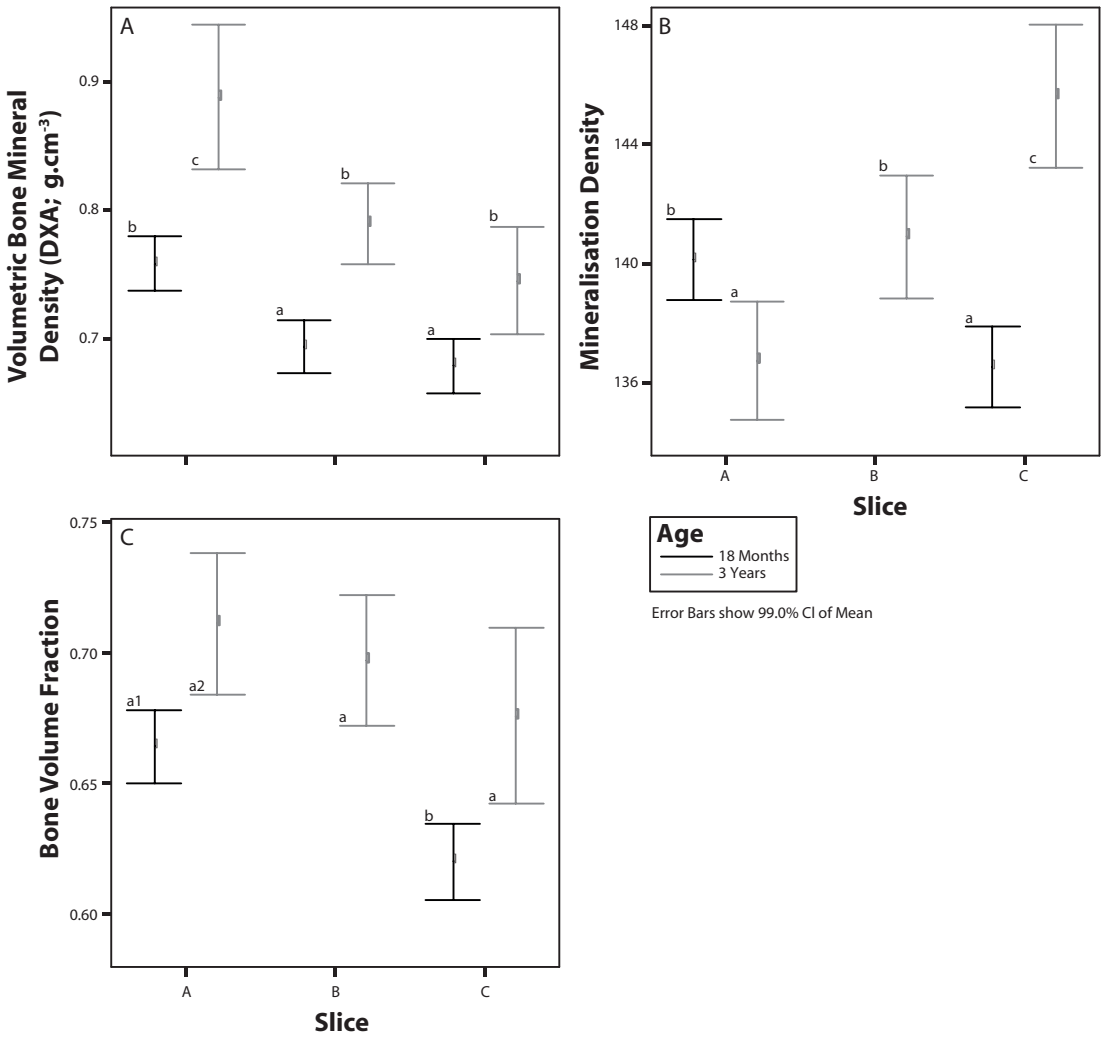

Figure 8-8: Age Effects in Condylar Bone

Significant slice- and age-dependent differences were found in vBMD, bone volume fraction and matrix mineralisation density. Note the similar trends in DXA-determined vBMD (A) and qBSE-determined bone volume fraction, which is not present in matrix mineralisation density (B). 18-month-old B-slices were not available for qBSE, so are not represented in these graphs.

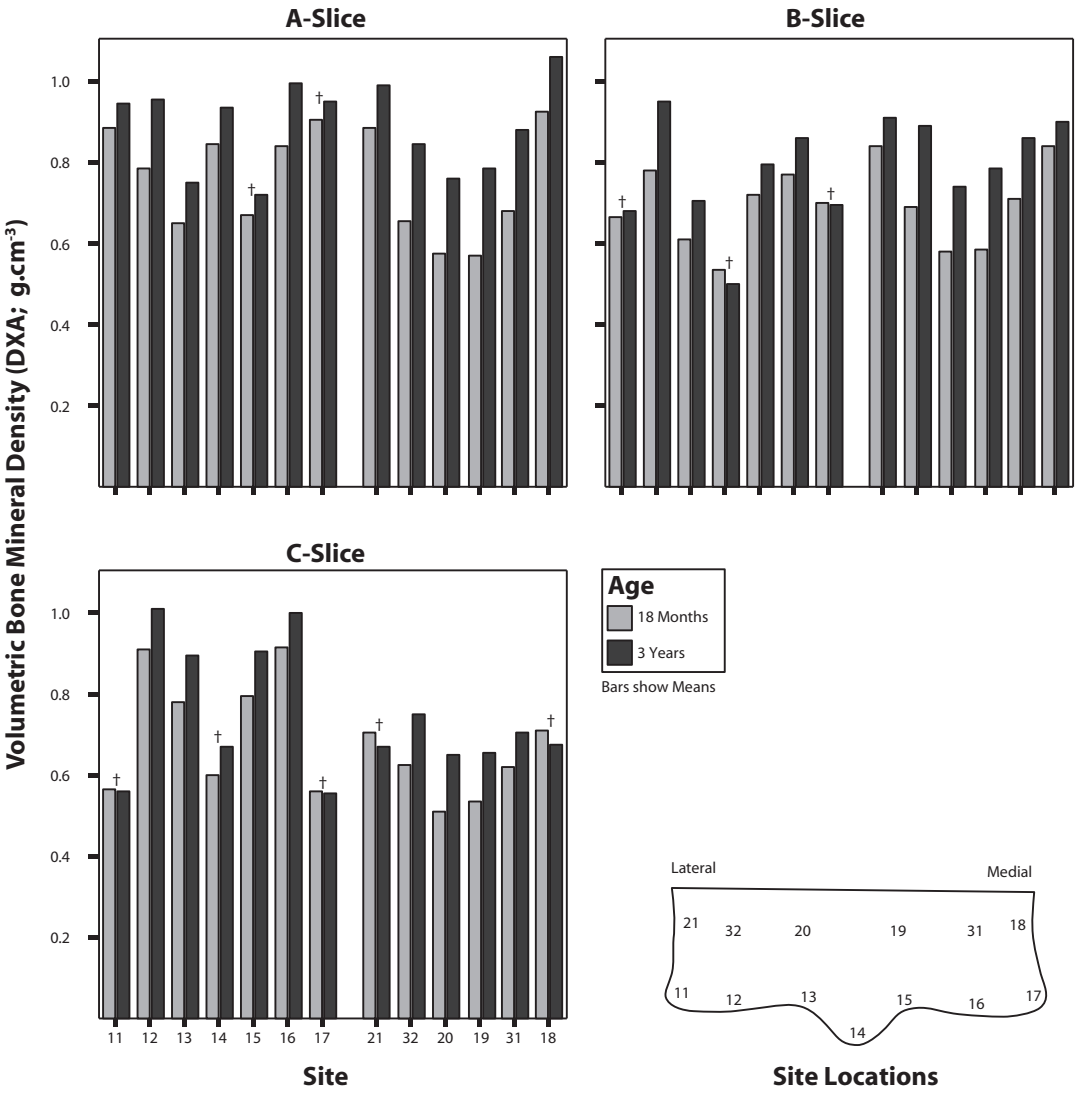

Figure 8-9: vBMD by Site and Age

Breakdown by site showed greater vBMD in 3-year-old Mc3 than 18-month-old Mc3 in most sites. Non-significant ($p \geq 0.05$) differences denoted by †.

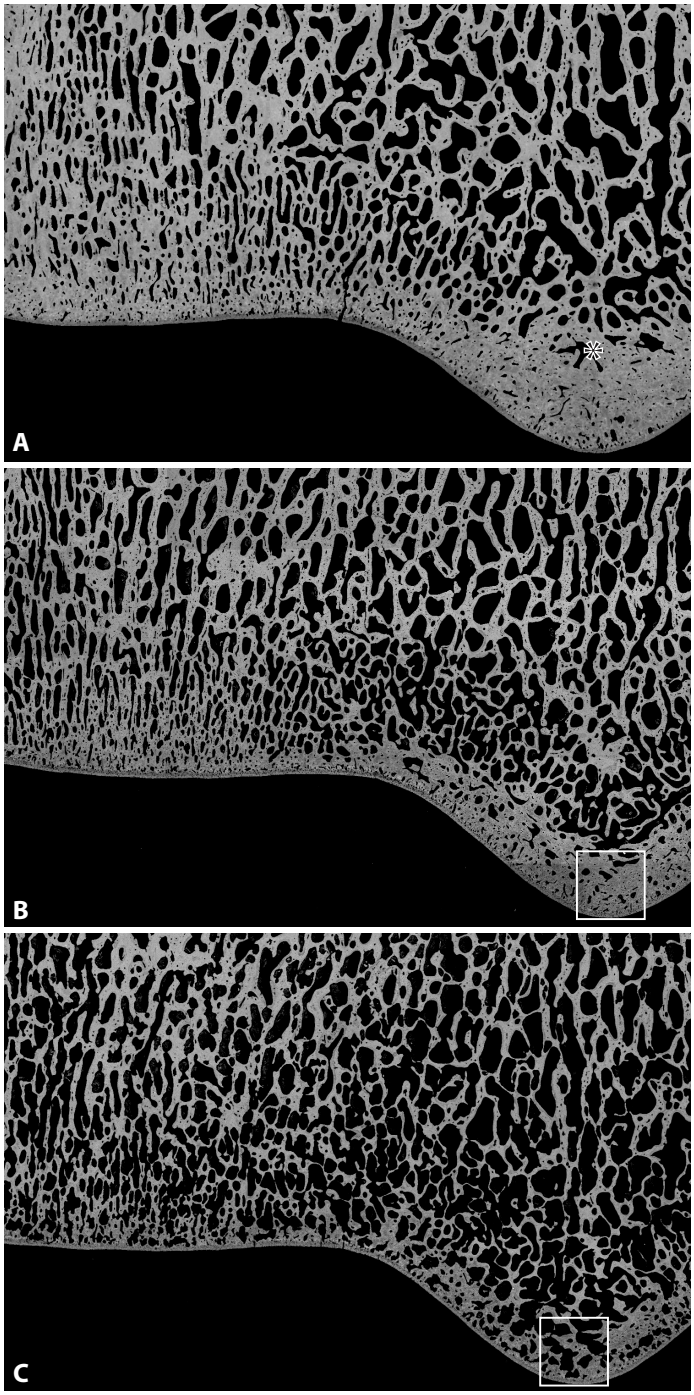

Figure 8-10: Bone Resorption in the Face of Unloading

One horse was euthanised at 19 months of age due to a fractured right humerus. It had been lame for approximately 4 weeks prior to euthanasia, prior to which it had received 2 weeks' box rest. (A) A-slice from a normal 18-month-old Mc3 (horse 16). Note the high VFb in the sagittal ridge (*) and general trabecular thickness. (B) A-slice from left (unaffected) limb. Note the reduced thickness of the subchondral bone plate in the sagittal ridge and notably thinner trabeculae than in (A). (C) A-slice from right (fractured) limb. Note the generalised resorption and very thin, almost absent, subchondral bone plate. Boxes enlarged in Figure 8-11. Field width 26.1 mm.

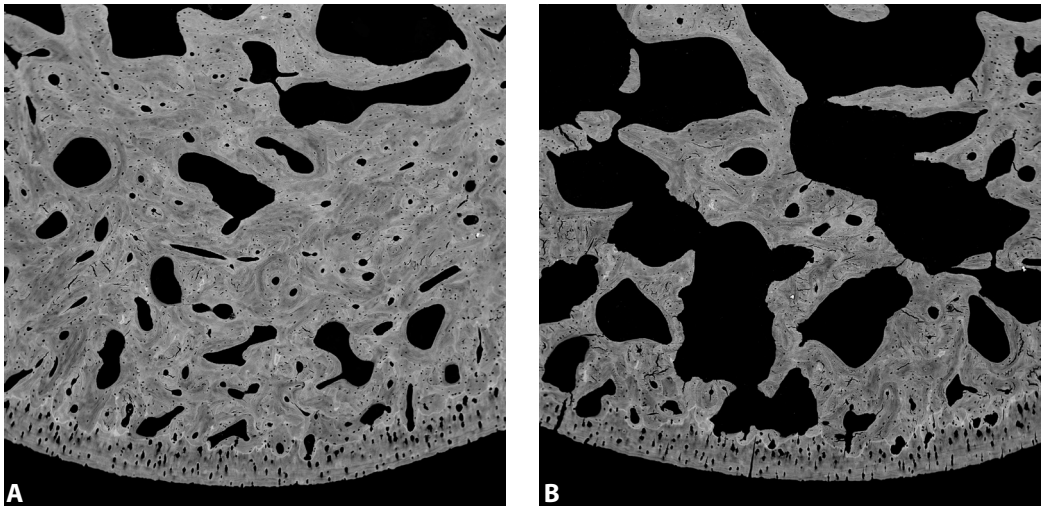

Figure 8-11: Enlargements from Figure 8–10

(A) Sagittal ridge from left A-slice. (B) Sagittal ridge from right A-slice. This horse was non-weight bearing on the right forelimb for 4 weeks prior to euthanasia. Massive, generalised bone resorption is undermining the integrity of the subchondral bone plate. Field width 2.7 mm.

9: General Discussion

9.1 Technical Advances

This study represents the first comprehensive mapping of combined mineralisation density and LAR information for bone and cartilage at the sub micron scale in any joint. The technique of registering CSLM images to qBSE images allowed direct comparison of LAR and mineralisation density. Alternative approaches may have included averaging LAR and backscatter coefficient by site then correlating them, however, the registration technique validated in Chapter 4 allowed comparisons to be made at the pixel scale – and pixels were submicron – so individual data pairs related very closely, giving information on the control of matrix mineralisation on a cellular scale.

The registration technique was only possible if the CSLM and qBSE images were representations of exactly the same region of the subject. Because backscattered electrons emanate from the upper few 10's or 100's of nanometres of the specimen, qBSE imaging is fundamentally a surface imaging technique. CSLM is often used to image below the specimen surface in order to geneate 3D images or to reach features of interest that would otherwise be invisible, however, in order for registration to work the CSLM focal plane had to be positioned at the very top surface of the specimen block. Using one of the CSLM channels to capture reflected light allowed accurate determination of the surface position through visualisation of surface glare; additionally, slope in the surface could be identified and corrected. The parabolic dish-shaped (non flat field) focal plane of the CSLM was obvious as the central portion of the image field would always lie slightly deeper in the specimen than edge regions, so surface glare was often present in the image corners as the parabolic focal plane intersected with the milled flat specimen surface. Three points, present and matching in both images, had to be identified by the operator each time a registration was attempted. Osteocyte lacunae were ideal for this purpose as they were small, their positions and centres were easily identified and they were often visible in both qBSE and CSLM images. Other landmarks such as mineralising front outcrops or bays were much less reliable. Failure of registration occurred if matching features could not be identified.

Previous studies on ACC dynamics have been unable to attribute changes in ACC thickness either to the mineralising front or to chondroclastic resorption. The simple method described in this thesis of dividing ACC thickness by LAR at the tidemark allows an estimate of 'lag time' to be calculated. Lag time is the time between cartilage mineralisation and eventual chondroclastic resorption and gives some idea as to the relative speeds of the two fronts. Decreased lag time implies rapid chondroclastic invasion into ACC, and vice versa. There is no known method for the direct measurement of chondroclastic invasion rate (i.e. in $\mu m \bullet d^{-1}$) although some authors describe quantifying chondroclastic activity by counting actively ossifying endochondral buds or osteochondral junction irregularity (Norrdin, Kawcak, Capwell and McIlwraith 1999). Interestingly, Norrdin et al. (1999) did not report double labelling of ACC or measure ACC LAR despite injections of oxytetracycline 13 and 3 days prior to euthanasia and their publication of

a monochrome image displaying bright bands at the mineralising front (Figure 4 in Norrdin, Kawcak, Capwell and McIlwraith (1999)).

Combined nanoindentation testing and qBSE imaging was performed on a very large number of sites, which was only feasible because correlation of nanoindentation to qBSE images was streamlined by an ImageJ macro (UmisArray, Appendix 3.1.4, p.170). UmisArray reproduced the indentation array on a qBSE image based on the array definition file and 3 marker indents. The macro then interactively stepped through each array while the user determined tissue type at each point. Once it was obvious that review of individual indentations would be required to examine outliers in the data, small adjustments to the macro allowed the user to enter an indentation number, which the macro could immediately locate in the qBSE image. Previous methods (Ferguson, Bushby and Boyde 2002; Ferguson, Bushby and Boyde 2003) required laborious map generation and cross-matching of image sites and array positions, which was not tenable for this very large dataset.

DXA is commonly employed in clinical practice to determine areal bone mineral density (aBMD), from which a Z-score is determined based on the population distribution of aBMD. Subsequently, risk of fracture is inferred from the Z-score and clinical management instituted. The current study compared laboratory DXA (~170 μm•pixel^{-1}) to qBSE (4.35 μm•pixel^{-1}) images and found a strong correlation between vBMD and VFb, but no correlation between vBMD and BMMD. There is a current explosion of interest in determining the inherent strength and fracture resistance of bone, which is somewhat vaguely termed ‘bone quality’ (Jones and Boyde 1994; Benhamou and Roux 2007), to which aBMD is generally assumed to be an important contributor. However, the usefulness of DXA in determining aBMD as equipment manufacturers purport is under severe scrutiny (Bolotin 2007). In the controlled scenario in this study, bone slices of known thickness with minimal overlying soft tissue had closely-related aBMD and VFb. As Bolotin (2007) points out, if any soft tissue overlies the bone of interest the absorptiometric result is not an accurate representation of aBMD because DXA cannot simultaneously determine the amount of bone, fat and water in the beam path (the ‘two-component limitation’). PIXImus-style DXA of plane parallel sections offers a practical advantage to qBSE as specimens need much less preparation, and instrument time per specimen is an order of magnitude or two lower (a minute or two in DXA rather than at least 2 hours in qBSE). However, DXA can only offer an estimate (at best) of VFb and only in specially-prepared specimens so is very unlikely to ever have any clinical use in the living horse.

9.2 Experimental Evidence

The experiments conducted in the course of this thesis have resulted in new information on ACC regulation and bone microstructure in the distal condyle of Mc3, with particular reference to preconditioning exercise.

Individual variation was a notable feature of Mc3 morphology. In particular, the radius of curvature of the parasagittal grooves and bone orientation directly deep to the parasagittal grooves was clearly different between individuals (Chapter 3: Variation in Condylar Microanatomy, p.66). Macroscopic osteochondral defect severity also varied between individuals but was not related to preconditioning exercise (Figure 3-2, p.72); A-slice sagittal ridge and C-slice parasagittal groove sites showed more severe changes than other sites on the condyle. Cracks penetrating ACC and subchondral bone were present in the parasagittal grooves of some horses and were assumed to be precursors to the linear defects reported in previous literature (Riggs, Whitehouse and Boyde 1999a). The relatively large degree of individual variation, small *n* (6 horses in each group) and relatively small experimental effect size conspired to obscure any effects, beneficial or otherwise, of preconditioning exercise. This result is disappointing after previous studies demonstrated clear bone responses to race-training level exercise in adult horses (Firth and Rogers 2005a; Firth, Rogers, Doube and Jopson 2005). However, it must be noted that no detrimental effect of preconditioning exercise was seen in the distal Mc3, leading to the conclusion that preconditioning exercise may be applied with minimal risk to Mc3, if it is required for the experimental study or specific pre-training modification of other body systems.

Several site-related changes were noted at both 18 months old and 3 years old. ACC thickness was consistently less at joint edges and on the sagittal ridge of the C-slice, regions that do not support large loads between bones. ACC tended to be thicker on more highly loaded portions of the condyles and was very thick on the A-slice sagittal ridge and in the C-slice parasagittal grooves. Contrary to previous reports (Murray, Whitton, Vedi, Goodship and Lekeux 1999) ACC thickness was not positively correlated with mineralising front LAR, rather it was negatively correlated – meaning that as LAR increases there is a general trend towards decreased ACC thickness. This can only occur if chondroclastic resorption increases in synchrony with increased LAR, and indeed, if chondroclastic resorption has the capacity to exceed LAR and catch up to the mineralising front and in so doing, reducing ACC thickness. It was commonly observed in this study that regions of thin ACC had bright, clear calcein labels, high LAR and high ACC mineralisation density, suggesting an overall activation of endochondral ossification. Taken together, it seems that when ACC is in a situation of low mechanical load, LAR, mineralisation density and chondroclastic resorption increase. This is in general agreement with O'Connor (1997) who found that joint unweighting resulted in increased ACC LAR and that joint immobilisation led to increased chondroclastic resorption. The significance of this finding is that low mechanical load may encourage ACC invasion into healthy HAC, reducing its already finite thickness, so leading to cartilage loss and contributing to osteoarthritis.

Lag time estimation allowed for the first time estimation of the time between ACC mineralisation at the mineralising front and removal by chondroclastic resorption. The functional significance of lag time estimation was that the very thick ACC in C-slice parasagittal grooves could be attributed to decreased chondroclastic resorption rather than increased LAR. LAR was found to be in the normal range in very thick ACC, but lag times were well beyond the normal 6 months and in one case was slightly longer than that horse's post-natal life. Earlier studies have found linear defects in already fractured Mc3 and non-fractured Mc3 of adult animals and postulated that linear defects contribute to condylar fracture (Riggs, Whitehouse and Boyde 1999a; Swindlehurst 2007). The finding of increased lag time, combined with the observation of cracks penetrating poorly-formed ACC and subchondral bone in C-slice parasagittal grooves, led to the conclusion that the linear defects thought to be involved in condylar fracture may have their genesis during early growth. Endochondral ossification is bone formation within a cartilage precursor (Ross, Romrell and Kaye 1995a), and osteochondrosis is a focal disturbance in endochondral ossification (Ytrehus, Carlson and Ekman 2007). It follows that because thickened ACC in the parasagittal grooves resulted from delayed chondroclastic resorption, which is a component of endochondral ossification, linear defects can be considered a manifestation of osteochondrosis, and Mc3 condylar fracture can now be considered to have an important developmental element rather than being solely degenerative.

LAR and mineralisation density have a very subtle interrelationship, which appears to be inverted between bone and ACC. In ACC, the slight trend was for increased LAR to be related to increased mineralisation density; this phenomenon was particularly apparent on the joint edges and the C-slice sagittal ridge. In bone, however, LAR and mineralisation density were negatively correlated so as LAR increased, inter-label mineralisation density decreased. The finding that bone and ACC have different relationships between LAR and mineralisation density supports the hypothesis that the mineralisation process in the two tissues is different. Bone and growth plate cartilage are known to mineralise by matrix vesicle production (Kirsch 2007), whereas matrix vesicles are not produced at the ACC mineralising front (Boyde and Jones 1983).

Spatial variation in bone marrow cavity orientation and size was a feature in the distal Mc3. In common with other parameters, preconditioning exercise did not result in significant changes to bone microstructure in the distal Mc3. Substantial variation in marrow space orientation and size was seen in bone supporting the C-slice parasagittal grooves. Larger marrow spaces were seen deep to parasagittal groove cracks, which may act in the short term to prevent fracture growth by increasing crack tip radius (Anderson 2005), but which do not provide the structural support provided by the normal subchondral bone buttress seen in other horses' parasagittal grooves. VFb varied throughout the condyle in a pattern consistent with previous findings (Boyde and Firth 2005b; Firth, Rogers, Doube and Jopson 2005), which presumably reflects the stress distribution within a normally-loaded Mc3.

Nanoindentation testing of ACC and subchondral bone from normal and 'affected' parasagittal grooves and a condylar control site showed that defective mineralisation and thickened ACC was related to lower than expected E in ACC, suggestive of aberrant mineral organisation. Subchondral bone was stiffer and had a higher mineralisation density in affected parasagittal grooves, suggestive of an adaptive increase in stiffness in the face of increased stress transmitted by affected ACC. Reduced E in affected parasagittal grooves is likely to result in an overall reduction in structural integrity and accelerate the development of cracks in subchondral bone.

A number of differences were noted between 18 months old and 3 years old. ACC was generally thicker in 3-year-old horses than 18-month-old horses, indicating that LAR continues at a slightly higher rate than chondroclastic resorption. Unfortunately, lag times could not be calculated for the 3-year-old ACC because intra-vital labels were not visible. ACC also became more highly mineralised in the older horses, although it could not be determined whether the increase in mineralisation density had occurred due to increased mineralisation at the mineralising front or whether mineral had gradually accreted in previously mineralised ACC. VFb/vBMD was markedly greater in 3-year-old horses than 18-month-old horses. The 3-year-olds had received 2 seasons of race training, which is substantially more intense than the preconditioning exercise regime, so an increase in VFb in the face of training exercise was the expected response (Boyde 2003; Firth, Rogers, Doube and Jopson 2005).

Regions of cracked, poorly-mineralised or unmineralised ACC were incorporated into the subchondral bone structure between 18 months old and 3 years old (Figure 8-1, Figure 8-2, Figure 8-4). Unmineralised cartilage appeared not to be efficiently removed by chondroclastic resorption resulting, in one parasagittal ridge, in an island of HAC surrounded by subchondral bone. Cracks in ACC were sealed with an amorphous, highly mineralised material that was then removed by chondroclastic resorption. Crack-infilling was only observed in ACC from the 3-year-old specimens and not the 18-month-old specimens, suggesting that cracks in 18-month-old specimens were too recent or were preparation artefacts, so could not have been in-filled. Deeper cracks in HAC and ACC that had escaped in-filling or were too large to be in-filled were integrated into the subchondral bone structure by endochondral ossification of the flanking, normally-mineralised ACC. This led (in one 3-year-old C-slice) to trenches in both parasagittal grooves, approximately 2 mm deep and 140 μm wide – a very similar size to the crack-starting defects introduced into bone for controlled fracture in materials testing. The adult bone response to cartilage damage during early life can result in formation of linear defects in the parasagittal grooves of Mc3, which have the characteristics of stress concentrating crack starters.

9.3 Caveats

Horses were not randomly allocated to cohorts; rather, grouping decisions were based on behavioural problems or awkward birth timing, or predisposition to injury (Rogers, Firth, McIlwraith, Barneveld, Goodship, Kawcak, Smith and Van Weeren (in press, *Equine Veterinary Journal*)). While *n* was always going to be small, this 'convenience' sampling may have biased the incidence of linear defects or increased apparent individual variation, obscuring subtle effects of preconditioning.

While every attempt was made to ensure the standardisation of sites examined throughout the study, it is likely that some variation in slice location occurred at cutting. If a slice was cut slightly too far dorsal or palmar, small linear lesions may have been missed. In addition, the method used to determine the proximodistal axis in qBSE montages (Section 6.3, p.113) may not be truly representative of anatomic proximodistal axis, but is an easily performed and repeated method that may applied in the absence of the whole Mc3.

Despite careful specimen clamping and tool alignment, diamond ultramilling caused surface defects on some blocks. Pieces of PMMA and tissue were torn from the block surface, particularly in regions of poorly mineralised ACC. This may have been a result of incompletely hardened PMMA, or inadequate infiltration of the specimen with methacrylate monomer prior to polymerisation. It was probably also due to poor connectivity between islands of mineralised calcified cartilage forming boundaries at which tearing and shear could more easily occur. Surface defects are likely to have added topographic noise to qBSE results, since backscattered electrons are emitted more strongly from surface ridges and less strongly from valleys than from a flat specimen. Apparent nanoindentation modulus would be affected if the indenter tip made its contact with a non-flat surface. In some sites the tip travel was over the indenter's limit of 20 μm due to surface roughness and E could not be calculated, while in other sites the indentation would lie in a crack and measured E would not be representative of true material stiffness.

9.4 Clinical Relevance

The discovery of a developmental component to parasagittal groove linear defects is an important new addition to the paradigm of Mc3 condylar fracture. Early models proposed that out-of plane 'asynchronous' rotation of Mc3 against PP might be sufficient to cause fracture (Rooney 1974), but were never experimentally validated. Later evidence based on post-mortem examination and clinical imaging supported fatigue failure of the Mc3 condyle emanating from linear defects in the parasagittal groove (Riggs, Whitehouse and Boyde 1999a). At the time, linear defects were thought to be solely degenerative, with microcracks forming through mechanical loading, then large resorption spaces growing to remove microcracks or prevent microcrack growth. It is now clear that linear defects in the parasagittal grooves are highly prevalent in 18-month-old horses, the age at which horses enter pre-training for their 2-year-old racing season. In other words, linear defects precede the intense loading of race training. This thesis has shown that ACC and bone in the parasagittal grooves did not develop normally in a substantial proportion of individuals, and that this developmental variation was not affected by the preconditioning exercise regime. Delayed chondroclastic resorption in the parasagittal grooves led to thickened ACC, although the reasons for the delay are not yet known. Linear defects appear to persist through race training, and in some cases worsen, as seen in the 3-year-old specimens examined in this study. Importantly, none of the horses was lame or had any clinically apparent abnormalities in their fetlock joins, meaning that even quite severe linear defects are clinically silent up to 18 months old and are likely to remain so until fracture occurs.

Early identification of individuals at risk of condylar fracture presents a clinical opportunity to alter the management of 'risky' horses with the aim of reducing fracture incidence. Before that can be done, the contributions to condylar fracture risk of linear defects and other conformational and kinematic variables must be determined, efficient screening methods must be in place and effective interventional strategies must be developed. The discovery of linear defects existing prior to race-training should stimulate interest in this area, since they can be observed prior to entry to race training and are likely to contribute to later fracture risk.

Preconditioning exercise resulted in few changes, as observed at 18 months. This thesis supports the small amount of data already published from experiments on tissue from the GEXA horses (Nugent, Law, Wong, Temple, Bae, Chen, Kawcak and Sah 2004), in which preconditioning exercise was not related to structural or biochemical parameters in HAC. Dykgraaf (2003) found that preconditioning exercise was related to an increased proportion of viable HAC chondrocytes but that the effect level attributable to exercise (a 14% increase in viable proportion) was much less that the effect level attributable to site, as the viable proportion was 34% greater in the palmar condyle than the dorsal condyle. To date, none of the results from the GEXA study have found overtly detrimental effects of preconditioning exercise, clearing the way for more extensive and/or more intense studies of its kind. Rogers et al. noted that preconditioned horses tended to be ready to race earlier, to complete more training starts (jump-outs) and to develop musculoskeletal injury later than non-preconditioned horses (Rogers, Firth, McIlwraith, Barneveld, Goodship, Kawcak and Smith (in press, *Equine Veterinary Journal*), lending practical support to preconditioning exercise. It is possible that preconditioning exercise results in numerous marginally- or non-significant tissue-level changes in several body systems, and that these changes combine to result in observable, large scale outcomes as Rogers et al observed.

9.5 Future Direction

The suspicion that endochondral ossification in the parasagittal grooves might vary in early life needs to be confirmed by the examination of tissue from young horses (0-18 months) at multiple ages. A survey of developmental variants would help to identify the critical stages at which endochondral ossification begins to fail, in common with the work on porcine osteochondrosis by Ytrehus and colleagues (Ytrehus, Carlson and Ekman 2007). Tissue from either a small number of horses raised in a controlled manner, or a larger number of random horses could be examined. A range of ages should be sampled in a cross-sectional design to give an estimate of the incidence and severity of parasagittal groove lesions at each age, and enable deduction of the natural course of such lesions.

Further identification of developmental variations in Thoroughbred foals' parasagittal grooves will be helpful in identifying the underlying mechanism(s) of linear defect formation. Identifying patterns of chondrocyte hypertrophy, apoptosis or necrosis in the parasagittal grooves of Mc3 during growth will be useful. Analysis of gene expression during endochondral ossification of the distal epiphysis, deep to articular cartilage will be essential.

An initial attempt to design probes for in-situ hybridisation (ISH) of equine cartilage was made as an adjunct to the work presented in this thesis because ISH is a technique that can identify spatial variations in gene expression on histological specimens. The development of equine-specific mRNA probes is substantially cheaper, quicker and more convenient than the development of antibodies for immunohistochemistry, although the techniques are complementary. A number of candidate genes involved in endochondral ossification were identified (OPN, MGP, VEGF), and several more of relevance could be studied, for example Cbfa1, HMGB1 and Ihh. In-situ hybridisation can locate gene expression to the level of individual cells in a histological preparation, while other molecular techniques, such as real-time RT-PCR or gene chip analysis are limited by the accuracy with which tissue samples can be excised. However, real time RT-PCR and gene chip approaches may aid in the identification of candidate genes to study with ISH out of large panels of genes. Unfortunately, there is not yet a horse gene chip in production. An initial horse genome assembly was published in January 2007, so the horse gene chip cannot be far off the horizon (Antczak 2007).

Correlation of detailed histological results to non-invasive imaging modalities such as MRI and CT will be beneficial to the development of prospective studies that will be required to determine the contribution of pre-existing linear defects to the risk of Mc3 condylar fracture. The relative risk of condylar fracture with and without pre-existing linear defects is unknown. The argument that linear defects contribute to condylar fracture is based on morphological association – that they are consistently found in the fracture predilection site – and the assumption (based on fracture mechanics) that linear defects act as stress risers. While Swindlehurst has made a positive association between fatal lateral condylar fracture and the presence of linear defects (Swindlehurst 2007), the defects' contribution to overall Mc3 fracture risk has not been ascertained. This is at least partly due to there being no practical, non-invasive method for the mass screening of horses for linear defects so longitudinal studies are currently impossible. Study of linear defects is limited at present to post-mortem examination, which (for now) precludes the option of prospective study. MRI technology for the standing horse continues to improve and may soon be adequate for a large-scale prospective study on fetlock morphology and fracture risk.

Until their contribution to fracture is clearly defined, the presence of linear defects is at most a leading suspect rather than confirmed culprit in the initiation of Mc3 condylar fracture. It would be premature for clinicians to make recommendations to their clients before clear risk data comes to light. Condylar fracture of Mc3 is undoubtedly multifactorial, with linear defects, training regime, conformation, kinematics and genetics playing as-yet-undetermined roles. At best, a relative risk of condylar fracture may be developed based on epidemiological analysis of training data and non-invasive imaging, and mechanical analysis of the fetlock joint. Such a score might be analogous to the relationship in human medicine between a patient's DXA Z-score and risk of hip fracture. Such relationships remain hotly debated despite thorough investigation. The sensible outcome for a clinician and their clients may be to discuss relative risk and make training adjustments, along with increased frequency of clinical examination or imaging for at-risk individuals.

Investigation into heritability of condylar fracture is warranted; the suspicion that condylar fracture has a genetic component has existed since at least 1994 when Ellis identified an unusually high incidence of condylar fractures amongst Mill Reef's offspring (Ellis 1994). Such a study might utilise the extremely well-organised and meticulously maintained Thoroughbred stud book, placing fracture cases within the family tree and identifying case clusters. This study would not be trivial and would require stringent internal controls so that environmental influences (for example, number of career starts) did not bias the result.

The current study provides data supporting the argument that developmental variations in the parasagittal grooves of Mc3, as seen at 18 months, persist into adulthood. The relationship between linear defects at 18 months old and later condylar fracture is associative rather than causative; it seems more than coincidental that condylar fractures usually originate in the same position that linear osteochondral defects are found. The finding of defects in the parasagittal grooves of 3-year-old Thoroughbreds involving deranged endochondral ossification lends further weight to the hypothesis. A long-term, longitudinal study is required to confirm the hypothesis that developmental osteochondral lesions of the parasagittal groove of Mc3 and Mt3 contribute to condylar fracture risk. Such a study would require high-resolution non-invasive imaging of fetlock joints at intervals throughout a large number of horses' lives combined with accurate training, racing and injury data. Multivariable analysis would enable a web of risk factors to be created, so that individual horses could be identified and protected from injury, for example by screening for linear defects or nascent stress fractures in Mc3 and tailoring training programmes accordingly.

Comprehensive mechanical models of failure modes in the Mc3 do not exist. Finite element (FE) models have greater predictive value for bone failure strength than mineralisation density alone (Crawford, Cann and Keaveny 2003) and can be developed from MRI and CT data, but the resolution of both methods as exemplified in the litearture to date is too poor. Testing Mc3 failure strength by placing entire distal limbs in material testing rigs with and without experimental parasagittal groove defects, and with or without naturally-occurring parasagittal groove defects would help validate FE models. Such a model would help to explain the importance of parasagittal groove defects and the effects of fetlock joint conformation. Up to the present, strength-testing of Mc3 has relied upon highly artificial loading of the whole bone (or machined beams) in 3- or 4- point bending across the mid-diaphysis. The results, while informative on bone material in a general sense, are entirely useless in modelling failure loading of the Mc3 in the living horse. No account has yet been taken for normal fetlock or carpometacarpal joint kinematics or the considerable tension in the suspensory apparatus. Identification of mechanical risk factors such as linear defects, condylar width or tendon stiffness, and their interactions, would be of great clinical usefulness in preventing condylar fracture.

References

Anonymous (1966). Veterinary Surgeons Act (United Kingdom).

Alexander, JT and JR Rooney (1974). The biomechanics, surgery and prognosis of equine fractures 1967-1971. *Proceedings of the American Association of Equine Practitioners* 18.

Alini, M, Y Matsui, GR Dodge and AR Poole (1992). The Extracellular-Matrix of Cartilage In The Growth Plate Before and During Calcification - Changes In Composition and Degradation of Type-Ii Collagen. *Calcified Tissue International* 50: 327-35.

Allen, DM and JJ Mao (2004). Heterogeneous nanostructural and nanoelastic properties of pericellular and interterritorial matrices of chondrocytes by atomic force microscopy. *Journal of Structural Biology* 145: 196-204.

Alvarez, J, L Costales, A Lopez-Muniz and JM Lopez (2005). Chondrocytes are released as viable cells during cartilage resorption associated with the formation of intrachondral canals in the rat tibial epiphysis. *Cell and Tissue Research* 320: 501-7.

Alvarez, J, L Costales, R Serra, M Balbin and JM Lopez (2005). Expression patterns of matrix metalloproteinases and vascular endothelial growth factor during epiphyseal ossification. *Journal of Bone and Mineral Research* 20: 1011-21.

Amil, B, M Fernandez-Fuente, I Molinos, J Rodriguez, E Carbajo-Perez, E Garcia, T Yamamoto and F Santos (2004). Chondromodulin-I expression in the growth plate of young uremic rats. *Kidney International* 66: 51-9.

Amizuka, N, D Davidson, H Liu, G Valverde-Franco, S Chai, T Maeda, H Ozawa, V Hammond, DM Ornitz, D Goltzman and JE Henderson (2004). Signalling by fibroblast growth factor receptor 3 and parathyroid hormone-related peptide coordinate cartilage and bone development. *Bone* 34: 13-25.

Anderson, HC (1969). Vesicles associated with calcification in the matrix of epiphyseal cartilage. *Journal of Cell Biology* 41: 59-72.

Anderson, HC, PT Hodges, XM Aguilera, L Missana and PE Moylan (2000). Bone morphogenetic protein (BMP) localization in developing human and rat growth plate, metaphysis, epiphysis, and articular cartilage. *Journal of Histochemistry & Cytochemistry* 48: 1493-502.

Anderson, TL (2005). Fracture Mechanics, Fundamentals and Applications. Boca Raton, FL, Taylor & Francis.

Anderson, TM, CW McIlwraith and R Douay (2004). The role of conformation in musculoskeletal problems in the racing Thoroughbred. *Equine Veterinary Journal* 36: 571-5.

Angker, L, C Nockolds, MV Swain and N Kilpatrick (2004a). Correlating the mechanical properties to the mineral content of carious dentine - a comparative study using an ultra-micro indentation system (UMIS) and SEM-BSE signals. *Archives of Oral Biology* 49: 369-78.

Angker, L, C Nockolds, MV Swain and N Kilpatrick (2004b). Quantitative analysis of the mineral content of sound and carious primary dentine using BSE imaging. *Archives of Oral Biology* 49: 99-107.

Animal Aid. (2006). Animal Aid: Horse Racing. Retrieved 10/01/2006, 2006, from http://www.animalaid.org.uk/racing/index.htm

Antczak, DF (2007). The Genetics Revolution. 46th Congress of the British Equine Veterinary Association, Edinburgh.

Archer, L and JF Wade (2006). Veterinary Newsletter. London, Horserace Betting Levy Board. Issue 10.

Bahrami, S, U Plate, R Dreier, A DuChesne, GH Willital and P Bruckner (2001). Endochondral ossification of costal cartilage is arrested after chondrocytes have reached hypertrophic stage of late differentiation. *Matrix Biology* 19: 707-15.

Bai, XW, S Lu and C Bai (1995). Advances in the study of cartilaginous type X collagen. *Progress in Biochemistry and Biophysics* 22: 521-5.

Ballock, RT, A Heydemann, LM Wakefield, KC Flanders, AB Roberts and MB Sporn (1993). Tgf-Beta-1 Prevents Hypertrophy of Epiphyseal Chondrocytes - Regulation of Gene-Expression For Cartilage Matrix Proteins and Metalloproteases. *Developmental Biology* 158: 414-29.

Ballock, RT and RJ O'Keefe (2003). The biology of the growth plate. *Journal of Bone and Joint Surgery-American Volume* 85A: 715-26.

Barclay, WP, JJ Foerner and TN Phillips (1985). Axial sesamoid injuries associated with lateral condylar fractures in horses. *Journal of the American Veterinary Medical Association* 186: 278-9.

Barr, AR, B Sridhar and HR Denny (1989). Long incomplete longitudinal fractures of the third metacarpal and metatarsal bone in horses. *Veterinary Record* 124: 580-2.

Bassage, LH, 2nd and DW Richardson (1998). Longitudinal fractures of the condyles of the third metacarpal and metatarsal bones in racehorses: 224 cases (1986-1995). *Journal of the American Veterinary Medical Association* 212: 1757-64.

Bathe, AP (1994). 245 fractures in thoroughbred racehorses: Prospective study in Newmarket. Proceedings of The Fortieth Annual Convention of The American Association of Equine Practitioners: 175-6.

Batschelet, E (1981). Circular Statistics in Biology. London, Academic Press.

Belchier, JB (1738a). An account of the bones of animals being changed to a red colour by aliment only. *Philosophical Transactions of London* 39: 287.

Belchier, JB (1738b). A further account of the bones of animals being made red by aliment only. *Philosophical Transactions of London* 39: 288.

Bell, RA, BD Nielsen, K Waite, D Rosenstein and M Orth (2001). Daily access to pasture turnout prevents loss of mineral in the third metacarpus of Arabian weanlings. *Journal of Animal Science* 79: 1142-50.

Bembey, A (2007). Micro-mechanical Properties and Composite Models of Bone. Department of Materials. London, Queen Mary, University of London. PhD.

Benhamou, CL and C Roux (2007). First meeting on bone quality, Abbaye des Vaux de Cernay, France, 15-16 june 2006: Bone architecture. *Osteoporosis International* 18: 837-+.

Bianco, P, FD Cancedda, M Riminucci and R Cancedda (1998). Bone formation via cartilage models: The "borderline" chondrocyte. *Matrix Biology* 17: 185-92.

Biewener, AA, J Thomason, A Goodship and LE Lanyon (1983). Bone stress in the horse forelimb during locomotion at different gaits: a comparison of two experimental methods. *Journal of Biomechanics* 16: 565-76.

Biewener, AA, J Thomason and LE Lanyon (1983). Mechanics of Locomotion and Jumping In The Forelimb of The Horse (Equus) - Invivo Stress Developed In The Radius and Metacarpus. *Journal of Zoology* 201: 67-82.

Biewener, AA, JJ Thomason and LE Lanyon (1988). Mechanics of Locomotion and Jumping In The Horse (Equus) - Invivo Stress In The Tibia and Metatarsus. *Journal of Zoology* 214: 547-65.

Bird, JL, D Platt, T Wells, SA May and MT Bayliss (2000). Exercise-induced changes in proteoglycan metabolism of equine articular cartilage. *Equine Veterinary Journal* 32: 161-3.

Bloebaum, RD, JL Holmes and JG Skedros (2005). Mineral content changes in bone associated with damage induced by the electron beam. *Scanning* 27: 240-8.

Bolotin, HH (2007). DXA in vivo BMD methodology: An erroneous and misleading research and clinical gauge of bone mineral status, bone fragility, and bone remodelling. *Bone* 41: 138-54.

Borrelli, J, Jr., Y Zhu, M Burns, L Sandell and MJ Silva (2004). Cartilage tolerates single impact loads of as much as half the joint fracture threshold. *Clinical Orthopaedics and Related Research*: 266-73.

Borrelli, J and WM Ricci (2004). Acute effects of cartilage impact. *Clinical Orthopaedics and Related Research*: 33-9.

Borrelli, J, K Tinsley, WM Ricci, M Burns, IE Karl and R Hotchkiss (2003). Induction of chondrocyte apoptosis following impact load. *Journal of Orthopaedic Trauma* 17: 635-41.

Boston, RC and DM Nunamaker (2000). Gait and speed as exercise components of risk factors associated with onset of fatigue injury of the third metacarpal bone in 2-year-old Thoroughbred racehorses. *American Journal of Veterinary Research* 61: 602-8.

Boutroy, S, ML Bouxsein, F Munoz and PD Delmas (2005). In vivo assessment of trabecular bone microarchitecture by high-resolution peripheral quantitative computed tomography. *Journal of Clinical Endocrinology & Metabolism* 90: 6508-15.

Boyde, A (2003). The real response of bone to exercise. *Journal of Anatomy* 203: 173-89.

Boyde, A, JC Elliott and SJ Jones (1993). Stereology and histogram analysis of backscattered electron images: age changes in bone. *Bone* 14: 205-10.

Boyde, A and EC Firth (2004). Articular calcified cartilage canals in the third metacarpal bone of 2-year-old thoroughbred racehorses. *Journal of Anatomy* 205: 491-500.

Boyde, A and EC Firth (2005a). Musculoskeletal responses of 2-year-old Thoroughbred horses to early training. 8. Quantitative back-scattered electron scanning electron microscopy and confocal fluorescence microscopy of the epiphysis of the third metacarpal bone. *New Zealand Veterinary Journal* In Press.

Boyde, A and EC Firth (2005b). Musculoskeletal responses of 2-year-old Thoroughbred horses to early training. 8. Quantitative back-scattered electron scanning electron microscopy and confocal fluorescence microscopy of the epiphysis of the third metacarpal bone. *New Zealand Veterinary Journal* 53: 123-32.

Boyde, A, Y Haroon, SJ Jones and CM Riggs (1999). Three dimensional structure of the distal condyles of the third metacarpal bone of the horse. *Equine Veterinary Journal* 31: 122-9.

Boyde, A, PGT Howell, T Bromage, JC Elliott, CM Riggs, LS Bell, M Kneissel, SA Reid, JAP Jayasinghe and SJ Jones (1992). Applications of mineral quantitation of bone by histogram analysis of backscattered electron images. Chemistry and biology of mineralised tissues. H Slavkin and P Price. Amsterdam, Elsevier Science Publishers: 47-60.

Boyde, A and SJ Jones (1983). Scanning Electron Microscopy of Cartilage. Cartilage. Volume 1: Structure, Function and Biochemistry. BK Hall. New York, Academic Press. 1: 105-48.

Boyde, A, L Lovicar and J Zamecnik (2004). Combining confocal and BSE SEM imaging for bone and implant interfaces. *European Cells and Materials* 7: 27.

Boyde, A, SA Reid and PGT Howell (1983). Stereology of bone using both backscattered electron and cathodoluminescence imaging for the SEM. *Beitr elektronenmikroskop Direktabb Oberfl* 16: 419-30.

Boyde, A and IM Shapiro (1983). Is There Life After Calcification - Micro-Dissection Analysis of Normal and Rachitic Tibial Growth Cartilage. *Calcified Tissue International* 35: 638-.

Boyde, A, R Travers, FH Glorieux and SJ Jones (1999). The mineralization density of iliac crest bone from children with osteogenesis imperfecta. *Calcified Tissue International* 64: 185-90.

Brama, PA, RA Bank, JM Tekoppele and PR Van Weeren (2001). Training affects the collagen framework of subchondral bone in foals. *Veterinary Journal* 162: 24-32.

Brama, PA, JM Tekoppele, RA Bank, A Barneveld, EC Firth and PR van Weeren (2000). The influence of strenuous exercise on collagen characteristics of articular cartilage in Thoroughbreds age 2 years. *Equine Veterinary Journal* 32: 551-4.

Brama, PA, JM Tekoppele, RA Bank, A Barneveld and PR van Weeren (2000). Functional adaptation of equine articular cartilage: the formation of regional biochemical characteristics up to age one year. *Equine Veterinary Journal* 32: 217-21.

Brama, PA, JM Tekoppele, RA Bank, D Karssenberg, A Barneveld and PR van Weeren (2000). Topographical mapping of biochemical properties of articular cartilage in the equine fetlock joint. *Equine Veterinary Journal* 32: 19-26.

Brama, PA, JM Tekoppele, RA Bank, PR van Weeren and A Barneveld (1999a). Influence of different exercise levels and age on the biochemical characteristics of immature equine articular cartilage. *Equine Veterinary Journal Supplement*: 55-61.

Brama, PA, JM Tekoppele, RA Bank, PR van Weeren and A Barneveld (1999b). Influence of site and age on biochemical characteristics of the collagen network of equine articular cartilage. *American Journal of Veterinary Research* 60: 341-5.

Brama, PAJ (1999). Dynamics of equine articular cartilage. The biochemical response to biomechanical challenges. Faculteit Diergeneeskunde. Utrecht, Universiteit Utrecht. PhD.

Brommer, H, PAJ Brama, MS Laasanen, HJ Helminen, RR van Weeren and JS Jurvelin (2005). Functional adaptation of articular cartilage from birth to maturity under the influence of loading: a biomechanical analysis. *Equine Veterinary Journal* 37: 148-54.

Broom, ND, A Oloyede, R Flachsmann and M Hows (1996). Dynamic fracture characteristics of the osteochondral junction undergoing shear deformation. *Medical Engineering & Physics* 18: 396-404.

Bullough, PG and A Jagannath (1983). The Morphology of The Calcification Front In Articular- Cartilage - Its Significance In Joint Function. *Journal of Bone and Joint Surgery-British Volume* 65: 72-8.

Burr, DB (2004). Anatomy and physiology of the mineralized tissues: role in the pathogenesis of osteoarthrosis. *Osteoarthritis and Cartilage* 12 *Supplement* A: S20-30.

Burr, DB and MB Schaffler (1997). The involvement of subchondral mineralized tissues in osteoarthrosis: Quantitative microscopic evidence. *Microscopy Research and Technique* 37: 343-57.

Bushby, AJ (2001). Nano-indentation using spherical indenters. *Nondestructive Testing and Evaluation* 17: 213-34.

Bushby, AJ, VL Ferguson and A Boyde (2004). Nanoindentation of bone: Comparison of specimens tested in liquid and embedded in polymethylmethacrylate. *Journal of Materials Research* 19: 249-59.

Butcher, MT and MA Ashley-Ross (2002). Fetlock joint kinematics differ with age in thoroughbred racehorses. *Journal of Biomechanics* 35: 563-71.

Byers, PD and RA Brown (2006). Cell columns in articular cartilage physes questioned: a review. *Osteoarthritis and Cartilage* 14: 3-12.

Cameron, DA and RA Robinson (1956). Electron microscopy of cartilage and bone matrix at the distal epiphyseal line of the femur in the newborn infant. *Journal of Biophysical and Biochemical Cytology* 2: 253-60.

Carlevaro, MF, S Cermelli, R Cancedda and FD Cancedda (2000). Vascular endothelial growth factor (VEGF) in cartilage neovascularization and chondrocyte differentiation: auto- paracrine role during endochondral bone formation. *Journal of Cell Science* 113: 59-69.

Carpenter, RS, LD Galuppo and SM Stover (2006). Effect of diameter of the drill hole on torque of screw insertion and pushout strength for headless tapered compression screws in simulated fractures of the lateral condyle of the equine third metacarpal bone. *American Journal of Veterinary Research* 67: 895-900.

Carstanjen, B, F Duboeuf, J Detilleux and OM Lepage (2003). Equine third metacarpal bone assessment by quantitative ultrasound and dual energy X-ray absorptiometry: an ex vivo study. *Journal of Veterinary Medicine Series A* 50: 42-7.

Carstanjen, B, OM Lepage, O Hars, P Langlois, F Duboeuf and H Amory (2003). Speed of sound measurements of the third metacarpal bone in young exercising thoroughbred racehorses. *Bone* 33: 411-8.

Casey, RC, CL Fhied and TR Oegema (2004). Regulatory factors of tidemark progression in adult human articular cartilage (Abstract). *Osteoarthritis and Cartilage* 12: S42-S3.

Chappard, D, N Retailleau-Gaborit, E Legrand, MF Basle and M Audran (2005). Comparison insight bone measurements by histomorphometry and microCT. *Journal of Bone and Mineral Research* 20: 1177-84.

Chateau, H, C Degueurce, H Jerbi, N Crevier-Denoix, P Pourcelot, F Audigie, V Pasqui-Boutard and JM Denoix (2001). Normal three-dimensional behaviour of the metacarpophalangeal joint and the effect of uneven foot bearing. *Equine Veterinary Journal Supplement* 33: 84-8.

Chenu, C and PD Delmas (1998). Physiology of bone remodeling. Molecular and cellular biology of bone. M Zaidi, OA Adebanjo and CF Huang. London, JAI Press Inc. 5A: 45-64.

Cherdchutham, W, CK Becker, ER Spek, WF Voorhout and PR van Weeren (2001). Effects of exercise on the diameter of collagen fibrils in the central core and periphery of the superficial digital flexor tendon in foals. *American Journal of Veterinary Research* 62: 1563-70.

Cherdchutham, W, LS Meershoek, PR van Weeren and A Barneveld (2001). Effects of exercise on biomechanical properties of the superficial digital flexor tendon in foals. *American Journal of Veterinary Research* 62: 1859-64.

Choi, KY, SW Lee, MH Park, YC Bae, HI Shin, SH Nam, YJ Kim, HJ Kim and HM Ryoo (2002). Spatio-temporal expression patterns of Runx2 isoforms in early skeletogenesis. *Experimental and Molecular Medicine* 34: 426-33.

Claassen, H and T Kirsch (1994). Immunolocalization of Type-X Collagen Before and After Mineralization of Human Thyroid Cartilage. *Histochemistry* 101: 27-32.

Clayton, HM, D Sha, J Stick and N Elvin (2007). 3D kinematics of the equine metacarpophalangeal joint at walk and trot. *Veterinary Comparative Orthopaedics and Traumatology* 20: 86-91.

Cohen, ND, GK Carter, JP Watkins and MS O'Conor (2006). Association of racing performance with specific abnormal radiographic findings in thoroughbred yearlings sold in Texas. *Journal of Equine Veterinary Science* 26: 462-74.

Colahan, P, G Piotrowski and P Poulos (1988). Kinematic analysis of the instant centers of rotation of the equine metacarpophalangeal joint. *American Journal of Veterinary Research* 49: 1560-5.

Colnot, C, L de la Fuente, S Huang, D Hu, CY Lu, B St-Jacques and JA Helms (2005). Indian hedgehog synchronizes skeletal angiogenesis and perichondrial maturation with cartilage development. *Development* 132: 1057-67.

Colnot, C, Z Thompson, T Miclau, Z Werb and JA Helms (2003). Altered fracture repair in the absence of MMP9. *Development* 130: 4123-33.

Cornelissen, BP, PR van Weeren, AG Ederveen and A Barneveld (1999). Influence of exercise on bone mineral density of immature cortical and trabecular bone of the equine metacarpus and proximal sesamoid bone. *Equine Veterinary Journal Supplement* 31: 79-85.

Cosslett, VE and WC Nixon (1952). An experimental x-ray shadow microscope. *Proceedings of the Royal Society B: Biological Sciences* 140: 422-31.

Costouros, JG, AC Dang and HT Kim (2004). Comparison of chondrocyte apoptosis in vivo and in vitro following acute osteochondral injury. *Journal of Orthopaedic Research* 22: 678-83.

Cotton, JR, P Zioupos, K Winwood and M Taylor (2003). Analysis of creep strain during tensile fatigue of cortical bone. *Journal of Biomechanics* 36: 943-9.

Cramer, T, E Schipani, RS Johnson, B Swoboda and D Pfander (2004). Expression of VEGF isoforms by epiphyseal chondrocytes during low-oxygen tension is HIF-1 alpha dependent. *Osteoarthritis and Cartilage* 12: 433-9.

Crawford, RP, CE Cann and TM Keaveny (2003). Finite element models predict in vitro vertebral body compressive strength better than quantitative computed tomography. *Bone* 33: 744-50.

Currey, JD, K Brear and P Zioupos (2004). Notch sensitivity of mammalian mineralized tissues in impact. *Proceedings of the Royal Society B: Biological Sciences* 271: 517-22.

D'Angelo, M, PC Billings, M Pacifici, PS Leboy and T Kirsch (2001). Authentic matrix vesicles contain active metalloproteases (MMP). a role for matrix vesicle-associated MMP-13 in activation of transforming growth factor-beta. *Journal of Biological Chemistry* 276: 11347-53.

D'Angelo, M, Z Yan, M Nooreyazdan, M Pacifici, D Sarment, PC Billings and PS Leboy (2000). MMP-13 is induced during chondrocyte hypertrophy. *Journal of Cellular Biochemistry* 77: 678-93.

Davies, HM (2001). Relationships between third metacarpal bone parameters and surface strains. *Equine Veterinary Journal Supplement* 33: 16-20.

Davies, HM and KM Watson (2005). Third metacarpal bone laterality asymmetry and midshaft dimensions in Thoroughbred racehorses. *Australian Veterinary Journal* 83: 224-6.

Davies, HMS (1994). Strain in the yearling equine metacarpus during locomotion. *Equine Veterinary Journal Supplement* 17: 25-8.

Davies, HMS (1996). The effects of different exercise conditions on metacarpal bone strains in Thoroughbred racehorses. *Pferdeheilkunde* 12: 666-70.

Davies, HMS (2005). The timing and distribution of strains around the surface of the midshaft of the third metacarpal bone during treadmill exercise in one Thoroughbred racehorse. *Australian Veterinary Journal* 83: 157-62.

Davies, HMS (2006). Personal communication to M Doube: Email.

Davies, HMS, SM Gale and DC Baker (1999). Radiographic measures of bone shape in young Thoroughbreds during training for racing. *Equine Veterinary Journal Supplement* 30: 262-5.

Davis, GR and JC Elliott (2003). High definition X-ray microtomography using a conventional impact X-ray source. *Journal De Physique IV* 104: 131-4.

deBri, E, FP Reinholt, D Heinegard, S MengarelliWidholm, M Norgard and O Svensson (1996). Bone sialoprotein and osteopontin distribution at the osteocartilaginous interface. *Clinical Orthopaedics and Related Research*: 251-60.

Deckers, MML, M Karperien, C van der Bent, T Yamashita, SE Papapoulos and C Lowik (2000). Expression of vascular endothelial growth factors and their receptors during osteoblast differentiation. *Endocrinology* 141: 1667-74.

Deckers, MML, ER Van Beek, G Van Der Pluijm, A Wetterwald, L Van Der Wee-Pals, MG Cecchini, SE Papapoulos and C Lowik (2002). Dissociation of angiogenesis and osteoclastogenesis during endochondral bone formation in neonatal mice. *Journal of Bone and Mineral Research* 17: 998-1007.

Deckers, MML, RL van Bezooijen, G van der Horst, J Hoogendam, C van der Bent, SE Papapoulos and C Lowik (2002). Bone morphogenetic proteins stimulate angiogenesis through osteoblast-derived vascular endothelial growth factor A. *Endocrinology* 143: 1545-53.

Denoix, JM (1999). The equine distal limb. London, Manson.

Dowling, BA and AJ Dart (2005). Mechanical and functional properties of the equine superficial digital flexor tendon. *Veterinary Journal* 170: 184-92.

Dunn, EJ, DW Bowes, SW Rothert and RB Greer, 3rd (1975). Letter: Microradiography of bone, a new use for the versatile Faxitron. *Archives of Pathology* 99: 62.

Dyce, KM, WO Sack and CJG Wensing (1996). The Forelimb of the Horse. Textbook of Veterinary Anatomy. Philadelphia, W.B. Saunders Company: 573-610.

Dykgraaf, S (2003). The Effect of Early Exercise on the Articular Cartilage and Subchondral Bone of the Distal Third Metacarpal / Metatarsal Bones of Young Thoroughbred Horses. Institute of Veterinary, Animal and Biomedical Sciences. Palmerston North, Massey University. MVSc.

Easton, KL and CE Kawcak (2007). Evaluation of increased subchondral bone density in areas of contact in the metacarpophalangeal joint during joint loading in horses. *American Journal of Veterinary Research* 68: 816-21.

Eggli, PS, EB Hunziker and RK Schenk (1988). Quantitation of structural features characterizing weight- and less-weight-bearing regions in articular cartilage: a stereological analysis of medial femoral condyles in young adult rabbits. *Anatomical Record* 222: 217-27.

El-Maadawy, S, MT Kaartinen, T Schinke, M Murshed, G Karsenty and MD McKee (2003). Cartilage formation and calcification in arteries of mice lacking matrix Gla protein. *Connective Tissue Research* 44: S272-8.

El Shorafa, WM, JP Feaster and EA Ott (1979). Horse metacarpal bone: age, ash content, cortical area and failure stress interrelationships. *Journal of Animal Science* 49: 979-82.

Elliott, JC and SD Dover (1985). X-ray microscopy using computerized axial tomography. *Journal of Microscopy* 138 (Pt 3): 329-31.

Ellis, DR (1994). Sir Frederick Hobday Memorial Lecture. Some observations on condylar fractures of the third metacarpus and third metatarsus in young thoroughbreds. *Equine Veterinary Journal* 26: 178-83.

Ely, ER, KLP Verheyen and JLN Wood (2004). Fractures and tendon injuries in National Hunt horses in training in the UK: a pilot study. *Equine Veterinary Journal* 36: 365-7.

Estberg, L, SM Stover, IA Gardner, BJ Johnson, JT Case, A Ardans, DH Read, ML Anderson, BC Barr, BM Daft, H Kinde, J Moore, J Stoltz and LW Woods (1994). Case-control study of a cluster estimate of cumulative exercise distance as a risk factor for fatal musculoskeletal injury in Thoroughbred racehorses. *Proceedings of the American Association of Equine Practitioners* 40: 171.

Ferguson, VL, AJ Bushby and A Boyde (2002). Modulus and mineralisation of articular calcified cartilage and subchondral bone in osteoarthritis via nanoindentation and quantitative backscattered electron imaging. *Journal of Bone and Mineral Research* 17: OC15.

Ferguson, VL, AJ Bushby and A Boyde (2003). Nanomechanical properties and mineral concentration in articular calcified cartilage and subchondral bone. *Journal of Anatomy* 203: 191-202.

Field, JS and MV Swain (1993). A simple predictive model for spherical indentation. *Journal of Materials Research* 8: 297-306.

Firth, EC and PW Poulos (1982). Blood vessels in the developing growth plate of the equine distal radius and metacarpus. *Research in Veterinary Science* 33: 159-66.

Firth, EC and PW Poulos (1983). Microangiographic studies of metaphyseal vessels in young foals. *Research in Veterinary Science* 34: 231-5.

Firth, EC and CW Rogers (2005a). Musculoskeletal responses of 2-year-old Thoroughbred horses to early training. 7. Bone and articular cartilage response in the carpus. *New Zealand Veterinary Journal* 53: 113-22.

Firth, EC and CW Rogers (2005b). Musculoskeletal responses of 2-year-old Thoroughbred horses to early training. Conclusions. *New Zealand Veterinary Journal* 53: 377-83.

Firth, EC, CW Rogers, M Doube and NB Jopson (2005). Musculoskeletal responses of 2-year-old Thoroughbred horses to early training. 6. Bone parameters in the third metacarpal and third metatarsal bones. *New Zealand Veterinary Journal* 53: 101-12.

Firth, EC, CW Rogers, NR Perkins, BH Anderson and ND Grace (2004). Musculoskeletal responses of 2-year-old Thoroughbred horses to early training. 1. Study design, and clinical, nutritional, radiological and histological observations. *New Zealand Veterinary Journal* 52: 261-71.

Firth, EC, HC Schamhardt and W Hartman (1988). Measurements of bone strain in foals with altered foot balance. *American Journal of Veterinary Research* 49: 261-5.

Franz-Odendaal, TA, BK Hall and PE Witten (2006). Buried alive: how osteoblasts become osteocytes. *Developmental Dynamics* 235: 176-90.

Fretz, PB, NF Cymbaluk and JW Pharr (1984). Quantitative analysis of long-bone growth in the horse. *American Journal of Veterinary Research* 45: 1602-9.

Frost, HM (1962). Tetracycline labelling and the zone of demarcation of osteoid seams. *Canadian Journal of Biochemistry and Physiology* 40: 485-9.

Frost, HM (1987). Bone "mass" and the "mechanostat": a proposal. *Anatomical Record* 219: 1-9.

Frost, HM (1996). Perspectives: A proposed general model of the "mechanostat" (Suggestions from a new skeletal-biologic paradigm). *Anatomical Record* 244: 139-47.

Frost, HM (2003). Bone's mechanostat: A 2003 update. *Anatomical Record Part A-Discoveries In Molecular Cellular and Evolutionary Biology* 275A: 1081-101.

Galuppo, LD, EL Simpson, SL Greenman, JP Dowd, GL Ferraro and DM Meagher (2006). A Clinical Evaluation of a Headless, Titanium, Variable-Pitched, Tapered, Compression Screw for Repair of Nondisplaced Lateral Condylar Fractures in Thoroughbred Racehorses. *Veterinary Surgery* 35: 423.

Gannon, JM, G Walker, M Fischer, R Carpenter, RC Thompson and TR Oegema (1991). Localization of Type-X Collagen In Canine Growth Plate and Adult Canine Articular-Cartilage. *Journal of Orthopaedic Research* 9: 485-94.

Gee, E, M Davies, E Firth, L Jeffcott, P Fennessy and T Mogg (2007). Osteochondrosis and copper: Histology of articular cartilage from foals out of copper supplemented and non-supplemented dams. *Veterinary Journal* 173: 111-9.

Gibson, VA, SM Stover, JC Gibeling, SJ Hazelwood and RB Martin (2006). Osteonal effects on elastic modulus and fatigue life in equine bone. *Journal of Biomechanics* 39: 217-25.

Gibson, VA, SM Stover, RB Martin, TC Gibeling, NH Willits, MB Gustafson and LV Griffin (1995). Fatigue behavior of the equine third metacarpus: Mechanical property analysis. *Journal of Orthopaedic Research* 13: 861-8.

Glade, MJ, NK Luba and HF Schryver (1986). Effects of age and diet on the development of mechanical strength by the third metacarpal and metatarsal bones of young horses. *Journal of Animal Science* 63: 1432-44.

Gläser, KE, ME Davies and LB Jeffcott (2003). Differential distribution of cathepsins B and L in articular cartilage during skeletal development in the horse. *Equine Veterinary Journal* 35: 42-7.

Goldman, HM, A Blayvas, A Boyde, PG Howell, JG Clement and TG Bromage (2000). Correlative light and backscattered electron microscopy of bone--part II: automated image analysis. *Scanning* 22: 337-44.

Goldstein, JI (1975a). Electron Beam-Specimen Interaction. Practical Scanning Electron Microscopy. JI Goldstein and H Yakowitz. New York, Plenum Press: 49-94.

Goldstein, JI (1975b). Electron Optics. Practical Scanning Electron Microscopy. JI Goldstein and H Yakowitz. New York, Plenum Press: 21-48.

Gomez, S and A Boyde (1994). Correlated Alkaline-Phosphatase *Histochemistry* and Quantitative Backscattered Electron Imaging In The Study of Rat Incisor Ameloblasts and Enamel Mineralization. *Microscopy Research and Technique* 29: 29-36.

Goodfellow, JW and PG Bullough (1967). The pattern of ageing of the articular cartilage of the elbow joint. *Journal of Bone and Joint Surgery - British Volume* 49: 175-81.

Greet, TR (1987). Condylar fracture of the cannon bone with axial sesamoid fracture in three horses. *Veterinary Record* 120: 223-5.

Gross, TS, KJ McLeod and CT Rubin (1992). Characterizing bone strain distributions in vivo using three triple rosette strain gages. *Journal of Biomechanics* 25: 1081-7.

Gupta, HS, S Schratter, W Tesch, P Roschger, A Berzlanovich, T Schoeberl, K Klaushofer and P Fratzl (2005). Two different correlations between nanoindentation modulus and mineral content in the bone-cartilage interface. *Journal of Structural Biology* 149: 138-48.

Hernandez, J and DL Hawkins (2001). Training failure among yearling horses. *American Journal of Veterinary Research* 62: 1418-22.

Hernandez, J, DL Hawkins and MC Scollay (2001). Race-start characteristics and risk of catastrophic musculoskeletal injury in Thoroughbred racehorses. *Journal of the American Veterinary Medical Association* 218: 83-6.

Hernandez, JA, MC Scollay, DL Hawkins, JA Corda and TM Krueger (2005). Evaluation of horseshoe characteristics and high-speed exercise history as possible risk factors for catastrophic musculoskeletal injury in Thoroughbred racehorses. *American Journal of Veterinary Research* 66: 1314-20.

HernandezVidal, G, LB Jeffcott and ME Davies (1997). Cellular heterogeneity in cathepsin D distribution in equine articular cartilage. *Equine Veterinary Journal* 29: 267-73.

Hill, T, D Carmichael, G Maylin and L Krook (1986). Track condition and racing injuries in thoroughbred horses. *Cornell Veterinarian* 76: 361-79.

Hogan, PM, CW McIlwraith, CM Honnas, JP Watkins and LR Bramlage (1997). Surgical treatment of subchondral cystic lesions of the third metacarpal bone: results in 15 horses (1986-1994). *Equine Veterinary Journal* 29: 477-82.

Holmbeck, K, P Bianco, J Caterina, S Yamada, M Kromer, SA Kuznetsov, M Mankani, P Gehron Robey, AR Poole, I Pidoux, JM Ward and H Birkedal-Hansen (1999). MT1-MMP-Deficient Mice Develop Dwarfism, Osteopenia, Arthritis, and Connective Tissue Disease due to Inadequate Collagen Turnover. *Cell* 99: 81-92.

Howell, PGT and A Boyde (1999). Surface roughness of preparations for backscattered electron- scanning electron microscopy: The image differences and their Monte Carlo simulation. *Scanning* 21: 361-7.

Howell, PGT, KMW Davy and A Boyde (1998). Mean atomic number and backscattered electron coefficient calculations for some materials with low mean atomic number. *Scanning* 20: 35-40.

Howell, PGT and SA Reid (1986). A microcomputer-based system for rapid on-line stereological analysis in the scanning electron microscope. *Scanning* 8: 139-44.

Hunziker, EB, W Herrmann, RK Schenk, M Mueller and H Moor (1984). Cartilage ultrastructure after high pressure freezing, freeze substitution, and low temperature embedding. I. Chondrocyte ultrastructure--implications for the theories of mineralization and vascular invasion. *Journal of Cell Biology* 98: 267-76.

Hwang, WS, DA Cameron, RA Robinson, DA Cameron and RA Robinson (1978). Ultrastructure of human foetal and neonatal hyaline cartilage. *Journal of Pathology* 126: 209-14.

Inoué, S (1995). Foundations of confocal scanned imaging in light microscopy. Handbook of Biological Confocal Microscopy. JB Pawley. New York, Plenum Press: 1-17.

Invitrogen. (2006). Spectra - Calcein/pH 9.0. Retrieved 20/04/2006, from http://probes.invitrogen.com/servlets/spectra?fileid=481ph9

Jiang, Y, J Zhao, DL White and HK Genant (2000). Micro CT and Micro MR imaging of 3D architecture of animal skeleton. *Journal of Musculoskeletal and Neuronal Interactions* 1: 45-51.

Jockey Club. (2006). The Jockey Club Home Page. Retrieved 10/01/2006, 2006, from http://www.thejockeyclub.co.uk/

Johnson, BJ, A Ardans, SM Stover, BM Daft, H Kinde, DH Read, BC Barr, J Moore, L Woods, M Anderson, J Stoltz and P Blanchard (1994). California Racehorse Postmortem Program: A 4-Year Overview. *Proceedings of the American Association of Equine Practitioners* 40: 167-9.

Johnson, BJ, SM Stover, BM Daft, H Kinde, DH Read, BC Barr, M Anderson, J Moore, L Woods and J Stoltz (1994). Causes of death in racehorses over a 2 year period. *Equine Veterinary Journal* 26: 327-30.

Jones, SJ and A Boyde (1994). Questions of quality and quantity--a morphological view of bone biology. *Kaibogaku Zasshi* 69: 229-43.

Jones, SJ, A Boyde and NN Ali (1986). The interface of cells and their matrices in mineralized tissues: a review. *Scanning Electron Microscopy*: 1555-69.

Kak, AC and M Slaney (2001). Principles of Computerized Tomographic Imaging, *Society of Industrial and Applied Mathematics*. Retrieved from http://cobweb.ecn.purdue.edu/~malcolm/pct/pct-toc.html on 17/05/2007

Kane, AJ, SM Stover, IA Gardner, JT Case, BJ Johnson, DH Read and AA Ardans (1996). Horseshoe characteristics as possible risk factors for fatal musculoskeletal injury of thoroughbred racehorses. *American Journal of Veterinary Research* 57: 1147-52.

Kaneko, M, K Kiryu, MA Oikawa, T Kanemaru, T Yamamoto and H Satoh (1980). Longitudinal Cannon-Bone Fracture and Subchondral Osteosclerosis In The Racehorse - An Examination of The Cannon-Bones of 2 Cases With The Fracture. *Bulletin of Equine Research Institute*: 1-7.

Kaneko, M, M Oikawa and T Yoshihara (1993). Pathological analysis of bone fractures in race horses. *Journal of Veterinary Medical Science* 55: 181-3.

Kasashima, Y, RKW Smith, HL Birch, K Takahashi, K Kusano and AE Goodship (2002). Exercise-induced tendon hypertrophy: cross-sectional area changes during growth are influenced by exercise. *Equine Veterinary Journal Supplement* 34: 264-8.

Kawcak, CE, LR Bramlage and RM Embertson (1995). Diagnosis and management of incomplete fracture of the distal palmar aspect of the third metacarpal bone in five horses. *Journal of the American Veterinary Medical Association* 206: 335-7.

King, KB, CF Opel and DM Rempel (2005). Cyclical articular joint loading leads to cartilage thinning and osteopontin production in a novel in vivo rabbit model of repetitive finger flexion. *Osteoarthritis and Cartilage* 13: 971-8.

Kirsch, T (2006). Cellular regulation of mineralisation. *Calcified Tissue International* 78: S22.

Kirsch, T (2007). Physiological and pathological mineralization: a complex multifactorial process. *Current Opinion in Orthopaedics* 18: 425-7.

Kirsch, T, W Wang and D Pfander (2003). Functional differences between growth plate apoptotic bodies and matrix vesicles. *Journal of Bone and Mineral Research* 18: 1872-81.

Kitahara, H, T Hayami, K Tokunaga, N Endo, H Funaki, Y Yoshida, E Yaoita and T Yamamoto (2003). Chondromodulin-I expression in rat articular cartilage. *Archives of Histology and Cytology* 66: 221-8.

Kiviranta, I, J Jurvelin, M Tammi, AM Saamanen and HJ Helminen (1987). Weight bearing controls glycosaminoglycan concentration and articular cartilage thickness in the knee joints of young beagle dogs. *Arthritis and Rheumatism* 30: 801-9.

Klein-Nulend, J, RG Bacabac and MG Mullender (2005). Mechanobiology of bone tissue. *Pathologie Biologie* 53: 576-80.

Kostenuik, PJ (2005). Osteoprotegerin and RANKL regulate bone resorption, density, geometry and strength. Curr Opin Pharmacol 5: 618-25.

Kronenberg, HM (2003). Developmental regulation of the growth plate. *Nature* 423: 332-6.

Krook, L and GA Maylin (1988). Fractures In Thoroughbred Race Horses. *Cornell Veterinarian* 78: 7-133.

Kuboki, T, M Kanyama, T Nakanishi, K Akiyama, K Nawachi, H Yatani, K Yamashita, T Takano-Yamamoto and M Takigawa (2003). Cbfa1/Runx2 gene expression in articular chondrocytes of the mice temporomandibular and knee joints in vivo. *Archives of Oral Biology* 48: 519-25.

Kusafuka, K, Y Hiraki, C Shukunami, T Kayano and T Takemura (2002). Cartilage-specific matrix protein, chondromodulin-I (ChM-I), is a strong angio-inhibitor in endochondral ossification of human neonatal vertebral tissues in vivo: relationship with angiogenic factors in the cartilage. *Acta Histochemica* 104: 167-75.

Lane, LB, A Villacin and PG Bullough (1977). The vascularity and remodelling of subchondral bone and calcified cartilage in adult human femoral and humeral heads. An age- and stress-related phenomenon. *Journal of Bone and Joint Surgery - British Volume* 59: 272-8

Lanyon, LE (1974). Experimental Support For Trajectorial Theory of Bone-Structure. *Journal of Bone and Joint Surgery-British Volume* 56: 160-6.

Lanyon, LE (1987). Functional strain in bone tissue as an objective, and controlling stimulus for adaptive bone remodelling. *Journal of Biomechanics* 20: 1083-93.

Lawrence, LA, EA Ott, GJ Miller, PW Poulos, G Piotrowski and RL Asquith (1994). The mechanical properties of equine third metacarpals as affected by age. *Journal of Animal Science* 72: 2617-23.

Lawson, SE, H Chateau, P Pourcelot, JM Denoix and N Crevier-Denoix (2007). Sensitivity of an equine distal limb model to perturbations in tendon paths, origins and insertions. *Journal of Biomechanics* 40: 2510-6.

Le Jeune, SS, MH Macdonald, SM Stover, KT Taylor and M Gerdes (2003). Biomechanical investigation of the association between suspensory ligament injury and lateral condylar fracture in thoroughbred racehorses. *Veterinary Surgery* 32: 585-97.

Leach, DH, NF Cymbaluk, A Hendrix and K Williams (1994). Mechanical properties of metacarpal bones of foals fed different energy and phosphorus levels. *Equine Veterinary Journal Supplement* 17: 61-6.

Lemperg, R (1971). Subchondral Bone Plate of Femoral Head In Adult Rabbits .1. Spontaneous Remodelling Studied By Microradiography and Tetracycline Labelling. *Virchows Archiv Abteilung A Pathologische Anatomie* 352: 1-13.

Lewiecki, EM (2005). Clinical applications of bone density testing for osteoporosis. *Minerva Medica* 96: 317-30.

Limaye, A (2007). Drishti.

Lin, YL, PA Brama, GH Kiers, PR Vanweeren and J Degroot (2005). Extracellular matrix compositon of the equine superficial digital flexor tendon: relationship with age and anatomical site. *Journal of Veterinary Medicine Series A* 52: 333-8.

Love, S, CA Wyse, AJ Stirk, MJ Stear, P Calver, LC Voute and DJ Mellor (2006). Prevalence, heritability and significance of musculoskeletal conformational traits in Thoroughbred yearlings. *Equine Veterinary Journal* 38: 597-603.

Loveridge, N, J Power, J Reeve and A Boyde (2004). Bone mineralization density and femoral neck fragility. *Bone* 35: 929-41.

Luo, G, P Ducy, MD McKee, GJ Pinero, E Loyer, RR Behringer and G Karsenty (1997). Spontaneous calcification of arteries and cartilage in mice lacking matrix GLA protein. *Nature* 386: 78-81.

Maes, C, P Carmeliet, K Moermans, I Stockmans, N Smets, D Collen, R Bouillon and G Carmeliet (2002). Impaired angiogenesis and endochondral bone formation in mice lacking the vascular endothelial growth factor isoforms VEGF(164) and VEGF(188). *Mechanisms of Development* 111: 61-73.

Maes, C, I Stockmans, K Moermans, R Van Looveren, N Smets, P Carmeliet, R Bouillon and G Carmeliet (2004). Soluble VEGF isoforms are essential for establishing epiphyseal vascularization and regulating chondrocyte development and survival. *Journal of Clinical Investigation* 113: 188-99.

Martin, GS (2000). Factors associated with racing performance of Thoroughbreds undergoing lag screw repair of condylar fractures of the third metacarpal or metatarsal bone. *Journal of the American Veterinary Medical Association* 217: 1870-7.

Martin, RB, VA Gibson, SM Stover, JC Gibeling and LV Griffin (1997). Residual strength of equine bone is not reduced by intense fatigue loading: Implications for stress fracture. *Journal of Biomechanics* 30: 109-14.

Martin, RB, ST Lau, PV Mathews, VA Gibson and SM Stover (1996). Collagen fiber organization is related to mechanical properties and remodeling in equine bone. A comparison of two methods. *Journal of Biomechanics* 29: 1515-21.

Martinelli, MJ, GJ Baker, RB Clarkson, JC Eurell, GJ Pijanowski, IV Kuriashkin and BO Carragher (1996). Correlation between anatomic features and low-field magnetic resonance imaging of the equine metacarpophalangeal joint. *American Journal of Veterinary Research* 57: 1421-6.

Martinelli, MJ, J Eurell, CM Les, D Fyhrie and D Bennett (2002). Age-related morphometry of equine calcified cartilage. *Equine Veterinary Journal* 34: 274-8.

Martinelli, MJ, IV Kuriashkin, BO Carragher, RB Clarkson and GJ Baker (1997). Magnetic resonance imaging of the equine metacarpophalangeal joint: three-dimensional reconstruction and anatomic analysis. *Veterinary Radiology and Ultrasound* 38: 193-9.

McCarthy, RN and LB Jeffcott (1988). Monitoring the effects of treadmill exercise on bone by non-invasive means during a progressive fitness programme. *Equine Veterinary Journal Supplement*: 88-92.

McCarthy, RN and LB Jeffcott (1992). Effects of Treadmill Exercise On Cortical Bone In The 3rd Metacarpus of Young Horses. *Research in Veterinary Science* 52: 28-37.

McClure, SR, JP Watkins, NW Glickman, JF Hawkins and LT Glickman (1998). Complete fractures of the third metacarpal or metatarsal bone in horses: 25 cases (1980-1996). *Journal of the American Veterinary Medical Association* 213: 847-50.

McKee, SL (1995). An update on racing fatalities in the UK. *Equine Veterinary Education* 7: 202-4.

Meagher, DM (1976). Lateral condylar fractures of the metacarpus and metatarsus in horses. *Proceedings of the American Association of Equine Practitioners* 22: 147-54.

Mechanic, GL, SB Arnaud, A Boyde, TG Bromage, P Buckendahl, JC Elliott, EP Katz and GN Durnova (1990). Regional distribution of mineral and matrix in the femurs of rats flown on Cosmos 1887 biosatellite. *FASEB Journal* 4: 34-40.

Mente, PL and JL Lewis (1994). Elastic modulus of calcified cartilage is an order of magnitude less than that of subchondral bone. *Journal of Orthopaedic Research* 12: 637-47.

Misof, BM, P Roschger, W Tesch, PA Baldock, A Valenta, P Messmer, JA Eisman, AL Boskey, EM Gardiner, P Fratzl and K Klaushofer (2003). Targeted overexpression of vitamin D receptor in osteoblasts increases calcium concentration without affecting structural properties of bone mineral crystals. *Calcified Tissue International* 73: 251-7.

Moger, CJ, R Barrett, P Bleuet, DA Bradley, RE Ellis, EM Green, KM Knapp, P Muthuvelu and CP Winlove (2007). Regional variations of collagen orientation in normal and diseased articular cartilage and subchondral bone determined using small angle X-ray scattering (SAXS). *Osteoarthritis and Cartilage* 15: 682-7.

Mohammed, HO, T Hill and J Lowe (1991). Risk factors associated with injuries in thoroughbred horses. *Equine Veterinary Journal* 23: 445-8.

Mohammed, HO, T Hill and J Lowe (1992). The risk of severity of limb injuries in racing thoroughbred horses. *Cornell Veterinarian* 82: 331-41.

Mohsin, S, FJ O'Brien and TC Lee (2006). Osteonal crack barriers in ovine compact bone. *Journal of Anatomy* 208: 81-9.

Morgan, EF and ML Bouxsein (2005). Use of finite element analysis to assess bone strength. *BoneKEy-Osteovision* 2: 8-19.

Morgan, JW, EM Santschi, LJ Zekas, MC Scollay-Ward, MD Markel, CL Radtke, SJ Sample, NS Keuler and P Muir (2006). Comparison of radiography and computed tomography to evaluate metacarpo/metatarsophalangeal joint pathology of paired limbs of thoroughbred racehorses with severe condylar fracture. *Veterinary Surgery* 35: 611-7.

Mow, VC, WY Gu and FH Chen (2005). Structure and function of articular cartilage and meniscus. Basic Orthopaedic Biomechanics and Mechano-Biology. VC Mow and R Huiskes. Philadelphia, Lippincott Williams & Wilkins: 181-258.

Mow, VC and R Huiskes (2005). A brief history of science and orthopaedic biomechanics. Basic orthopaedic biomechanics and mechano-biology. VC Mow and R Huiskes. Philadelphia, Lippincott Williams &Wilkins: 1-27.

Muir, P, J McCarthy, CL Radtke, MD Markel, EM Santschi, MC Scollay and VL Kalscheur (2006). Role of endochondral ossification of articular cartilage and functional adaptation of the subchondral plate in the development of fatigue microcracking of joints. *Bone* 38: 342-9.

Murray, RC, RC Whitton, S Vedi, AE Goodship and P Lekeux (1999). The effect of training on the calcified zone of equine middle carpal articular cartilage. *Equine Veterinary Journal Supplement* 30: 274-8.

Murshed, M, T Schinke, MD McKee and G Karsenty (2004). Extracellular matrix mineralization is regulated locally; different roles of two gla-containing proteins. *Journal of Cell Biology* 165: 625-30.

Newbury, DE (1975). Image Formation in the Scanning Electron Microscope. Practical Scanning Electron Microscopy. JI Goldstein and H Yakowitz. New York, Plenum Press: 95-148.

Nielsen, BD, GD Potter, EL Morris, TW Odom, DM Senor, JA Reynolds, WB Smith and MT Martin (1997). Changes in the third metacarpal bone and frequency of bone injuries in young quarter horses during race training - Observations and theoretical considerations. *Journal of Equine Veterinary Science* 17: 541-9.

Niida, S, T Kondo, S Hiratsuka, S Hayashi, N Amizuka, T Noda, K Ikeda and M Shibuya (2005). VEGF receptor 1 signaling is essential for osteoclast development and bone marrow formation in colony-stimulating factor 1-deficient mice. *Proceedings of the National Academy of Sciences USA* 102: 14016-21.

Nixon, AJ (1990). Osteochondrosis and Osteochondritis-Dissecans of The Equine Fetlock. *Compendium On Continuing Education For The Practicing Veterinarian* 12: 1463.

Norrdin, RW, CE Kawcak, BA Capwell and CW McIlwraith (1998). Subchondral bone failure in an equine model of overload arthrosis. *Bone* 22: 133-9.

Norrdin, RW, CE Kawcak, BA Capwell and CW McIlwraith (1999). Calcified cartilage morphometry and its relation to subchondral bone remodeling in equine arthrosis. *Bone* 24: 109-14.

Norrdin, RW and SM Stover (2006). Subchondral bone failure in overload arthrosis: A scanning electron microscopic study in horses. *Journal of Musculoskeletal and Neuronal Interactions* 6: 251-7.

Nugent, GE, AW Law, EG Wong, MM Temple, WC Bae, AC Chen, CE Kawcak and RL Sah (2004). Site- and exercise-related variation in structure and function of cartilage from equine distal metacarpal condyle. *Osteoarthritis and Cartilage* 12: 826-33.

Nunamaker, DM, DM Butterweck and MT Provost (1989). Some geometric properties of the third metacarpal bone: a comparison between the thoroughbred and standardbred racehorse. *Journal of Biomechanics* 22: 129-34.

O'Brien, FJ, D Taylor and TC Lee (2005). The effect of bone microstructure on the initiation and growth of microcracks. *Journal of Orthopaedic Research* 23: 475-80.

O'Brien, TR, WJ Hornof and DM Meagher (1981). Radiographic detection and characterization of palmar lesions in the equine fetlock joint. *Journal of the American Veterinary Medical Association* 178: 231-7.

O'Connor, KM (1997). Unweighting accelerates tidemark advancement in articular cartilage at the knee joint of rats. *Journal of Bone and Mineral Research* 12: 580-9.

Oegema, TR, RJ Carpenter, F Hofmeister and RC Thompson (1997). The interaction of the zone of calcified cartilage and subchondral bone in osteoarthritis. *Microscopy Research and Technique* 37: 324-32.

Ohashi, N, AG Robling, DB Burr and CH Turner (2002). The effects of dynamic axial loading on the rat growth plate. *Journal of Bone and Mineral Research* 17: 284-92.

Oikawa, M, T Yoshihara and M Kaneko (1989). Age-Related-Changes In Articular-Cartilage Thickness of The 3rd Metacarpal Bone In The Thoroughbred. *Japanese Journal of Veterinary Science* 51: 839-42.

Parisuthiman, D, Y Mochida, WR Duarte and M Yamauchi (2005). Biglycan modulates osteoblast differentiation and matrix mineralization. *Journal of Bone and Mineral Research* 20: 1878-86.

Park, H, YK Jung, OJ Park, YJ Lee, JY Choi and Y Choi (2005). Interaction of Fas ligand and Fas expressed on osteoclast precursors increases osteoclastogenesis. *Journal of Immunology* 175: 7193-201.

Parkin, TD, PD Clegg, NP French, CJ Proudman, CM Riggs, ER Singer, PM Webbon and KL Morgan (2004a). Risk of fatal distal limb fractures among Thoroughbreds involved in the five types of racing in the United Kingdom. *Veterinary Record* 154: 493-7.

Parkin, TD, PD Clegg, NP French, CJ Proudman, CM Riggs, ER Singer, PM Webbon and KL Morgan (2006). Catastrophic fracture of the lateral condyle of the third metacarpus/metatarsus in UK racehorses - fracture descriptions and pre-existing pathology. *Veterinary Journal* 171: 157-65.

Parkin, TDH, RD Clegg, NP French, CJ Proudman, CM Riggs, ER Singer, PM Webbon and KL Morgan (2004b). Horse-level risk factors for fatal distal limb fracture in racing Thoroughbreds in the UK. *Equine Veterinary Journal* 36: 513-9.

Peloso, JG, GD Mundy and ND Cohen (1994). Prevalence of, and factors associated with, musculoskeletal racing injuries of thoroughbreds. *Journal of the American Veterinary Medical Association* 204: 620-6.

Perez, E, J Luna, L Rojas and JB Kouri (2005). Chondroptosis: An immunohistochemical study of apoptosis and Golgi complex in chondrocytes from human osteoarthritic cartilage. *Apoptosis* 10: 1105-10.

Perkins, NR, SW Reid and RS Morris (2005a). Risk factors for musculoskeletal injuries of the lower limbs in Thoroughbred racehorses in New Zealand. *New Zealand Veterinary Journal* 53: 171-83.

Perkins, NR, SWJ Reid and RS Morris (2005b). Profiling the New Zealand Thoroughbred racing industry. 2. Conditions interfering with training and racing. *New Zealand Veterinary Journal* 53: 69-76.

Perkins, NR, CW Rogers, EC Firth and BH Anderson (2004). Musculoskeletal responses of 2-year-old Thoroughbred horses to early training. 3. In vivo ultrasonographic assessment of the cross-sectional area and echogenicity of the superficial digital flexor tendon. *New Zealand Veterinary Journal* 52: 280-4.

Peterlik, H, P Roschger, K Klaushofer and P Fratzl (2006). From brittle to ductile fracture of bone. *Nature Materials* 5: 52-5.

Petrie, A and P Watson (1999). Statistics for Veterinary and Animal Science. London, Blackwell Science Ltd.

Pilsworth, RC, R Hopes and TRC Greet (1988). A Flexed Dorso-Palmar Projection of The Equine Fetlock In Demonstrating Lesions of The Distal 3rd Metacarpus. *Veterinary Record* 122: 332-3.

Piotrowski, G, M Sullivan and PT Colahan (1983). Geometric properties of equine metacarpi. *Journal of Biomechanics* 16: 129-39.

Pool, RR and DM Meagher (1990). Pathologic findings and pathogenesis of racetrack injuries. *Veterinary Clinics of North America Equine Practice* 6: 1-30.

Poole, KE, RL van Bezooijen, N Loveridge, H Hamersma, SE Papapoulos, CW Lowik and J Reeve (2005). Sclerostin is a delayed secreted product of osteocytes that inhibits bone formation. *FASEB Journal* 19: 1842-4.

Poole, KES and J Reeve (2005). Parathyroid hormone -- a bone anabolic and catabolic agent. *Gastrointestinal/ Endocrine and Metabolic Diseases* 5: 612.

Pourmand, EP, I Binderman, SB Doty, V Kudryashov and AL Boskey (2007). Chondrocyte apoptosis is not essential for cartilage calcification: Evidence from an in vitro avian model. *Journal of Cellular Biochemistry* 100: 43-57.

Radtke, CL, NA Danova, MC Scollay, EM Santschi, MD Markel, T Da Costa Gomez and P Muir (2003). Macroscopic changes in the distal ends of the third metacarpal and metatarsal bones of Thoroughbred racehorses with condylar fractures. *American Journal of Veterinary Research* 64: 1110-6.

Rahm, C, K Ito and J Auer (2000). Screw fixation in lag fashion of equine cadaveric metacarpal and metatarsal condylar bone specimens: a biomechanical comparison of shaft and cortex screws. *Veterinary Surgery* 29: 564-71.

Rasband, W (2005). ImageJ, United States National Institutes of Health.

Raub, RH, SG Jackson and JP Baker (1989). The effect of exercise on bone growth and development in weanling horses. *Journal of Animal Science* 67: 2508-14.

RCVS. (2006). Guide to Professional Conduct. Retrieved 14/6/2006, from http://www.rcvs.org.uk/PrintFullArticle.asp?NodeID=89642

Reid, SA and A Boyde (1987). Changes in the mineral density distribution in human bone with age: Image Analysis using backscattered electrons in SEM. *Journal of Bone and Mineral Research* 2: 13-22.

Revell, PA, C Pirie, G Amir, S Rashad and F Walker (1990). Metabolic activity in the calcified zone of cartilage: observations on tetracycline labelled articular cartilage in human osteoarthritic hips. *Rheumatology International* 10: 143-7.

Richardson, DW (1984). Medial condylar fractures of the third metatarsal bone in horses. *Journal of the American Veterinary Medical Association* 185: 761-5.

Richardson, DW (1998). The metacarpal and metatarsal bones. Current techniques in equine surgery and lameness. NA White and JN Moore. Philadelphia, J.B. Lippincott Co: 810-6.

Rick, MC, TR O'Brien, RR Pool and D Meagher (1983). Condylar fractures of the third metacarpal bone and third metatarsal bone in 75 horses: radiographic features, treatments, and outcome. *Journal of the American Veterinary Medical Association* 183: 287-96.

Riggs, CM (1990). The Relationship Between Mechanical Function and Microstructural Properties of Cortical Bone in the Racehorse. Department of Surgery and Obstetrics, Royal Veterinary College. London, University of London. PhD.

Riggs, CM (1999). Aetiopathogenesis of parasagittal fractures of the distal condyles of the third metacarpal and third metatarsal bones--review of the literature. *Equine Veterinary Journal* 31: 116-20.

Riggs, CM (2002). Fractures--a preventable hazard of racing thoroughbreds? *Veterinary Journal* 163: 19-29.

Riggs, CM, GH Whitehouse and A Boyde (1999a). Pathology of the distal condyles of the third metacarpal and third metatarsal bones of the horse. *Equine Veterinary Journal* 31: 140-8.

Riggs, CM, GH Whitehouse and A Boyde (1999b). Structural variation of the distal condyles of the third metacarpal and third metatarsal bones in the horse. *Equine Veterinary Journal* 31: 130-9.

Roach, HI (1999). Association of matrix acid and alkaline phosphatases with mineralization of cartilage and endochondral bone. *Histochemical Journal* 31: 53-61.

Roach, HI, T Aigner and JB Kouri (2004). Chondroptosis: A variant of apoptotic cell death in chondrocytes? *Apoptosis* 9: 265-77.

Rogers, CW, E Firth, CW McIlwraith, A Barneveld, A Goodship, C Kawcak, RK Smith and PR Van Weeren (In press). Evaluation of a new strategy to modulate skeletal development in the equine athlete by imposing track-based exercise during growth. *Equine Veterinary Journal*.

Rogers, CW, E Firth, CW McIlwraith, A Barneveld, AE Goodship, CE Kawcak and RKW Smith (In press). Evaluation of a new strategy to modulate skeletal development in the equine athlete by imposing track-based exercise during growth: the effects on 2-year-old and 3-year-old racing careers. *Equine Veterinary Journal*.

Rogers, CW and EC Firth (2004). Musculoskeletal responses of 2-year-old Thoroughbred horses to early training. 2. Measurement error and effect of training stage on the relationship between objective and subjective criteria of training workload. *New Zealand Veterinary Journal* 52: 272-9.

Rooney, JR (1974). Distal condylar fractures of the cannon bone in the horse. *Modern Veterinary Practice* 55: 113-4.

Rooney, JR and JL Robertson (1996). Fore Leg. Equine Pathology. JR Rooney and JL Robertson, Iowa State University Press: 158-62.

Roschger, P, P Fratzl, J Eschberger and K Klaushofer (1998). Validation of quantitative backscattered electron imaging for the measurement of mineral density distribution in human bone biopsies. *Bone* 23: 319-26.

Ross, MH, LJ Romrell and GI Kaye (1995a). Bone Formation. Histology. A Text and Atlas. Baltimore, Maryland, USA, Williams & Wilkins: 160-7.

Ross, MH, LJ Romrell and GI Kaye (1995b). Cartilage. Histology. A Text and Atlas. Baltimore, Maryland, USA, Williams & Wilkins: 132-46.

Ross, MW (1998). Scintigraphic and clinical findings in the Standardbred metatarsophalangeal joint: 114 cases (1993-1995). *Equine Veterinary Journal* 30: 131-8.

Rossdale, PD, R Hopes, NJ Digby and K Offord (1985). Epidemiological study of wastage among race-horses 1982 and 1983. *Veterinary Record* 116: 66-9.

Roux, W (1881). Der Kampf der Teile im Organismus. Leipzig, Engelmann.

RSPCA. (2006). Website General - Horseracing. Retrieved 10/01/2006, 2006, from http://www.rspca.org.uk/

Rubin, CT and LE Lanyon (1985). Regulation of bone mass by mechanical strain magnitude. *Calcified Tissue International* 37: 411-7.

Russell, TM and AA Maclean (2006). Standing surgical repair of propagating metacarpal and metatarsal condylar fractures in racehorses. *Equine Veterinary Journal* 38: 423-7.

Schneider, R and B Jackman (1996). Fractures of the third metacarpus and metatarsus. Equine Fracture Repair. AJ Nixon. Philadelphia, Saunders: 179-94.

Schriefer, JL, SJ Warden, LK Saxon, AG Robling and CH Turner (2005). Cellular accommodation and the response of bone to mechanical loading. *Journal of Biomechanics* 38: 1838-45.

Schryver, HF (1978). Bending properties of cortical bone of the horse. *American Journal of Veterinary Research* 39: 25-8.

Seeman, E (2007). Bone's material and structural strength. *Current Opinion in Orthopaedics* 18: 494-8.

Semevolos, SA, ML Strassheim, JL Haupt and AJ Nixon (2005). Expression patterns of hedgehog signaling peptides in naturally acquired equine osteochondrosis. *Journal of Orthopaedic Research* 23: 1152-9.

Sherman, KM, GJ Miller, TJ Wronski, PT Colahan, M Brown and W Wilson (1995). The effect of training on equine metacarpal bone breaking strength. *Equine Veterinary Journal* 27: 135-9.

Skedros, JG, TR Grunander and MW Hamrick (2005). Spatial distribution of osteocyte lacunae in equine radii and third metacarpals: considerations for cellular communication, microdamage detection and metabolism. *Cells Tissues Organs* 180: 215-36.

Skedros, JG, JL Holmes, EG Vajda and RD Bloebaum (2005). Cement lines of secondary osteons in human bone are not mineral-deficient: New data in a historical perspective. *Anatomical Record* 286: 781-803.

SkyScan. (2006). SkyScan micro-CT: Model 2011 X-ray Nanotomograph (Nano-CT). Retrieved 29/05/2006, 2006, from http://www.skyscan.be/next/spec_2011.htm

Sloet van Oldruitenborgh-Oosterbaan, MM, JA Mol and A Barneveld (1999). Hormones, growth factors and other plasma variables in relation to osteochondrosis. *Equine Veterinary Journal Supplement* 31: 45-54.

Stashak, TS (2001). Fractures of the condyles of the third metacarpal and metatarsal bones. Adams' Lameness in Horses. TS Stashak. Philadelphia, Williams & Wilkins.

Steendijk, R and A Boyde (1973). Scanning Electron-Microscopic Observations On Bone From Patients With Hypophosphatemic (Vitamin-D Resistant) Rickets. *Calcified Tissue Research* 11: 242-50.

Stepnik, MW, CL Radtke, MC Scollay, PE Oshel, RM Albrecht, EM Santschi, MD Markel and P Muir (2004). Scanning electron microscopic examination of third metacarpal/third metatarsal bone failure surfaces in thoroughbred racehorses with condylar fracture. *Veterinary Surgery* 33: 2-10.

Stock, KF and O Distl (2005). Evaluation of expected response to selection for orthopedic health and performance traits in Hanoverian Warmblood horses. *American Journal of Veterinary Research* 66: 1371-9.

Stock, KF, H Hamann and O Distl (2005). Estimation of genetic parameters for the prevalence of osseous fragments in limb joints of Hanoverian Warmblood horses. *Journal of Animal Breeding and Genetics* 122: 271-80.

Stover, SM, RR Pool, RB Martin and JP Morgan (1992). Histological Features of The Dorsal Cortex of The 3rd Metacarpal Bone Mid-Diaphysis During Postnatal-Growth In Thoroughbred Horses. *Journal of Anatomy* 181: 455-69.

Stover, SM, DH Read, BJ Johnson, T Harrington, A Ardans, ML Anderson, BC Barr, BM Daft, H Kinde, J Moore, J Stoltz and Woods (1994). Lateral condylar fracture histomorphology in racehorses. *Proceedings of the American Association of Equine Practitioners* 40: 173-4.

Strand, E, GS Martin, MP Crawford, SG Kamerling and DJ Burba (1998). Intra-articular pressure, elastance and range of motion in healthy and injured racehorse metacarpophalangeal joints. *Equine Veterinary Journal* 30: 520-7.

Suzumoto, R, M Takami and T Sasaki (2005). Differentiation and function of osteoclasts cultured on bone and cartilage. *Journal of Electron Microscopy (Tokyo)* 54: 529-40.

Swindlehurst, J (2007). Skeletal Risk Factors for Fatal Lateral Condylar Fractures in racing Thoroughbreds. Liverpool, University of Liverpool. MPhil.

Swindlehurst, J, TDH Parkin and KL Morgan (2006). Subchondral Bone Pathology Associated With Fatal Lateral Condylar Fracture In Racehorses - A Case-Control Study.

Swindlehurst, JC, TDH Parkin and KL Morgan (2005). Fatal lateral condylar fractures in racehorses: associations with pathology and conformation? British Equine Veterinary Association Congress, Harrogate.

Taniguchi, N, K Yoshida, T Ito, M Tsuda, Y Mishima, T Furumatsu, L Ronfani, K Abeyama, K Kawahara, S Komiya, I Maruyama, M Lotz, ME Bianchi and H Asahara (2007). Stage-specific secretion of HMGB1 in cartilage regulates endochondral ossification. *Molecular and Cellular Biology* 27: 5650-63.

Tapprest, J, F Audigie, C Radier, MC Anglade, MC Voisin, N Foucher, C Collobert-Laugier, D Mathieu and JM Denoix (2003). Magnetic resonance imaging for the diagnosis of stress fractures in a horse. *Veterinary Radiology and Ultrasound* 44: 438-42.

Tomioka, Y, M Kaneko, M Oikawa, T Kanemaru, T Yoshihara and R Wada (1985). Bone mineral content of metacarpus in racehorses by photon absorption technique: In vitro measurement. *Bulletin of Equine Research Institute* 22: 22-9.

Trueta, J and AJ Buhr (1963). The Vascular Contribution To Osteogenesis. V. The Vasculature Supplying The Epiphysial Cartilage In Rachitic Rats. *Journal of Bone and Joint Surgery - British Volume* 45: 572-81.

Trueta, J and JD Morgan (1960). The vascular contribution to osteogenesis. I. Studies by the injection method. *Journal of Bone and Joint Surgery - British Volume* 42-B: 97-109.

Trueta, J and A Trias (1961). The vascular contribution to osteogenesis. IV. The effect of pressure upon the epiphysial cartilage of the rabbit. *Journal of Bone and Joint Surgery - British Volume* 43-B: 800-13.

Turner, AS, EJ Mills and AA Gabel (1975). In vivo measurement of bone strain in the horse. *American Journal of Veterinary Research* 36: 1573-9.

Vajda, EG, JG Skedros and RD Bloebaum (1995). Consistency In Calibrated Backscattered Electron Images of Calcified Tissues and Minerals Analyzed In Multiple Imaging Sessions. *Scanning Microscopy* 9: 741-55.

van de Lest, CH, PA Brama and PR Van Weeren (2002). The influence of exercise on the composition of developing equine joints. *Biorheology* 39: 183-91.

van den Hoogen, BM, CHA van de Lest, PR van Weeren, LMG van Golde and A Barneveld (1999). Effect of exercise on the proteoglycan metabolism of articular cartilage in growing foals. *Equine Veterinary Journal Supplement* 31: 62-6.

van Weeren, PR and A Barneveld (1999). The effect of exercise on the distribution and manifestation of osteochondrotic lesions in the Warmblood foal. *Equine Veterinary Journal Supplement*: 16-25.

van Weeren, PR, J Knaap and EC Firth (2003). Influence of liver copper status of mare and newborn foal on the development of osteochondrotic lesions. *Equine Veterinary Journal* 35: 67-71.

Vaughan, LC and BJE Mason (1975). A clinico-pathological study of racing accidents in horses. A report of a study on equine fatal accidents on racecourses. London, Horserace Betting Levy Board.

Verheyen, KL, WE Henley, JS Price and JL Wood (2005). Training-related factors associated with dorsometacarpal disease in young Thoroughbred racehorses in the UK. *Equine Veterinary Journal* 37: 442-8.

Verheyen, KL and JL Wood (2004). Descriptive epidemiology of fractures occurring in British Thoroughbred racehorses in training. *Equine Veterinary Journal* 36: 167-73.

Vilar, JM, M Pinedo, J Demier, F Castejon and C Riber (1995). Equine Metacarpophalangeal Joint Surface-Contact Changes During Walk, Trot and Gallop. *Journal of Equine Veterinary Science* 15: 315-9.

von Meyer, GH (1867). Die architektur der spongiosa. *Archiv für Anatomie, Physiologie und wissenschaftliche Medicin* 34: 615-25.

Walker, GD, M Fischer, J Gannon, RC Thompson and TR Oegema (1995). Expression of Type-X Collagen In Osteoarthritis. *Journal of Orthopaedic Research* 13: 4-12.

Wallace, JM, RM Rajachar, X-D Chen, S Shi, MR Allen, SA Bloomfield, CM Les, PG Robey, MF Young and DH Kohn (2006). The mechanical phenotype of biglycan-deficient mice is bone- and gender-specific. *Bone*: In Press, Corrected Proof.

Walter, J (2004). Sync Windows, United States National Institutes of Health.

Wittwer, C, K Lohring, C Drogemuller, H Hamann, E Rosenberger and O Distl (2007). Mapping quantitative trait loci for osteochondrosis in fetlock and hock joints and palmar/plantar osseus fragments in fetlock joints of South German Coldblood horses. *Animal Genetics* 38: 350-7.

Wolff, J (1892). Das Gesetz der Transformation der Knochen. Berlin, Hirschwald.

Wyn-Jones, G (1988). Lateral Condylar Fractures. Equine Lameness. G Wyn-Jones. London, Blackwell Scientific: 253-8.

Yoshihara, T, M Kaneko, M Oikawa, R Wada and Y Tomioka (1989). An Application of The Image Analyzer To The Soft Radiogram of The 3rd Metacarpus In Horses. *Japanese Journal of Veterinary Science* 51: 184-6.

Yovich, JV, CW McIlwraith and TS Stashak (1985). Osteochondritis dissecans of the sagittal ridge of the third metacarpal and metatarsal bones in horses. *Journal of the American Veterinary Medical Association* 186: 1186-91.

Yovich, JV, AS Turner and FW Smith (1985a). Holding Power of Orthopedic Screws In Equine 3rd Metacarpal and Metatarsal Bones .1. Foal Bone. *Veterinary Surgery* 14: 221-9.

Yovich, JV, AS Turner and FW Smith (1985b). Holding Power of Orthopedic Screws In Equine 3rd Metacarpal and Metatarsal Bones .2. Adult Horse Bone. *Veterinary Surgery* 14: 230-4.

Ytrehus, B, CS Carlson and S Ekman (2007). Etiology and pathogenesis of osteochondrosis. *Veterinary Pathology* 44: 429-48.

Zekas, LJ, LR Bramlage, RM Embertson and SR Hance (1999a). Characterisation of the type and location of fractures of the third metacarpal/metatarsal condyles in 135 horses in central Kentucky (1986-1994). *Equine Veterinary Journal* 31: 304-8.

Zekas, LJ, LR Bramlage, RM Embertson and SR Hance (1999b). Results of treatment of 145 fractures of the third metacarpal/metatarsal condyles in 135 horses (1986-1994). *Equine Veterinary Journal* 31: 309-13.

Zhou, Z, SS Apte, R Soininen, R Cao, GY Baaklini, RW Rauser, J Wang, Y Cao and K Tryggvason (2000). Impaired endochondral ossification and angiogenesis in mice deficient in membrane-type matrix metalloproteinase I. *Proceedings of The National Academy of Sciences USA* 97: 4052-7.

Zizak, I, P Roschger, O Paris, BM Misof, A Berzlanovich, S Bernstorff, H Amenitsch, K Klaushofer and P Fratzl (2003). Characteristics of mineral particles in the human bone/cartilage interface. *Journal of Structural Biology* 141: 208-17.

Appendix 1: Publications

1.6 Papers

Doube, M, EC Firth and A Boyde (2005). Registration of confocal scanning laser microscopy and quantitative backscattered electron images for the temporospatial quantification of mineralization density in 18-month old thoroughbred racehorse articular calcified cartilage. *Scanning* **27**: 219-26.

Doube, M, EC Firth and A Boyde (2007). Variations in articular calcified cartilage by site and exercise in the 18-month-old equine distal metacarpal condyle. *Osteoarthritis and Cartilage* **15**: 1283-92.

1.7 Meeting Abstracts

Doube, M., E. C. Firth and A. Boyde (2005a). Correlated confocal and backscattered electron (BSE) SEM studies of the articular cartilage mineralising front in 18 month old thoroughbred racehorse distal third metacarpal bones. *Journal of Anatomy* **206**: 494.

Doube, M., E. C. Firth and A. Boyde (2005b). Registration of CSLM and qBSE images for the temporospatial quantification of mineralization density in 18-month old thoroughbred racehorse articular calcified cartilage. *Scanning* **27**: 74-5.

Doube, M., E. C. Firth and A. Boyde (2006a). ImageJ and analysis of correlated confocal and BSE-SEM imaging. *Scanning* **28**: 93-4.

Doube, M., E. C. Firth and A. Boyde (2006b). Preconditioning exercise and anatomic site relate to mineralisation and thickness in equine third metacarpal articular calcified cartilage. *Calcified Tissue International* **78**: S47.

Doube, M., E. C. Firth and A. Boyde (2006c). Site- and exercise-related variations in equine articular calcified cartilage thickness, mineralization density and linear accretion rate. *Journal of Anatomy* **209**: 564-5.

Doube, M. E. C. Firth and A. Boyde (2007a). Bone mineralisation density and marrow space orientation vary by site in the equine third metacarpal condyle. *Calcified Tissue International* **80**: S51

Doube, M., E. C. Firth, G. R. Davis, A. J. Bushby and A. Boyde (2007b). Early development of linear defects in the third metacarpal parasagittal groove. British Equine Veterinary Association Congress, Edinburgh.

Appendix 2: Abbreviations

3D	three dimensional, three dimensions
ACC	articular calcified cartilage
ALP	alkaline phosphatase
BMP	bone morphogenetic protein
BMU	basic multicellular unit
BSE-SEM	backscattered electron scanning electron microscopy
CL	cathodluminescence
CDET	common digital extensor tendon
CT	computed tomography
CWI	cumulative work index
DDFT	deep digital flexor tendon
Dm	mineralisation density
DNA	deoxyribonucleic acid
DXA	dual x-ray absorptiometry
E	Nanoindentation modulus
ECM	extracellular matrix
GERA	Global Equine Research Alliance
GEXA	GERA exercise
HAC	hyaline articular cartilage
IGF	insulin-like growth factor
Ihh	Indian hedgehog
IOT	interosseus tendon
ISH	in-situ hybridisation
LAR	linear accretion rate
LDET	lateral digital extensor tendon
LUT	look-up table
Mc3	third metacarpal bone
MCPJ	metacarpophalangeal joint
MCSJ	metacarposesamoidean joint
µCT	micro computed tomography
MMP	matrix metalloproteinase
MRI	magnetic resonance imaging
mRNA	messenger ribonucleic acid
Mt3	third metatarsal bone
MT-MMP	membrane-type matrix metalloproteinase
OC	osteochondrosis
OCD	osteochondritis dissecans
OPG	osteoprotegrin
PP	proximal phalangeal bone
PMMA	polymethylmethacrylate, poly (methyl 2-methylpropenoate)
pQCT	peripheral quantitative computed tomography
PSB	proximal sesamoid bone
PTH	parathyroid hormone
PTHrP	parathyroid hormone related peptide

QUS	quantitative ultrasound
RANK	receptor activator of NF- κB
RANKL	receptor activator of NF- κB ligand
RNA	ribonucleic acid
SDFT	superficial digital flexor tendon
Shh	sonic hedgehog
SOS	speed of sound
TEM	transmission electron microscope
TRAP	tartrate-resistant acid phosphatase
TUNEL	terminal deoxyribonucleotidyl transferse (TdT)-mediated biotin-16-dUTP nick-end labelling
vBMD	volumetric bone mineral density
VEGF	vascular endothelial growth factor
VEGFR-1	vascular endothelial growth factor receptor 1
VFb	volume fraction of bone

Appendix 3: Computer Program Code

3.1 ImageJ Macros

3.1.1 TwinPeaks.txt

```
macro "Standard Grey Peak Finder [j]" {
setBatchMode(true);
run("Raw...", "image=8-bit width=512 height=512 offset=128 number=1
gap=0");
row=nResults;
getRawStatistics(area, mean, min, max, std, histogram);
f=0;
for(n=10;n<128;n++){
      if(histogram[n]>f){
            f=histogram[n];
            peak1=n;
      }
}
setResult("Brominated",row,peak1);
g=0;
for(o=220; o>127; o--) {
      if(histogram[o]>g){
            g=histogram[o];
            peak2=o;
      }
}
setResult("Iodinated",row,peak2);
      name = getTitle();
      setResult("Label", row, name);
updateResults();
}
```

3.1.2 Cartilage.txt

```
var milled;
var left;
var scale;
macro "Show Dialog... [b]" {
makeRectangle(500, 500, 1024, 1024);
//Make a dialog box
Dialog.create("Specimen Information");
Dialog.addCheckbox("Lateral to left (uncheck if to right)", true);
Dialog.addNumber("Scale", scale, 4, 6, "µm / pixel");
Dialog.show();
left = Dialog.getCheckbox();
scale = Dialog.getNumber();
setVoxelSize(scale, scale, 1, "micron");
//set logical values
if (left==true) left = 1;
else left = 0;
}
macro "Calcified Cartilage [t]" {
requires("1.34h");
var bmmd;
var fraction;
//get the pixel information from inside the ROI
getRawStatistics(count, mean, min, max, std, histogram);
row = nResults;
//get the number of image fields in the stack from ImageJ
fields = nSlices();
//use this line if dealing with a stacked series of images
name=getMetadata();
```

```
//use this line if dealing with single images
//    name = getTitle();
//  The following section gets useful information from the filename
horse = substring(name, 0, 2);
setResult("Horse ID", row, horse);
leg = substring(name, 2, 3);
setResult("Leg", row, leg);
section = substring(name, 3, 4);
setResult("Slice", row, section);
ni = getSliceNumber();
//use these lines to manually control the threshold
lower=1;
upper=255;
for (k=0; k<lower; k++) {
                  background = background + histogram[k];
fraction = (count - background) / count;
setResult("Vfc ", row, fraction);
      }
      for(j=lower; j<upper; j++) {
cumulative = cumulative + histogram[j];
av = av + j * histogram[j];
bmmd = av / cumulative;
setResult("Mean Matrix", row, bmmd);
}
      modep=0;
mode = 0;
for (p=lower; p<upper; p++) {
            if (mode < histogram[p]) {
mode = histogram[p];
setResult("Mode", row, p);
modep = p;
}}
setResult("Mean ROI ", row, mean);
//get the coordinates of the ends of the straight line selection
getLine(a,b,c,d,w);
//calculate line length - go pythagoras
thickness=scale*sqrt((a-c)*(a-c)+(b-d)*(b-d));
setResult("Thickness", row, thickness);
//Calculate relative position from left, lateral is always left, image
sequences //start on left
if (left == 1) pos = ni / fields;
else if (left == 0) pos = (fields - ni +1) / fields;
setResult("Pos", row, pos);
setResult("Finish", row, milled);
//still can't get strings into the results table...
//updateResults();
//the next line prints results in a log window
print(horse, " \t", leg, "\t", section, "\t", milled,"\t", modep, "
\t", mean, " \t", bmmd, " \t", fraction, "\t", thickness, "\t", pos, "
\n");
//draw a 250 micron radius circle to guide unbiased placement of next
ROI
r=500/scale;
x=a-r/2;
y=b-r/2;
makeOval(x,y,r,r);
}
```

3.1.3 UmisArrayDesigner.txt

```
//Umis Array Designer
//Open an image and set scale [b]
//Draw and rotate a rectangular ROI
//Create array [u]:
//Enter parameters (spacing, force)
//Print array file to log window
//Draw array on image
//Umis Array Designer v0.3
//ImageJ macro for designing UMIS nanoindentation arrays
//Copyright (C) 2007 Michael Doube
//m.doube at qmul.ac.uk
//This program is free software; you can redistribute it and/or
//modify it under the terms of the GNU General Public License
//as published by the Free Software Foundation (version 2).
//http://www.gnu.org/copyleft/gpl.html
//This program is distributed in the hope that it will be useful,
//but WITHOUT ANY WARRANTY; without even the implied warranty of
//MERCHANTABILITY or FITNESS FOR A PARTICULAR PURPOSE.  See the
//GNU General Public License for more details.
//You should have received a copy of the GNU General Public License
//along with this program; if not, write to the Free Software
//Foundation, Inc., 51 Franklin Street, Fifth Floor, Boston, MA
02110-1301, USA.

//Declare some global variables
var xspacing = 20; var yspacing = 20; var force = 20; var scale = 1;
var radius = 3; var thetax; var pos; var marker_offset = 50; var mark-
er_force = 50;
macro "Open Image...[b]"{
open();
run("Set Scale...", "distance=1 known=1 pixel=1 unit=pixel");
//default colour
setColor(255);
scale = abs(scale);
Dialog.create("Set Pixel Size");
Dialog.addNumber("microns / pixel", scale);
Dialog.show();
scale = Dialog.getNumber();
if (scale != 1) run("Set Scale...", "distance=1 known="+scale+"
pixel=1 unit=micron");
}
macro "Generate Array... [u]" {
scale = abs(scale);
type = selectionType();
if (type < 0) exit("Please draw a rectangular ROI");
if (type != 0 && type != 2) exit("I can only handle rectangular ar-
rays!");
Dialog.create("Adjust Indent Parameters");
Dialog.addNumber("X Spacing", xspacing);
Dialog.addNumber("Y Spacing", yspacing);
Dialog.addNumber("Force", force);
Dialog.addNumber("Marker Y Offset", marker_offset);
Dialog.addNumber("Marker Force", marker_force);
Dialog.addCheckbox("Show Outline", false);
Dialog.addCheckbox("Include Marker Indents", true);
Dialog.show();
xspacing = Dialog.getNumber();
yspacing = Dialog.getNumber();
force = Dialog.getNumber();
marker_offset = Dialog.getNumber();
```

```
marker_force = Dialog.getNumber();
outline = Dialog.getCheckbox();
include_marker = Dialog.getCheckbox();
getSelectionCoordinates(x, y);
yrefx = x[0];
yrefy = y[0];
xrefx = x[2];
xrefy = y[2];
startx = x[3];
starty = y[3];
//work out the baseline angle
thetax = atan((starty-xrefy)/(xrefx-startx));
//work out the mast angle
thetay = atan((starty-yrefy)/(yrefx-startx));
lengthx = sqrt((xrefx-startx)*(xrefx-startx)+(xrefy-starty)*(xrefy-
starty));
lengthy = sqrt((yrefx-startx)*(yrefx-startx)+(yrefy-starty)*(yrefy-
starty));
width = lengthx * scale;
length = lengthy * scale;
xcount = floor(width / xspacing)+2;
ycount = floor(length / yspacing)+2;
//handle top-right start positions
if (starty < yrefy) scale = -1*scale;
//handle reflected axes
if ((starty > yrefy && startx > xrefx)||(starty < yrefy && startx <
xrefx)){
            scale = -1*scale;
}
if (include_marker == true) marker_count = 2 + floor(sqrt(xcount));
else marker_count = 0;
//extra 2*marker_count is for marker rows
npos = xcount * ycount + 2 * marker_count;
xpos = newArray(npos);
ypos = newArray(npos);
//clear the log file
print("\\Clear");
k=0;
if (include_marker == true){
//calculate first marker row
for (h = k; h < marker_count-1; h++){
//marker_tally = marker_tally + xspacing;
                  ypos[h] = 0;
                  if (h*h*xspacing < (xcount-1) * xspacing){
                        xpos[h] = h*h*xspacing;
                        print(xpos[h]+"\,"+ypos[h]+"\,"+marker_force);
                        k++;
                  }
}
//calculate the bottom right corner
xpos[k] = (xcount-1) * xspacing;
ypos[k] = 0;
print(xpos[k]+"\,"+ypos[k]+"\,"+marker_force);
k++;
}
//calculate body of array
ytally = marker_offset;
for (i = 0; i < ycount; i++){
            xtally =0;
            for (j = 0; j < xcount; j++){
                  xpos[k] = xtally;
```

```
                    xtally = xtally + xspacing;
                    ypos[k] = ytally;
                    print(xpos[k]+"\,"+ypos[k]+"\,"+force);
                    k++;
               }
        ytally = ytally + yspacing;
}
if (include_marker == true){
//calculate top marker row
for (h = 0; h < marker_count-1; h++){
                    ypos[k] = (ycount-1)*yspacing + 2*marker_offset;
                    if (h*h*xspacing < (xcount-1) * xspacing){
                          xpos[k] = h*h*xspacing;
                          print(xpos[k]+"\,"+ypos[k]+"\,"+marker_force);
                          k++;
                    }
}
//calculate the top right corner
xpos[k] = (xcount-1) * xspacing;
ypos[k] = (ycount-1)*yspacing + 2*marker_offset;
print(xpos[k]+"\,"+ypos[k]+"\,"+marker_force);
}

//print the selection outline
if (outline == true) run("Draw");
//print the array
for (pos=0; pos<npos;pos++){
                    drawarray();
                    fill();
}
minutes = (k+1)*3.727;
days = floor(minutes / (60 * 24));
hours = floor(minutes / 60 - days * 24);
minutes = round(minutes - hours * 60 - days * 24 * 60);
xcount = xpos[k] / xspacing+1;
ycount = (ypos[k]-2*marker_offset) / yspacing+1;
showMessage("Array Layout",(k+1)+" indents total\n"+xcount+" x
"+ycount+" array size\n"+xpos[k]+" x "+ypos[k]+" microns\n\nTime to
complete:\n"+days+" days, "+hours+" hours, "+minutes+" mins");
}
//drawarray() function
function drawarray() {
//set the x scale
            x = xpos[pos]/scale;
//set the y scale
            y = ypos[pos]/scale;
//work out the rotated positions
            newx = (x-y*(tan(thetax)))*(cos(thetax));
            newy = y/cos(thetax)+sin(thetax)*(x-y*tan(thetax));
//adjust the positions for the marker offset
            markery = abs(marker_offset*sin(thetay)/scale)*scale/
abs(scale);
if (thetax == 0) markerx = 0;
else markerx = abs(marker_offset*cos(thetay)/scale)*thetax/
abs(thetax)*scale
/abs(scale);
//draw a circular ROI at the rotated, skewed position
makeOval(startx+newx+markerx-radius,starty-newy+markery-ra-
dius,2*radius,2*radius);
}}
```

3.1.4 Umis_Array0.521.txt

```
//Umis_Array
//Read layout file
//Determine position of array within image
//Draw an ROI at each point
//Adjust position, store adjustment and apply to next position
//log and recall error values for each position
//Classify tissue at each point
//Measure greyscale at each position
//GoTo any indent within an array
//Go forward or backwards through the array
//Handles arrays in any orientation
//Correlates qBSE backscatter coefficient
//to nanoindentation elastic modulus

//Umis_Array v0.52 ImageJ macro for combined qBSE and nanoindentation
analysis
//Copyright (C) 2007 Michael Doube
//m.doube at qmul.ac.uk
//2007-03-28 19:06 GMT

//This program is free software; you can redistribute it and/or
//modify it under the terms of the GNU General Public License
//as published by the Free Software Foundation (version 2).
//http://www.gnu.org/copyleft/gpl.html
//This program is distributed in the hope that it will be useful,
//but WITHOUT ANY WARRANTY; without even the implied warranty of
//MERCHANTABILITY or FITNESS FOR A PARTICULAR PURPOSE.  See the
//GNU General Public License for more details.
//You should have received a copy of the GNU General Public License
//along with this program; if not, write to the Free Software
//Foundation, Inc., 51 Franklin Street, Fifth Floor, Boston, MA
02110-1301, USA.

//declare some global variables
var xyf; var row; var pos; var width; var height; var nindents; var
radius; var startx; var starty; var newx; var newy; var scalex; var
scaley; var thetax; var thetay; var lengthy; var lengthx; var lines;
var imagelist; var xerror; var yerror; var goto = -1; var xerrors; var
yerrors; var errorlogged; var xfactor = 1; var factor = 1; var batch =
-1; var moduli; var force_macro = -1; var nimages = 0; var xrefx; var
xrefy; var yrefx; var yrefy; var win_size = 300;
//set the ROI radius - usually 15 pixels
var radius = 15;

//first macro starts here
macro "Setup Array... [b]" {
nimages = 0;
imagelist = newArray(3);
//open the qBSE image
open();
imagelist[0]=getImageID();
nimages++;
run("Set Scale...", "distance=1 known=1 pixel=1 unit=pixel global");
//open the array map
open();
imagelist[1]=getImageID();
nimages++;
run("Set Scale...", "distance=1 known=1 pixel=1 unit=pixel global");
sync = isOpen("Sync Windows 1.6");
if (sync == false) run("Sync Windows");
```

```
//Open the array file which must be a csv list like x,y,f
string = File.openAsString("");
//Initialise the results window
if(isOpen("Results")==false) row = 0;
else row = pos;
//initialise the position stepper
pos=-1;
//Split the CSV file into an array of lines
lines = split(string, "\n");
nindents = lengthOf(lines);
//initialise the error log arrays
xerrors = newArray(nindents);
yerrors = newArray(nindents);
errorlogged = newArray(nindents);
//find the dimensions of the indent array
dimension = lines[nindents-1];
dimension = split(dimension, "\,");
width = parseFloat(dimension[0]);
height = parseFloat(dimension[1]);
//Clear old selections
run("Select None");
//Locate important array landmarks on the image
//bottom left (start), bottom right (xref), top left (yref)
leftButton=16;
shift=1;
alt=8;
rightButton=23;
ctrl=2;
x2=-1;
y2=-1;
z2=-1;
flags2=-1;
//set the last value to be determined to be the loop escape value
yrefy = -1;
while (yrefy==-1) {
getCursorLoc(x, y, z, flags);
if (x!=x2 || y!=y2 || z!=z2 || flags!=flags2) {
// the "-radius" bits are to shift the ROI's to the centre of the cur-
sor position
//since the x,y position of each ROI is determined by the top left
corner of its //bounding box
//capture the start position with left click plus ctrl
       if (flags == 18){
startx = x-radius;
starty = y-radius;
print("start position captured",x, y,"\n");
}
//capture the bottom right indent point with left click plus alt
if (flags == 24){
xrefx = x-radius;
xrefy = y-radius;
print("x reference point captured",x,y,"\n");
}
//capture the top left indent point with left click plus shift
if (flags == 17){
yrefx = x-radius;
yrefy = y-radius;
print("y reference point captured",x,y,"\n");
}
}
x2=x; y2=y; z2=z; flags2=flags;
```

```
wait(10);
}
//work out the baseline angle
thetax = atan((starty-xrefy)/(xrefx-startx));
print ("baseline angle", thetax,"\n");
//work out the baseline length
lengthx = sqrt((xrefx-startx)*(xrefx-startx)+(xrefy-starty)*(xrefy-
starty));
print ("Baseline length", lengthx, width, "\n");
//work out the mast angle
thetay = atan((starty-yrefy)/(yrefx-startx));
print ("Mast angle", thetay,"\n");
//work out the mast length
lengthy = cos((thetax)-(thetay)+(PI/2))*sqrt((yrefx-startx)*(yrefx-
startx)+(yrefy-starty)*(yrefy-starty));
print("Mast length", abs(lengthy), height, "\n");
//work out a scale factor in x
scalex = (lengthx)/(width);
//work out a scale factor in y
scaley = abs((lengthy)/(height));
//handle top-right start positions
if (starty < yrefy){
scaley = -1*scaley;
scalex = -1*scalex;
}
//handle reflected axes
if ((starty > yrefy && startx > xrefx)||(starty < yrefy && startx <
xrefx)){
scalex = -1*scalex;
}
}

//macro - adjust the scale factors
macro "Adjust Scale... [u]" {
Dialog.create("Adjust Zoom");
Dialog.addNumber("Window Size", win_size);
Dialog.show();
win_size = Dialog.getNumber();
drawarray();
}

//macro - draw the whole array
macro "Draw array... [y]" {
Dialog.create("Draw Options");
array_styles = newArray("Outline", "Numbered", "Filled");
Dialog.addChoice("Style", array_styles, array_styles[0]);
Dialog.show();
array_style = Dialog.getChoice();
batch = 1;
setBatchMode(true);
for (pos=0; pos<nindents;pos++){
drawarray();
if (array_style == array_styles[0]) run("Draw");
else if (array_style == array_styles[1]){
run("Draw");
//print the number
drawString(pos+1,startx+newx+xerror,starty-newy-yerror);
}
else fill();
}
batch = -1;
```

```
setBatchMode(false);
run("Select None");
pos = 0;
}

//macro - advance to the next indent
macro "Next Indent... [l]" {
poserror();
if (pos < nindents-1) pos++; else exit("End of indentation array!");
drawarray();
}

//macro - go to the previous indent
macro "Previous Indent... [j]" {
poserror();
if (pos > 0) pos--; else exit("Beginning of indentation array!");
drawarray();
}

//macro: make a dialog box where the user can enter the indent they
want to go to
macro "Go To Indent... [g]" {
poserror();
Dialog.create("Go To Indent");
Dialog.addString("Indent No.", "");
Dialog.addMessage("Indent range 1-"+nindents+"\n");
Dialog.show();
goto = parseFloat(Dialog.getString());
if (goto > nindents || goto < 1) showMessage("Oops!", "Please enter a
value between 1 and "+nindents+"\n");
else {
goto = goto - 1;
drawarray();
}
}

//macro - set tissue type, measure pixels and record results
macro "Tissue type... [t]" {
if(isOpen("Results")==false) row = 0;
//update the row in the results table that relates to the indent
if (pos <= nResults) row = pos;
//else fill up the intervening rows with 0
else if (pos > nResults && nResults == 0) {
for (i = 0; i <= pos; i++){
setResult("N", i, i+1);
updateResults;
}
row = pos;
}
else if (pos > nResults) {
for (i = nResults-1; i <= pos; i++){
setResult("N", i, i+1);
updateResults;
}
row = pos;
}
xyf= split(lines[pos], "\,");
for (p=0; p<lengthOf(xyf); p++){
      setResult("N", row, pos+1);
      setResult("X", row, xyf[0]);
      setResult("Y", row, xyf[1]);
```

```
      setResult("Force", row, xyf[2]);
}
selectImage(imagelist[0]);
//Make a dialog box where the user can enter tissue type
//and go to the next indent
Dialog.create("Classify Tissue");
Dialog.addMessage("Indent no.: "+(pos+1)+"\n\n0 Lacuna\n1 Hyaline ar-
ticular cartilage\n2 Articular calcified cartilage\n3 Cement line\n4
Bone\n5 Marrow space");
Dialog.addString("Tissue Type", "");
Dialog.show();
type = Dialog.getString();
setResult("Tissue", row, type);
if (type == 0) setColor(100);
if (type == 1) setColor(150);
if (type == 2) setColor(210);
if (type == 3) setColor(240);
if (type == 4) setColor(250);
//collect data on pixels in ROI
getRawStatistics(count, mean, min, max, std, histogram);
//set the threshold (qBSE images use lots of 0's for non-mineralised
tissue)
lower = 1;
upper = 255;
//work out the non-zero area fraction
background = 0;
for (k=0; k<lower; k++){
background = background + histogram[k];
fraction = (count - background) / count;
setResult("AF", row, fraction);
}
//work out the mean mineral density of the mineralised fraction
cumulative = 0;
av= 0;
for (j=lower; j<upper; j++) {
cumulative = cumulative + histogram[j];
av = av + j * histogram[j];
bmmd = av / cumulative;
setResult("Mean Matrix", row, bmmd);
}
//work out the modal mineral density of the mineralised fraction
mode = 0;
for (p=lower; p<upper; p++) {
if (mode < histogram[p]) {
mode = histogram[p];
setResult("Mode Matrix", row, p);
modep = p;
}
setResult("Mean ROI", row, mean);
      }
print ('row', row, 'pos', pos);
updateResults;
//    fill();
//    row++;
poserror();
if (pos < nindents-1) pos++;
else exit("End of indentation array!");
drawarray();
}

//Macro: set the fill colour based on the indentation modulus
```

```
//requires a CSV list in (n,mean,sd) format
macro "Colour Code Array... [f]"{
force_macro = 1;
//parse the moduli file
modulus_min = 99999999;
modulus_max = 0;
moduli_file = File.openAsString("");
moduli_lines = split(moduli_file, "\n");
moduli = newArray(nindents);
for (m=0; m<lengthOf(moduli_lines); m++){
moduli_n= split(moduli_lines[m], "\,");
if (isNaN(moduli_n[1]) == true) moduli[m] = 0;
else moduli[m] = parseFloat(moduli_n[1]);
if (moduli[m] < modulus_min) modulus_min = moduli[m];
if (moduli[m] > modulus_max) modulus_max = moduli[m];
}
//ask the user for the array spacing
Dialog.create("Array Spacing");
Dialog.addMessage("Please enter\nthe array spacing");
Dialog.addNumber("x (microns)", 20);
Dialog.addNumber("y (microns)", 20);
Dialog.show;
xspacing  = parseFloat(Dialog.getNumber());
yspacing = parseFloat(Dialog.getNumber());
selectImage(imagelist[0]);
name = getTitle();
w = getWidth();
h=getHeight();
newImage("moduli_"+name, "8-bit Black", w, h, 1);
imagelist[2] = getImageID();
nimages++;
scale = 250/(modulus_max-modulus_min);
//Draw the array
batch = 1;
setBatchMode(true);
for (pos=0; pos<nindents;pos++){
if (20+(moduli[pos]-modulus_min)*scale < 255 )
setColor(20+(moduli[pos]-modulus_min)*scale);
else setColor(255);
drawarray();
fill();
}
batch = -1;
setBatchMode(false);
pos = 0;
run("Select None");
run("Interactive 3D Surface Plot");
//only plot the values from the array area, not the background black
makePolygon(startx-radius, starty+radius, xrefx+radius, xrefy+radius,
yrefx+xrefx-startx+radius, yrefy+xrefy-starty-radius, yrefx-radius,
yrefy-radius);
run("Interactive 3D Surface Plot");
force_macro = -1;
}

//poserror() - determine the error at each position
function poserror() {
if (pos > -1){
//measure the manual adjustment to add to the auto adjust value
getSelectionBounds(adjposx,adjposy,wi, he);
//recall the logged error values for that position if they exist
```

```
if (errorlogged[pos] == -8){
   xerror = xerrors[pos];
   yerror = yerrors[pos];
}
xerroradj = adjposx-(startx+floor(newx)+xerror);
yerroradj = adjposy-(starty-floor(newy)-yerror);
//if the selection is accidentally deselected, fix the way-out error
value
if (adjposx==0 && adjposy==0){
xerroradj = 0;
yerroradj = -1;
}
xerror = xerror+xerroradj;
//yerror needs to be adjusted by -1 to correct for float to integer
rounding errors
yerror = yerror-yerroradj-1;
if (yerror == -1) yerror = 0;
//log the x and y errors
xerrors[pos] = xerror;
yerrors[pos] = yerror;
errorlogged[pos] = -8;
print(pos, xerrors[pos], yerrors[pos]);
}
}

//drawarray() function
function drawarray() {
if (batch>0) setBatchMode(true);
//Get each x,y coordinate and display it
if (goto != -1) pos = goto;
xyf= split(lines[pos], "\,");
//set the x scale
x = (xyf[0])*(scalex);
//set the y scale
y = (xyf[1])*(scaley);
//work out the rotated positions
newx = (x-y*(tan(thetax)))*(cos(thetax));
newy = y/cos(thetax)+sin(thetax)*(x-y*tan(thetax));
//work out the skew
skewx = cos(thetax)*y*tan(thetax+(PI/2)-thetay);
skewy = sin(thetax)*y*tan(thetax+(PI/2)-thetay);
//adjust the positions
newx = (newx + skewx)*xfactor;
newy = (newy + skewy)*yfactor;
//reset the error values when returning to the origin (1st indent)
if (pos == 0){
xerroradj = 0;
yerroradj = -1;
xerror = 0;
yerror = 0;
}
//recall the logged error values for the position if they exist
if (errorlogged[pos] == -8){
xerror = xerrors[pos];
yerror = yerrors[pos];
}
//Zoom and centre the window
for (n = 0; n<nimages; n++){
if (batch < 0){
selectImage(imagelist[n]);
makeRectangle(startx+newx+xerror-win_size/2+radius, starty-newy-yer-
```

```
ror-win_size/2+radius, win_size, win_size);
run("To Selection");
}
//if we are running the modulus macro then draw a polygon
if (force_macro > 0){
xp = startx+newx+radius+xerror;
yp = starty-newy+radius-yerror;
h = abs(yspacing * lengthy / height);
l = xspacing * lengthx / width;
x0 = xp - (h * cos(thetay) / 2) - (l * cos(thetax) / 2);
y0 = yp - (h * sin(thetay) / 2) - (l * sin(thetax) / 2);
x1 = x0 - h*cos(thetay);
y1 = y0 + h*sin(thetay);
x3 = x0 + l*cos(thetax);
y3 = y0 - l*sin(thetax);
x2 = x1 + x3 - x0;
y2 = y1 + y3 - y0;
makePolygon(x0,y0, x1, y1, x2, y2, x3, y3);
} else {
//draw a circular ROI at the rotated, skewed and error adjusted posi-
tion
makeOval(startx+newx+xerror,starty-newy-yerror,2*radius,2*radius);
}
}
//Tell us which indent we are looking at
if (nimages == 3) showStatus("Indent: "+(pos+1)+", x="+xyf[0]+",
y="+xyf[1]+", E="+round(10*moduli[pos])/10);
else showStatus("Indent: "+(pos+1)+", x="+xyf[0]+", y="+xyf[1]);
//reset the GoTo value
goto = -1;
}
```

3.1.5 VolumeFractionOfBone.txt

```
//VolumeFractionOfBone
//ImageJ macro for the determination of bone volume fraction in
//3D image sets
//Copyright (C) 2007 Michael Doube
//m.doube at qmul.ac.uk
//Last modified 2007-02-28 17:53 UTC

//This program is free software; you can redistribute it and/or
//modify it under the terms of the GNU General Public License
//as published by the Free Software Foundation (version 2).
//http://www.gnu.org/copyleft/gpl.html
//This program is distributed in the hope that it will be useful,
//but WITHOUT ANY WARRANTY; without even the implied warranty of
//MERCHANTABILITY or FITNESS FOR A PARTICULAR PURPOSE.  See the
//GNU General Public License for more details.
//You should have received a copy of the GNU General Public License
//along with this program; if not, write to the Free Software
//Foundation, Inc., 51 Franklin Street, Fifth Floor, Boston, MA
02110-1301, USA.
var startslice; var endslice;
macro "Start Slice [j]" {
startslice = getSliceNumber();
}
macro "End Slice [l]" {
endslice = getSliceNumber();
}
macro "Volume Fraction of Bone [q]" {
requires("1.34h");
```

```
n = getSliceNumber();
row = nResults;
vroihisto = newArray(256);
getThreshold(lower, upper);
if (lower==-1) exit("Use Image>Adjust>Threshold to set the thresh-
old");
setBatchMode(true);
vmax = 0;
if (startslice < 1) startslice = 1;
if (endslice < 1) endslice = nSlices;
if (startslice > endslice) exit ("Start slice must be a lower number
than end slice!");
print("For slice "+startslice+" to slice "+endslice);
for (i=startslice; i<=endslice; i++) {
            setSlice(i);
            getRawStatistics(count, mean, min, max, std, histogram);
            vcount = vcount + count;
            if (max > vmax) vmax = max;
            if (max < upper) top = max;
            else top = upper;
            for (m=0; m<=top;m++){
                  vroihisto[m] = vroihisto[m] + histogram[m];
            }
                  for (k=0; k<lower; k++) {
                        background = background + histogram[k];
                  }
}
vfraction = (vcount - background) / vcount;
if (vmax < upper) top = vmax;
else top = upper;
av=0;
cumulative = 0;
for (q = lower; q<=top; q++){
            cumulative = cumulative + vroihisto[q];
av = av + q * vroihisto[q];
}
vbmmd = av / cumulative;
for (q = 0; q<=vmax; q++){
            roiav = roiav + q * vroihisto[q];
}
roiav = roiav / vcount;
if (vfraction == 0) mode = 0/0;
else {
            mode = lower;
            for (q=lower; q<=top;q++){
                  if (vroihisto[q] > vroihisto[mode]) mode = q;
            }
}
name = getTitle();
setResult("Label", row, name);
setResult("Vfb", row, vfraction);
setResult("Mean Matrix", row, vbmmd);
setResult("Mode Matrix", row, mode);
setResult("Mean ROI", row, roiav);
updateResults();
setSlice(n);
setBatchMode(false);
}
```

3.2 Perl Scripts

3.2.1 kittyflip.pl

```
#!/usr/bin/perl
#kittyflip.plx
use warnings;
use strict;
my $fname; my $line; my @pre_profile; my $element; my $interval; my
$count; my @profile; my $density; my $pixel_time; my $i; my @line; my
$row; my $col; my $array; my @array; my @namechars; my $out;

print "Please ensure that the input filename takes\nthe general form,
hhlsppxxxxx, where\nhh is the horse id, l is the leg, s is the slice
and pp is the site.\nData will be added at the bottom of an existing
output file, otherwise a new file will be created.\nPlease enter an
output file name\n: ";
$out = <STDIN>;
open FH, ">> $out" or die $!;
print "How many days between labels?: ";
$interval = <STDIN>;
foreach $fname(@ARGV) {
open(FILE, $fname) || die("Could not open $fname\n");
@namechars = split(//,$fname);
$row=0;
while (<FILE>) {
            s/[\n\r]+$//;
            s/(^ +| +$)//g;
            @line=split(/\t/,$_);
            for ($col=0;$col <= $#line;$col++) {
                  $array[$col][$row]=$line[$col];
            }
            $row++;
}
for ($row=1;$row <= $#array;$row++) {
            $line='';
            for ($col=0;$col <= $#{$array[$row]};$col++) {
                  $line.="\t$array[$row][$col]";
            }
            $line =~ s/^\t//;
            chomp $line;
            @pre_profile=split(/\t/,$line);
            shift @pre_profile;
            @profile = ();
            for $element(@pre_profile) {
                  unless($element == 0) {
                        push @profile, $element;
                  }
            }
            $count = @profile;
            $pixel_time = $interval/$count;
            $i = $pixel_time;
            for $density(@profile) {
print FH $namechars[0],$namechars[1],"\t", $namechars[2], \t",
$namechars[3], "\t", $namechars[4],$namechars[5], "\t",$i,"\
t",$density, "\n";
                  $i = $i + $pixel_time;
            }
}
close(FILE);
}
print "Data written to ", $out;
```

Appendix 4: Equipment and Suppliers

Acer Aspire 3023 WLMi Notebook Computer

Technoworld Plc.
Unit B2, Connaught Business Centre
Hyde Estate Road
West Hendon
London
NW9 6JL

Calcein

Sigma-Aldrich Company Ltd
Fancy Road
Poole
Dorset
BH12 4QH
Cat. C0875

Excel

Microsoft Corporation
One Microsoft Way
Redmond, California
United States of America

ImageJ

National Institutes of Health
Bethesda, Maryland
United States of America
http://rsb.info.nih.gov/ij/

Kontron IBAS SEM Controller

Zeiss UK Ltd.
Welwyn Garden City
Herts
United Kingdom

Leica SP2 Confocal Scanning Laser Microscope

Leica Microsystems (UK) Ltd
Davy Avenue
Knowlhill
Milton Keynes
MK5 8LB
Bucks
United Kingdom

MySQL 5

MySQL AB
Bangårdsgatan 8
S-75320 Uppsala
Sweden

PIXImus DXA Scanner

Qados Ltd.
Unit 8, Lakeside Business Park
Swan Lane, Sandhurst, Berks, GU47 9DN
http://www.faxitron.com/piximus_specifications.htm

SEM Calibration Grid

Agar Scientific Cat S171
Stansted
Essex
United Kingdom

Solvents, general reagents

BDH Ltd.,
Poole
BH15 1TD
United Kingdom

Methyl-methacrylate (Prod. 2923467)
α-Azo-iso-butyronitrile (Prod. 27918)

UMIS 2000 Nanoindentation Testing Rig

CSIRO
Lindfield
New South Wales
Australia

Windows XP SP2

Microsoft Corporation
One Microsoft Way
Redmond, California
United States of America

X-ray Microtomography Imager

MuCat2
Biophysics in Relation to Dentistry
Barts and The London School of Medicine and Dentistry
Queen Mary, University of London
Mile End
London

Zeiss DSM962 Scanning Electron Microscope

Zeiss UK Ltd.
Welwyn Garden City
Herts
United Kingdom